2012

Synthesis of PDMS-metal oxide hybrid nanocomposites using an in situ sol-gel route

Qiaoyu Lu
Michigan Technological University

SYNTHESIS OF PDMS-METAL OXIDE HYBRID NANOCOMPOSITES USING AN *IN SITU* SOL-GEL ROUTE

By

Qiaoyu Lu

A DISSERTATION

Submitted in partial fulfillment of the requirements for the degree of

DOCTOR OF PHILOSOPHY

(Chemical Engineering)

MICHIGAN TECHNOLOGICAL UNIVERSITY

2012

This dissertation, “Synthesis of PDMS-Metal Oxide Hybrid Nanocomposites Using an *In Situ* Sol-Gel Route” is hereby approved in partial fulfillment of the requirements for the Degree of DOCTOR OF PHILOSOPHY IN CHEMICAL ENGINEERING.

Department of Chemical Engineering

Signatures:

Dissertation Advisor _____
Michael E. Mullins

Department Chair _____
Komar Kawatra

Date _____

Table of Contents

List of Figures

List of Tables

Preface

Chapter 4 is an article that was previously published in MRS Proceedings 2012 1400: mrsf11-1400-s06-02. Qiaoyu Lu designed and conducted the experiments, analyzed the data, and wrote the paper.

Acknowledgements

First of all I would like to express deepest gratitude to my advisor Dr. Michael E. Mullins, for his constant help, guidance, and encouragement. Thanks for his good advice and support to my research experiment, and walked me through the writing of this dissertation. Without his help this work could not have reached this present form.

I would also like to thank Dr. Tony R. Rogers, Dr. Gerard T. Caneba, and Dr. Christopher T. Middlebrook for being my committee and spend time reading my dissertation. Thanks to Dr. Tony R. Rogers for his encouragement and setting me a good sample of hardworking. Thanks to Dr. Gerard T. Caneba for his instructions and lending me the chemicals I need. Thanks to Dr. Christopher T. Middlebrook for his professional suggestions for my experiment design and for his kindness to let me use his instrument.

I wish to express my special appreciation of Dr. Jacek Borysow's help with the light scattering apparatus set-up and his gentleness to loan me his instruments. I especially appreciate the guidance of Dr. Bahne C. Cornilsen on the instrument of FT-IR and FT-Raman. My special gratitude also goes to Dr. Jeffrey B. Burl for lending me his instrument and Michael R. Chase for teaching me how to use it. Thanks to Dr. Miguel Levy for training me to operate the prism coupler.

I gratefully acknowledge Dr. David R. Shonnard, Dr. Tomas B. Co, and Dr. Michael E. Mullins for helping me during the time being their teaching assistant. Thanks to Dr. Tomas B. Co and Dr. Faith A. Morrison for being there as friends.

I would extend my sincere thanks to Xiaochu Ding and Ning Chen, for the help of running polymerization experiments in their labs. I would like to thank Daw Don Cheam, Thomas Daunais, and William Knudsen for their training and assisting on the instruments in Material Science and Engineering.

I would like to express my gratitude to Jerry A. Norkol, David W. Caspary, Tim P. Gasperich for their technical help of my research and my lab. Thanks to Alexis Snell and David Zei for assisting me with all the graduate paperwork and ordering chemicals and instruments.

I would like to take this opportunity to thank my colleagues and friends Hanbing Wang, ChoHui Lim, Qi Gao, Huan Yang, Jifei Liu, Wen Nee Yeo, Felix Adom, Shuo Huang, Xiaodao Chen, Yuan Liang, Fanyu Kong, Zhuoer Xie, Sheng Hu, Justin Carlson, Abby Carlson, Ran An, Le Xin, Zhichao Wang, Jiqing Fan, and Zhiyong Zhang for giving me a hand whenever I need, thanks for their friendship.

Last but not least, I want to give my heartfelt thanks to my parents, my husband, and my son for their love, support, and patience.

Abstract

Organic-inorganic hybrid nanocomposites are widely studied and applied in broad areas because of their ability to combine the flexibility, low density of the organic materials with the hardness, strength, thermal stability, good optical and electronic properties of the inorganic materials. Polydimethylsiloxane (PDMS) due to its excellent elasticity, transparency, and biocompatibility has been extensively employed as the organic host matrix for nanocomposites. For the inorganic component, titanium dioxide and barium titanate are broadly explored as they possess outstanding physical, optical and electronic properties.

In our experiment, PDMS-TiO_2 and PDMS-$BaTiO_3$ hybrid nanocomposites were fabricated based on in-situ sol-gel technique. By changing the amount of metal precursors, transparent and homogeneous PDMS-TiO_2 and PDMS-$BaTiO_3$ hybrid films with various compositions were obtained. Two structural models of these two types of hybrids were stated and verified by the results of characterization.

The structures of the hybrid films were examined by a conjunction of FTIR and FT-Raman. The morphologies of the cross-sectional areas of the films were characterized by FESEM. An Ellipsometer and an automatic capacitance meter were utilized to evaluate the refractive index and dielectric constant of these composites respectively. A simultaneous DSC/TGA instrument was applied to measure the thermal properties. For PDMS-TiO_2 hybrids, the higher the ratio of titanium precursor added, the higher the

refractive index and the dielectric constant of the composites are. The highest values achieved of refractive index and dielectric constant were 1.74 and 15.5 respectively for sample PDMS-TiO_2 (1-6). However, when the ratio of titanium precursor to PDMS was as high as 20 to 1, phase separation occurred as evidenced by SEM images, refractive index and dielectric constant decreased. For PDMS-$BaTiO_3$ hybrids, with the increase of barium and titanium precursors in the system, the refractive index and dielectric constant of the composites increased. The highest value was attained in sample PDMS-$BaTiO_3$ (1-6) with a refractive index of 1.6 and a dielectric constant of 12.2. However, phase separation appeared in SEM images for sample PDMS-$BaTiO_3$ (1-8), the refractive index and dielectric constant reduced to lower values. Different compositions of PDMS-TiO_2 and PDMS-$BaTiO_3$ hybrid films were annealed at 60 °C and 100 °C, the influences on the refractive index, dielectric constant, and thermal properties were investigated.

1. Introduction

1.1 Hybrid Nanocomposites

Materials used today could be broadly separated into two types: organic and inorganic. Polymers and elastomers, that are organic materials, own favorable mechanical properties such as softness, elasticity, light weight, and flexibility which make them easy to process and utilize. However, they generally have poor electronic properties (e.g. dielectric constant, conductivity, etc.), and modest optical properties (e.g. refractive index) compared to their inorganic counterparts. Inorganic materials such as glasses, ceramics, and metals have high hardness, firmness, and thermal resistance; but are much more difficult to process into films, coatings, fibers, or extruded shapes. Combining the flexibility of organic materials and the thermal stability and high refractive index of inorganic materials, hybrid composites composed of organic and inorganic components have been developed due to combine the favorable properties of both within a single system. This term 'nanocomposites' was first proposed by Theng in 1970 (1). The terms 'hybrid nanocomposites', 'nanohybrids', and 'nanostructural composites' are used interchangeably in the literature to describe these systems.

Nanocomposites are composites that have at least one characteristic scale in the order of nanometers. Nanocomposites combine the most significant properties of their constituents, such as low processing temperature (polymeric), thermal stability (metal oxides) and high transparency. Nanocomposite materials can be separated into three broad types (2): ceramic matrix; metal matrix; and polymer matrix nanocomposites.

Although ceramics have good wear resistance and high thermal and chemical stability, they are typically brittle. The low toughness of ceramics has blocked their use for many applications; however, ceramic matrix nanocomposites have significantly enhanced mechanical properties which can overcome this problem. By the incorporation of energy-dissipating components such as whiskers, fibers, platelets or particles which can hinder further opening of a crack, the ceramic matrix exhibits increased fracture toughness (3-5). The potential of ceramic matrix nanocomposites were revealed by the pioneering work of Niihara (6,7), on the Al_2O_3/SiC system. By adding of a low volume fraction of SiC particles of suitable size and hot pressing the resulting mixture, the Al_2O_3 matrix had a noticeable strength improvement. The mechanism of this toughening was explained by some studies based upon the crack-bridging role of the nanosized reinforcements (8). Subsequently, the preparation of advanced nanocomposites with high toughness was also demonstrated by the incorporation of high strength nanofibers into ceramic matrices (9).

Metal matrix nanocomposites consist of a ductile metal or alloy matrix wherein some nanosized reinforcements are implanted. By combining the ductility and toughness of metal with the high strength and modulus of ceramic, nanocomposites with high strength in shear/compression processes and for high service temperature applications can be made. These are widely applied in many areas, such as the aerospace and automotive industries and for advanced structural materials (10).

Polymer materials are broadly used in industry because of their ease of production, light weight, and ductile nature. However, compared with metals and ceramics they have

relatively low modulus and strength. In order to overcome these disadvantages, polymers may be filled with inorganic compounds, either synthetic or natural. Depending on the fill material, the polymers may exhibit increased heat and impact resistance, flame retardancy and mechanical strength, or decreased electrical conductivity and gas permeability (11). For more advanced applications, the fill materials can combine the unique magnetic, electronic, or optical properties of metal and ceramics with useful polymer properties such as processibility and film forming capability. Utilizing this approach, the weaker attributes of polymers can be improved while keeping their lightweight and ductile nature (12-17). Due to the high surface area of nanometer scale particles versus micrometer scaled particles, nanocomposites can exhibit much larger changes in these special properties than microcomposites.. The efficiency of reinforcement particles in nanocomposites, even at low volume fractions, is comparable to 40-50% for fibers in microcomposites (18). That is because the larger surface area of nanocomposites provides much better phase interaction compared to microcomposites.

When the size of material is reduced to a value that significant changes of properties can be observed, it is called “the critical size”. (19) Therefore, during the preparation of nanocomposites, the ratio of surface area to volume is a crucial factor to be considered to better understand the relationships between structure and properties. The amount and characteristics of the interphase will affect the properties of composites. The characteristics of the interphase mostly depend on the formation mechanism and the properties of the components. For interphase formed by chemical reactions, it is hard to predict its properties. For example, when silane is treated to fibers or fillers and a

polysiloxane layer formed, the thickness of this layer is mostly affected by the amount of silane applied for treatment and the properties are determined by the functional groups of the component. For interphase formed by physicochemical interactions, its thickness is controlled by interaction strength and its properties are decided by the properties of the components and the amount of material bonded in the interphase. Although nanocomposites can have unique properties not found in conventional composites, there are still challenges in controlling elemental composition and stoichiometry in the nanocluster phase.

1.2 Organic-Inorganic Hybrid Nanocomposites with High Refractive Index

Producing an organic-inorganic hybrid nanocomposite with a high refractive index is an important goal of this work. Although they can have excellent optical transparence and processability, optical polymers have limited refractive indices. Inorganic ceramics having high refractive indices, but are difficult to process and their optical dispersion needs to be improved. Therefore, combining the merits of polymeric and inorganic optical materials is a potential route to prepare nanocomposites with high refractive indices. Many organic-inorganic hybrid nanocomposites with high refractive index are discussed in the literature. (20-36) Triethoxysilane-capped polymer titania hybrid materials, based on poly(tetramethylene oxide) (20), poly(arylene ether ketone) (21), poly(arylene ether sulfone) (21) and poly(arylene ether phosphine oxide) (22) were successfully prepared by Wilkes and co-workers. TiO_2 as an inorganic component is

particularly introduced into polymer matrixes to synthesize nanocomposites with high refractive indices (30-36). By changing the ratio of the organic component to the inorganic component, the refractive index of these hybrid materials could be controlled. The properties of organic and inorganic components as well as the nanocomposite's phase morphology and interfacial properties will affect the final hybrid's optical, mechanical and thermal properties. Therefore, morphology and phase separation are important factors in organic-inorganic hybrid nanocomposites. (37-49) The microstructure and properties of these nanocomposite materials are controlled by the interfacial strength between organic and inorganic components, where the extensive hydrogen bonds (40-43) and covalent bonds (44-46) may prevent phase separation.

1.3 Organic-Inorganic Nanocomposites Synthesis

1.3.1 Sol-gel Reaction

In order to improve the compatibility between organic and inorganic components, several types of approaches have been developed. Among the numerous methods under development, the sol-gel route has been broadly applied because of its capability to control the miscibility between organic and inorganic components at the molecular level (50,51). The sol-gel route is a process in which molecular precursors, such as metal alkoxides, undergo hydrolysis and condensation reactions to form a three-dimensional network of inorganic or organic-inorganic hybrid materials. This route requires low temperature and less energy compared to physical mixing. It can fabricate organic-inorganic hybrid nanocomposites with a domain size approaching molecular level under

mild conditions. A large amount of literature has been published in this field recently (52-65). The hydrolysis and condensation reactions for the sol-gel reaction processes are shown below:

Hydrolysis

$$M(OR)_4 + H_2O \rightarrow M(OR)_X(OH)_{4-X} + R - OH$$

Condensation

$$\equiv M - OR + \equiv M - OH \rightarrow \equiv M - O - M \equiv + R - OH$$

$$\equiv M - OH + \equiv M - OH \rightarrow \equiv M - O - M \equiv + H - OH$$

Organic matrix materials used in sol-gel synthesis of organic-inorganic nanocomposites can be broadly separated into two categories: organo (alkoxy) silanes with polymerizable or reactive organic substituents and functional group modified oligomers (prepolymers) or polymers. ORMOSILs or ORMOCERs are two commercially available organic-inorganic hybrid nanocomposites, which are prepared using this hydrolysis-condensation reaction of these organo (alkoxy) silanes.(60,65) Because of their high refractive index, titanium alkoxides and zirconium alkoxides are usually used as precursors for the synthesis of the inorganic phase in hybrid nanocomposites. In an acid catalyzed system, these precursors can be introduced into the ORMOSILs directly via a co-condensation reaction to synthesize nanocomposites. (66,67) However, compared to silicon alkoxides, titanium and zirconium alkoxides have much higher reactivity towards water, which may cause immediate hydrolysis and the precipitation of the oxo-polymers. (54,55) The reaction rate of the metal alkoxides in the sol-gel reaction highly depends on the catalysts (acidic, basic or nucleophilic activation) in the system. Therefore, to control the reactivity

of these transition-metal alkoxides and avoid phase separation (producing an opaque appearance) in the resultant nanocomposites, chemical additives can be introduced into the system. Normally, the organic acids, β-diketones or allied derivatives are used as chelating agents to decrease the reactivity of these transition-metal alkoxides. (66,68) Although adding chemical additives is an efficient method for preparing transparent high performance nanocomposites, it is hard to fully remove the additives from the system because of their strong affinity with the transition metals, and the remaining additives may affect the thermal, mechanical and optical properties of the nanocomposites.

Functional group modified oligomers, prepolymers or polymers are the second type of organic matrix materials used in sol-gel synthesis of nanocomposites, such as triethoxysilane end or side chain capped polymers etc. (69-75) In this case, the nanoscale building blocks produced by sol-gel reaction are generated in the organic matrices. The morphology of the inorganic phase produced is well controlled by the functional groups of polymers or oligomers, which is restricted to the nanoscale. These functional groups offer strong covalent linkages between nanoscale building blocks and organic matrices, preventing phase separation in nanocomposites. The interfacial force between organic and inorganic phases is a significant factor in controlling the structure and properties of nanocomposites, by which even with high inorganic loading level, homogeneous transparent nanocomposites can be obtained. Fig. 1 shows a sol-gel preparation route for titania-polymer nanocomposites with covalent linkages. The reactive functional groups of polymers may cause the form of dual organic-inorganic hybrid nanocomposites. (56) If the polymer matrix has a high content of functional groups, triethoxysilane for example,

due to the fast hydrolysis and condensation reactions of titanium alkoxides, a gelation phenomenon is usually observed in the system. Therefore under high titania content, instead of conventional acid catalysis, acid-free polymerization is applied to produce organic-inorganic nanocomposites. (72) However, the disadvantage of the sol-gel route is that the titania or zirconia domains formed during the reaction are normally amorphous and the refractive index is relatively low. Also, the drying process cause large shrinkage in the system and therefore results in high inner stress in the nanocomposites, which may lead to poor mechanical properties.

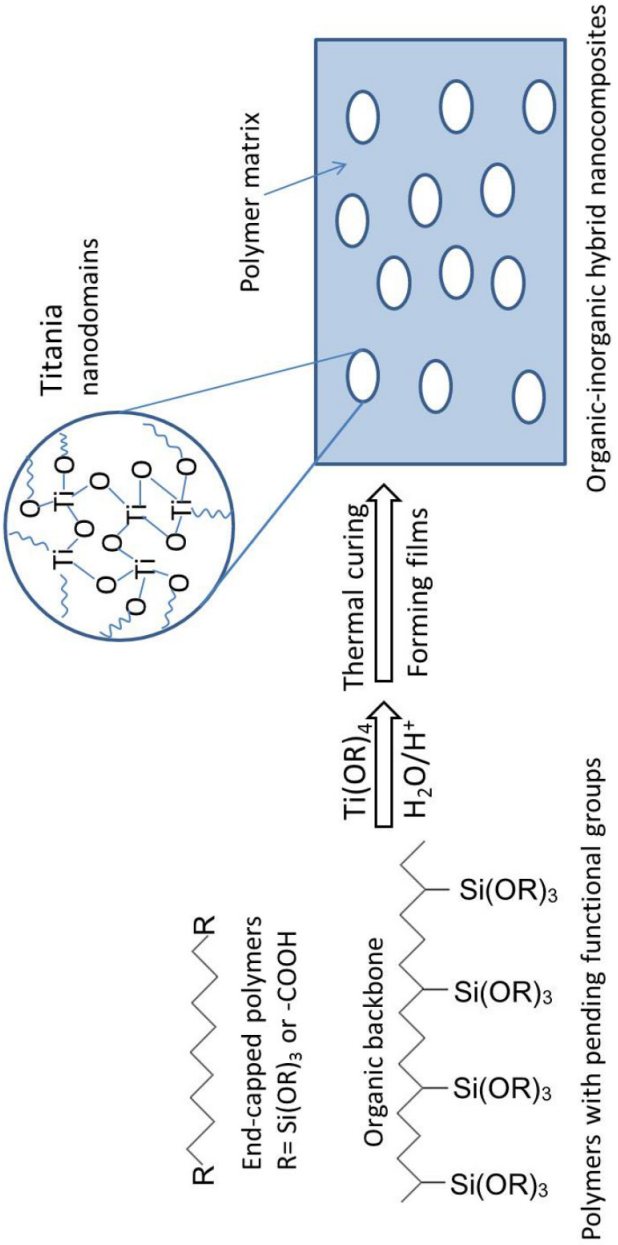

Figure 1.1 Synthetic scheme for high RI titania-polymer nanocomposites via the sol-gel route (modified from (76))

1.3.2 In situ formation of nanoparticles in polymer matrices

The *in situ* method synthesizes inorganic nanoparticles directly within the polymer matrix to prepare nanocomposites in one step. In this route, the particle aggregation caused by

handling and mixing processes can be avoided, since the nanoparticles are nucleated and grown inside the polymer matrix. Additionally, the polymer chain functional groups have passivating or stabilizing effect on the nanoparticles formed. This effect provides an even spatial distribution in polymer matrices by preventing them from agglomerating, since there is an insufficient fluid environment in the polymer matrices to allow individual particles to meet by diffusion. These nanocomposites are stable compared to colloidal solutions and can be applied in the design of optical and optoelectronic devices. However, the disadvantage of this method is that the unreacted educts or byproducts of the *in situ* reaction may affect the properties of the final product.

The strong interaction between the inorganic precursor and the polymer matrix is a very important factor for controlling the particle size and polydispersity. Polymers with hydroxyl, mercapto and sulfonic functional groups can offer strong interactions between metal elements of inorganic precursors and polymer matrices. (77-82) The *in situ* preparation scheme of semiconductor nanoparticle-polymer nanocomposites is shown below in Figure 1.2. As shown in Figure 1.2, the polymer and metal ions are first mixed in a solution, and then a counter-ion such as S^{-2} in the form of a gas or as liquid phase ions is introduced into the solution. The composite can be cast to a film before or after the introduction of the counterion. This *in situ* synthesis method was performed to fabricate high refractive index nanocomposites with PbS nanoparticles. (83-85)

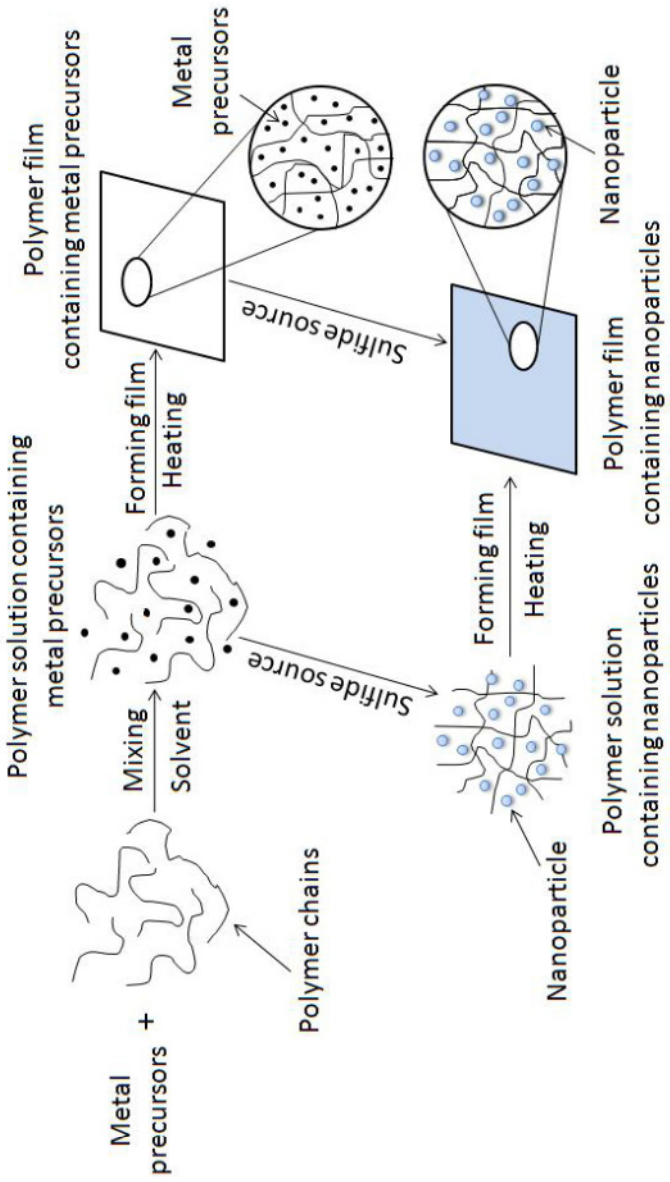

Figure1.2 Schematic of *in situ* synthesis of metal sulfide nanoparticles in a polymer matrix (modified from (76))

The highest refractive index for a PbS-gelatin film is about 2.5 with 70wt% PbS. Some water-soluble polymers such as poly(vinyl alcohol) (PVA), poly(ethylene oxide) (PEO),

poly(acrylic acid) (PAA) and poly(acrylamide) have been chosen as polymer matrices to produce PbS-polymer nanocomposites with high refractive index. (84)

Stable semiconductor-polymer nanocomposites can be fabricated by H_2S gas reacting with a soluble metal-containing microgel which is formed by copolymerizing the polymerizable metal salts with styrene. These nanocomposites have a well-controlled particle content, size and surface state. Yang et al. copolymerized lead methacrylate or zinc methacrylate with styrene, and then treated them with H_2S gas to prepare metal sulfide nanoparticles in polymer networks. (86-88) These cross-linked nanocomposites consist of PbS nanoparticles by polymerizing lead dimethacrylate. (89) By covalent bonds grown between the nanocomposites and the substrates, composite films with enhanced stability, controlling film thickness and structure are obtained. Researchers have used reactive lead precursors ($Pb(SCH_2CH_2OH)_2$) and polythiourethane (PTU) oligomers terminated with isocyanate groups, followed by *in situ* gas-solid reaction to design and synthesize PbS-polymer nanocomposites with a high refractive index. (90)

1.3.3 *Ex situ* synthesis method

Another important route for the preparation of organic-inorganic nanocomposites is called "*ex situ* synthesis" of nanocomposites. In this method, pre-made nanoscale building blocks such as inorganic nanoparticles (NPs) are integrated into the polymer (blending route) or monomers which are then polymerized to fabricate composites (*in situ* polymerization). The process of this "ex situ synthesis" method is shown below in Figure 1.3.

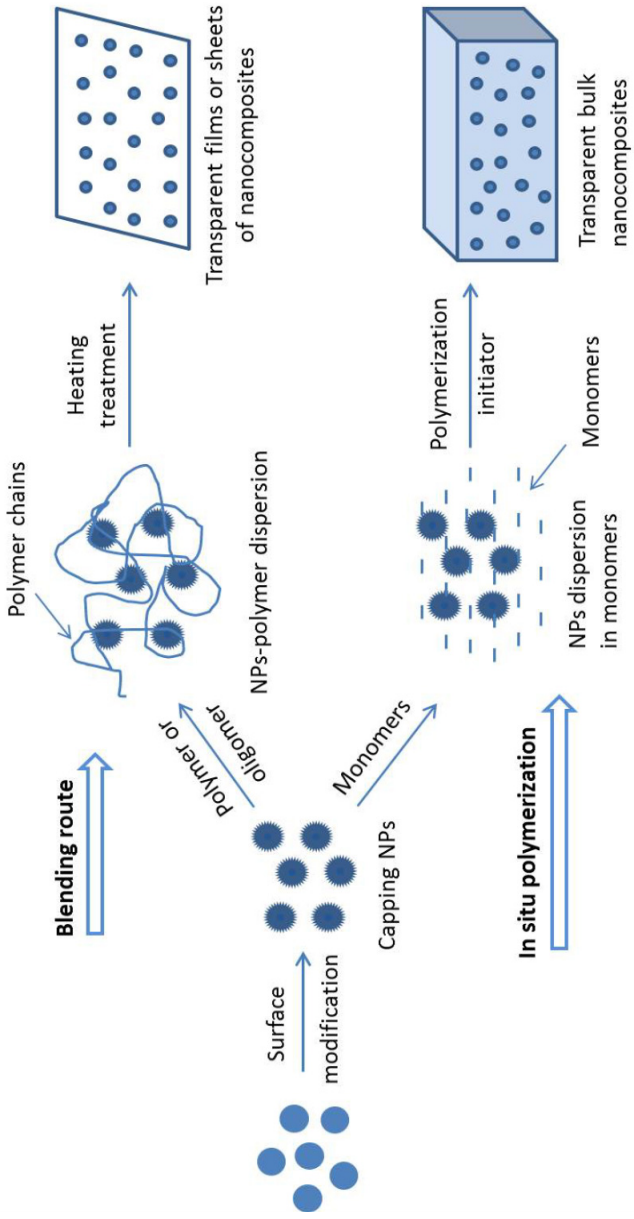

Figure1.3 Ex situ synthesis of nanocomposites from blending route and in situ polymerization process (modified from (76))

As shown in the scheme, the nanoparticles used in this method are prepared separately, isolated and purified and modified by surface capping agents before incorporated into the polymer matrix. In this method, the surface properties of nanoparticles, particle size and

size distribution are well controlled. Therefore, compared with other methods, this “ex situ synthesis” method is mostly applied in large scale industrial area. Although this approach is a quite promising route for practical application, the pre-made nanoparticles tend to aggregate unless their surfaces are modified to decrease the inter-particle attraction. So, the main challenge of this approach is to prepare nanoparticles with long-term stability against aggregation, and disperse them well into the polymer or monomers to obtain a positive interference in large enough amounts. To solve this problem, based on surface engineering of nanoparticles it is very important to minimize the interface energies between nanoparticles and the polymer matrix. Generally, in both synthesis and post-treatment processes, the nanoparticles are modified by chemi- or physisorption of surfactant molecules onto the surface to terminate the growth of particles. The surface modified nanoparticles can be readily dispersed in an organic medium after isolation. For the preparation of nanocomposites with high refractive index, if a large amount of surface capping agent or surfactant is incorporated, their refractive index should be higher than the conventional ones in order to avoid the decrease of the resultant nanocomposites refractive index.

1.3.3.1 Blending Route

The blending route is the simplest approach to prepare nanocomposites. Usually, a solution of polymer or oligomers consisting of dispersed nanoparticles (NPs) is cast into a container or deposited on a glass or plastic substrate by a spin coating or dip coating process, after which the sample is heated and finally a transparent nanocomposite film or sheet is obtained. This preparation method contains two major steps: the preparation of

surface modified nanoparticles and the synthesis of polymers, from which a crucial issue to improve the transparency of nanocomposites is the compatibility of nanoparticles and polymer matrices. For example, Lee et al. based on ligand molecule engineering, incorporated surface modified ZrO_2 nanoparticles into a polydimethylsiloxane (PDMS) matrix to prepare high refractive index transparent nanocomposites. (91) With PDMS-like siloxane tail structure, the designed ligand molecule has good chemical compatibility with the PDMS matrix. It strongly adsorbs on ZrO_2 nanoparticles surface by its diamine head group, and forms a strong steric barrier due to its double-tailed structure. This ligand molecule is a key factor to efficiently disperse ZrO_2 particles in a PDMS matrix.

To improve the compatibility and avoid phase separation, it not only needs the rational design and tailoring of the nanoparticles and the structures of the polymer matrix, also proper cosolvents are necessary. Nakayama et al. used n-butanol and toluene as the cosolvents to prepare high refractive index (1.58-1.81) transparent free-standing nanocomposite films by dispersing propionic acid modified TiO_2 nanoparticles into poly(bisphenol-A and epichlorohydrin). (92)

1.3.3.2 In situ polymerization

In situ polymerization is widely reported as an effective route to obtain transperant nanocomposites. (93-98) It also has been developed to prepare organic-inorganic nanocomposites with high refractive index. Additionally, as compared with other approaches, this method is particularly suitable to prepare thicker bulk nanocomposites. However, it is very important to attain stable and transparent dispersions of nanoparticles before subsequent polymerization; otherwise the low viscosity of particle dispersions in

monomers may cause the inorganic particles to precipitate during the long polymerization process. Normally, in order to offer strong interfacial interaction between the monomer molecules and the inorganic particles or the inorganic particle cores protected with organic capping shells, the design and tailoring of the surface characteristics of the inorganic particles is necessary.

Later, Inkyo et al. capped TiO_2 nanoparticles well dispersed in MMA with APTMOS, and through in situ polymersization to prepare transparent TiO_2-PMMA nanocomposites with a higher refractive index than pure PMMA. (99) Wegner et al. also used this approach to prepare acid modified ZnO-PMMA transparent nanocomposites. (100) In addition, the influence of various metal oxide nanoparticles (ZnO, TiO_2, ZrO_2 etc.) on the free radical polymerization in the in situ polymerization method was also studied. (97) However, to increase the refractive index of nanocomposites, the metal oxide content in the polymer matrix still need to be improved.

1.4 Applications of Organic-Inorganic Nanocomposites

For the 21st century, it is widely agreed that active optical applications of sol-gel derived hybrid polymers or nanocomposites might be one of the most attractive fields. (101,102) There are a large number of literature recent or throughout the past decade concerning these applications.

1.4.1 Application of High Refractive Index Nanocomposites

Organic-inorganic nanocomposites with high refractive index are expected to play an important role in future optical, optoelectric and information fields, including antireflection coatings, ophthalmic lenses, prisms, optical waveguides, non-linear optical materials and adhesives for optical components, etc.

1.4.1.1 Antireflective Coatings

To reduce the reflection loss at the surface of an optical material and obtain a clear view, antireflective coatings are the most important coating designs by applying which light transmittance will be increased and negative effects on the visual observation will be avoided, like double image and reflection, etc. (103-105) Back in 1817, antireflective coatings on glass substrates were discovered by Fraunhofer. Since then, they have been applied to broad technological fields, such as ophthalmic lenses, optical filters, photovoltaics, photodetectors, display screens, optical data storage and optoelectronic devices. (103-104) Low-cost multilayer antireflective coatings with high performance are most favorable in the development of optical and electro-optical systems in the visible and near infrared regions. (106) The recently developed sol-gel route used to fabricate antireflective coatings needs a thermal or chemical curing stage during processes, which is unlike conventional method requiring expensive vacuum processes. (107-109) It is very important for choosing materials for the high refractive index layer in the design and fabrication of multilayer antireflective coatings.

A facile procedure of spin-coating metal oxide nanoparticles on polymer substrates to make antireflective films was first developed by Krogman et al. (110) Antireflective coatings of high refractive index was fabricated by introducing commercially available aqueous colloidal ceria nanoparticles with refractive index of 2.18 at 500nm into a UV curable monomer. By loading ceria nanoparticles from 0 to 90 wt%, the refractive index of polymer layers can be increased. By incorporating SiO_2 into polymer matrix, films with low refractive index 1.46-1.54 were also manufactured. The properties of the fabricated nanocomposites antireflective coatings are as good as those manufactured by other methods. For example, an uncoated acrylic substrate of 90% transmission can be increased to 96.3% by applying two layer antireflective coatings. In addition, by changing the thickness and refractive index of the coated layers, the wavelength of minimum reflection of the cured films can also be controlled. Recently, Chen and coworkers coated optical glass using multilayer antireflective coatings made of polyimide-titania nanocomposite. (74) Also polymethyl silesquioxane was used to produce a three –layer antireflective coating, at the same time 90 wt% and 30 wt% titania nanocomposites were used as alternate depositing layers. The reflectance of original glass was decreased from 5% to an average value of 0.5% in the visible region. Organic-inorganic nanocomposites with high refractive index can be used to fabricate antireflective coatings. However, during the producing of antireflective coatings, attention needs to be paid in case that the solvent or monomers of nanocomposites systems may destroy the substrates, particularly for plastic substrates. In addition, because of their tunable refractive index, organic-inorganic nanocomposites are highly

valuable in the design of gradient index antireflective coatings on higher refractive index substrates or device surfaces.

1.4.1.2 Optical Waveguide Materials

Optical waveguide devices are the main factor in developing high speed broadband communication, especially for very large scale integration photonics and optoelectronics. (111) Organic-inorganic hybrid nanocomposites are utilized to fabricate flexible optical waveguide because of their outstanding benefits, such as low processing temperature, enhanced thermal and mechanical properties compared to equivalent pure polymers, higher thickness without cracking and their micropatternable by photolithographic techniques(68,112-114). In addition, by changing the chemical composition of nanocomposites, their optical properties can be precisely tailored and furthermore well-defined, and reproducible refractive index differences can be obtained to fabricate step-index or graded-index optical waveguide structures. It is an effective strategy to incorporate high refractive index nanoscale building blocks into nanocomposites to precisely tailor the optical properties in a very broad range. Because of the high refractive index of titania, titania based polymer nanocomposites have been widely studied as waveguide materials recently. Prasad et al used the sol-gel method fabricating SiO_2-TiO_2-poly(vinylpyrrolidone) nanocomposites to be applied for an optical waveguide. (68) By changing the ratio of SiO_2 to TiO_2, the nanocomposites refractive index was controlled in the range of 1.39-1.65 at 633nm. In order to avoid the precipitation of TiO_2 particles, the hydrolysis rate of titanium precursors was controlled by the author with the incorporation of acetic acid as a co-solvent. In the resultant nanocomposites, there was a low optical

propagation loss of 0.62 dB cm^{-1} or lower at 633nm in the slab waveguide configuration. In a reverse micellar micro reactor, fluorinated polyimide and pre-made TiO_2 nanoparticles were combined by an ex situ method successfully fabricating a transparent titania-polyimide composite waveguide. (115) The refractive index of the nanocomposites fabricated were increased from 1.55 for pure polyimide to 1.56 with 4 wt% TiO_2 nanoparticles dispersed into polymer matrix, and an optical propagation loss of 1.4 dB cm^{-1} at 633nm were obtained in the resultant slab composite waveguide. Chen et al. manufactured oligomeric phenylsilsesquioxane (OPSQ)-titania hybrid nanocomposites with an absorption in 277-322 nm and a high refractive index in the range of 1.527-1.759. (75) OPSQ-titania nanocomposites were used as the core layer to produce planar waveguides. When the titania content was increased from 0 to 15.9 wt%, the optical loss was decreased from 0.568 to 0.415 dB cm^{-1} due to the reduction of C-H bonding density in the nanocomposites. ORMOSIL systems were also studied for applying in waveguide production.(116-118) Optical waveguides were fabricated using ORMOSIL matix incorporated with high refractive index titania nanoscale building blocks. (119, 120) From the results of the experiments, planar waveguides with optical losses typically below 1 dB cm^{-1} in various communication windows are possible to produce using this method.

1.4.1.3 Non-linear Optical Materials

Non-linear optical materials, because of their potential applications in fields such as optical data storage, information processing and telecommunications, are widely studied. (121,122) The requirements for these materials are to have high mechanical and

dimensional stability, high thermal stability, high laser damage threshold and good transparency in the IR-vis region with low optical loss. The application of Organic-inorganic nanocomposites containing metal or semiconductor nanoparticles has attracted the most interest due to large optical non-linearities. (123) By increasing the nanoparticle concentration and dielectric confinement effect which depends on the dielectric constant ratio of nanoparticles and their surroundings, the optical non-linearities of nanocomposite materials can be improved. Therefore, two methods can be applied to improve the dielectric confinement effect: high refractive index nanoparticles such as CdS, PbS doping low refractive index matrixes such as PMMA, PVA, or applying high refractive index nanoparticles coated with a low refractive index layer. (124) Additionally, it is a critical issue to control the particle size and size distribution in the nanocomposites to apply them in non-linear optical applications. (125) It is possible to satisfy the above mentioned conditions and find applications in non-linear optical fields if some high refractive index transparent nanocomposites with high inorganic nanophase loading. The unique non-linear optical behavior of titania-PMMA nanocomposites with high refractive index was studied by Wang and coworkers recently. (126) These nanohybrid films were prepared by an in situ sol-gel route followed by spin-coating on quartz substrates with a titania nanocrystalline content up to 80%. It is demonstrated that the obtained nanohybrid films have outstanding non-linear optical behaviors with an ultrafast response of < 1.5 ps. (126) However, there were no signals for pure PMMA and TiO_2 thin films fabricated under the same conditions. The loading level of titania strongly affected the non-linear optical properties of nanohybrid films. It is the TiO_2 nanocrystalline phase, which has a much higher refractive index than that of the surrounding polymer matrix, that cause the

observed non-linear optical behavior. This is caused by the dielectric confinement effect of surface polarization that accelerates taking apart the excited charges and improves the electric field inside the nanoparticles. The author also found that both linear and non-linear optical responses can be increase by controlling the crystallinity of titania in PMMA nanocomposites. (127) The nanocomposites with highest titania crystallinity were observed to have a two photon absorption coefficient as high as 2260 cm GW^{-1} and a non-linear refractive index as high as 6.2×10^{-2} cm^2 GW^{-1}. Transparent, highly homogeneous linear and non-linear optical nanocomposites were prepared using PMMA-co-MA copolymer incorporated with oleic acid capped TiO_2 nanorods by a direct blending route. (128) In this system, a nearly negligible non-linear absorption and a negative value for non-linear refractive index were obtained. Theoretically, the quadratic Stark effect, which overcomes both the positive non-linearity of solvent and the positive non-linearity related to indirect transition, results in the negative non-linear refractive index. To effectively improve the non-linear optical behavior of organic-inorganic nanocomposites, many methods have been tried in the design of high refractive index nanocomposites to tailor or control the structure and dispersion state of the nanophase in organic matrix.

1.4.1.4 Volume Holographic Recording Materials

Organic-inorganic nanocomposites can be applied as volume holographic recording materials for optical data storage. The principal challenge in the field of holographic data storage is to develop an optimum recording material. (129) Holographic recording is usually obtained by photo induced refractive index modulation resulting from periodic

changing of composition and density caused by photopolymerization of monomers, and in turn two directional diffusion of the components in the process of exposing to the interference pattern. To maximize the dynamic range or the data storage capacity of materials, a large refractive index modulation is needed. So far, various types of photopolymers and photopolymerizable composites have been studied to apply high refractive index change with higher dimensional stability. However, it is rather difficult for pure polymer materials to achieve large refractive index modulation. That is not only because the restricted diffusion of monomer molecules in the binders, but also because the correspondingly limited refractive index differences between the available monomers and the binders. (130) High refractive index species (HRIS), such as Zr-based HRIS (131) and various nanoparticles (132-137) were incorporated into photopolymerizable monomers to improve the refractive index modulation, obtaining volume holographic gratings with refractive index modulation up to 2.4×10^{-2}. It has been demonstrated that the formation of volume grating in these nanocomposites is caused by the spatial rearrangement of nanoparticles and monomers in the period of holographic exposure. Nanoparticles are mostly located in the fringes relating to the interference pattern's dark regions in nanoparticle-polymer composites.

Generally, the inorganic nanoparticles incorporated into nanoparticle-polymer derived volume holographic recording materials should satisfy the following requirements: a much higher refractive index than that of typical polymers, colorlessness (absence of absorption in visible and near IR regions), small particle size and narrow size distribution. Additionally, the aggregation of the inorganic nanoparticles in hybrid

composites will cause an obvious reduction in the scattering loss which is vital for holographic data storage applications.

1.4.1.5 High Refractive Index Hard Coatings for Plastic Lenses

The optical plastics used as ophthalmic lenses have many advantages, such as low weight, excellent impact resistance, good processability and dyeability compared to glasses, but the uncoated plastics may cause a faster decrease of the optical quality resulting from the low surface hardness and poor abrasion resistance. For example, resins like polythiourethane (PTU, n=1.61) and polycarbonate (PC, n=1.59) having a higher refractive index but show a lower abrasion resistance. Therefore, coatings in high demand are the ones with a high abrasion resistance and a good adhesion to the substrate. In addition, to avoid the generation of an interference fringe between the lens surface and the coating layer, the refractive index of lens and coatings must be matched. Most of the work studied before was focused on crosslinking the vinyl and thiol groups to synthesize organo (alkoxy) silane coatings. The coatings can be modified through co-condensation reaction with transition metal alkoxides such as zirconium alkoxides by a sol-gel route to increase the refractive index of the resulting coatings. However, by addition of around 12 mol% of zirconium alkoxides, the refractive index of the resultant coating was only increased to 1.53. Therefore, hard coatings with higher refractive index are desirable to make high refractive index lenses. (138)

Hwang et al. used a sol-gel route incorporating commercially available colloidal TiO_2 particles into an ORMOSIL system to prepare scratch-resistant, UV protective and transparent organic-inorganic nanocomposites coatings. (139) The TiO_2 particles were modified with 3-glycidoxypropyltrimethoxysilane (GPTMS), and ORMOSIL system was obtained from methoxytrimethylsilane (MTMS), dimethydimethoxysilane (DMDMS) and acetic acid. An excellent abrasion resistance and a maximum hardness were obtained in the resultant nanocomposite coatings with a refractive index of 1.6.

1.4.2 Application of nanocomopsites with high dielectric constant

An electrical insulator being polarized when it is put in an electric field is called dielectric. If a dielectric is charged by an electric field, the electric charges do not go through the material like in conducting materials, but move lightly from original positions which cause the dielectric to be polarized. Materials with a high polarizability are usually described as “Dielectric”, and it is expressed by a number called the dielectric constant.

When designing capacitors or materials possibly used to introduce capacitance into a circuit, the dielectric constant is an essential factor. If a material with a high dielectric constant is placed in an electric field, the magnitude of that field will have an obvious decrease in the volume of the dielectric. When designing a particular capacitor, this information is usually used to increase the capacitance.

For use as capacitors, materials need to have low capacitance tolerance, but high dielectric constant, easy to be processed as well as low cost. However, single materials can hardly own these properties at the same time, such as thin film capacitors fabricated by vacuum deposition. They contain the benefits of relatively high capacitance, whereas with drawbacks of requiring high temperature to be processed and high cost. Organic-inorganic composites which are made of polymers and ceramics are among the most favorable materials applied as capacitors. (140-142) They have good the processability of polymers and the high dielectric constant of ceramics, which cause a process with lower temperature and lower cost.

Because of excellent dielectric and mechanical properties, composites made by polymer and ceramic with high dielectric constant have been widely used. By increasing the amount of ceramic material, the dielectric constant of composites is increased. Polymer-ceramic composite materials have properties, such as low process temperature, flexibility, lightness and small size which make them applicable to various products.

Organic-inorganic composites with a high dielectric constant can be applied in a variety of fields (143-156): (1) Capacitors having high power and high energy used in defibrillators, hybrid cars, pulsed plasma thrusters and electric ships. High dielectric constant, high breakdown voltage and low dielectric loss are desired in these applications to provide a high and quick burst of power. High dielectric constant materials are cost effective and simplified volume manufacturing with improved performance. (2) Transistors applied in printed circuit boards, electronic switches and converters, in which

the device dimensions are preferred to be scaled down without sacrificing the performance. Materials with a high dielectric constant can be applied to provide enhanced capacitance, lower leakage current and a longer lifetime. (3) Memory storage. (4) Photonic band gap materials applied in optical quantum computing, optical switches, microlasers and as biological probes for detecting tumors.

Composites with high dielectric constant can be used as lossy materials that dissipate electromagnetic or acoustic energy passing through them. From the results of Eric Chikando's work, lossy materials with high dielectric constant provided a significant reduction in emissions across a wide frequency range to greatly improve a system's chance to meet regulatory compliance limits. They can be widely used in communication facilities, such as resonators, compacted antennas and filters.

Organic-inorganic nanocomposites with high dielectric constants can also be applied as electrorheological fluids. Electrorheological fluids are made of liquid and suspended particles whose dielectric constants are mismatched. Therefore, when applying an AC or DC electric field on electrorheological fluids, dipolar particle interactions will be created. And the rheological properties can be changed immediately as fluids transit between the liquid and the solid-like phases in a few milliseconds. Rheological fluids can be used as a power amplifier, since they can control considerably more mechanical power than the electrical power applied to control the effect. Rheological fluids also have a broad range of industrial applications, including hydraulic valves, clutches, brakes and shock absorbers. Although currently, the utilization of electrorheological technology in medical device development is low, those favorable properties including less

agglomeration, low power consumption, better dispersability and faster response are being considered for use in device development applications.

1.5 Polydimethylsiloxane Based Nanocomposites

Because of the existence of Si-O-Si bonds in the polymeric backbone, polydimethylsiloxane (PDMS), one of the most important members of the polysiloxane class, is thermal stable, water repellent, extensively resistant to oxygen, ozone and UV-light, non-stick and low reactive. For a disadvantage, PDMS has poor mechanical properties, which needs the addition of reinforcing additives to improve the mechanical properties to satisfy the final required application.

Normally, PDMS is reinforced by the addition of silica. The –OH terminal groups on silica surface interact with the oxygen atoms in PDMS backbone. To optimize the interactions between silica and PDMS, it is necessary to modify the surface of silica particles. Since the Si-O group is present in both silica and PDMS, this system is widely studied for in situ generating silica with the presence of polymeric matrix. (157,158)

1.5.1 Chemical Modification of Metal Alkoxides

Because of the relatively low reaction temperature, sol-gel is one of the favorable approaches to hybridize inorganic materials including ceramics and glasses into organic materials which are unstable at high temperature. Metal alkoxides, $M(OR)_n$ as a starting precursor of the sol-gel reaction to prepare ceramics and glasses, are readily hydrolyzed

and condensated to obtain an inorganic network containing M-O-M bonds at low temperature. (159-161)

The reactivity of metal precursors relies on types of metals and alkoxy groups. Si alkoxides because of its lower reactivity, for example TEOS, is easy to control; while most other metal alkoxides with high reactivity are hard to control, especially in the atmosphere. Therefore, to avoid an inorganic network largely growing to precipitate without reacting with PDMS and the corresponding oxide or hydroxide, highly reactive metal precursors are modified by chemical chelating agents such as EAcAc to slow down their hydrolysis rate. (162,163)

1.5.2 PDMS-Silica Nanocomposites

Rajan et al. in situ produced silica particles in the matrix of PDMS. In his experiment, the moisture in the air was used for hydrolysis reaction and tin salts (dibutyltin diacetate or dilaurate) was applied as catalyst, from which method a PDMS nanocomposites with 14 wt% silica was obtained. Electron microscopy was used to characterize the nanocomposites. As shown in the SEM images, silica particles were small and uniformly distributed to form transparent composites.

The effects of molecular weight of polymer chains, amount of particles incorporated and catalyst concentration on the final particle size were widely studied. (164) The smallest silica particle size was obtained for the smallest value of polymer molecular weight, probably because shorter polymer chains have more obvious constraining effects. When polymer molecular weight and incorporated particle concentration are constant, the

higher the catalyst concentration the larger the particles are. Although incorporating particles with low or high concentration hardly affects the size of the particles, it obviously increased sizes at intermediate loading (10-20 wt%), resulting from coalescence of individual particles to form larger ones.

Bokobza et al. (165,166) used a cross-linked vinyl-terminated PDMS to fabricate similar composites based on the same synthetic procedure. It is shown that the in situ formed silica particles were homogeneously distributed in the polymer matrix, but various morphologies were attained corresponding to the introduced tin based catalyst and therefore the way of growth processes. The mechanical properties of the final nanocomposites were significantly improved by the extensive interaction between the hydrophilic surface of silica particles and the PDMS chains.

Bokobza also published a paper comparing PDMS reinforced with various methods. (167) Three types of approaches for incorporating silica particles were compared. They were the "conventional mechanical mixing process, in situ filling process and incorporation of spherical colloidal silicas", among which the in situ filling process was the most favorable approach.

1.5.3 PDMS-Titania and PDMS-Zirconia Nanocomposites

Murugesan and Mark (168,169) used in situ generation method to prepare PDMS-titania and PDMS-zirconia utilizing corresponding metal alkoxides. The composites prepared

were characterized and the results were reported. The UV-VIS analysis showed that PDMS-ZrO_2 nanocomposites had much higher transmittance than PDMS-TiO_2 nanocomposites, since compared to zirconia, titania particles are more likely to form small aggregates which leads to a higher opacity. However, because of phase separation at high temperatures, PDMS/ZrO_2 composites were less stable compared to PDMS/TiO_2 composites as shown by the thermal analysis results.

1.6 References:

1. B K G Theng. Interactions of clay minerals with organic polymers. Some practical applications. Clays and Clay Minerals. 1970; 18: 357.
2. Pedro Henrique Cury Camargo, Kestur Gundappa Satyanarayana*, Fernando Wypych. Nanocomposites: Synthesis, Structure, Properties and New Application Opportunities. Materials Research. 2009; 12(1):1-39.
3. Lange FF. Effect of microstructure on strength of Si_3N_4-SiC composite system. Journal of the American Ceramic Society. 1973; 56(9):445-450.
4. Becher PF. Microstructural design of toughened ceramics. Journal of the American Ceramic Society. 1991; 74(2):255-269.
5. Harmer M, Chan HM, Miller GA. Unique opportunities for microstructural engineering with duplex and laminar ceramic composites. Journal of the American Ceramic Society. 1992; 75(2):1715-1728.
6. Niihara K. New design concept of strctural ceramics-ceramic nanocomposite. Journal of the Ceramic Society of Japan *(*Nippon Seramikkusu Kyokai Gakujutsu Ronbunshi). 1991; 99(6):974-982.
7. Nakahira A, Niihara K. Strctural ceramics-ceramic nanocomposites by sintering method: roles of nano-size particles. Journal of the Ceramic Society of Japan. 1992; 100(4):448-453.
8. Ferroni LP, Pezzotti G, Isshiki T, Kleebe HJ. Determination of amorphous interfacial phases in Al_2O_3/SiC nanocomposites by computer-aided high-resolution electron microscopy. Acta Materialia. 2001; 49(11):2109-2113.
9. She J, Inoue T, Suzuki M, Sodeoka S, Ueno K. Mechanical properties and fracture behavior of fibrous Al_2O_3/SiC ceramics. Journal of European Ceramic Society. 2000; 20(12):1877-1881.
10. Tjong SC, Wang GS. High-cycle fatigue properties of Al-based composites reinforced with in situ TiB_2 and Al_2O_3 particulates. Materials Science and Engineering: A. 2004; 386(1-2):48-53.
11. Fischer H. Polymer nanocomposites: from fundamental research to specific applications. Materials Science and Engineering: C. 2003; 23(6-8):763-772.

12. Jordan J, Jacob KI, Tannenbaum R, Sharaf MA, Jasiuk I. Experimental trends in polymer nanocomposites: a review. Materials Science and Engineering: A. 2005; 393(1-2):1-11.
13. Ray SS, Bousmina M. Biodegradable polymers and their layered silicate nanocomposites: in greening the 21st century materials world. Progress in Matererials Science. 2005; 50(8):962-1079.
14. Akita H, Hattori T. Studies on molecular composite. I. Processing of molecular composites using a precursor polymer for poly (P-Phenylene benzobisthiazole). Journal of Polymer Science: Part B: Polymer Physics. 1999; 37(3):189-197.
15. Akita H, Kobayashi H. Studies on molecular composite. III. Nano composites consisting of poly (P-phenylene benzobisthiazole) and thermoplastic polyamide. Journal of European Ceramic Society. 1999; 37(3):209-218.
16. Akita H, Kobayashi H, Hattori T, Kagawa K. Studies on molecular composite. II. Processing of molecular composites using copolymers consisting of a precursor of poly (P-phenylene benzobisthiazole) and aromatic polyamide. Journal of European Ceramic Society. 1999; 37(3):199-207.
17. Chang JH, An YU. Nanocomposites of polyurethane with various organoclays: thermomechanical properties, morphology, and gas permeability. Journal of European Ceramic Society. 2002; 40(7):670-677.
18. Zavyalov SA, Pivkina AN, Schoonman J. Formation and characterization of metal-polymer nanostructured composites. Solid State Ionics. 2002; 147(3-4):415-419.
19. Kamigaito O. What can be improved by nanometer composites? Journal of Japan Society of Powder Metalurgy. 1991; 38: 315-321.
20. Wang B., Wilkes G. L. New Ti-PTMO and Tr-PTMO Ceramer Hybrid Materials Prepared by the Sol-Gel Method: Synthesis and Characterization. Journal of Polymer Science Part A: Polymer Chemistry. 1991; 29: 905-909.
21. Wang B., Wilkes G. L., Hedrick J. C., Liptak S. C. McGrath J. E. New high refractive index organic/inorganic hybrid materials from sol-gel processing. Macromolecules. 1991; 24: 3449-3450.
22. Wang B., Wilkes G. L., Smith C. D., McGrath J. E. High Refractive Index Hybrid Ceramer Materials Prepared from Titanium Tetraisopropoxide and Poly(arylene

ether phosphine oxide) Through Sol-Gel Processing. Polymer Communications. 199; 32: 400-402.

23. Chen W. C., Lee S. J., Lee L. H., Lin J. L. Synthesis and Characterization of Trialkoxysilane-Capped Poly(methyl methacrylate)-Titania Hybrid Optical Thin Films. Jouranl of Materials Chemistry 1999; 9(12): 2999-3003.
24. Lee L. H., Chen W. C. High refractive-index thin films prepared from trialkoxysilane-capped poly(methyl methacrylate)-titania materials. Chemistry of Materials. 2001; 13(3): 1137-1142.
25. L. Zimmermann, M. Weibel, W. Caseri, U. W. Suter. High refractive index films of polymer nanocomposites. Journal of Materials Research. 1993; 8: 1742.
26. F. Papadimitrakopoulos, P. Wisniecki, D. E. Bhagwagar. Mechanically attrited silicon for high refractive-index nanocomposites. Chemistry of Materials. 1997; 9(12): 2928.
27. D. L. Thomsen, T. Phely-Bobin, F. Papadimitrakopoulos. Zinc-Bisquinoline Coordination Assemblies of High Refractive Index and Film Uniformity. Journal of the American Chemical Society. 1998; 120: 6177.
28. M. Weibel, W. Caseri, U. W. Suter, H. Kiess, E. Wehrli. Polymer nanocomposites with 'ultrahigh' refractive index. Polymers for Advanced Technologies. 1991; 2: 75.
29. T. Kyprianidou-Leodidou, W. Caseri, U. W. Suter. Size variations of PbS particles in high-refractive-index nanocomposites. Journal of Physical Chemistry. 1994; 98: 8992.
30. B. Wang, G. L. Wilkes, J. C. Hedrick, S. C. Liptak, J. E. Mcgrath. New High Refractive Index Organic/Inorganic Hybrid Materials from Sol-Gel Processing. Macromolecules. 1991; 24: 3449.
31. B. Wang, H. Huang, G. L. Wilkes. Polymeric Materials: Science and Engeering. 1990; 63: 892.
32. B. Wang, G. L. Wilkes, C. D. Smith, J. E. McGrath. High Refractive Index Hybrid Ceramer Materials Prepared from Titanium Tetraisopropoxide and Poly(arylene ether phosphine oxide) Through Sol-Gel Processing. Polymer Communication. 1991; 32: 400.

33. M. Yoshida, P. N. Prasad. Sol-gel-processed SiO2/TiO2/poly(vinylpyrrolidone) composite materials for optical waveguides. Chemistry of Materials. 1996; 8: 235.
34. W. F. Su, H. K. Yuan, Polym. Prepr. (Am. Chem. Soc., Div. Polym. Chem.) 2000; 41: 574.
35. L. H. Lee, W. C. Chen. High refractive-index thin films prepared from trialkoxysilane-capped poly(methylmethacrylate)-titania materials. Chemistry of Materials. 2001; 13: 1137.
36. C. C. Chang, W. C. Chen. High-refractive-index thin films prepared from amino alkoxysilane-capped pyromellitic dianhydride-titania hybrid materials. Journal of Polymer Science Part A: Polymer Chemistry. 2001; 39: 3419.
37. B. M. Novak. Hybrid Nanocomposite Materials—between inorganic glasses and organic polymers. Advanced Materials. 1993; 5(6): 422.
38. P. Judeinstein, C. Sanchez. Hybrid Organic-Inorganic Materials : A Land of Multidisciplinarity. Journal of Materials Chemistry. 1996; 6: 511.
39. C. Sanchez, F. Ribot, B. Lebeau. Molecular design of hybrid organic-inorganic nanocomposites synthesized via sol-gel chemistry. Journal of Materials Chemistry. 1999; 9: 35.
40. C. K. Chan, S. L. Peng, I. M. Chu, S. C. Ni. Effects of heat treatment on the properties of poly(methyl methacrylate)/silica hybrid materials prepared by sol-gel process. Polymer. 2001; 42: 4189.
41. Q. Hu, E. Marand. In situ formation of nanosized TiO2 domains within poly(amide–imide) by a sol–gel process. Polymer. 1999; 40(17): 4833.
42. C. Sanchez, B. Alonso, F. Chapusot, F. Ribot, P. Audebert. Molecular design of hybrid organic-inorganic materials with electronic properties. Journal of Sol-Gel Science and Technology. 1994; 2(1-3): 161.
43. M. Yoshida, P. N. Prasad. Sol-gel-processed SiO2/TiO2/poly(vinylpyrrolidone) composite materials for optical waveguides. Chemistry of Materials. 1996; 8: 235.
44. Z. Ahmad, J. E. Mark. Polyimide-ceramic hybrid composites by the sol-gel route. Chemistry of Materials. 2001; 13: 3320.
45. Y. Wei, J. M. Yeh, D. Jin, X. Jia, J. Wang. Composites of electronically conductive polyaniline with polycrylate-silica hybrid sol-gel materials. Chemistry of Materials.

1995; 7(5): 969.

46. Y. Wei, D. Jin, D. J. Brennan, D. N. Rivera, Q. Zhuang, N. J. DiNardo, K. Qiu, Atomic Force Microscopy Study of Organic-Inorganic Hybrid Materials. Chem. Mater. 1998; 10(3): 769.
47. W. E. van Zyl, M. Garcìa, B. A. G. Schrauwen, B. J. Kooi, J. T. M. de Hosson, H. Verweij. Hybrid polyamide/silica nanocomposites: Synthesis and mechanical testing. Macromolecular Materials and Engineering. 2002; 287(2): 106.
48. J. Jang, H. Park. In situ sol-gel process of polystyrene/silica hybrid materials: Effect of silane-coupling agents. Journal of Applied Polymer Science. 2002; 85(10): 2074.
49. M.I. Sarwar, Z. Ahmad. Interphase bonding in organic–inorganic hybrid materials using aminophenyltrimethoxysilane. European Polymer Jouranl. 2000; 36: 89-94.
50. R.A. Zoppi, C.R. de Castro, I.V.P. Yoshida, S.P. Nunes. Hybrids of SiO2 and poly(amide 6-b-ethylene oxide). Polymer. 1997; 38: 5705.
51. W. C. Chen, S. J. Lee, L. H. Lee, J. L. Lin. Synthesis and characterization of trialkoxysilane-capped poly(methyl methacrylate)-titania hybrid optical thin films. Journal of Materials Chemistry. 1999; 9: 2999.
52. B. M. Novak. Hybrid nanocomposite materials-between inorganic glasses and organic polymers. Advanced Materials. 1993; 5: 422.
53. H. R. Allcock. Inorganic—Organic Polymers. Advanced Materials. 1994; 6: 106.
54. P. Judeinstein, C. Sanchez. Hybrid Organic-Inorganic Materials: A Land of Multidisciplinarity. Journal of Materials Chemistry. 1996; 6: 511.
55. D. Pomogailo. Hybrid polymer-inorganic nanocomposites. Russian Chemical Reviews. 2000; 69(1): 53.
56. G. Kickelbick. Concepts for the incorporation of inorganic building blocks into organic polymers on a nanaoscale. Progress in Polymer Science. 2003; 28: 83.
57. F. Mammeri, E. Le Bourhis, L. Rozes, C. Sanchez. Mechanical properties of hybrid organic-inorganic materials. Journal of Materials Chemistry. 2005; 15: 3787.
58. C. Sanchez, G. J. de, A. A. Soler-Illia, F. Ribot, T. Lalot, C. R. Mayer, V. Cabuil. Designed hybrid organic-inorganic nanocomposites from functional nanobuilding blocks. Chemistry of Materials. 2001; 13: 3061.
59. C. Sanchez, F. Ribot, B. Lebeau. Molecular design of hybrid organic-inorganic

nanocomposites synthesized via sol-gel chemistry. Journal of Materials Chemistry. 1999; 9(1): 35.

60. G. Schottner. Hybrid Sol-Gel-Derived Polymers: Applications of Multifunctional Materials. Chemistry of Materials. 2001; 13: 3422.
61. P. Innocenzi, B. Lebeau. Organic-inorganic hybrid materials for non-linear optics. Journal of Materials Chemistry. 2005; 15: 3821.
62. C. Sanchez, B. Lebeau, F. Chaput, J.-P. Boilot. Optical Properties of Functional Hybrid Organic-Inorganic Nanocomposites. Advanced Materials. 2003; 15(23): 1969.
63. L. Nicole, C. Boissi_ere, D. Grosso, A. Quach, C. Sanchez. Mesostructured hybrid organic-inorganicthin films. Journal of Materials Chemistry. 2005; 15: 3598.
64. C. Sanchez, B. Juli_an, P. Belleville, M. Popall. Applications of hybrid organic-inorganic nanocomposites. Journal of Materials Chemistry. 2005; 15: 3559.
65. A.-L. P_enard, T. Gacoin, J.-P. Boilot. Functionalized sol-gel coatings for optical applications. Accounts of Chemical Research. 2007; 40(9): 895.
66. W. Que, Z. Sun, Y. Zhou, Y. L. Lam, Y. C. Chan, C. H. Kam. Optical and mechanical properties of TiO2/SiO2/organically modified silane composite films prepared by sol–gel processing. Thin Solid Films, 2000; 359(2): 177.
67. B. Yang, Y. Liu, C. Lu, Chin. Pat. ZL2005 1 0016828.7, 2005.
68. M. Yoshida, P. N. Prasad. Sol-gel-processed SiO2/TiO2/poly(vinylpyrrolidone) composite materials for optical waveguides. Chemistry of Materials. 1996; 8: 235.
69. B. Wang, H. Huang and G. L. Wilkes. Polymeric Materials: Science and Engeering. 1990; 63: 892.
70. B. Wang, G. L. Wilkes, J. C. Hedrick, S. C. Liptak, J. E. McGrath. New high refractive index organic/inorganic hybrid materials from sol-gel processing. Macromolecules. 1991; 24: 3449.
71. B. Wang, G. L. Wilkes, C. D. Smith, J. E. McGrath. High Refractive Index Hybrid Ceramer Materials Prepared from Titanium Tetraisopropoxide and Poly(arylene ether phosphine oxide) Through Sol‐Gel Processing. Polymer Communications. 1991; 32(13): 400.

72. L. H. Lee, W. C. Chen. High-Refractive-Index Thin Films Prepared from Trialkoxysilane-Capped Poly(methyl methacrylate)- Titania Materials. Chemistry of Materials. 2001; 13: 1137.
73. C. C. Chang, W. C. Chen. High-refractive-index thin films prepared from amino alkoxysilane-capped pyromellitic dianhydride-titania hybrid materials. Journal of Polymer Science Part A: Polymer Chemistry. 2001; 39(19): 3419.
74. H. W. Su, W. C. Chen. High Refractive Index Polyimide-Nanocrystalline Titania Hybrid Optical Materials. Journal of Materials Chemistry. 2008; 18: 1139.
75. W. C. Chen, W. C. Liu, P. T. Wu, P. F. Chen. Synthesis and characterization of oligomeric phenylsilsesquioxane-titania hybrid optical thin films. Materials Chemistry and Physics. 2004; 83(1): 71.
76. C. Lu, B. Yang. High refractive index organic-inorganic nanocomposites: design, synthesis and application. Journal of Materials Chemistry. 2009; 19: 2884-2901.
77. M. Moffitt, A. Eisenberg. Size Control of Nanoparticles in Semiconductor-Polymer Composites. 1. Control via Multiplet Aggregation Numbers in Styrene-Based Random Ionomers. Chemistry of Materials. 1995; 7(6): 1178.
78. M. Moffitt, L. McMahon, V. Pessel, A. Eisenberg. Size Control of Nanoparticles in Semiconductor-Polymer Composites. 2. Control via Sizes of Spherical Ionic Microdomains in Styrene-Based Diblock Ionomers. Chemistry of Materials. 1995; 7(6): 1185.
79. R. S. Kane, R. E. Cohen and R. Silbey. Synthesis of PbS Nanoclusters within Block Copolymer Nanoreactors. Chemistry of Materials. 1996; 8(8): 1919.
80. R. S. Kane, R. E. Cohen, R. Silbey. Synthesis of doped ZnS nanoclusters within block copolymer nanoreactors. Chemistry of Materials. 1999; 11: 90.
81. J. Huang, Y. Yang, B. Yang, S. Liu, J. Shen. Synthesis of the CdS nanoparticles in polymer networks. Polymer Bulletin. 1996; 36(3): 337.
82. G. Carrot, S. M. Scholz, C. J. G. Plummer, J. G. Hilborn. Synthesis and Characterization of Nanoscopic Entities Based on Poly(caprolactone)-Grafted Cadmium Sulfide Nanoparticles. Chemistry of Materials. 1999; 11(12): 3571
83. T. Kypriandou-Leodidou, H. J. Althaus, Y. Wyser, D. Vetter, M. Buchler, W. Caseri, U. W. Suter. High refractive index materials of iron sulfides and

poly(ethylene oxide). Journal of Materials Research. 1997; 12: 2198.

84. L. Zimmermann, M. Weibel, W. Caseri, U. W. Suter. High refractive index films of polymer nanocomposites. Journal of Materials Research. 1993; 8: 1742.
85. T. Kypriandou-Leodidou, W. Caseri, U. W. Suter. Size variation of PbS particles in high-refractive-index nanocomposites. Journal of Physical Chemistry. 1994; 98(36): 8992.
86. M. Gao, Y. Yang, B. Yang, F. Bian, J. Shen. Synthesis of PbS Nanoparticles in Polymer Matrices. Journal of the Chemical Society, Chemical Communications. 1994, 2779.
87. M. Gao, Y. Yang, B. Yang, J. Shen. Effect of the surface chemical modification on the optical properties of polymer-stabilized PbS nanoparticles. Journal of the Chemical Society, Faraday Transactions. 1995; 91: 4121.
88. Y. Yang, J. Huang, S. Liu, J. Shen. Preparation, characterization and electroluminescence of ZnS nanocrystals in a polymer matrix. Journal of Materials Chemistry. 1997; 7(1): 131.
89. J. Wang, W. Chen, A. Liu, G. Lu, G. Zhang, J. Zhang, B. Yang. Controlled Fabrication of Cross-Linked Nanoparticles/Polymer Composite Thin Films through the Combined Use of Surface-Initiated Atom Transfer Radical Polymerization and Gas/Solid Reaction. Journal of the American Chemical Society. 2002; 124(45): 13358-13359.
90. C. Lu, C. Guan, Y. Liu, Y. Cheng, B. Yang. PbS/polymer nanocomposites optical materials with high refractive index. Chemistry of Materials. 2005; 17: 2448-2454.
91. S. Lee, H. J. Shin, S. M. Yoon, D. K. Yi, J. Y. Choi, U. Paik. Refractive index engineering of transparent ZrO_2-polydimethylsiloxane nanocomposites. Journal of Materials Chemistry. 2008; 18: 1751-1755.
92. N. Nakayamaa and T. Hayashi. Preparation and characterization of TiO_2 and polymer nanocomposite films with high refractive index. Journal of Applied Polymer Science. 2007; 105(6): 3662-3672.
93. M. Avella, M. E. Errico, E. Martuscelli. Novel PMMA/CaCO3 nanocomposites abrasion resistant prepared by an in situ polymerization process. Nano Letters. 2001; 1(4): 213-217.

94. H. Zhang, Z. Cui, Y. Wang, K. Zhang, X. Ji, C. Lu, B. Yang, M. Gao. From water-soluble CdTe nanocrystals to fluorescent nanocrystal-polymer transparent composites using polymerizable surfactants. Advanced Materials. 2003; 15: 777-780.
95. C. H. Hung, W. T. Whang. Effect of surface stabilization of nanoparticles on luminescent characteristics in ZnO/poly(hydroxyethyl methacrylate) nanohybrid films. Journal of Materials Chemistry. 2005; 15(2): 267-274.
96. S. M. Khaled, R. Sui, P. A. Charpentier, A. S. Rizkalla. Synthesis of TiO_2-PMMA Nanocomposite: Using Methacrylic Acid as a Coupling Agent. Langmuir. 2007; 23: 3988-3995.
97. M. M. Demir, P. Castignolles, U. Akbey, G. Wegner. In-situ bulk polymerization of dilute Particle/MMA dispersions. Macromolecules, 2007; 40(12): 4190-4198.
98. H. Althues, R. Palkovits, A. Rumplecker, P. Simon, W. Sigle, M. Bredol, U. Kynast, S. Kaskel. Synthesis and Characterization of Transparent Luminescent ZnS:Mn/PMMA Nanocomposites. Chemistry of Materials. 2006; 18(4): 1068-1072.
99. M. Inkyo, Y. Tokunaga, T. Tahara, T. Iwaki, F. Iskandar, C. J. Hogan, K. Okuyama. Beads Mill-Assisted Synthesis of Poly Methyl Methacrylate (PMMA)-TiO2 Nanoparticle Composites. Industrial Engineering Chemistry Research. 2008; 47: 2597-2604.
100. M. M. Demir, K. Koynov, U. Akbey, C. Bubeck, I. Park, I. Lieberwirth, G. Wegner. Optical Properties of Composites of PMMA and Surface-Modified Zincite Nanoparticles. Macromolecules. 2007; 40: 1089-1100.
101. Uhlmann D. R., Teowee G. Sol-gel science and technology: Current state and future prospects. Journal of Sol-Gel Science and Technology. 1998; 13: 153-162.
102. Mackenzie J. D., Bescher E. P. Structures, properties and potential applications of ormosils. Journal of Sol-Gel Science and Technology. 1998; 13(1-3): 371-377.
103. H. A. Macleod. Thin Film Optical Filters. 2nd ed. UK: Adam Hilger Ltd, Bristol; 1986.
104. A. Thelen. Design of Optical Interference Coatings. New York: McGraw-Hill; 1989.

105. L. Martinu, D. Poltras. Plasma deposition of optical films and coatings: A review. Journal of Vaccumm Science & Technology A. 2000; 18: 2619-2645.
106. H. G. Shanbhogue, C. L. Nagendra, M. N. Annapurna, S. A. Kumar, G. K. M. Thutupalli. Multilayer antireflection coatings for the visible and near-infrared regions. Applied Optics. 1997; 36: 6339-6351.
107. E. Spiller, I. Haller, R. Feder, J. E. E. Baglin and W. N. Hammer. Graded-index AR surfaces produced by ion implantation on plastic materials. Applied Optics. 1980; 19(17): 3022-3026.
108. B. S. Dunn, J. D. Mackenzie, E. J. A. Pope, H. K. Schmidt, M. Yamane. Sol–Gel Optics. 4th ed. San Diego, CA: SPIE; 1997. 452 p.
109. E. Brinley, S. Seal, R. Folks, E. Braunstein, L. Kramer, S. Seal. High efficiency SiO_2–TiO_2 hybrid sol-gel antireflective coating for infrared applications. Journal of Vacuum Science and Technology A. 2006; 24: 1141.
110. K. C. Krogman, T. Druffel, M. K. Sunkara. Anti-reflective optical coatings incorporating nanoparticles. Nanotechnology. 2005; 16(7): S338-343.
111. C. Vassallo. Optical Waveguide Concepts. New York: Elsevier; 1991.
112. C. Xu, L. Eldada, C. Wu, R. A. Norwood, L. W. Shacklette, J. T. Yardley, Y. Wei. Photoimageable, low shrinkage organic-inorganic hybrid materials for practical multimode channel waveguides. Chemistry of Materials. 1996; 8: 2701-2703.
113. Y. K. Kwon, J. K. Han, J. M. Lee, Y. S. Ko, J. H. Oh, H. S. Lee, E. H. Lee. Organic–inorganic hybrid materials for flexible optical waveguide applications. Journal of Materials Chemistry. 2008; 18(5): 579-585.
114. Y. Enami, G. Meredith, N. Peyghambarian, M. Kawazu and A. K.-Y. Jen. Hybrid Electro-optic Polymer/Selective Buried Sol-gel Waveguides for the Integration of Phase-Modulator at 1.55 mm. Applied Physics Letters. 2003; 82(4): 490.
115. M. Yoshida, M. Lal, N. D. Kumar, P. N. Prasad. TiO_2 nano-particle-dispersed polyimide composite optical waveguide materials through reverse micelles. Journal of Materials Science. 1997; 32: 4047.
116. S. Motakef, T. Suratwala, R. L. Roncone, J. M. Boulton, G. Teowee, G. F. Neilson, D. R. Uhlmann. Processing and optical properties of inorganic-organic hybrids

(polycerams). I. MPEOU-based waveguides. Journal of Non-Crystalline Solids. 1994; 178: 31-36.

117. S. Jeong, J. Moon. Fabrication of inorganic–organic hybrid films for optical waveguide. Journal of Non-Crystalline Solids. 2005; 351: 3530-3535.
118. D. C. Oliveira, A. G. Macedo, N. J. O. Silva, C. Molina, R. A. S. Ferreira, P. S. Andr_e, K. Dahmouche, V. D. Z. Bermudez, Y. Messaddeq, S. J. L. Ribeiro, L. D. Carlos. Photopatternable di-ureasil-zirconium oxocluster organic-inorganic hybrids as cost effective integrated optical substrates. Chemistry of Materials. 2008; 20(11): 3696-3705.
119. R. Buestrich, F. Kahlenberg, M. Popall, P. Dannberg, R. Muller- Fiedler, O. S. Rosch. Ormocers for optical interconnection technology. Journal of Sol–Gel Science and Technology. 2001; 20(2): 181-186.
120. X. Luo, C. Zha, B. L. Davies. Preparation and optical properties of titania-doped hybrid polymer via anhydrous sol–gel process. Journal of Non-Crystalline Solids. 2005; 351(1): 29-34.
121. Y. Shi, C. Zhang, H. Zhang, J. H. Bechtel, L. R. Dalton, B. H. Robinson ,W. H. Steier. Halfwave Voltage Polymeric Electro-optic Modulators Achieved by Controlling Chromophore Shape. Science. 2000; 288: 119-122.
122. J. A. Delaire, K. Nakatani. Linear and Nonlinear Optical Properties of Photochromic Molecules and Materials. Chemical Reviews. 2000; 100: 1817-1846.
123. A. Martucci, P. Innocenzi, J. Fick, J. D. Mackenzie. Zirconia-ormosil films doped with PbS quantum dots. Journal of Non-Crystalline Solids. 1999; 244: 55-62.
124. F. Gan. Optical nonlinearity of hybrid and nano compostie materials prepared by the Sol-Gel method. Journal of Sol–Gel Science and Technology. 1998; 13: 559-563.
125. F. Qin, J. L.Shi, C. Y.Wei, J. L.Gu. Large incorporation amount and enhanced nonlinear optical properties of sulfide nanoparticles within mesoporous thin films. Journal of Materials Chemistry. 2008; 18(6): 634-636.
126. H. Yuwono, J. Xue, J. Wang, H. I. Elim, W. Ji, Y. Li, T. J. White. Transparent nanohybrids of nanocrystalline TiO_2 in PMMA with unique nonlinear optical behavior. Journal of Materials Chemistry. 2003; 13: 1475-1479.

127. H. Yuwono, B. Liu, J. Xue, J. Wang, H. I. Elim, W. Ji, Y. Li, T. J. White. Controlling the crystallinity and nonlinear optical properties of transparent TiO_2 PMMA nanohybrids. Journal of Materials Chemistry. 2004; 14: 2978-2987.
128. C. Sciancalepore, T. Cassano, M. L. Curri, D. Mecerreyes, A. Valentini, A. Agostiano, R. Tommasi, M. Striccoli. TiO_2 nanorods / PMMA co-polymer based nanocomposites: highly homogeneous linear and nonlinear optical material. Nanotechnology. 2008; 19: 205705-205713.
129. M. Haw. Holographic data storage: The light fantastic. Nature. 2003; 422: 556.
130. T. J. Trout, J. J. Schmieg, W. J. Gambogi, A. M. Weber. Optical photopolymers: design and applications. Advanced Materials. 1998; 10: 1219-1224.
131. F. del Monte, O. Martı´nez, J. A. Rodrigo, M. L. Calvo, P. Cheben. A Volume Holographic Sol-Gel Material with Large Enhancement of Dynamic Range by Incorporation of High Refractive Index Species. Advanced Materials. 2006; 18: 2014-2017.
132. R. A. Vaia, C. L. Dennis, L. V. Natarajan, V. P. Tondiglia, D. W. Tomlin, T. J. Bunning. One-step, micrometer-scale organization of nano- and mesoparticles using holographic photopolymerization: A generic technique. Advanced Materials. 2001; 13: 1570-1574.
133. N. Suzuki, Y. Tomita and T. Kojima. Holographic recording in TiO2 nanoparticle-dispersed methacrylate photopolymer films. Applied Physics Letters. 2002; 81: 4121-4123.
134. C. S_anchez, M. J. Escuti, C. van Heesch, C. W. M. Bastiaansen, D. J. Broer, J. Loos, R. Nussbaumer. TiO2 nanoparticle-photopolymer composites for volume holographic recording. Advanced Functional Materials. 2005; 15: 1623-1629.
135. N. Suzuki, Y. Tomita. Highly transparent ZrO2 nanoparticle-dispersed acrylate photopolymers for volume holographic recording. Optics Express. 2006; 14: 12712.
136. O. V. Sakhno, L. M. Goldenberg, J. Stumpe and T. N. Smirnova. Surface Modified ZrO_2 and TiO_2 Nanoparticles Embedded in Organic Photopolymers for Highly Effective and UV-Stable Volume Holograms. Nanotechnology. 2007; 18(10): 105704.

137. G. Garnweitner, L. M. Goldenberg, O. V. Sakhno, M. Antonietti, M. Niederberger, J. Stumpe. Large-Scale Synthesis of Organophilic Zirconia Nanoparticles and Their Application in Organic–Inorganic Nanocomposites for Efficient Volume Holography. Small 2007; 3: 1626.
138. G. Schottner, K. Rose, U. Posset. Scratch and abrasion resistant coatins on plastic lenses-state of the art, current developments and perspectives. Journal of Sol–Gel Science and Technology. 2003; 27: 71-79.
139. D. K. Hwang, J. H. Moon, Y. G. Shul, K. T. Jung, D. H. Kim, D. W. Lee. Scratch resistant and transparent UV-protective coating on polycarbonate. Journal of Sol–Gel Science and Technology. 2003; 26: 783-787.
140. Bhattacharya, S. K., Tummala, R. R. Next generation integral passives: materials, processer, and integration of resistors and capacitors on PWB substrates. Journal of Materials Science: Materials in Electronics. 2000; 11: 253-268.
141. Bhattacharya, S. K., Tummala, R. R. Integral passives for next generation of electronic packaging: application of epoxy/ceramic nanocomposites as integral capacitors. Microelectronics Journal. 2001; 32: 11-19.
142. Rao, Y., Ogitani, S., Kohl, P., Wong, C. P. Novel polymer–ceramic nanocomposite based on high dielectric constant epoxy formula for embedded capacitor application. Journal of Applied Polymer Science. 2002; 83(5): 1084-1090.
143. Robertson, J. High dielectric constant oxides. The European Physical Journal-Applied Physics. 2004; 28: 265–291.
144. Dang, Z. M., Zhou, T., Yao, S. H., Yuan, J. K., Zha, J. W., Song, H. T., Li, J. Y., Chen, Q., Yang, W. T., Bai, J. B. Advanced Calcium Copper Titanate/Polyimide Functional Hybrid Films with High Dielectric Permittivity. Journal of Advanced Materials. 2009; 21(20): 2077–2082.
145. Rao, Y., Ogitani, S., Kohl, P., Wong, C. P. Novel polymer–ceramic nanocomposite based on high dielectric constant epoxy formula for embedded capacitor application. Journal of Applied Polymer Science. 2002; 83(5): 1084–1090.
146. Kim, C., Wang, Z. M., Choi, H. J., Ha, Y. G., Facchetti, A., Marks, T. J. Printable cross-linked polymer blend dielectrics. Design strategies, synthesis, microstructures, and electrical properties, with organic field-effect transistors as

testbeds. Journal of the American Chemical Society. 2008; 130: 6867–6878.

147. Ortiz, R. P., Facchetti, A., Marks, T. High-k Dielectrics for Low-Voltage Organic Field-Effect Transistors. Journal of Chemical Reviews. 2010; 110: 205–239.
148. Dimitrakopoulos, C. D., Purushothaman, S., Kymissis, J., Callegari, A., Shaw, J. M. Low-voltage organic transistors on plastic comprising high-dielectric constant gate insulators. Science. 1999; 283: 822–824.
149. Homes, C. C., Vogt, T., Shapiro, S. M., Wakimoto, S., Ramirez, A. P. Optical response of high-dielectric-constant perovskite-related oxide. Science 2001; 293: 673–676.
150. Carlson, C. M., Rivkin, T. V., Parilla, P. A., Perkins, J. D., Ginley, D. S., Kozyrev, A. B., Oshadchy, V. N., Pavlov, A. S. Large dielectric constant ($\varepsilon/\varepsilon 0>6000$) $Ba_{0.4}Sr_{0.6}TiO_3$ thin films for high-performance microwave phase shifters. Applied Physics Letters. 2000; 76(14): 1920–1922.
151. Scott, J. F. High dielectric constant thin films for dynamic random access memories. Annual Review of Materials Science. 1998; 28: 79–100.
152. Kotecki, D. E. A review of high dielectric materials for DRAM capacitors. Integrated Ferroelectrics. 1997; 16(1/4): 1–19.
153. Pelrine, R., Kornbluh, R., Kofod, G. High-Strain Actuator Materials Based on Dielectric Elastomers. Advanced Materials. 2000; 12: 1223–1225.
154. Jiang, S. L., Yu, Y., Zeng, Y. K. Novel Ag–$BaTiO_3$/PVDF three-component nanocomposites with high energy density and the influence of nano-Ag on the dielectric properties. Current Applied Physics. 2009; 9(5): 956–959.
155. Raval, H. N., Tiwari, S. P., Navan, R. R., Mhaisalkar, S. G., Rao, V. R. Solution-Processed Bootstrapped Organic Inverters Based on P3HT With a High-k Gate Dielectric Material. IEEE Electron Device Letters. 2009; 30(5): 484–486.
156. Khan, M. Z. R., Hasko, D. G., Saifullah, M. S. M., Welland, M. E. Trapped charge dynamics in a sol-gel based TiO_2 high-k gate dielectric silicon metal-oxide-semiconductor field effect transistor. Journal of Physics: Condensed Matter. 2009; 21: 215902.
157. Mark, J.E. Some novel polymeric nanocomposites. Accounts of Chemical Research. 2006; 39: 881–888.

158. Mark, J.E. Ceramic-modified elastomers. Current Opinion in Solid State & Materials Science. 1999; 4: 565–570.
159. Brinker, C., Scherer, G. Sol–Gel Science: the Physics and Chemistry of Sol–Gel Processing. Boston: Academic Press; 1990.
160. De Luca, M.A., Jacobi, M.M., Orlandini, L.F. Synthesis and characterization of elastomeric composites prepared from epoxidised styrene butadiene rubber, 3-aminopropyltriethoxysilane and tetraethoxysilane. Journal of Sol-Gel Science and Technology. 2009; 49: 150–158.
161. De Luca, M.A., Machado, T.E., Notti, R.B., et al. Synthesis and characterization of epoxidized styrene-butadiene rubber/silicon dioxide hybrid materials. Journal of Applied Polymer Science. 2004; 92: 798–803.
162. Kohjiya, S., Kato, A., Ikeda, Y. Visualization of nanostructure of soft matter by 3D-TEM: nanoparticles in a natural rubber matrix. Progress in Polymer Science. 2008; 33: 979–997.
163. Kohjiya, S., Katoh, A., Shimanuki, J., et al. Three-dimensional nano-structure of in situ silica in natural rubber as revealed by 3D-TEM/electron tomography. Polymer. 2005. 46: 4440–4446.
164. Breiner, J.M., Mark, J.E., Beaucage, G. Dependence of silica particle sizes on network chain lengths, silica contents, and catalyst concentrations in in situ-reinforced polysiloxane elastomers. Journal of Polymer Science: Polymer Physics. 1999; 37: 1421–1427.
165. Dewimille, L., Bresson, B., Bokobza, L. Synthesis, structure and morphology of poly(dimethylsiloxane) networks filled with in situ generated silica particles. Polymer. 2005; 46: 4135–4143.
166. Bokobza, L. New developments in rubber reinforcement. Kgk-Kaut Gummi Kunst. 2009; 62: 23–27.
167. Bokobza, L. Elastomeric composites. I. Silicone composites. Journal of Applied Polymer Science. 2004; 93: 2095–2104.
168. Murugesan, S., Mark, J.E., Beaucage, G. Structure-property relationships for poly(dimethylsiloxane) networks in situ filled using titanium 2-ethylhexoxide and zirconium n-butoxide. ACS Symposium Series. 2003; 838: 163–169.

169. Murugesan, S., Sur, G.S., Mark, J.E., et al. In situ catalyst generation and controlled hydrolysis in the sol–gel precipitation of zirconia and titania particles in poly(dimethylsiloxane). Journal of Inorganic and Organometallic Polymers. 2004; 14: 239–252.

2. Synthesis of PDMS-TiO_2 Hybrid Nanocomposites Using Sol-Gel Route

2.1 Abstract

The fabrication of organic-inorganic hybrid nanocomposites prepared with silanol-terminated polydimethylsiloxane (PDMS) and titanium isopropoxide (TTIP) was investigated. By changing the amount of titanium precursor, homogeneous and transparent PDMS-TiO_2 hybrid films with different compositions were obtained via an *in-situ* sol-gel process. The effect of TiO_2 content on the structures of hybrids was inspected by FT-IR and FT-Raman, and morphologies were explored by FESEM. The thermal properties were measured by a simultaneous DSC/TGA instrument. Ellipsometry and a Resistance, Capacitance, and Inductance (RCL) meter were utilized to measure the refractive index and dielectric constant respectively. As the percentage of titanium added increased, the refractive index increased from 1.4 for plain PDMS to a maximum value of 1.74, and the dielectric constant from 2.8 to as high as 15.5 for sample PDMS-TiO_2 (1-15) prepared by TTIP and PDMS with a molar ratio of 15 to 1. Homogeneous hybrid films were obtained up to a titanium isopropoxide: PDMS ratio as high as 20 to 1. Above this ratio phase separation occurred as evidenced by scanning electron microscope (SEM), and subsequently the refractive index and dielectric constant decreased. A structural model based on the ratios of PDMS to titanium precursor was proposed, which explained the structure of composites and may permit design of these hybrids for specific applications. The films were annealed at different temperatures, and the effect on the properties of the final products was investigated.

2.2 Introduction

Organic-inorganic hybrid materials have attracted great attention recently due to their versatility in tailoring compositions, structures, and properties (1). Hybrid nanocomposites combine the processibility of the organic polymers with the desirable optical and electrical properties of inorganic metal oxides making them very useful for applications in electronic and photonic devices. Numerous methods have been investigated for the preparation of hybrid nanocomposites, including: co-precipitation, hydrothermal synthesis, spray pyrolysis, and sol-gel technology (2). Among these techniques, the sol-gel route has been favored because of its ability to make a wide range of materials with compositional homogeneity at moderate processing temperatures (3).

Inorganic-polymer hybrids have been made with a wide range of polymer chemistries (4-9). However, due to the high elasticity, hydrophobicity, transparency, biocompatibility, and excellent relaxation properties of polydimethylsiloxane (PDMS), it has been extensively employed as the host matrix in nanocomposites (1). By introducing a metal oxide nanophase into the siloxane framework, the resulting hybrids can possess enhanced optical, electronic and mechanical properties. Titanium oxide and its associated metal titanates have been broadly studied, and as a group possess biocompatibility; outstanding physical, optical, and electrical properties; and chemically stable structures (10). Consequently, the oxides of titanium have often been used to prepare organic-inorganic hybrid nanocomposites (4, 11-15).

The preparation of PDMS-TiO_2 composites by the sol-gel method has already been reported in literature, but few studies have been performed without using modifier agents or in the absence of water. The introduction of complex modifiers will affect the kinetics of reaction and they may be difficult to remove from the final structure of the hybrids. For systems containing water, the hydrolysis rate of metal precursors is fast, especially for highly reactive metals like titanium. These may cause phase-separated hybrid materials and introduce inhomogeneities in the final structure. In addition, although some structural studies of PDMS-base hybrids have been reported, no systematic investigation of the effect of composition on hybrid structures has been conducted. In our experiments, PDMS-TiO_2 hybrid nanocomposites were fabricated *in situ* via the reaction of titanium alkoxides with silanol terminated PDMS without chemical modifiers and in the absence of water. The alkoxide served to cross link the polymer, and act as the site for the formation of a metal oxide nanophase. Over a wide range of titanium/PDMS compositions, flexible and transparent hybrid films were obtained.

2.3 Experimental

2.3.1 Materials

Titanium isopropoxide (TTIP) $Ti(OCH(CH_3)_2)_4$ (97%) purchased from Sigma Aldrich was used as the precursor of inorganic titanium components. Silanol terminated poly(dimethylsiloxane) (PDMS) with an average molecular weight of approximate 3500 was provided by the Dow Corning Corporation. Isopropanol (anhydrous, PHARMCO-

AAPER) was used as the solvent. All the chemicals were used without further purification.

2.3.2 Preparation of PDMS-TiO_2 hybrid nanocomposites

The synthesis of PDMS-TiO_2 hybrid nanocomposites was done in the liquid phase at ordinary pressure and moderate temperatures. The schematic of the process is shown below in Figure 2.1.

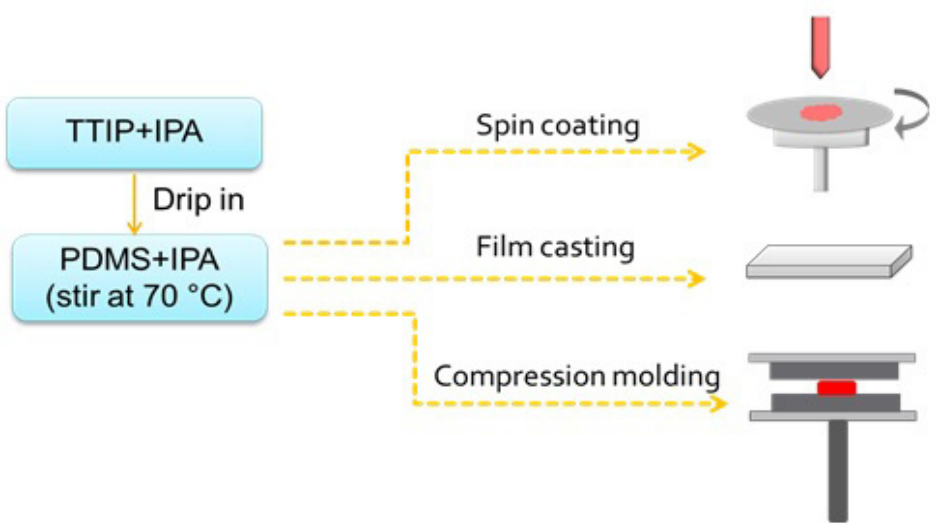

Figure 2.1 Schematic of the process for fabricating PDMS-TiO_2 samples

First, 0.715ml of polydimethylsiloxane (PDMS) and 2ml of isopropanol (IPA) were introduced into a sample vial and sonicated for 3-5 minutes to allow them to mix thoroughly. The desired amount of titanium isopropoxide was diluted with 1ml isopropanol in a separate sample vial and sonicated for a few minutes to obtain a clear, homogenous solution. Finally, the titanium isopropoxide solution was added into the PDMS solution, and then stirred and heated in an oil bath at 70°C. After reacting for 30 minutes, the mixture was removed from the heat, and either spin coated on silicon wafer

or cast into films for testing. The ratio of titanium isopropoxide to PDMS was varied, and four different compositions were chose as representative to examine their effects on the hybrids properties. The compositions of the PDMS-TiO_2 hybrids are summarized in Table 2.1.

Table 2.1

Composition of PDMS-TiO2 nanocomposites.

Sample	Molar ratio of PDMS:TTIP	Molar ratio of Ti:Si (theoretical value)	TiO_2 wt% (theoretical value)
PDMS-TiO_2 (1-5)	1:5	5:47	10%
PDMS- TiO_2 (1-10)	1:10	10:47	19%
PDMS- TiO_2 (1-15)	1:15	15:47	26%
PDMS- TiO_2 (1-20)	1:20	20:47	31%

2.3.3 Hypothesis

Although PDMS-TiO_2 hybrids have been studied by previous researchers, chemical modifier and acid catalysts were employed in their experiments which can be difficult to remove from the final products. In these experiments, PDMS-TiO_2 hybrids were synthesized without using any chemical modifier or acid; and the chemical structures developed by various titanium precursor compositions were investigated.

Silanol terminated PDMS was used as the polymer precursor since the terminal Si-OH groups readily react with titanium isopropoxide to form Si-O-Ti structures. Titanium isopropoxide in effect serves as a cross-linking agent. Since there is no water in the

solution, the initial reactions are between PDMS and titanium isopropoxide which may proceed as shown below:

$$HO-[Si(CH_3)_2O]_n-H+Ti(OC_3H_7)_4 \rightarrow\ HO-[Si(CH_3)_2O]_n-Ti(OC_3H_7)_3+\ C_3H_7OH$$

Equation 2-1

$$HO-[Si(CH_3)_2O]_n-Ti(OC_3H_7)_3+\ Ti(OC_3H_7)_4 \rightarrow$$

$$(OC_3H_7)_3Ti-O-[Si(CH_3)_2O]_n-Ti(OC_3H_7)_3+\ C_3H_7OH$$

Equation 2-2

$$2\ HO-[Si(CH_3)_2O]_n-Ti(OC_3H_7)_3 \rightarrow$$

$$HO-[Si(CH_3)_2O]_n-Ti(OC_3H_7)_2-O-[Si(CH_3)_2O]_n-Ti(OC_3H_7)_3+C_3H_7OH$$

Equation 2-3

When the resulting PDMS-TiO_2 hybrid solutions are spin-coated or cast into films, the moisture in the air can hydrolyze the unreacted Ti-OR bonds to form Ti-OH which in turn may react with each other to generate Ti-O-Ti bonds. Sufficient excess Ti-OR can thus create small regions of titanium oxide compounds. The relevant equations are shown below:

Hydrolysis:

$$Ti(OC_3H_7)_4+\ 4\ H_2O\ \rightarrow Ti(OH)_4+\ 4C_3H_7OH$$

Equation 2-4

$$-[Si(CH_3)_2O]_n-Ti(OC_3H_7)_3+\ 3H_2O\ \rightarrow\ -[Si(CH_3)_2O]_n-Ti(OH)_3+\ 3C_3H_7OH$$

Equation 2-5

$$-[Si(CH_3)_2O]_n-Ti(OC_3H_7)_2-\ O-[Si(CH_3)_2O]_m-\ +2H_2O\ \rightarrow$$

$$-[Si(CH_3)_2O]_n-Ti(OH)_2-\ O-[Si(CH_3)_2O]_m-\ +2C_3H_7OH$$

Equation 2-6

Condensation:

$$M \equiv Ti - OH + HO - Ti \equiv N \rightarrow M \equiv Ti - O - Ti \equiv N + H_2O$$

Equation 2-7

As suggested by the reactions outlined above, when in the solution the titanium isopropoxide acts first as a cross-linker reacting with PDMS, and then in a second curing step hydrolyzes with atmospheric moisture to produce titanium dioxide. It is proposed that the final dried hybrid nanocomposite forms networks with pores of nanometer dimensions, which still contains some isopropanol solvent in the pores of the network. There is titanium dioxide grafted to the PDMS backbone, and also free amorphous nanometric titanium dioxide dispersed in the matrix network. By varying the amount of titanium precursor, the structure of the final hybrid will be changed. Theoretically, if tetrafunctional bonds of titanium fully react with two silanol terminal groups of PDMS, the stoichiometric ratio of titanium isopropoxide to PDMS is 2 to 1. However, this is not necessarily the case. For the PDMS-TiO_2 (1-5) hybrid, since there are less titanium precursors in the solution, the main reactions are equation 2-1 and equation 2-3 which tend to form longer PDMS chains. On the opposite extreme, more titanium precursors are available in the solution of PDMS-TiO_2 (1-20), therefore the main reactions are equation 2-1 and equation 2-2 which are likely to generate shorter PDMS chains. After drying, PDMS-TiO_2 (1-20) with shorter chains can form more highly cross-linked structures than the PDMS-TiO_2 (1-5) with longer chains. The structures of hybrids PDMS-TiO_2 (1-10) and PDMS-TiO_2 (1-15) lie between these two hybrids. The higher the ratio of the titanium precursor, the larger and more numerous the titanium dioxide regions will be.

Schematics of the final structures of PDMS-TiO_2 hybrids with different compositions are shown below:

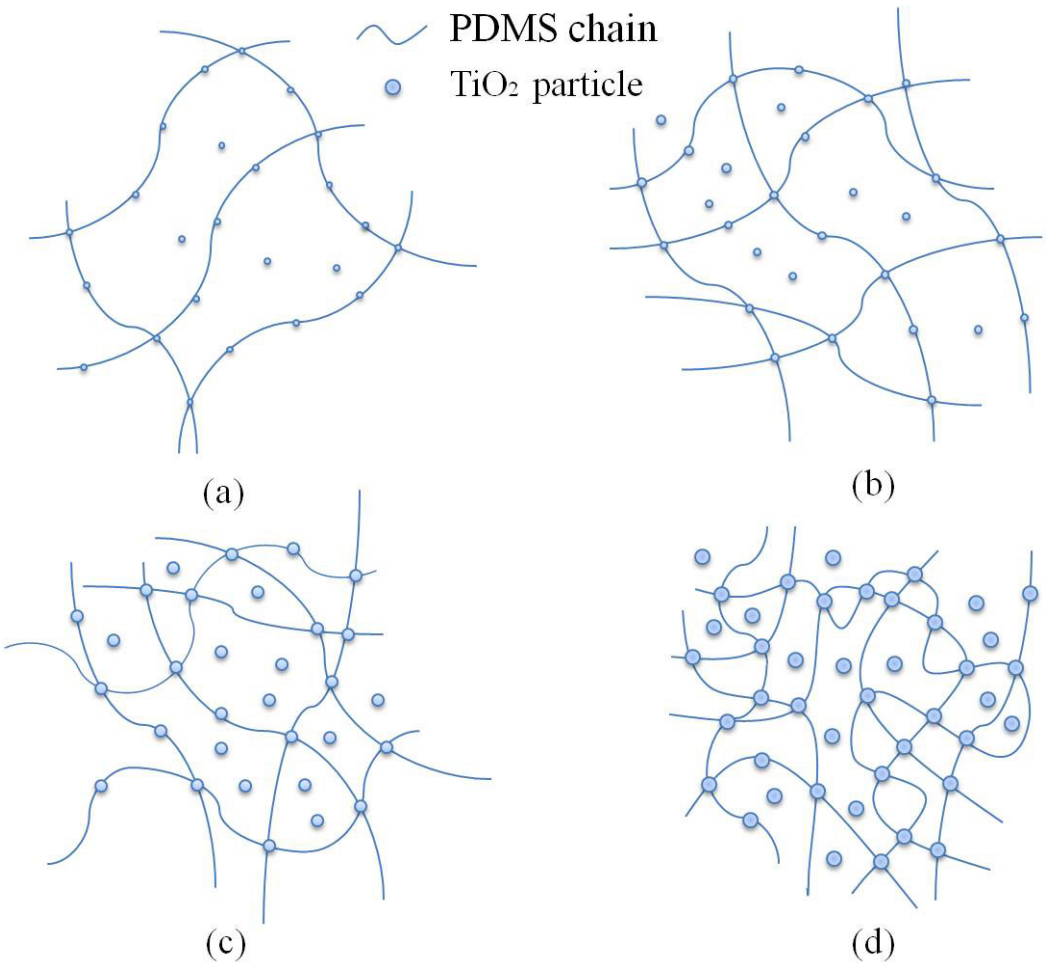

Figure 2.2 Structural models of PDMS-TiO_2 hybrids: (a) PDMS-TiO_2 (1-5), (b) PDMS-TiO_2 (1-10), (c) PDMS-TiO_2 (1-15), (d) PDMS-TiO_2 (1-20).

2.3.4 Characterization

To verify if the structures of the hybrids are as hypothesized in the models depicted above, PDMS-TiO_2 nanocomposites prepared with different compositions were characterized by various instruments to clarify their structure. The nanocomposites were

examined by a conjunction of a PerkinElmer FT-IR Spectrometer and a Bruker RFS 100 FT-Raman to give a better understanding of their bonding structure. The bulk film thickness was measured by a Mitutoyo Absolute Digimatic Calipers. A field emission scanning electron microscope (Model S-4700, Hitachi High Technologies America, Inc.) was also employed to examine the cross sectional areas of the samples. The hybrid precursor solution was first spin-coated on Si wafers with a spinner (Model WS-400BZ-6NPP, Laurell Technologies Co.) to produce films of 1-2 μm thick (measured by a STYLUS PROFILER), and then tested on an ellipsometer (V-VASE, J.A. Woollam Co., Inc.) for refractive indices. To determine the dielectric constants, the hybrid samples were placed in a homemade cell and pressed by a compression molder (WABASH 12-101T) to get solid films around 0.3 mm thick. These films were tested by an automatic capacitance meter (PM 6304, Fluke) to obtain the capacitances which were in turn used to calculate the dielectric constants of the sample films via the equation given below:

$$K = \frac{C * d}{\varepsilon * A}$$

Equation 2-8

Where C is the capacitance in F, d is the distance between the plates (i.e. the thickness of the film in m), ε is the vacuum permittivity ($8.85*10^{-12}$ F/m), and A is the surface area of the plates in m^2. Thermal analysis for the samples was done by a simultaneous DSC/TGA instrument (TA Instruments, SDT Q600). In these experiments, a small amount of sample (around 3mg) was studied in order to obtain clear and accurate thermograms. The sample was heated from room temperature to 1000°C at a rate of 20°C/min. Nitrogen gas was flowing through the sample chamber at a rate of 100 ml/min during the heating process.

As stated in the hypothesis, the prepared hybrid composites possess a network with pores of submicron dimensions, which may still contain some isopropanol. Annealing these hybrids can help release the solvent from the network and the properties of the final products will probably improve as a result. Two different annealing temperatures, 60 °C and 100 °C, were employed on PDMS-TiO_2 hybrids with various compositions to investigate their effects on the optical, electrical and thermal properties of the final products.

2.4 Results and Discussion

2.4.1 Effect of the titanium precursor amount

2.4.1.1 Structural properties

Hybrid nanocomposite films of PDMS-TiO_2 at the increasing Ti:Si ratios as shown in Table 2.1 were studied using FTIR and FT-Raman spectroscopy. The FT-IR spectra of the samples were measured by a PerkinElmer FT-IR Spectrometer in the range of 4000-650 cm^{-1} with a universal ATR sampling accessory. The cast sample films were placed on the ATR crystal area and held in contact with the crystal surface by a pressure arm. For each test, a background scan was run first and subtracted from the resulting sample spectrum. FT-Raman experiments were carried out using a Bruker RFS 100 FT-Raman with a liquid nitrogen cooled Ge detector. The bulk sample films were placed on the sample holder and excited by an Nd: YAG laser. For each sample, 1000 scans were recorded with a $4cm^{-1}$ resolution. Two samples of each composition of the hybrid films,

pure PDMS, and pure sol-gel synthesized TiO_2 were tested to identify the structural bonds in the hybrid network, to verify if there is TiO_2 in the hybrid and to validate the structural model proposed.

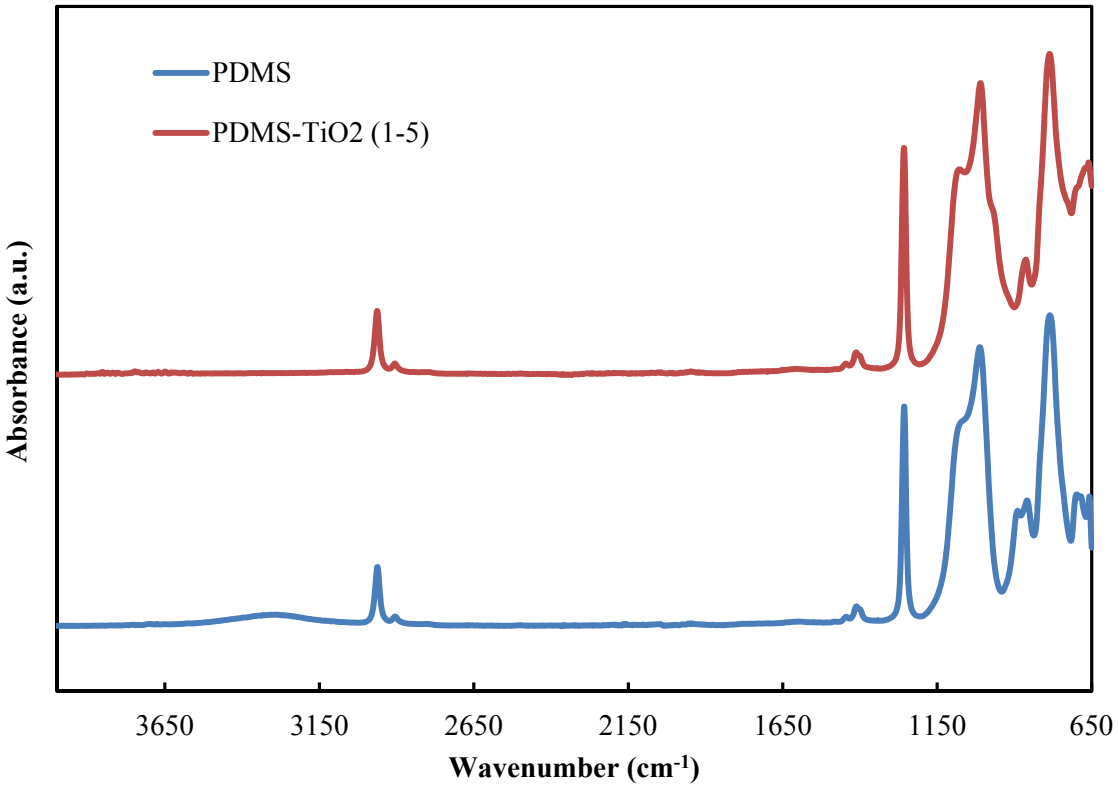

Figure 2.3 FT-IR spectra of PDMS and PDMS-TiO_2 (1-5)

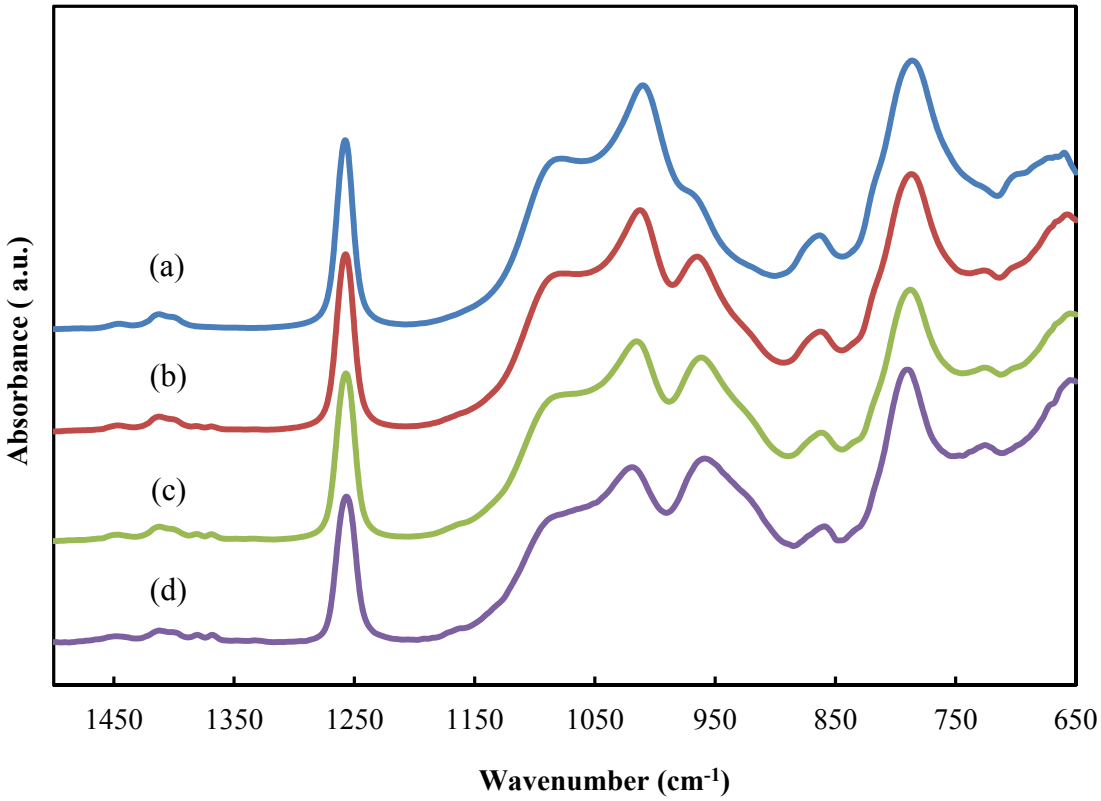

Figure 2.4 FT-IR spectra of PDMS-TiO_2 hybrid films (a) PDMS-TiO_2 (1-5), (b) PDMS-TiO_2 (1-10), (c) PDMS-TiO_2 (1-15), (d) PDMS-TiO_2 (1-20)

Figure 2.3 shows the FT-IR spectra of the pure PDMS and the hybrid composite PDMS-TiO_2 (1-5). The low, broad peak around 3200-3400 cm^{-1} may be assigned to hydroxyl (-OH) terminated groups in pure PDMS (16). This broad peak disappears in PDMS-TiO_2 (1-5) spectrum which indicates that most of the hydroxyl groups have reacted with the titanium isopropoxide. The shoulder around 960 cm^{-1} which appears in the spectrum of PDMS-TiO_2 (1-5) corresponds to Si-O-Ti bonds (17), which confirms the reaction between the titanium precursor and PDMS to form the hybrid composites. The FT-IR spectra of PDMS-TiO_2 hybrid nanocomposites with different compositions in the spectral range between 1500 and 650 cm^{-1} are depicted in Figure 2.4. All spectra show peaks

around 1400 and 1260 cm^{-1} assigned to Si-CH_3 groups of PDMS molecules (18). The bands around 1100 and 1022 cm^{-1} are attributed to asymmetric stretching motions of Si-O-Si (19), and the peak around 800 cm^{-1} corresponds to the symmetric stretching vibrations (16). The absorption peak centered around 960 cm^{-1} is ascribed to the Ti-O-Si band as in previous studies (17). The intensity of this peak increases with the amount of titanium precursor in the system, which means there are more Ti-O-Si bands in the hybrid containing a higher ratio of titanium precurcor. This is consistent with the proposed structural model, since a higher ratio of titanium precursor in the system generates shorter polymer chains, leading to denser structures which contain more tetrafunctional Ti units (Ti with four Si-O-Ti bonds) than difunctional Ti units (Ti with two Si-O-Ti bonds) or trifunctional Ti units (Ti with three Si-O-Ti bonds). Therefore, a higher ratio of titanium precursor in the system creates a more condensed structure with more tetrafunctional Ti units in the matrix. This indicates more Ti-O-Si bonds and leads to a stronger Ti-O-Si peak. On the contrary, for a given sample with a lower ratio of titanium precursor in the system, it possesses a relative loose structure consisting of mostly difunctional Ti units. As a result, this hybrid shows a weaker peak corresponding to Ti-O-Si, such as for the hybrid of PDMS-TiO_2 (1-5). From the results of FT-IR spectra, it can be concluded that in accord with the structural model proposed, titanium isopropoxide acts as a cross-linking agent with the silanol terminal groups of PDMS to link the polymers together. The PDMS-TiO_2 (1-20) hybrid has the most tetrafunctional Ti units and the most condensed structure.

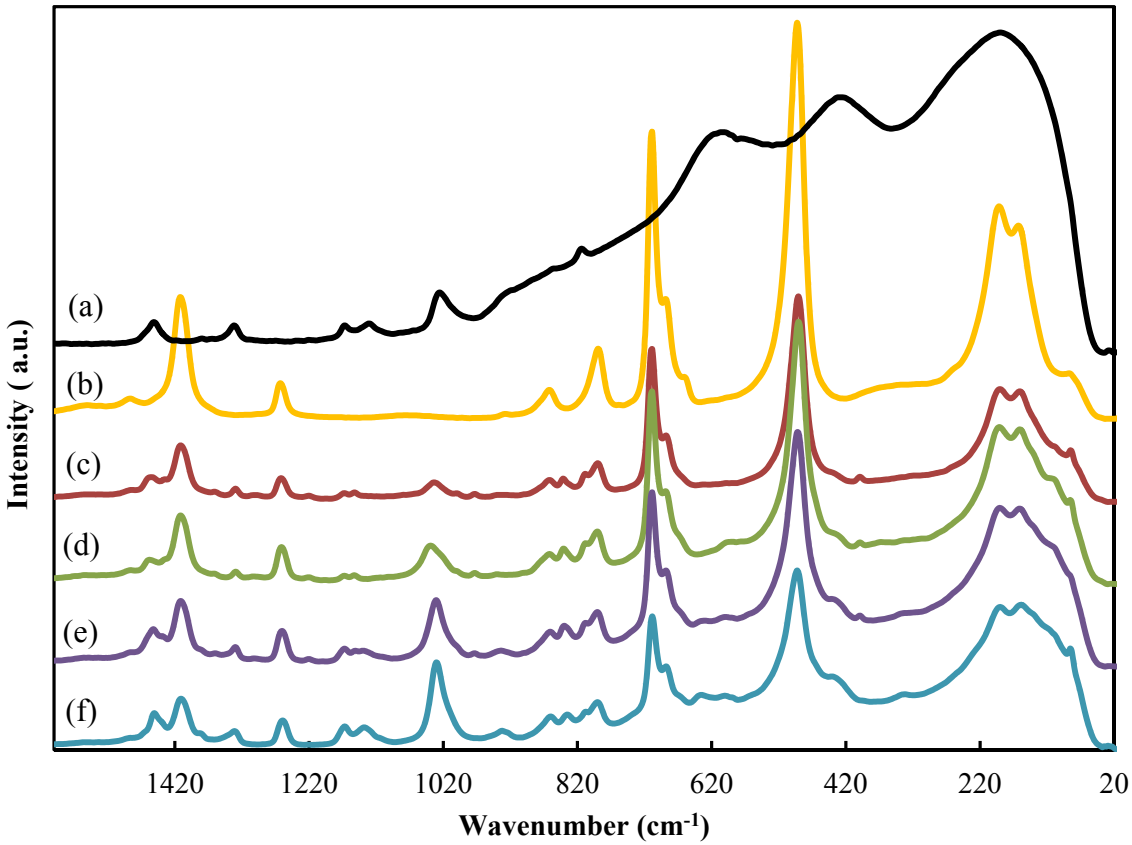

Figure 2.5 FT-Raman spectra of: (a) TiO_2 (sol-gel synthesis, unheated), (b) PDMS, (c) PDMS-TiO_2 (1-5), (d) PDMS-TiO_2 (1-10), (e) PDMS-TiO_2 (1-15), (f) PDMS-TiO_2 (1-20).

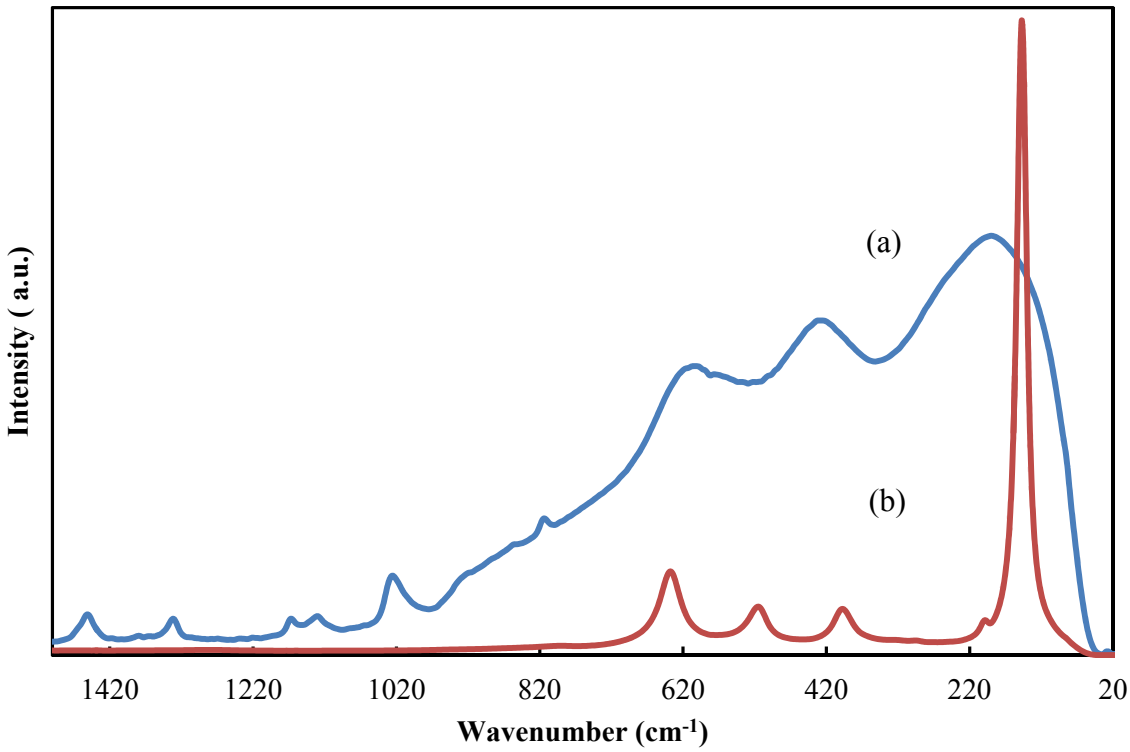

Figure 2.6 FT-Raman spectra of: (a) TiO_2 (sol-gel synthesis, unheated), (b) TiO_2 (sol-gel process, annealed at 400 °C)

Figure 2.5 shows the Raman spectra of pure PDMS, sol-gel synthesized TiO_2 without heating and several PDMS-TiO_2 composites. As shown in Figure 2.5 (b), the spectrum of the PDMS in our experiment is the same as a typical PDMS bulk liquid (20). The Si-O-Si and Si-CH_3 symmetric stretching bands are detected at 488 cm^{-1} and 708 cm^{-1}. The bands centered around 687 cm^{-1}, 787 cm^{-1}, and 862 cm^{-1} are assigned to Si-CH_3 symmetric rocking, Si-CH_3 asymmetric stretching, and CH_3 symmetric rocking respectively. Another two bands of CH_3 symmetric and asymmetric bending are ascribed to the peaks at 1262 cm^{-1} and 1412 cm^{-1} respectively. In the spectra of the PDMS-TiO_2 nanocomposites, along with the bands for PDMS, some additional bands corresponding to sol-gel TiO_2 (Figure 2.5 (a)) are detected. The bands of sol-gel derived TiO_2 located at

1451 cm^{-1}, 1331 cm^{-1}, 1167 cm^{-1}, 1138 cm^{-1} and 1026 cm^{-1} are also detectable in the spectra of the PDMS-TiO_2 composites. Three broad peaks of TiO_2 in the lower range of 660-70 cm^{-1} are not obviously seen in the PDMS-TiO_2 composites spectra, but their peaks in this range are widened compared to the original PDMS. As discussed above, it demonstrates that the PDMS-TiO_2 composites contain free TiO_2 particles with structures similar to those found for the sol-gel TiO_2. The higher the amount of titanium isopropoxide in the system, the more obvious the peaks corresponded to TiO_2 are. Since the intensity of the FT-Raman peak is proportional to the amount of material present, this means that the hybrids with higher ratios of titanium precursors have more free TiO_2 particles in the system. In Figure 2.6, the Raman spectra of the unheated sol-gel synthesized TiO_2 and annealed at 400 °C are shown. The spectrum of the TiO_2 heated to 400 °C is identical to TiO_2 anatase (21), which indicates that the TiO_2 sol-gel as-prepared *in situ* is amorphous and may crystallize to the anatase structure upon heating. From these two figures, it can be concluded that there are free, amorphous TiO_2 particles in the PDMS-TiO_2 composites, and their amount increases with increasing titanium isopropoxide in the system. This agrees with the structural model which predicts that the higher the ratio of the titanium precursor, the larger and more numerous the titanium dioxide regions will be.

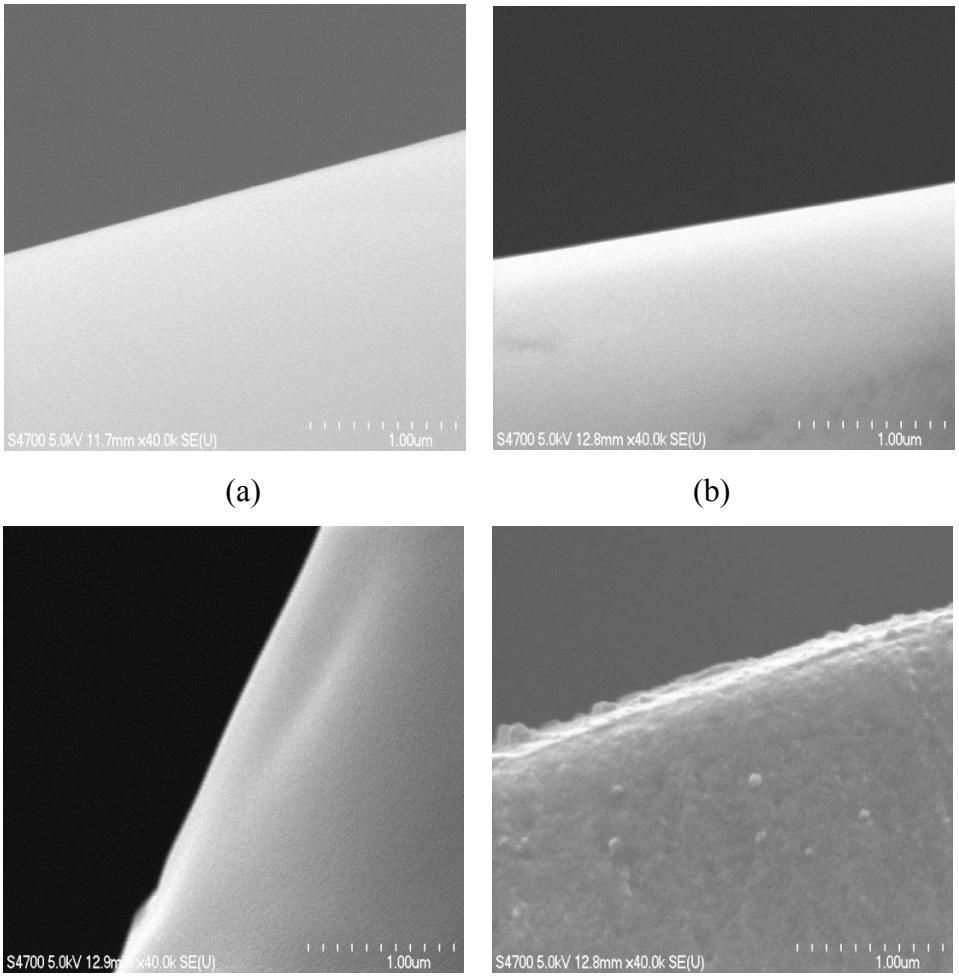

Figure 2.7 SEM images of cross-sectional areas of the PDMS-TiO_2 composite films.
(a) PDMS-TiO_2 (1-5), (b) PDMS-TiO_2 (1-10), (c) PDMS-TiO_2 (1-15), (d) PDMS-TiO_2 (1-20).

The morphology and microstructure of cross-sectional area of the PDMS-TiO_2 hybrid films were examined by SEM. As for lower Ti compositions, shown in Figure 2.7 (a), (b), and (c), the surfaces of the cross-sectional areas are smooth with no particulates evident. Here, the amorphous TiO_2 formed by excess titanium precursor are nanometer sized and uniformly distributed throughout the PDMS matrix. The dense structure shown in these images may be because the pores of network are < 10 nm dimensions as proposed by structural model and are not visible here. As stated in the structural model, the higher the

ratio of titanium precursor in the system, the larger the TiO_2 particles will form. It can be seen from figure 2.7 (d) that with the highest loading of TiO_2, the cross-sectional surface of the hybrid film is rougher, and TiO_2 particles between 50 nm and 100 nm resulting from phase separation are evident.

2.4.1.2 Optical and electronic properties

For application in optical and electric areas, the refractive indices and dielectric constants of the hybrids are important. The refractive index, n, is a number defines how light, or any other radiation propagates through the medium; and defines the amount of refraction a wave will undergo when it enters a medium. It is the most important property of an optical system such as an optical waveguide or lens that uses refraction. An ellipsometer (V-VASE, J.A. Woollam Co., Inc.) because of its high accuracy and a wide spectral range was used to test the refractive indices in our experiments. The theory of ellipsometer is based on measuring the change in polarization as the light reflected from material structure. From the measured response, the optical properties included refractive index and the thickness of the material can be deduced. The dielectric constant is also called static relative permittivity that indicates the extent to which it concentrates electrostatic lines of flux, which is the crucial information for designing capacitors. Materials with a high dielectric constant usually used to design capacitors with increased capacitance. In our experiments, the capacitances were determined by an automatic capacitance meter (PM 6304, Fluke) and using equation 2-8 to calculate the dielectric constants. By analyzing the results, the influence of introducing TiO_2 in the hybrids and its relationship with the refractive indices and dielectric constants were investigated.

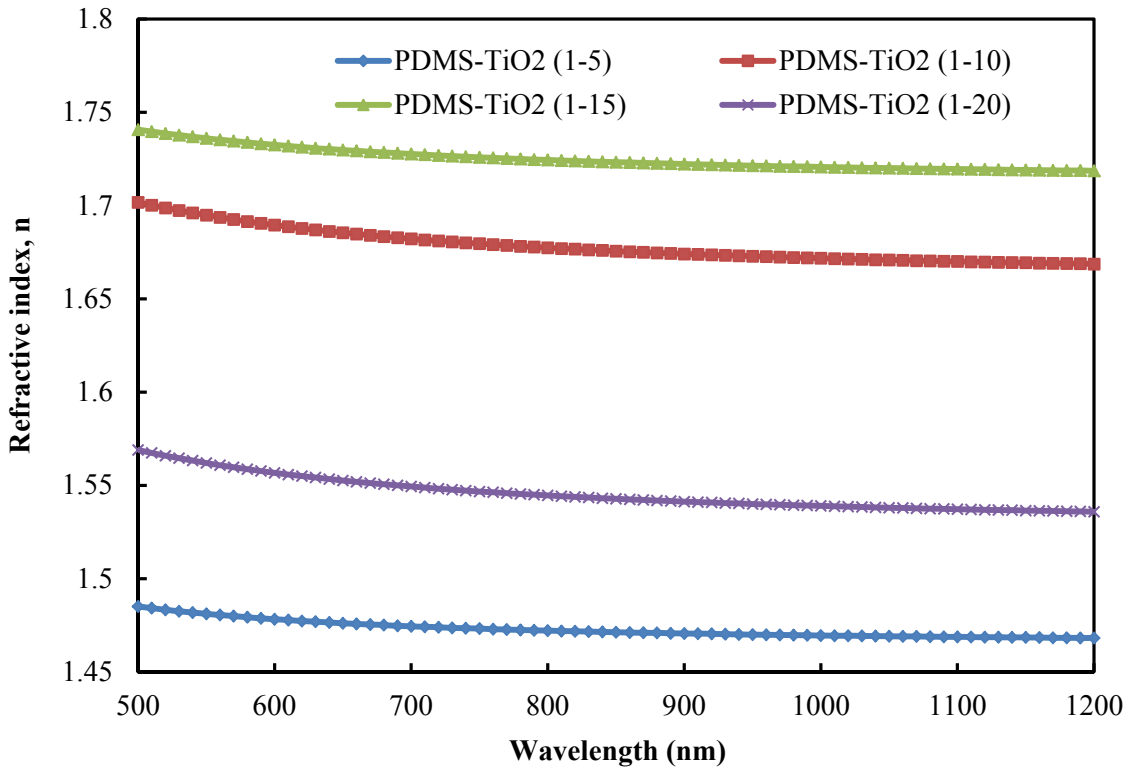

Figure 2.8 Refractive index of PDMS-TiO_2 hybrid composites

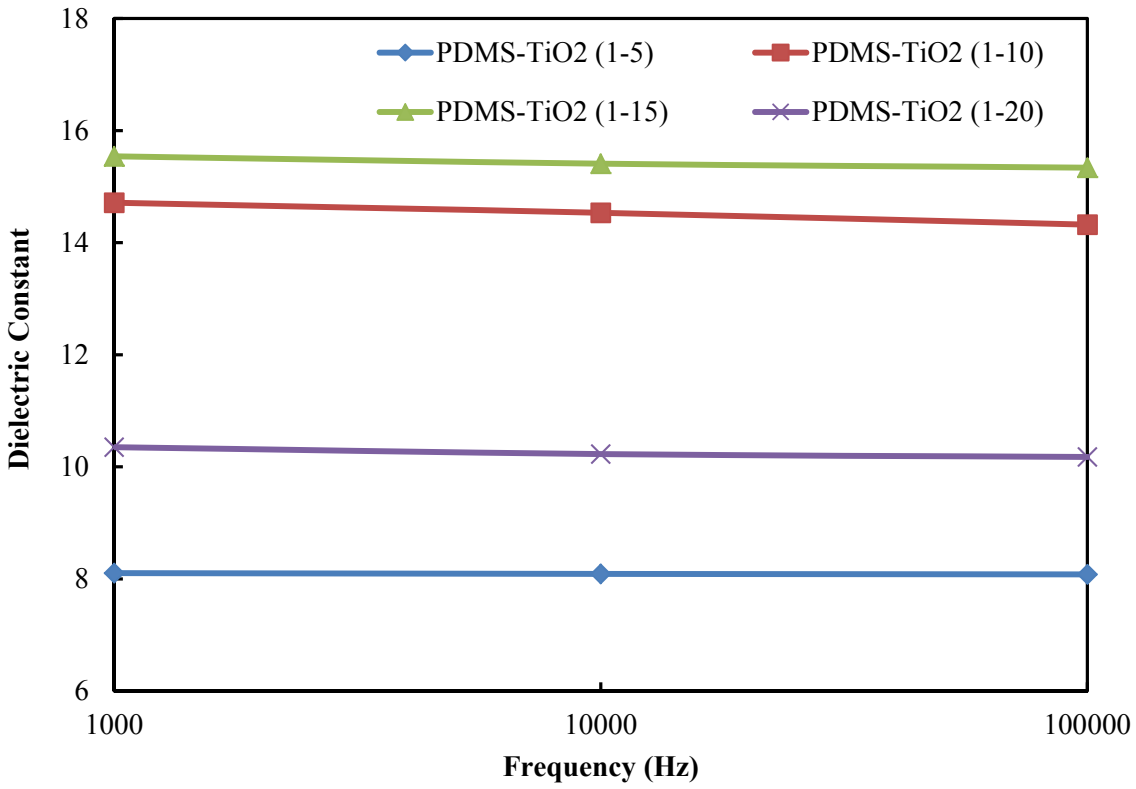

Figure 2.9 Variation of dielectric constant with frequency

Figure 2.8 shows the refractive index as a function of wavelength for various compositions of PDMS-TiO_2 composites. In general, all of the sample show that the larger the wavelength, the smaller the refractive index measured. The refractive index of pure PDMS is around 1.4 (22), and that of pure titanium dioxide is 2.4. As seen in the figure, all the composites show higher refractive indices by introducing more TiO_2 into the system. For PDMS-TiO_2 (1-5), PDMS-TiO_2 (1-10) and PDMS-TiO_2 (1-15), the more TiO_2 present in the hybrids, the higher the refractive indices are. However, when the amount of TiO_2 is very high, as PDMS-TiO_2 (1-20) shown in the figure, phase separation may occur, resulting in large particle formation, and the refractive index decreases. This theory is consistent with the statement of structural models and the results of SEM

images. The same compositional trends were noticed during the measurement of dielectric constants. The RCL meter with a homemade cell used to test capacitance of the composite films was first calibrated at different frequencies using standard materials. After the capacitance measurements were calibrated, they were substituted into equation 2-8 to calculate the dielectric constants and the results are plotted in Figure 2.9. It can be seen that in the measured frequency range of 10^3-10^5 Hz, the dielectric constants of the PDMS-TiO_2 composites decrease slightly with increasing frequency. For the PDMS-TiO_2 composites higher dielectric constant are attained as the amount of TiO_2 in the composites increases. However, it was found that for composites with a very high ratio of TiO_2 (PDMS-TiO_2 (1-20)) in the system, the value of dielectric constant decreased. This may also be due to the larger TiO_2 particles caused by phase separation as predicted by the structural model and shown in the SEM images.

2.4.1.3 Thermal properties

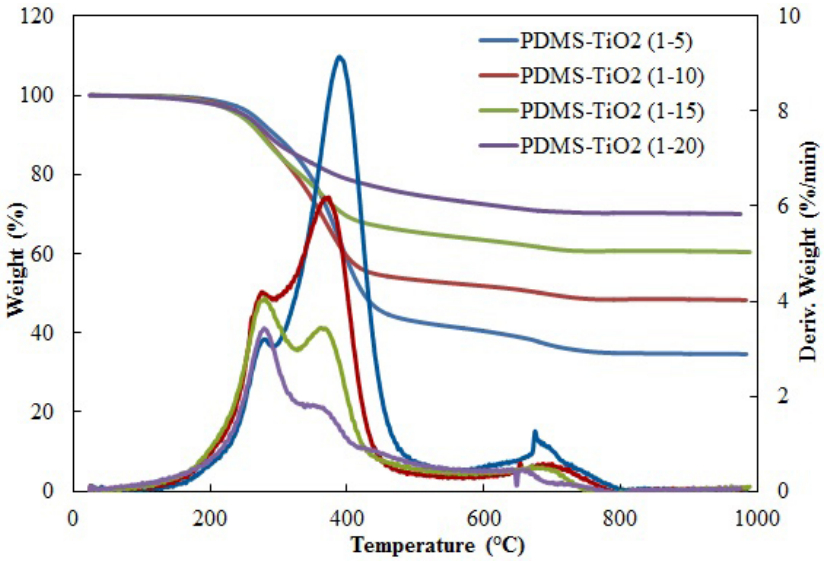

Figure 2.10 TGA curve of PDMS-TiO2 with various compositions

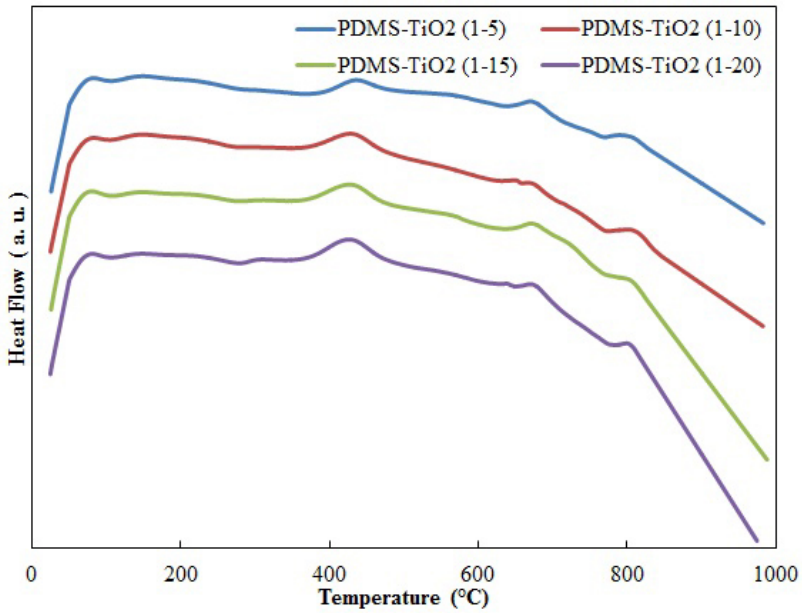

Figure 2.11 DSC curve of PDMS-TiO2 with various compositions

Differential scanning calorimetric (DSC) and thermogravimetric analysis (TGA) of PDMS-TiO_2 with various compositions are shown in the figures above. It can be seen that there is an endothermic DSC peak around 100 °C with no accompanying weight loss which may be attributed to the vaporization of surface moisture. As shown in the derivative weight change curves, the main weight loss from 200 °C to 500 °C is divided into two steps. The first step from 200 °C to 350 °C corresponds to an endothermic peak in DSC and is caused by the release of trapped solvent in the pores of the network matrix. The second step is related to an exothermic peak from 350 °C to 500 °C with a weight loss indicating the decomposition of PDMS composites (23-25). The relative height of these two derivative peaks changes with the composition of the hybrids. Since the trapped solvent are mostly created by the reaction of $Ti(OR)_4$ with –OH groups, PDMS-TiO_2 (1-20) with the largest amount of $Ti(OR)_4$ and the least amount of PDMS has the relatively highest peak for the first step. The PDMS-TiO_2 (1-5) sample has the opposite trend. It can be seen that the PDMS-TiO_2 sample (1-5) decomposes at a higher temperature compared to the other three samples. Since longer chains require higher decomposition temperatures, this demonstrates that the PDMS-TiO_2 (1-5) hybrid has the longest chains as described by structural model. As for the other three samples, there is no significant difference of their decomposition temperatures; this is maybe due to the smaller difference of their chain lengths. On further heating, an exothermic peak appears around 670 °C which can be ascribed to the formation of SiC or the re-crosslinking of polymers (26). From the results of the TGA curves, it is shown that the higher the ratio of TiO_2, the lower the total weight loss. This is because per mass, a composite with a higher ratio of

TiO_2 contains a lower amount of PDMS which is the main factor in weight loss. Finally, the exothermic peak at 800 °C corresponds to the TiO_2 transition to a rutile structure.

2.4.2 Effect of temperature

As proposed in the hypothesis and seen from the SEM images, the network of hybrids structure may consist of pores of nanometer dimensions containing isopropanol solvent, which is hard to remove until heated. One temperature of 60 °C below and the other temperature of 100 °C above the boiling point of isopropanol were chose as the annealing temperatures. After the PDMS-TiO_2 hybrid nanocomposites were made, they were dried in the air, and heated in an oven in air at either 60 °C or 100 °C to characterize the effect of temperature on the refractive index, dielectric constant and thermal properties of the hybrid films. Removal of solvent from hybrids would improve the refractive index, dielectric constant and thermal properties of the final products. Therefore, the cast sample films were annealed at 60 °C and 100 °C to release the solvent and explore the effect on the final properties.

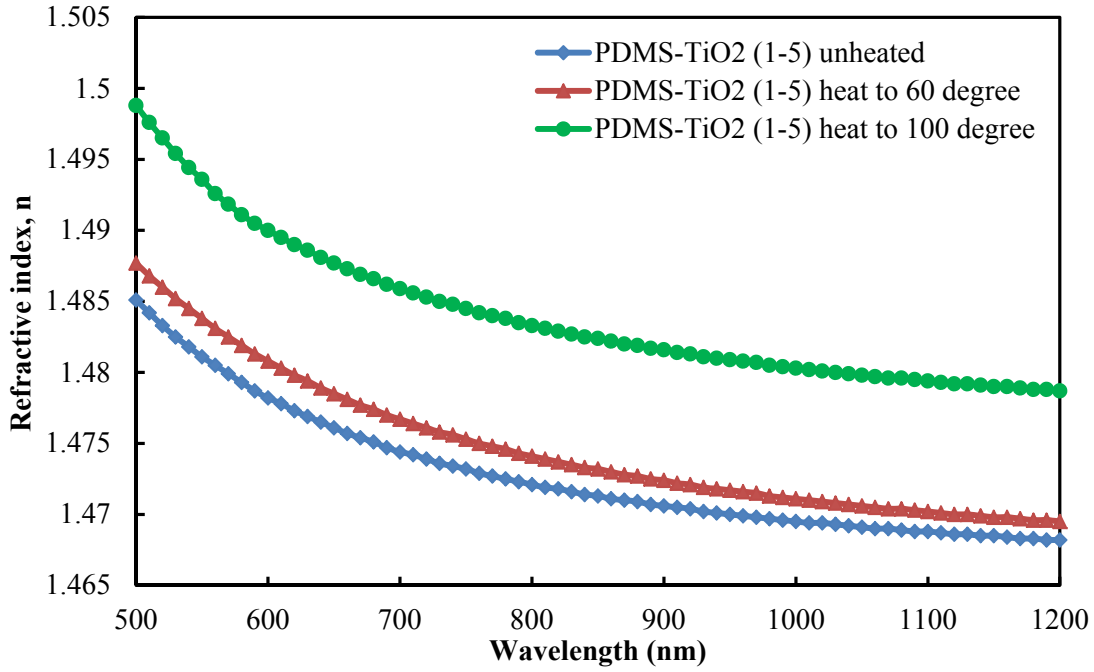

Figure 2.12 Refractive index of PDMS-TiO_2 (1-5) annealed at different temperatures

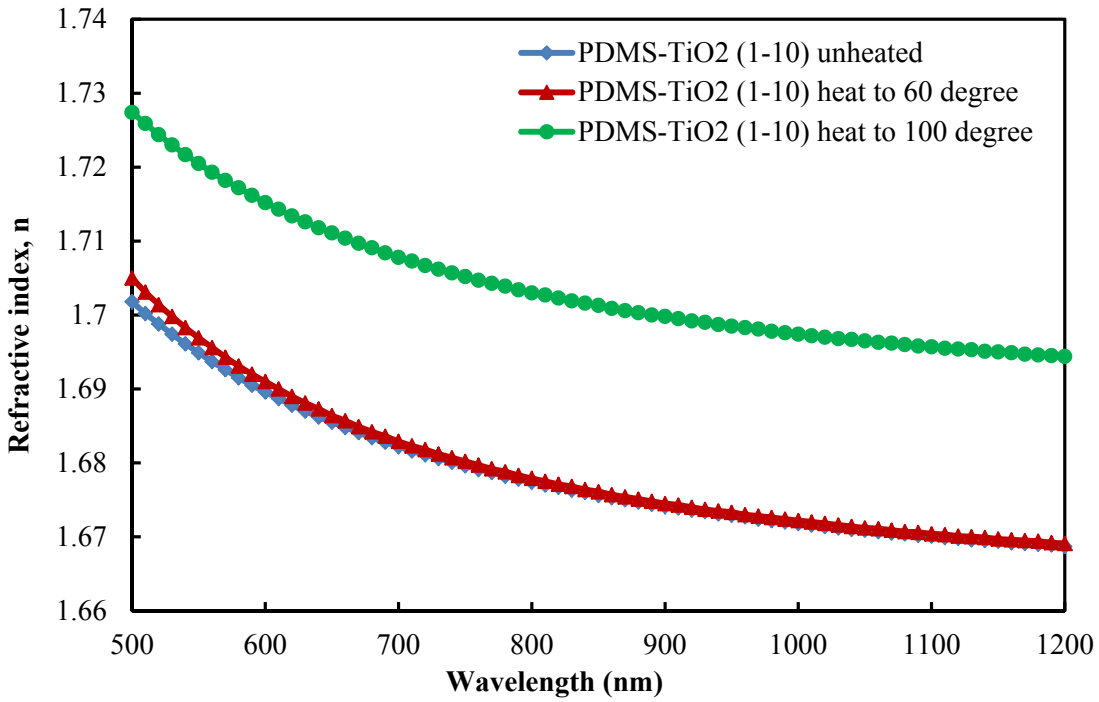

Figure 2.13 Refractive index of PDMS-TiO2 (1-10) annealed at different temperatures

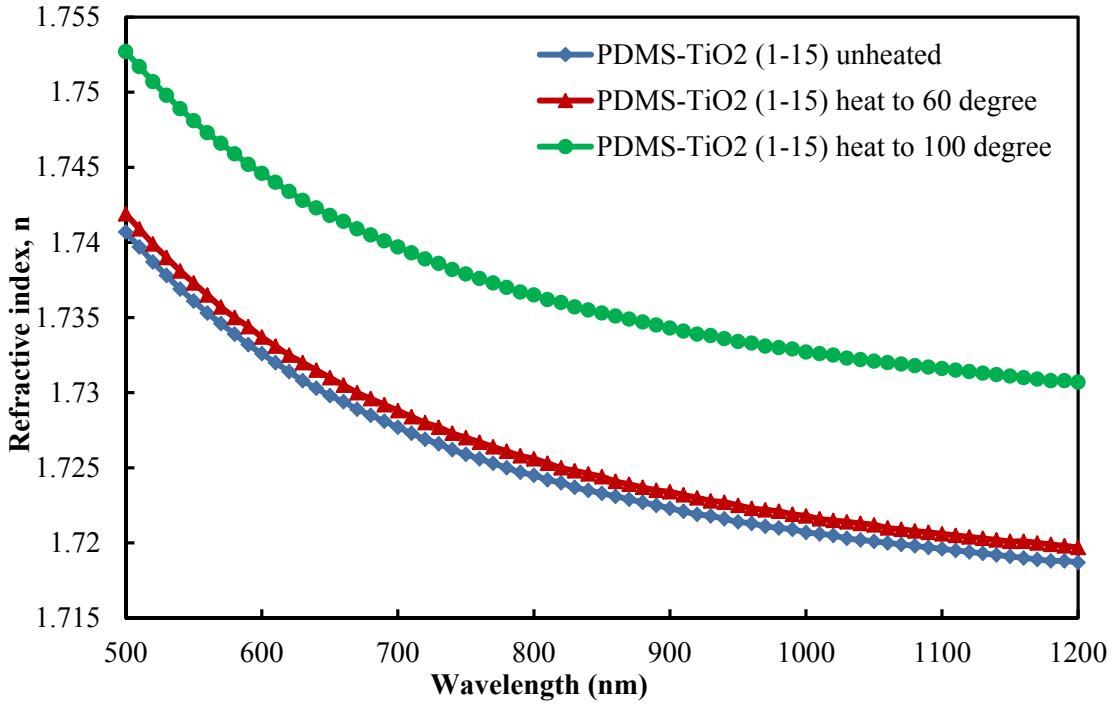

Figure 2.14 Refractive index of PDMS-TiO2 (1-15) annealed at different temperatures

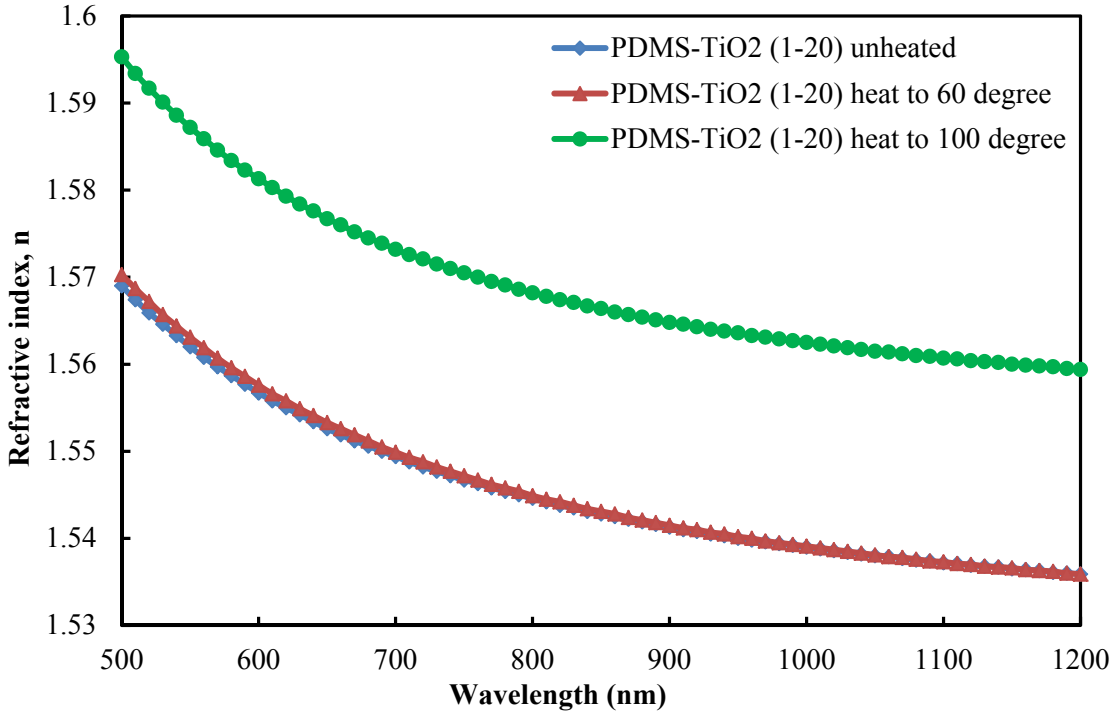

Figure 2.15 Refractive index of PDMS-TiO2 (1-20) annealed at different temperature

PDMS-TiO_2 composite samples were spin-coated on silicon wafers and tested on the ellipsometer for refractive index. The coated wafers were air dried, heated in an oven for 6h at 60 °C and 100 °C respectively. The refractive indices of four compositions of PDMS-TiO_2 composites annealed at different temperatures are plotted in Figure 2.12, Figure 2.13, Figure 2.14 and Figure 2.15. As shown in the figures above, the air dried and the 60 °C annealed PDMS-TiO_2 samples have almost the same refractive index in the measured wavelength range of 500-1200 nm. This is due to the lower annealing temperature, which is 60°C, doesn't change the structure of PDMS-TiO_2 composites or TiO_2 amorphous state in the system and therefore has no effect on the refractive index. When annealed at 100 °C, the refractive indices are increased significantly. This is probably due to the removal of solvent in the pores of the network, which evaporates out during annealing and as a result increases the refractive index.

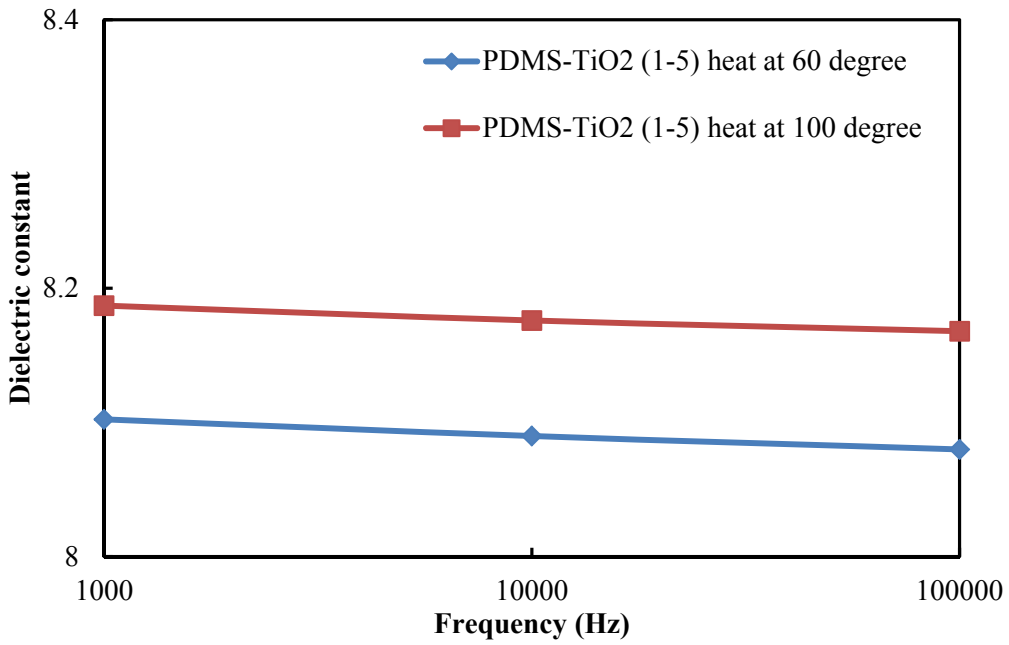

Figure 2.16 Dielectric constant of PDMS-TiO_2 (1-5) annealed at different temperatures

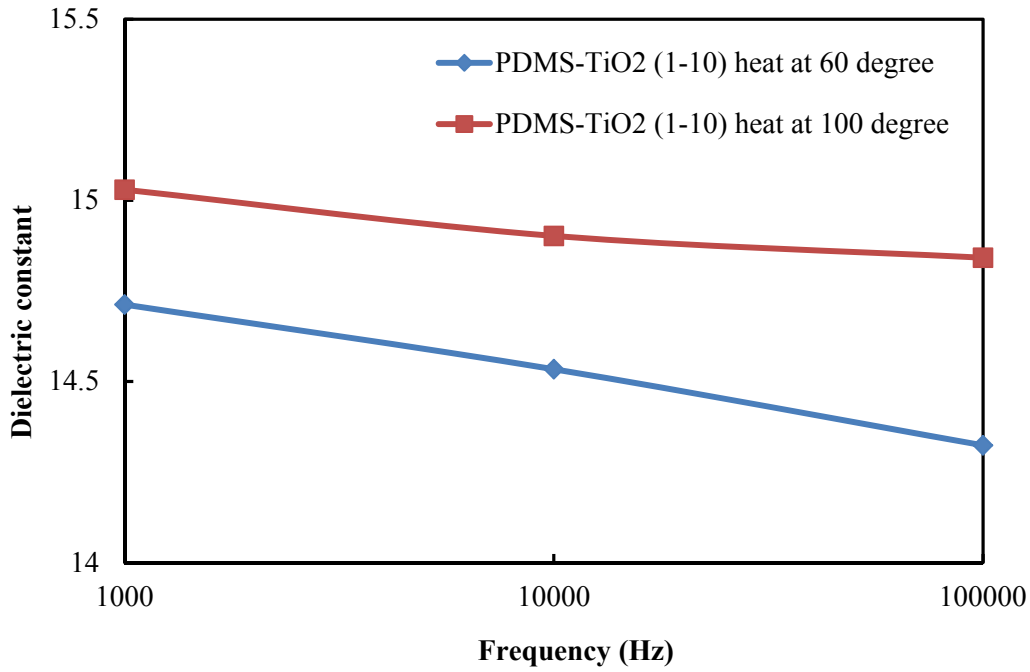

Figure 2.17 Dielectric constant of PDMS-TiO2 (1-10) annealed at different temperatures

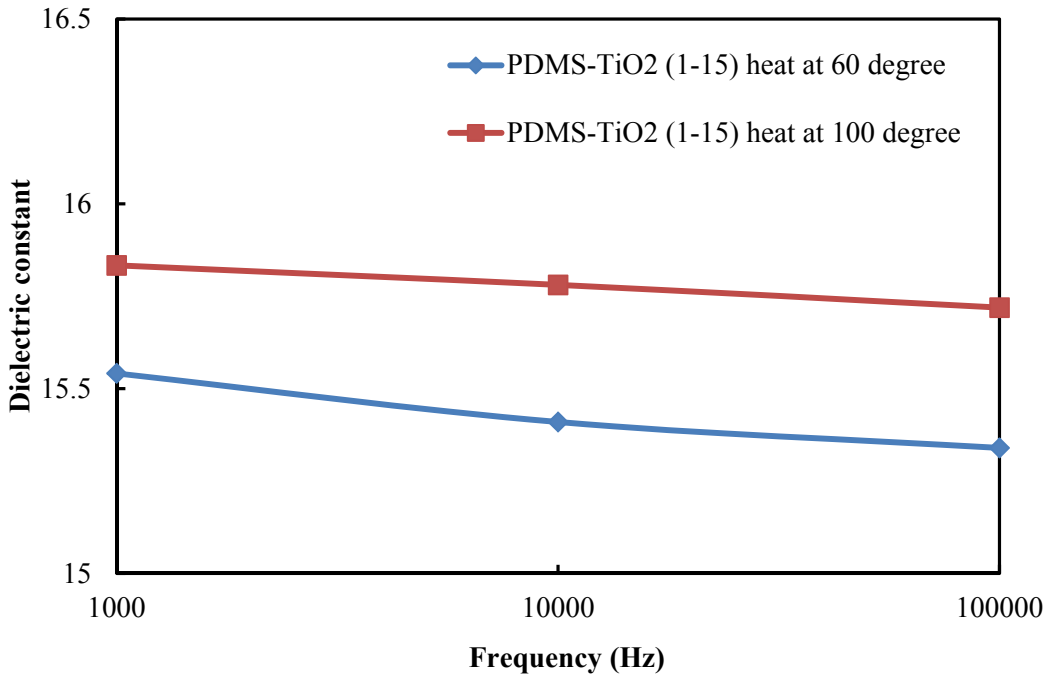

Figure 2.18 Dielectric constant of PDMS-TiO_2 (1-15) annealed at different temperatures

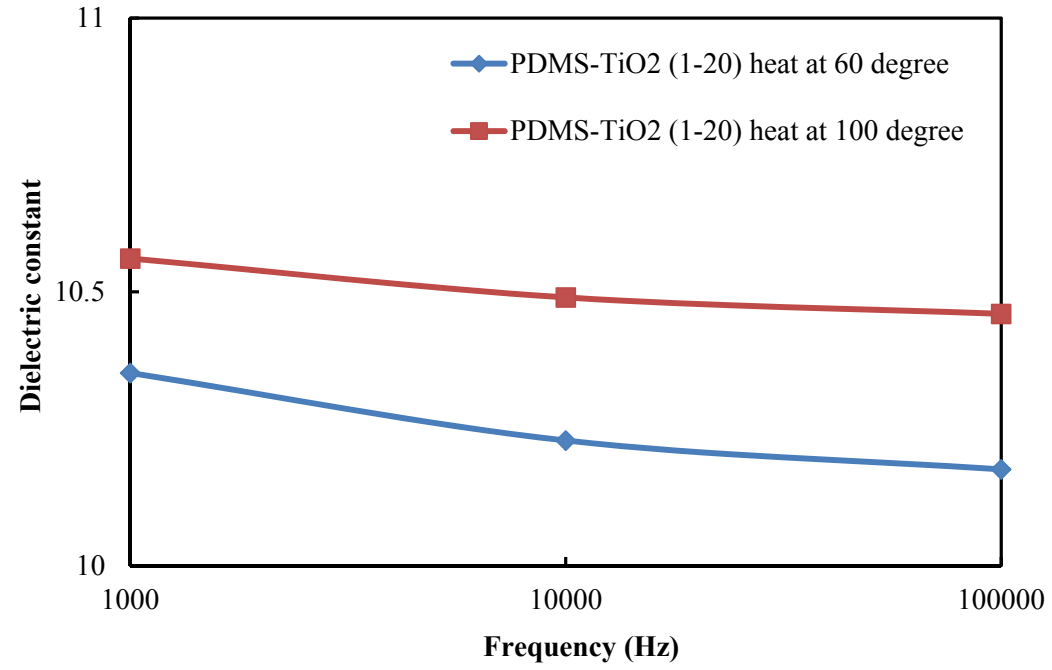

Figure 2.19 Dielectric constant of PDMS-TiO_2 (1-20) annealed at different temperatures

The dielectric constants of various compositions of PDMS-TiO_2 composites annealed at different temperatures are depicted in Figures 2.16 through 2.19. The trends observed are similar to those for refractive index. It is can be seen that there is a decrease for the dielectric constant with increase of frequency in the range of 10^3-10^5 Hz. When the annealing temperature is raised from 60 °C to 100 °C, the dielectric constants increases to higher values, which once again may be due to the evaporation of liquid in the network pores during annealing, as seen for the refractive index.

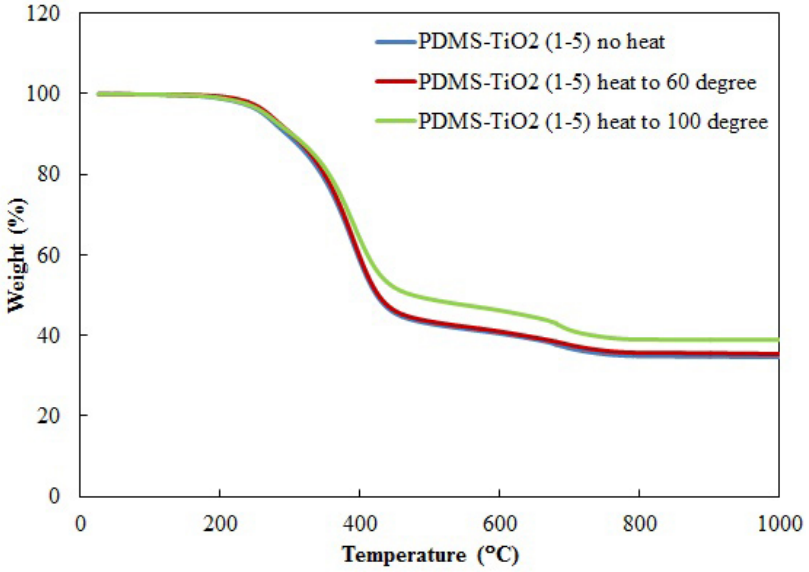

Figure 2.20 TGA curve of PDMS-TiO2 (1-5) annealed at different temperature

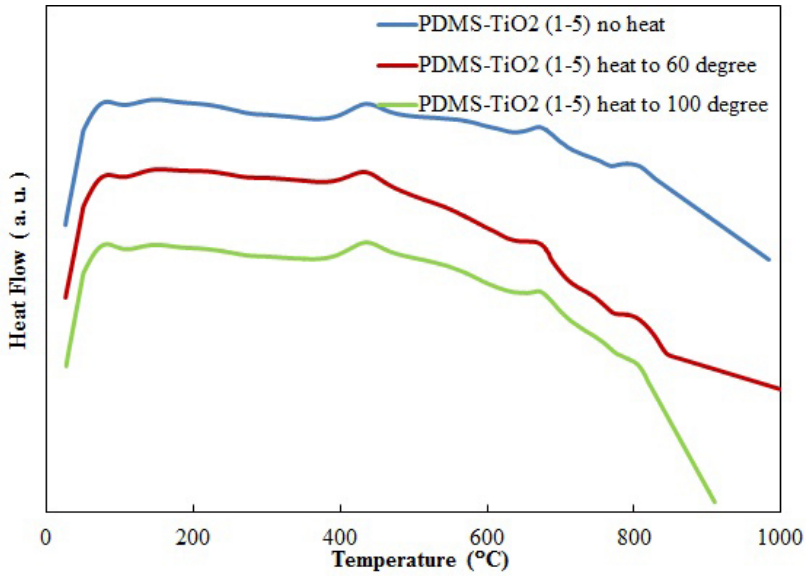

Figure 2.21 DSC curve of PDMS-TiO2 (1-5) annealed at different temperatures

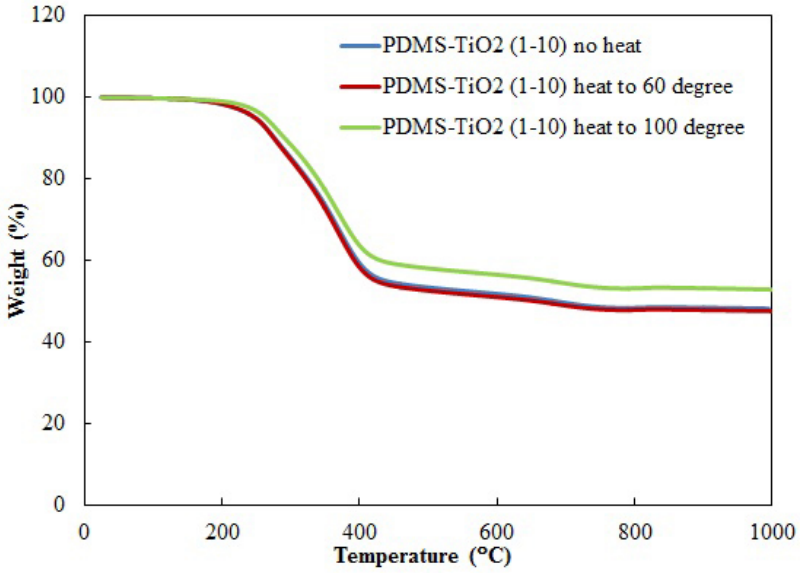

Figure 2.22 TGA curve of PDMS-TiO_2 (1-10) annealed at different temperatures

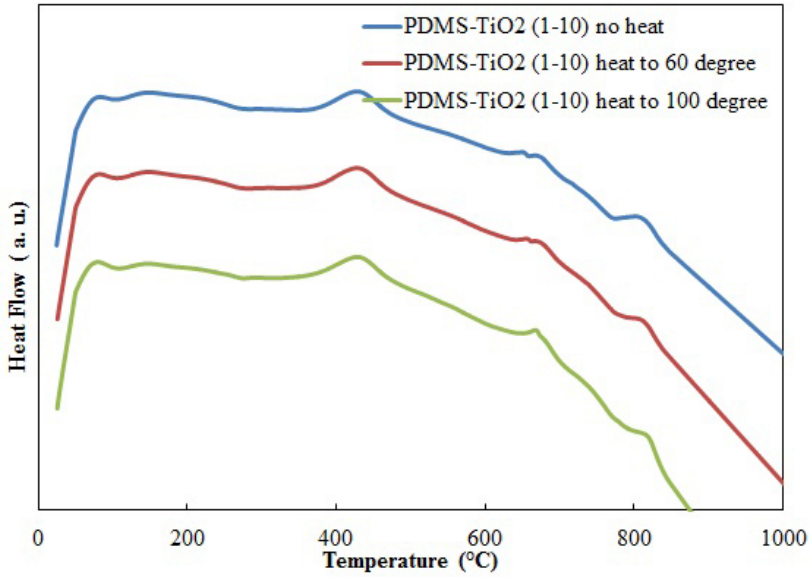

Figure 2.23 DSC curve of PDMS-TiO_2 (1-10) annealed at different temperatures

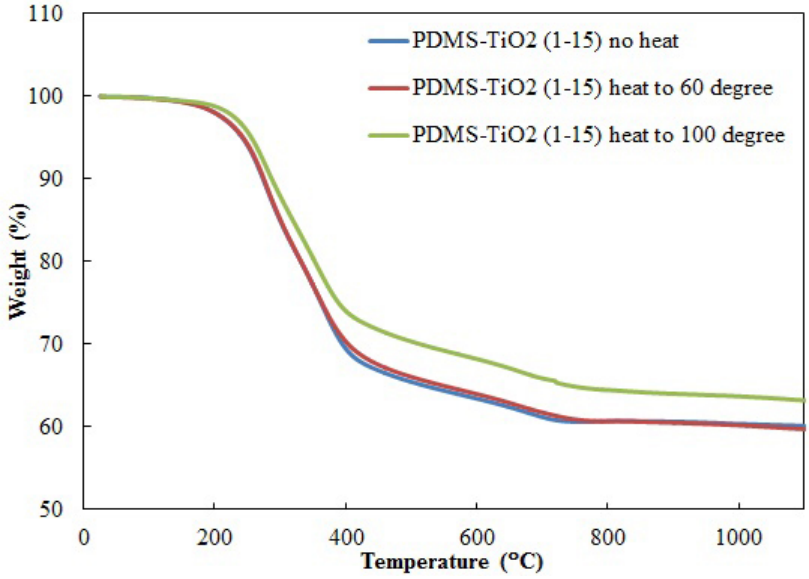

Figure 2.24 TGA curve of PDMS-TiO_2 (1-15) annealed at different temperatures

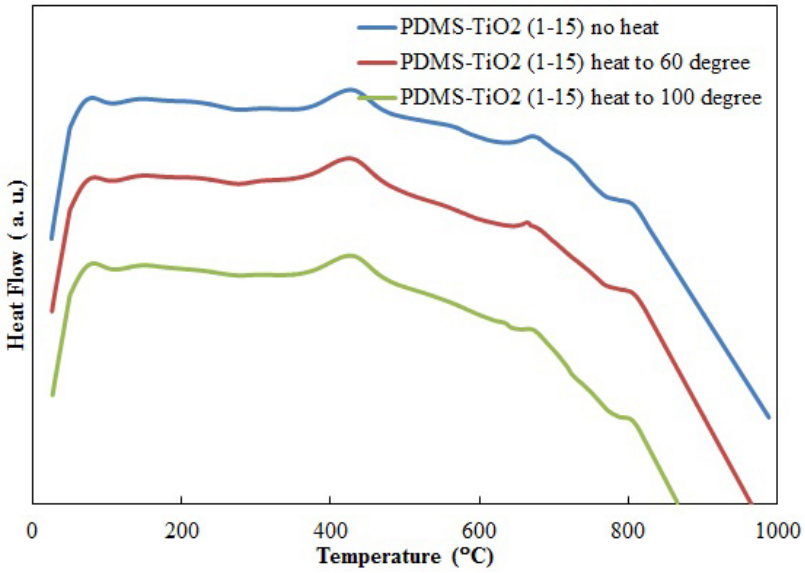

Figure 2.25 DSC curve of PDMS-TiO_2 (1-15) annealed at different temperatures

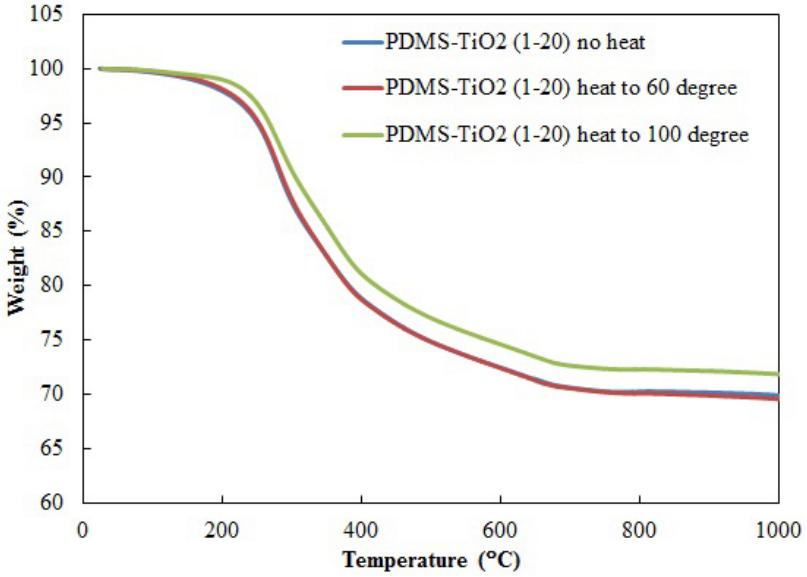

Figure 2.26 TGA curve of PDMS-TiO_2 (1-20) annealed at different temperatures

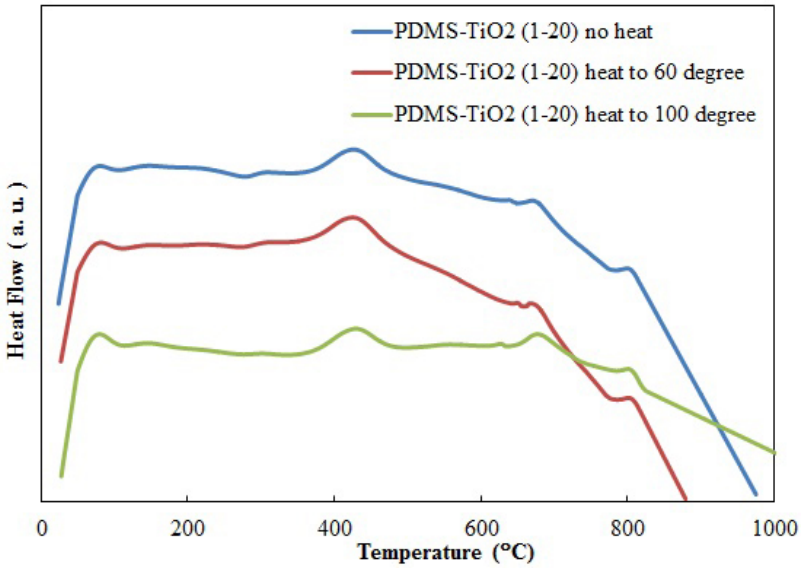

Figure 2.27 DSC curve of PDMS-TiO_2 (1-20) annealed at different temperatures

As shown in TGA-DSC curves above, there is no significant effect of annealing at 60 °C. However, when annealing at 100 °C, the weight losses in the TGA were reduced. This weight reduction corresponds to the evaporation of trapped solvent which is the product of Ti $(OR)_4$ reacting with PDMS. Most of the solvent didn't come out of the pores of the matrix until increase the annealing temperature to 100 °C. As indicated by the derivative weight loss curves, the PDMS-TiO_2 (1-20) sample has the largest relative amount of solvent trapped within the pores whereas PDMS-TiO_2 (1-5) has the least. Since PDMS-TiO_2 (1-20) contains the highest amount of isopropanol, it has the most significant reduction in weight loss after annealing at 100 °C. However, this reduction is not obvious in PDMS-TiO_2 (1-5), since there is relatively little isopropanol in this system, and the residual isopropanol is not easy removed until heated to a higher temperature.

2.5 Conclusion

The structural model stated in the hypothesis was verified by the results of experiments. PDMS is first cross-linked by the titanium precursor to form PDMS-TiO_2 nanocomposites. These precursors then form titanium dioxide during curing to produce a final hybrid structure with network containing pores in the sub-micron range. The titanium dioxide generated is located in the PDMS backbone and dispersed uniformly in the matrix as amorphous status. The ratio of titanium precursor to PDMS was varied from 5:1 to 20:1 to prepare composites with a variety of compositions. The higher the ratio of titanium precursor, the more condensed the structure created, and subsequently larger and more amorphous titanium dioxide particles were produced. The refractive index and

dielectric constants of the hybrids increased with an increase of TiO_2 in the system. The highest refractive index and dielectric constant obtained were 1.74 and 15.5 respectively for the PDMS-TiO_2 (1-15) sample. However, when the ratio of TiO_2 to PDMS reached as high as 20 to 1, phase separation occurs and the refractive index and dielectric constant decrease to lower values. When the composites were annealed at 60 °C, no significant effect on refractive index or dielectric constant due to the removal of residual solvents was observed. However, upon increasing the annealing temperature above the boiling point of isopropanol to 100 °C, the refractive index, dielectric constant and thermal stability of the composites were significantly improved.

2.6 References

1. Julian, B., et al. Synthesis and characterization of transparent PDMS-metal-oxo based organic anorganic nanocomposites. Chemistry of Materials. 2003; 15(15): 3026-3034.
2. Pomogailo, A.D. Polymer sol-gel synthesis of hybrid nanocomposites. Colloid Journal. 2005; 67(6): 658-677.
3. Niederberger, M. Nonaqueous sol-gel routes to metal oxide nanoparticles. Accounts of Chemical Research. 2007; 40(9): 793-800.
4. Nandi, M., et al. Molecular-Level Ceramic Polymer Composites. 2.1 Synthesis of Polymer-Trapped Silica and Titania Nanoclusters. Chemistry of Materials. 1991; 3(1): 201-206.
5. Mourey, T.H., et al. Hydrolysis and Condensation Coupling of (Trimethoxysilyl)Phenyl-Terminated Polystyrene Macromonomers. Macromolecules. 1992; 25(1): 45-52.
6. Chujo, Y., et al. Block Copolymer of 2-Methyl-2-Oxazoline with Silica-Gel - an Organic-Inorganic Hybrid Polymer. Makromolekulare Chemie-Macromolecular Symposia. 1991; 42(3): 303-312.
7. Noell, J.L.W., et al. The Preparation and Characterization of New Polyether Ketone-Tetraethylorthosilicate Hybrid Glasses by the Sol-Gel Method. Journal of Applied Polymer Science. 1990; 40(7-8): 1177-1194.
8. Glaser, R.H., G.L. Wilkes. Polymer Modified Mixed Metal Alkoxide-Metal Acetyl Acetonate Sol-Gel Materials. Polymer Bulletin. 1989; 22(5-6): 527-532.
9. Coltrain, B.K., et al. Role of Trialkoxysilane Functionalization in the Preparation of Organic-Inorganic Composites. Chemistry of Materials. 1993; 5(10): 1445-1455.
10. Macwan, D.P., P.N. Dave, S. Chaturvedi. A review on nano-TiO2 sol-gel type syntheses and its applications. Journal of Materials Science. 2011; 46(11): 3669-3686.
11. Hu, Q., E. Marand. In situ formation of nanosized TiO2 domains within poly(amide-imide) by a sol-gel process. Polymer. 1999; 40(17): 4833-4843.

12. Chen, W.C., et al. Synthesis and characterization of poly(methyl silsesquioxane) titania optical thin films. Journal of Materials Chemistry. 2002; 12(12): 3644-3648.
13. Lee, L.H., W.C. Chen. High refractive-index thin films prepared from trialkoxysilane-capped poly(methyl methacrylate)-titania materials. Chemistry of Materials. 2001; 13(3): 1137-1142.
14. Nussbaumer, R.J., et al. Polymer-TiO2 nanocomposites: A route towards visually transparent broadband UV filters and high refractive index materials. Macromolecular Materials and Engineering. 2003; 288(1): 44-49.
15. Zhang, J., et al. New observations on the optical properties of PPV/TiO2 nanocomposites. Polymer. 2001; 42(8): 3697-3702.
16. Yabuta, T., et al. Synthesis of blood compatible PDMS-based organic-inorganic hybrid coatings. Journal of Sol-Gel Science and Technology. 2004; 31(1-3): 273-276.
17. Shindou, T., et al. Effect of composition on surface properties of polydimethylsiloxane-based inorganic/organic hybrid films. Journal of Sol-Gel Science and Technology. 2004; 30(3): 229-237.
18. Pena-Alonso, R., et al., Surface chemical and physical properties of TEOS-TBOT-PDMS hybrid materials. Journal of Sol-Gel Science and Technology. 2006; 38(2): 133-145.
19. Nakade, M., M. Ogawa. Synthesis and characterization of zinc oxide fine particles coated with titania/PDMS hybrid. Journal of Materials Science. 2007; 42(12): 4254-4259.
20. Bae, S.C., et al. Chemical imaging in a surface forces apparatus: Confocal Raman spectroscopy of confined poly(dimethylsiloxane). Langmuir. 2005; 21(13): 5685-5688.
21. Aprile, C., et al. Long-lived (minutes) photoinduced charge separation in a structured periodic mesoporous titania containing 2,4,6-triphenylpyrylium as guest. Dalton Transactions. 2008; 40: 5465-5470.
22. Jang, J., et al. Self-reference quantitative phase microscopy for microfluidic devices. Optics Letters. 2010; 35(4): 514-516.

23. MASATO NAKADE, KOSUKE ICHIHASHI, MAKOTO OGAWA. Microporous materials derived from the thermal decomposition of the titania/PDMS hybrid particles. Journal of Porous Materials. 2005; 12: 79-85.
24. T. Howard, T. C. Kendrick. Thermal analysis of polydimethylsiloxane. I. Thermal degradation in controlled atmospheres. Journal of Polymer Sicence: Part A-2. 1969; 7: 537-549.
25. S. R. Gomes, F. M. A. Margaca, D. Faria Silva, L. M. Ferreira, I. M. Miranda Salvado, A. N. Falcao. Novel way to control PDMS cross-linking by gamma-irradiation. Nuclear Instruments and Methods in Physics Research B. 2008; 266: 1105-1108.
26. Shukla, S.K., et al. Some thermal studies of polysilanes and polycarbosilanes. Thermochimica Acta. 2004; 424(1-2): 209-217.

3. Synthesis of PDMS-$BaTiO_3$ Hybrid Nanocomposites Using an *In Situ* Sol-Gel Route

3.1 Abstract

PDMS-$BaTiO_3$ hybrid nanocomposites were fabricated using an *in situ* sol-gel process with silanol terminated polydimethylsiloxane (PDMS) as the host matrix to an inorganic phase prepared from titanium isopropoxide and barium acetate. By changing the ratio of titanium and barium precursors, homogeneous and transparent PDMS-$BaTiO_3$ hybrids with a range of compositions were obtained. The structure and thermal properties of these hybrids were characterized using several instruments, including FT-IR, FT-Raman, and TGA/DSC instruments. The hybrid samples were also spin-coated onto silicon wafers substrates and tested on an ellipsometer for refractive indices. Dielectric constants for these samples were calculated from the capacitances determined over a range of frequencies. As the ratio of titanium and barium precursors for the sample of PDMS-$BaTiO_3$ increased, the refractive index increased from 1.4 for plain PDMS to 1.6, and similarly the dielectric constant increased from 2.8 to 12.2 for PDMS-$BaTiO_3$ (1-6) sample. However, when the ratio of metal precursors to PDMS reached 8:1, phase separation of the inorganic region occurred as evidenced by scanning electron microscope (SEM) images, and consequently, the refractive index and dielectric constant decreased. A structural model based on the ratios of PDMS to titanium and barium precursors was proposed, which explained the structure of composites and may permit design of these hybrids for specific applications. The films were annealed at 60 °C and 100 °C, and the effect on the properties of the final products was investigated.

3.2 Introduction

Fabrication of organic-inorganic hybrids with high dielectric constants has attracted great attention due to their promise for electronic and photonic applications, including resistors, capacitors, and inductors (1,2). Ceramics with high dielectric constants and refractive indices are candidates for these applications. However, high processing temperatures are required for the ceramics, which are not compatible with the embedded capacitors (3). Numerous attempts have been made to solve this problem, including the preparation of polymer-ceramic composites, since this technique combines the low processing temperature of polymers with the high dielectric constant of ceramics (4,5). A variety of preparation approaches have been studied, such as co-precipitation, sol-gel route, and hydrothermal synthesis. The sol-gel route is particularly attractive due to its ability to produce good chemical homogeneity, and high purity hybrids at low temperatures (6,7).

Polydimethylsiloxane (PDMS) due to its high elasticity, hydrophobicity, transparency, and excellent relaxation properties was selected as the organic component to fabricate PDMS-metal oxide hybrid nanocomposites. Because of its exceptional dielectric and ferroelectric properties, barium titanate is an important ceramic to be applied as the inorganic component in organic-inorganic hybrid making. Many types of $BaTiO_3$-polymer composites have been synthesized, however most of them were obtained by mixing fine barium titanate particles into polymer solutions (8-10) where the compatibility and uniformity are the main challenges. Although the use of sol-gel method

to prepare PDMS/SiO_2-TiO_2 composites has been reported before (11), the difference in hydrolysis rate between the silicon and titanium precursors led to phase separation with a physical mixture of two oxides instead of a true binary oxide. In this study, PDMS-$BaTiO_3$ nanocomposites were fabricated for the first time based on an *in situ* sol-gel reaction to get transparent and homogenous polymer-binary metal oxide hybrids. Many types of barium precursors were investigated to react with the titanium isopropoxide to form barium titanate compounds, including: barium metal, barium ethoxide, barium hydroxide, barium chloride, and barium acetate. In general, the low solubility of most Ba compounds in water and their insolubility in alcohol and other organic solvents limited the utilization of Ba salts in sol-gel process. After trying several types of barium precursors, we found that barium acetate, which has a high water solubility, was successfully reacted with titanium isopropoxide to obtain homogeneous PDMS-$BaTiO_3$ composites. As a result it was selected as our barium source. In the following study, the effects of the ratio of barium titanate on the structures and the properties of the hybrids prepared with different compositions were investigated.

3.3 Experimental

3.3.1 Materials

Titanium isopropoxide (TTIP) Ti $(OCH(CH_3)_2)_4$ (97%) and barium acetate $(Ba(OAc)_2)$ (99%) purchased from Sigma Aldrich were used as the precursors of inorganic components. Silanol terminated poly(dimethylsiloxane) (PDMS) with an average molecular weight of approximate 3500 was provided by the Dow Corning Corporation.

Isopropanol and ethanol (anhydrous, PHARMCO-AAPER) were used as the solvents. Ethyl acetoacetate (EAcAc) (Sigma Aldrich) was used as a chemical modifier of the titanium alkoxide to decrease the hydrolysis rate. All the chemicals were used without further purification. Water was distilled and deionized.

3.3.2 Preparation of PDMS-$BaTiO_3$ hybrid nanocomposites

The PDMS-$BaTiO_3$ nanocomposites were fabricated in a three step process. Since titanium isopropoxide reacts with water instantly to generate particles, the chemical modifier EAcAc was employed to slow down its hydrolysis rate. The addition sequence of the reactants was studied to find one with the most transparent "sol" and shown in the schematic below.

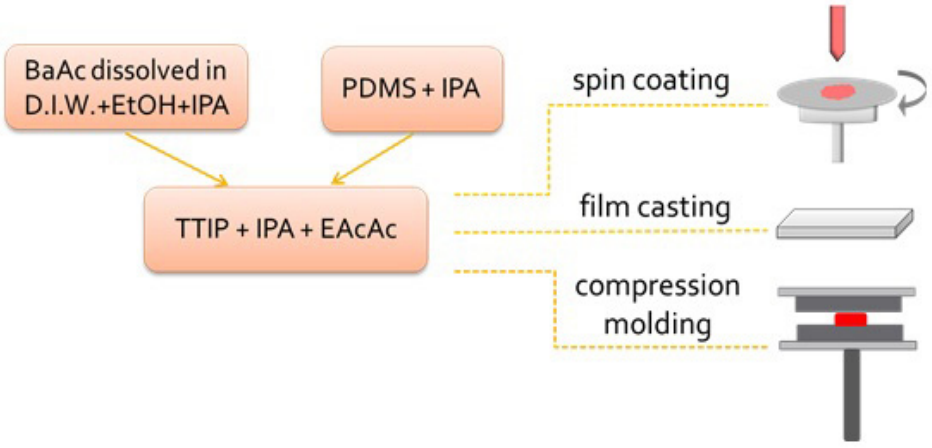

Figure 3.1 Schematic of process for the fabrication of PDMS-$BaTiO_3$ hybrid samples

First, solution "A" was formed by dissolving the desired amount of barium acetate in a mixture of D.I. water, isopropanol and ethanol (molar ratio of BaAc: D.I.W: IPA: EtOH= 3: 250: 50: 17). To fully dissolve the barium acetate, this mixture was stirred at room

temperature for 10 minutes and then sonicated for an additional 30 minutes. Solution "B" was prepared by adding a stoichiometric amount of titanium isopropoxide into a mixture of isopropanol and ethyl acetoacetate. The molar ratio of titanium isopropoxide to EAcAc was 1 to 4. Solution "C" was produced by 0.715ml of polydimethylsiloxane (PDMS) diluted with 2ml of propanol. Finally, solution A and solution C were quickly dripped into solution B while it stirred at room temperature. The final solution was poured into an aluminum sample dish to produce a light yellowish, transparent gel or spin-coated onto silicon wafers to obtain hybrid films. The ratio of metal precursors to PDMS was varied, and four different compositions were chose as representative to examine their effects on the hybrids properties. The compositions of the PDMS-$BaTiO_3$ composites examined are summarized in Table 3.1.

Table 3.1

Composition of PDMS-$BaTiO_3$ nanocomposites.

Sample	Molar ratio of PDMS: $Ba(OAc)_2$:TTIP	Molar ratio of Ba:Ti:Si (theoretical value)	$BaTiO_3$ wt% (theoretical value)
PDMS-$BaTiO_3$ (1-2)	1:2:2	2:2:47	12%
PDMS-$BaTiO_3$ (1-4)	1:4:4	4:4:47	21%
PDMS-$BaTiO_3$ (1-6)	1:6:6	6:6:47	29%
PDMS-$BaTiO_3$ (1-8)	1:8:8	8:8:47	35%

The various compositions of PDMS-$BaTiO_3$ composites were measured for their structures, morphologies, optical, electrical and thermal properties. These composites were annealed at 60 °C and 100 °C to investigate the effects of annealing on the structures and properties of the final hybrids.

3.3.3 Hypothesis

In this experiment, PDMS-$BaTiO_3$ hybrid nanocomposites were synthesized using an *in situ* sol-gel process for the first time. Silanol terminated PDMS was used as the organic component since the terminal Si-OH groups can react readily with metal precursors. EAcAc was introduced as a chemical modifier to slow down the hydrolysis rate of titanium isopropoxide. The related main reactions are shown below:

Solution A: (Barium acetate dissolved in water)

$$Ba(OAc)_2 + 2H_2O \rightarrow Ba^{2+} + 2OH^- + 2HOAc$$

Equation 3-1

Solution B:

In this system, titanium isopropoxide is attacked by four molecules of EAcAc, then through electron rearrangement, $Ti(OR)_2(EAcAc')_4^{2-}$ ($EAcAc'$ stands for the attached EAcAc which loses one -H) and the associated alcohol is formed.

$$Ti(OR)_4 + 4EAcAc \rightarrow Ti(OR)_2(EAcAc')_4{}^{2-} + 2ROH + 2H^+$$

Equation 3-2

Addition of solution A+ solution B:

When adding solution A into solution B, the titanium compound is hydrolyzed and then reacts preferentially with dissolved barium due to its small size and its easier access to the hydrolyzed titanium intermediate. After most of the titanium precursors react with barium, the condensation products, HO-Ba-O-Ti(OH)$(EAcAc')_4^{2-}$, would react with each other to produce bigger Ba-Ti regions. This process is summarized as depicted below:

$$Ti(OR)_2(EAcAc')_4{}^{2-} + 2H_20 \rightarrow Ti(OH)_2(EAcAc')_4{}^{2-} + 2ROH$$

Equation 3-3

$$Ba^{2+} + 2OH^- + Ti(OH)_2(EAcAc')_4{}^{2-} \rightarrow$$

$$HO - Ba - O - Ti(OH)(EAcAc')_4{}^{2-} + H_2O$$

Equation 3-4

$$2HO - Ba - O - Ti(OH)(EAcAc')_4{}^{2-} \rightarrow$$

$$HOBa - O - Ti(EAcAc')_4{}^{2-} - O - Ti(EAcAc')_4{}^{2-} - O - BaOH + H_2O$$

Equation 3-5

Final addition step: (Solution A+ Solution B) + Solution C:

As described by the equations shown above, when PDMS was added to system, most of the reactions were between PDMS terminal silanol groups (–OH) and HO-Ba-M (M presents the possible metal compounds connected to Ba).

$$H{-}[OSi(CH_3)_2]_n - OH + HO - Ba - M \rightarrow H{-}[OSi(CH_3)_2]_n - O - Ba - M + H_2O$$

Equation 3-6

$$M - Ba - OH + H{-}[OSi(CH_3)_2]_n - O - Ba - M$$

$$\rightarrow M - Ba - O - Si{-}[OSi(CH_3)_2]_{n-1} - O - Ba - M + H_2O$$

Equation 3-7

Curing step:

During curing, the EAcAc groups release and Ti fully hydrolyzes. The hydrolyzed Ti-OH groups reacte with each other to generate Ti-O-Ti bonds, in which step $BaTiO_3$ particles would form. Some TiO_2 particles may be generated as a byproduct.

$$M = Ti(EAcAc')_4^{2-} + 2H_2O \rightarrow M = Ti(OH)_2 + 2EAcAc$$

Equation 3-8

$$M \equiv Ti(OH) + (OH)Ti \equiv M \rightarrow M \equiv Ti - O - Ti \equiv M + H_2O$$

Equation 3-9

As discussed above, during the experiments, titanium isopropoxide was first hydrolyzed and then react with barium to form particles containing titanium, barium, and the residual EAcAc. When adding PDMS to the system, the Ba-OH bonds on the surface of the particles cross-link with the terminal silanol groups of PDMS to produce solid hybrids. Upon curing the hybrids in ambient air, titanium compounds fully hydrolyzed and much of the residual EAcAc evaporates from the matrix. The final hybrids fabricated have a structure of $BaTiO_3$ particles cross-linked with PDMS and free amorphous $BaTiO_3$ and TiO_2 particles dispersed in the matrix. The final structure consists of a polymer-nanoparticle network with pores of nanometer size containing some residual isopropanol solvent and EAcAc. By varying the amount of the titanium and barium precursors, the structure of the final hybrids is changed. As the amount of metal precursors in the solution increases, more inorganic regions are generated and some of these coalesce to form larger particles. Since larger particles diffuse more slowly in solution, for the hybrids with more metal precursors, there are more PDMS chains only cross-linked with the particles on one side, which means the matrix is less cross-linked. The schematic of the proposed final structures of the PDMS-$BaTiO_3$ hybrids with increasing inorganic content are shown below:

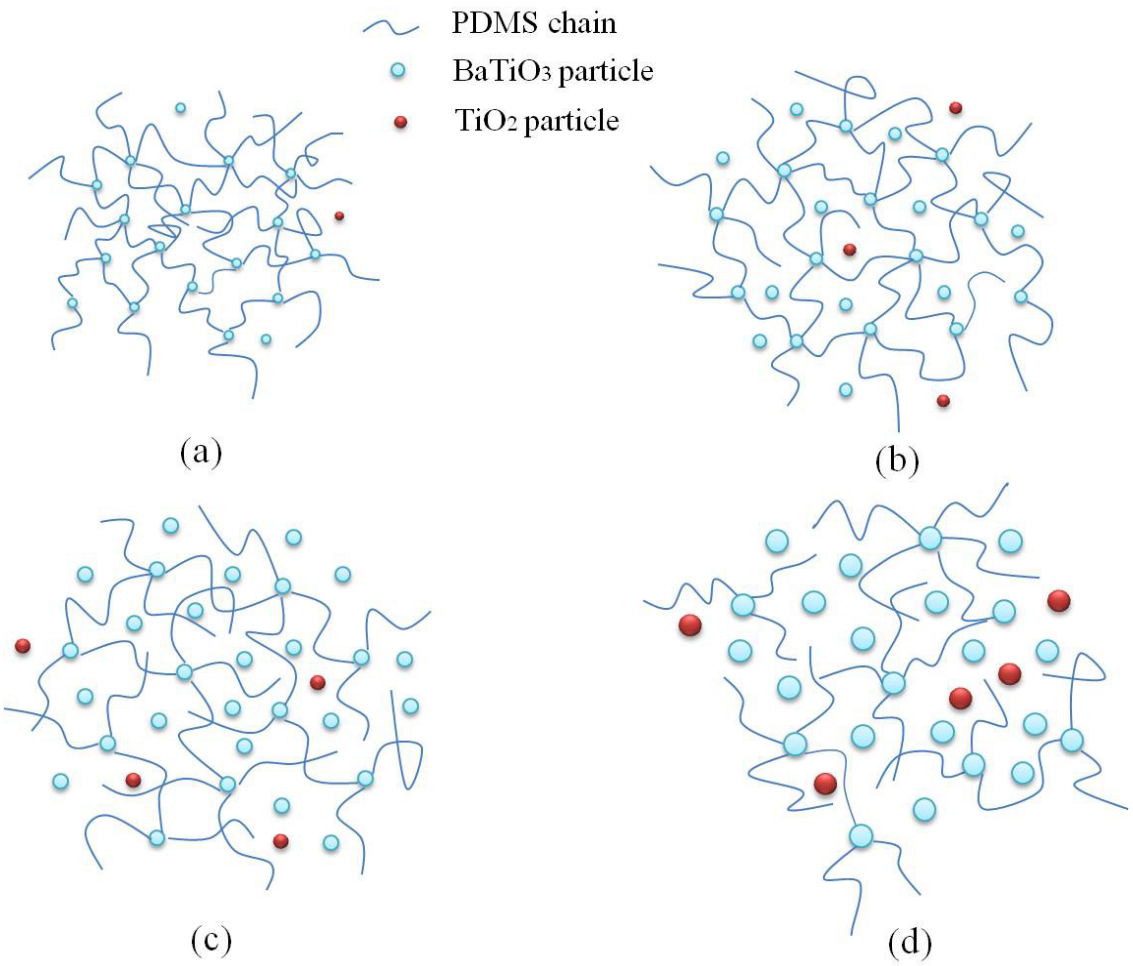

Figure 3.2 Proposed structural model for PDMS-$BaTiO_3$ hybrid nanocomposites: (a) PDMS-$BaTiO_3$ (1-2), (b) PDMS-$BaTiO_3$ (1-4), (c) PDMS-$BaTiO_3$ (1-6), (d) PDMS-$BaTiO_3$ (1-8).

3.3.4 Characterization

To verify if the structures of the hybrids are as the models above depict, PDMS-$BaTiO_3$ nanocomposites prepared with different compositions were characterized by various instruments for their chemical structure and physical properties. The bonding within the materials were measured at various synthesis steps by a combination of a PerkinElmer FT-IR Spectrometer and a Bruker RFS 100 FT-Raman which in conjunction may give a

better understanding of the structure. The bulk film thickness was measured by an ABSOLUTE DIGIMATIC Calipers. The physical morphology was examined by field emission scanning electron microscope (Model S-4700, Hitachi High Technologies America, Inc.) applied to cross sections of the samples. To determine the optical properties of the materials the hybrid solution was first spin-coated onto Si wafers with a spinner (Model WS-400BZ-6NPP, Laurell Technologies Co.), and then tested on an ellipsometer (V-VASE, J.A. Woollam Co., Inc.) for refractive indices as a function wavelength. The coated film thickness was measured by a STYLUS PROFILER. To determine the dielectric constants, the hybrid samples were placed on a homemade cell and pressed by a compression molder (WABASH 12-101T) to form thicker films. Then these films were tested by an automatic capacitance meter (PM 6304, Fluke) to obtain the capacitances which were in turn used to calculate the dielectric constants of the sample films via the equation given below:

$$K = \frac{C * d}{\varepsilon * A}$$

Equation 3-10

Where C is the capacitance in F, d is the distance between the plates and also the thickness of the film in m, ε is the vacuum permittivity ($8.85*10^{-12}$ F/m), and A is the surface area of the plates in m^2. The evaluated dielectric constant was a function of frequency in the range of 10^3-10^5Hz to satisfy diverse applications.

As stated in the hypothesis, the hybrid composites may possess a network with pores of nanometer dimensions, which may still contain some isopropanol or EAcAc. Annealing these hybrids helps the solvent release from the network, and the properties of the final products will be changed as a result. The thermal analysis was done by a simultaneous DSC/TGA instrument (TA Instruments, SDT Q600). In these experiments, a small amount of sample (around 3mg) was used. The sample was heated from room temperature to 1000°C at a rate of 20°C/min. Nitrogen gas was flowing through the sample chamber at a rate of 100 ml/min during the heating process.

3.4 Results and Discussion

3.4.1 Effect of the titanium and barium precursors amount

To understand more fully the in situ process, a comparison of the hybrid nanocomposite films of PDMS-$BaTiO_3$ prepared with different ratios of titanium isopropoxide and barium acetate was made, and the influence of composition on the structures and properties of the resulting products were studied.

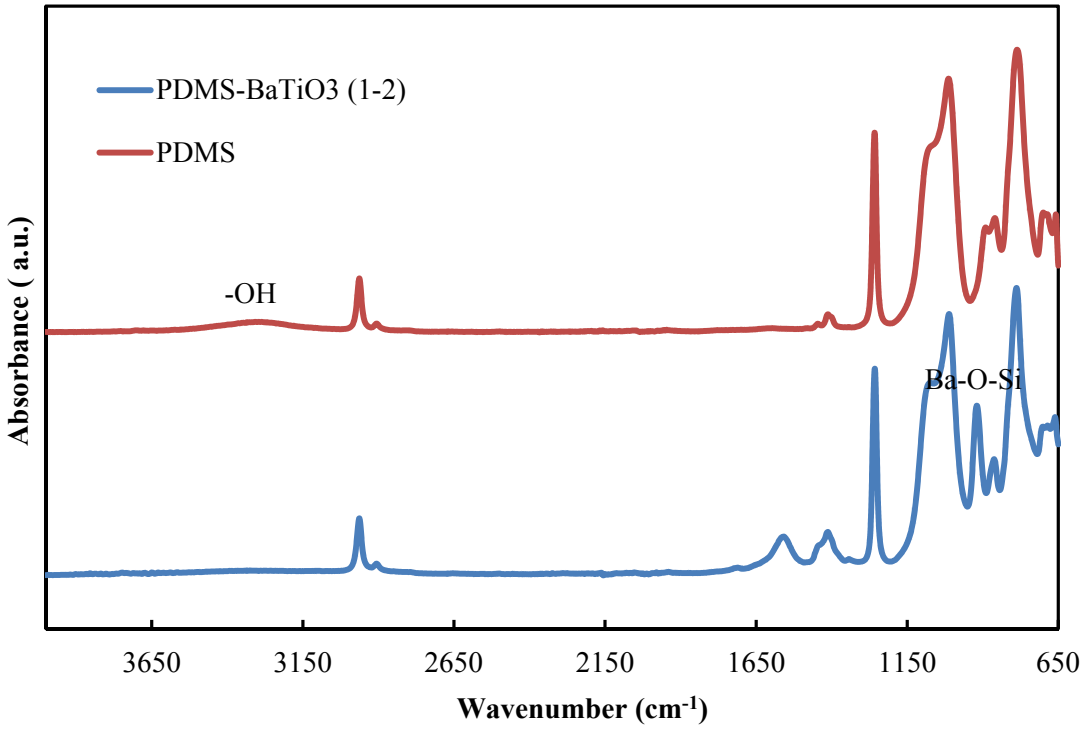

Figure 3.3 FT-IR spectra of PDMS and PDMS-$BaTiO_3$ (1-2)

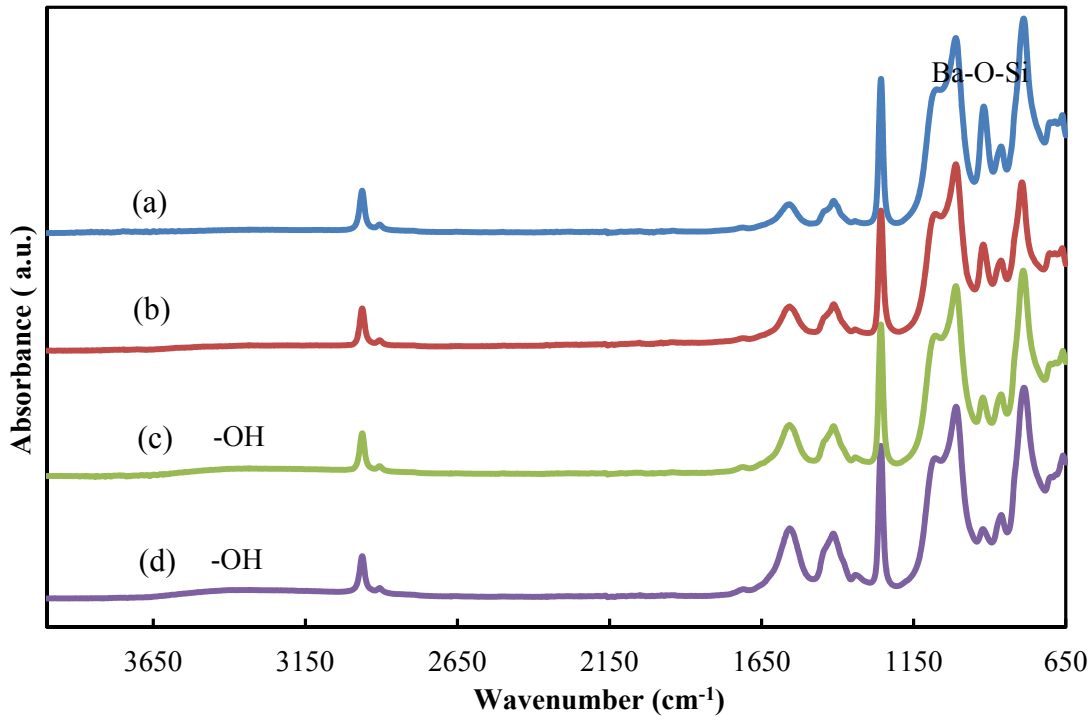

Figure 3.4 FT-IR spectra of PDMS-$BaTiO_3$ hybrid films (a) PDMS-$BaTiO_3$ (1-2), (b) PDMS-$BaTiO_3$ (1-4), (c) PDMS-$BaTiO_3$ (1-6), (d) PDMS-$BaTiO_3$ (1-8)

Figure 3.3 shows the FT-IR spectra of pure PDMS and the composite PDMS-$BaTiO_3$ (1-2). The low broad peak around 3200-3400 cm^{-1} may be assigned to the hydroxyl (-OH) terminated groups in the unreacted PDMS (12). This broad peak disappears in the PDMS-$BaTiO_3$ (1-2) spectrum which means that most of the hydroxyl groups have reacted with titanium isopropoxide and barium acetate when forming the composite. Two characteristic peaks at 1566 cm^{-1} and 1415 cm^{-1} are due to acetate stretching which may be ascribed to the unreacted barium acetate in the hybrid (13). In the spectrum of PDMS-$BaTiO_3$ (1-2), the peak corresponded to Si-O-Ti bonds at 960 cm^{-1}(14) is shifted to a lower wavenumber, 920 cm^{-1}, which we ascribe to the bonds of Si-O-Ba. This result demonstrates that the hydroxyl terminated PDMS was cross-linked with $BaTiO_3$ to form

hybrids as stated in the hypothesis. Figure 3.4 shows the FT-IR spectra of PDMS-$BaTiO_3$ hybrid nanocomposites with various compositions. All spectra show peaks around 2950, 1400 and 1260 cm^{-1} assigned to Si-CH_3 groups of PDMS molecules (12). The bands around 1100 and 1022 cm^{-1} are attributed to asymmetric stretching motions of Si-O-Si (15), and the peak around 800 cm^{-1} corresponds to the symmetric stretching vibrations (16). The intensity of the absorption peak centered around 920 cm^{-1} decrease with the increase of metal precursor in the matrix. Broad bands around 3200-3400 cm^{-1} start to reappear in the spectra of PDMS-$BaTiO_3$ (1-6) and PDMS-$BaTiO_3$ (1-8), which indicates the existence of residual –OH groups in these two composites. As described in the structural model, hybrids with higher amount of metal precursors create larger $BaTiO_3$ particles and more PDMS chains only connected to the particles on one side. So in a certain volume to be measured by FT-IR, PDMS-$BaTiO_3$ (1-8) has the strongest hydroxyl peak and the weakest peak for Si-O-Ba. From this analysis, the results of the FT-IR spectra are consistence with the structural model. The higher the ratio of metal precursors in the system, the stronger the intensity of the peaks at 1566 cm^{-1} and 1415 cm^{-1}, demonstrating more unreacted barium acetate in the hybrid.

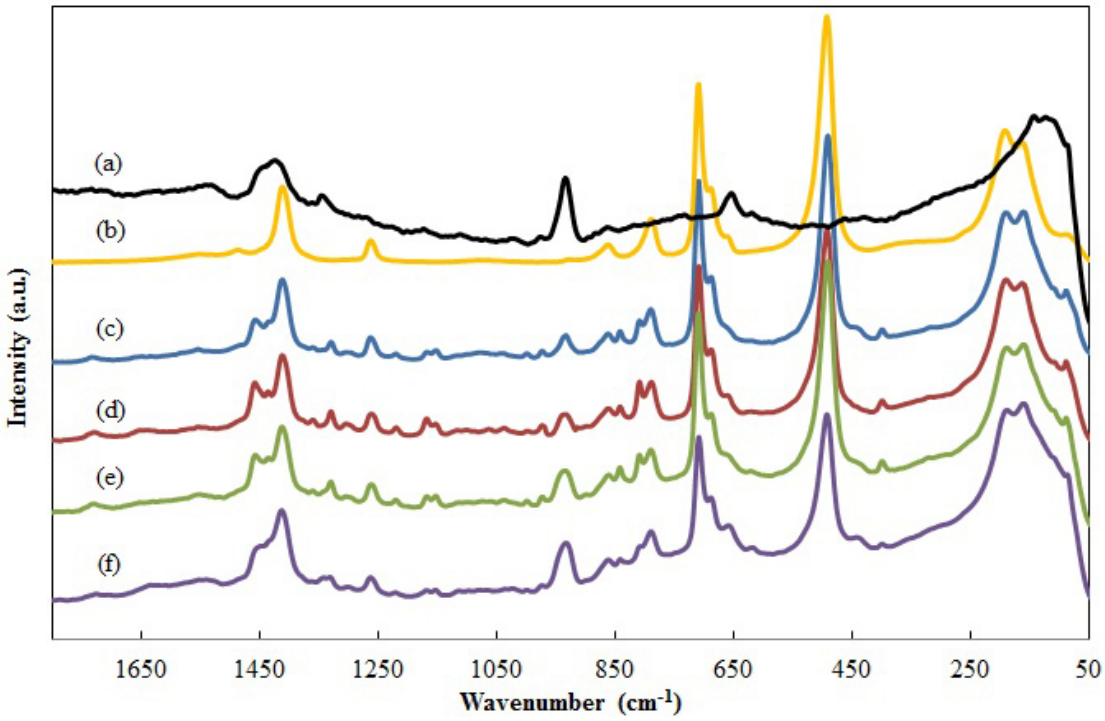

Figure 3.5 FT-Raman spectra of: (a) $BaTiO_3$ (sol-gel made unheated), (b) PDMS, (c) PDMS-$BaTiO_3$ (1-2), (d) PDMS-$BaTiO_3$ (1-4), (e) PDMS-$BaTiO_3$ (1-6), (f) PDMS- $BaTiO_3$ (1-8).

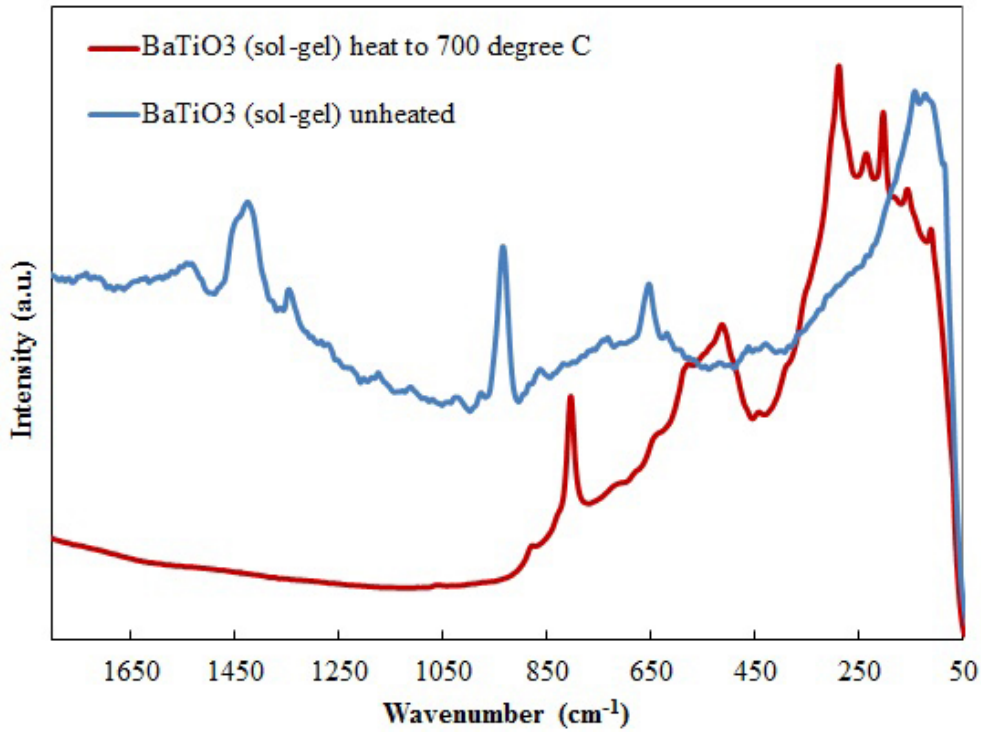

Figure 3.6 FT-Raman spectra of: (a) $BaTiO_3$ (sol-gel made unheated), (b) $BaTiO_3$ (sol-gel made heat to 800 °C)

Figure 3.5 shows the Raman spectra of pure PDMS, pure sol-gel synthesized $BaTiO_3$ without heating and the PDMS- $BaTiO_3$ composites. As shown in figure 3.5 (b), the spectrum of PDMS in our experiment is the same as a typical PDMS bulk liquid (17). The Si-O-Si and Si-CH_3 symmetric stretching bands are detected at 488 cm^{-1} and 708 cm^{-1}. The bands centered around 687 cm^{-1}, 787 cm^{-1}, and 862 cm^{-1} are assigned to Si-CH_3 symmetric rocking, Si-CH_3 asymmetric stretching, and CH_3 symmetric rocking respectively. Two additional bands for CH_3 symmetric and asymmetric bending are ascribed to 1262 cm^{-1} and 1412 cm^{-1}. In the spectra of the PDMS-$BaTiO_3$ nanocomposites, besides the bands for PDMS, some new bands corresponded to sol-gel synthesized $BaTiO_3$ (figure 3.5 (a)) are detected. The bands for$BaTiO_3$ which are located

around 935 cm^{-1}, are also detectable in the spectra of the PDMS-$BaTiO_3$ composites. Although two broad peaks are evident for the pure $BaTiO_3$ in the range of 1476-1375 cm^{-1} and 240-50 cm^{-1}, these are not obvious in the PDMS-$BaTiO_3$ composite spectra, and the original PDMS peaks at these wavelengths are broadened in the composite spectra. As discussed above, this indicates that the PDMS-$BaTiO_3$ composites contain structures similar to the sol-gel synthesized pure $BaTiO_3$. The higher the amount of titanium isopropoxide and barium acetate in the system, the more obvious the peaks corresponding to $BaTiO_3$ are. Since the intensity of the FT-Raman peak is proportional to the amount of characteristic bonds present, this means that the hybrids with higher ratios of precursors have more bonds identical to sol-gel made $BaTiO_3$. This is in accordance with the proposed structural, in that more inorganic precursors in the system create more and larger mixed metal oxide particles. In Figure 3.6, the Raman spectra of the unheated sol-gel $BaTiO_3$, and the $BaTiO_3$ heated to 700 °C are shown. When the sol-gel synthesized $BaTiO_3$ is heated, there two broad peaks appear around 305 cm^{-1} and 515 cm^{-1} which are identical to those for tetragonal crystalline $BaTiO_3$ (18). This indicates that the sol-gel made $BaTiO_3$ in the composites is initially amorphous, but can crystallize to the tetragonal crystalline structural form upon annealing at higher temperatures. Some of the other peaks in the spectra are due to the chemical modifier EAcAc or alcohol left in the matrix. In summary, these FT-Raman spectra support the hypothesis of the structural model that via *in situ* sol-gel synthesis amorphous $BaTiO_3$ particles produced within the PDMS matrix. Fewer particles which are smaller size are generated with lower amounts of metal precursors in the solution, and higher inorganic component ratios result in more numerous and larger particles.

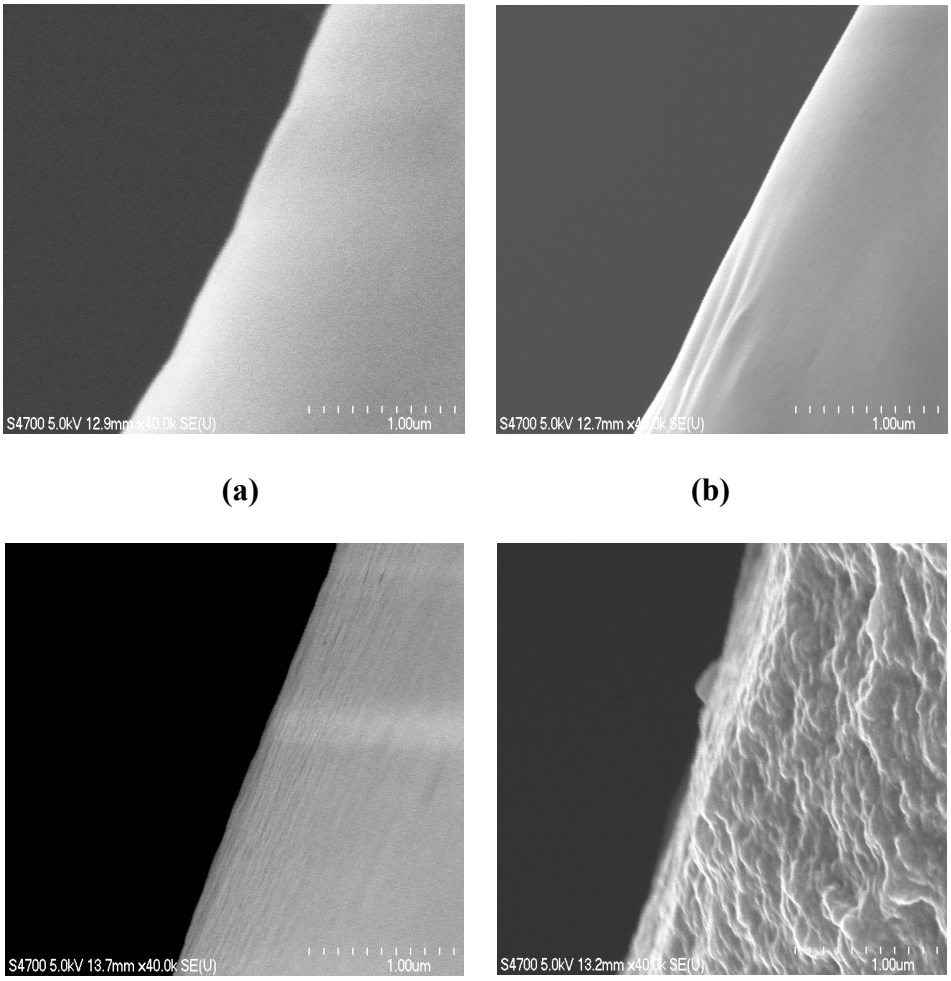

Figure 3.7 SEM images of cross-sectional areas of the PDMS-$BaTiO_3$ composite films. (a) PDMS-$BaTiO_3$ (1-2), (b) PDMS-$BaTiO_3$ (1-4), (c) PDMS-$BaTiO_3$ (1-6), (d) PDMS-$BaTiO_3$ (1-8).

The PDMS-$BaTiO_3$ sample films were cut to examine the morphology and microstructure of the cross-sectional areas by SEM. At lower metal: PDMS ratios, shown in figure 3.7 (a), (b), and (c), the films have a dense structure and the surfaces of the cross-sections are almost smooth. Considering the resolution of the image, it seems

evident that the amorphous $BaTiO_3$ regions formed by the titanium and barium precursors are less than 10 nanometers and uniformly distributed throughout the PDMS matrix. This image also supports the hypothesis of the structural model that the pores of the matrix network are in the single digit nanometer range. It can be seen from Figure 3.7 (d) that with a higher loading of $BaTiO_3$, the cross-sectional surface of the hybrid film becomes rough and grainy which is consistent with phase separation of the barium titanate from the PDMS. This phenomenon is predicted by the proposed structural model, wherein with higher amounts of metal precursors in the system, larger particles are generated which may coalesce to form even larger regions, and eventually phase separation between the inorganic and organic components can result.

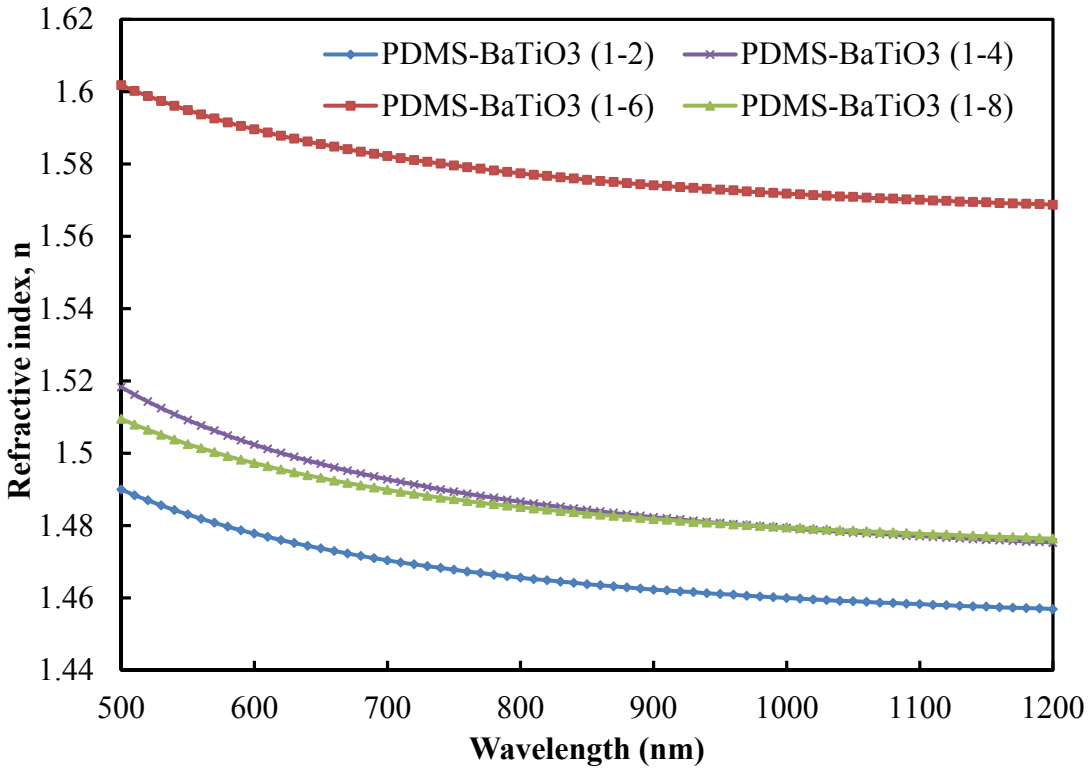

Figure 3.8 Refractive index of PDMS-$BaTiO_3$ hybrid composites

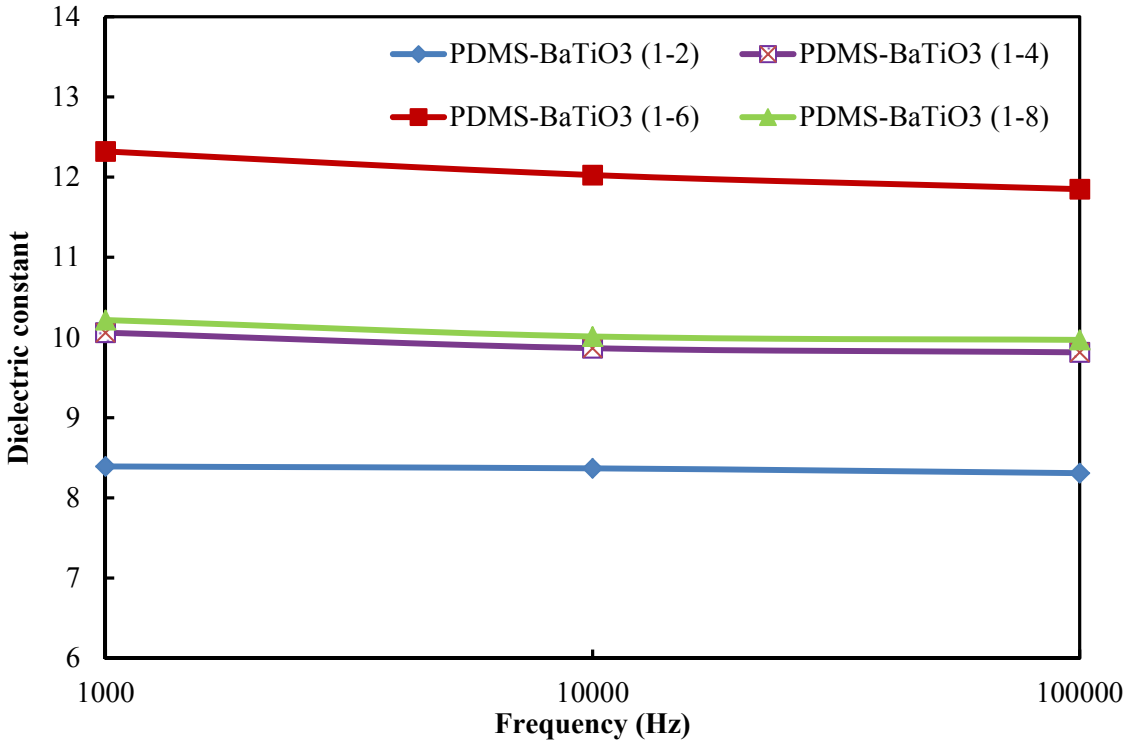

Figure 3.9 Variation of dielectric constant with frequency

Figure 3.8 shows the refractive index as a function of wavelength for various compositions of PDMS-$BaTiO_3$ composites. In general, these show that the longer the wavelength, the smaller the refractive index measured. The refractive index of pure PDMS is around 1.4 (19); and as may be seen in the figure, all of the hybrid materials have higher refractive indices by introducing $BaTiO_3$ in the system. For the lower concentration samples, PDMS-$BaTiO_3$ (1-2), PDMS-$BaTiO_3$ (1-4) and PDMS-$BaTiO_3$ (1-6), the refractive indices increase with an increasing ratio of $BaTiO_3$. However, when the amount of $BaTiO_3$ is too high (PDMS-$BaTiO_3$ (1-8)), phase separation occurs and the refractive index decreases significantly. This result is consistent with the structural model and the SEM images. The same trend is apparent in the measurement of dielectric constants for the hybrids. The automatic capacitance meter with our sample cell was first

calibrated at different frequencies using standard materials. Once calibrated, this apparatus was used to test the capacitance of our hybrid films. The capacitances measured were used in equation 3-10 to calculate the corresponding dielectric constants, and the results are plotted in Figure 3.9. As shown in Figure 3.9, it may be seen that over the measured frequency range of 10^3-10^5 Hz, the dielectric constants of the PDMS-$BaTiO_3$ composites decrease slightly with increasing frequency. For PDMS-$BaTiO_3$ composites with a ratio less than 1:8, higher dielectric constants are obtained with increasing $BaTiO_3$ concentration. However, for the hybrid films with a very high ratio of $BaTiO_3$ (PDMS-$BaTiO_3$ (1-8)) in the system, the value of dielectric constant greatly decreases. As with the refractive index, again this is most likely due to phase separation as described by the structural model and shown in the SEM images.

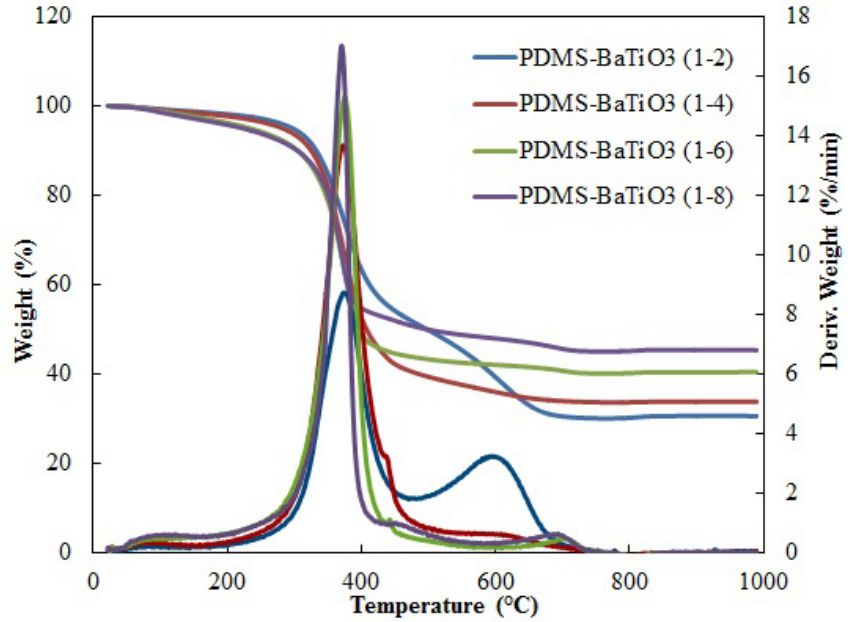

Figure 3.10 TGA curve of PDMS-$BaTiO_3$ with various compositions

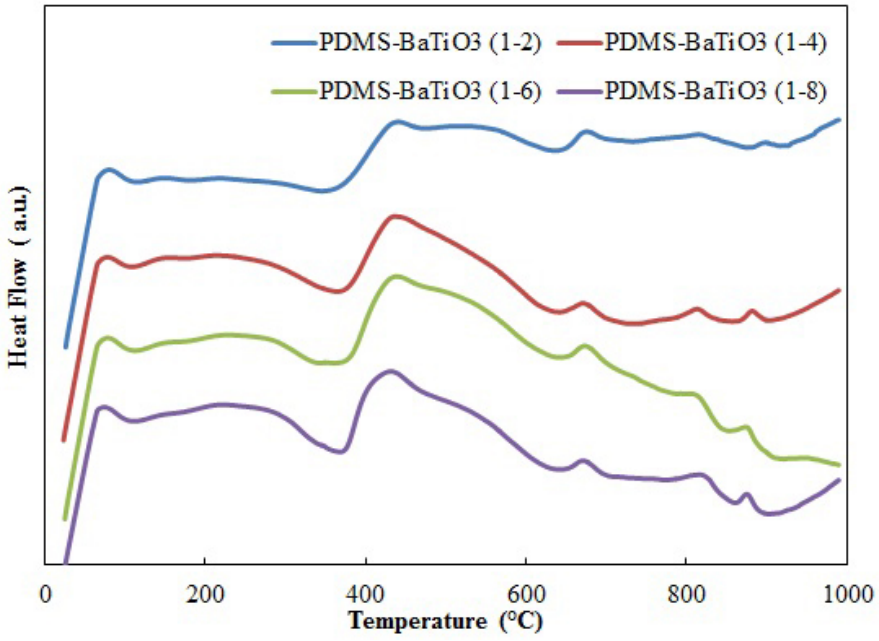

Figure 3.11 DSC curve of PDMS-$BaTiO_3$ with various compositions

Differential scanning calorimetry (DSC) and thermogravimetric analysis (TGA) of the PDMS-$BaTiO_3$ hybrids as a function of composition are shown in Figures 3.10 and 3.11. It can be seen that there is an endothermic peak around 100 °C with no significant weight loss which may be attributed to the vaporization of the water. As shown in the derivative weight curves from 200 °C to 500 °C, although the main weight loss occurs in one step, the derivative weight loss peaks are asymmetric, especially for samples with high metal compositions. The skewness of the peak to lower temperature (200 °C to 100 °C) is caused by the evaporation of trapped solvent and the chemical modifier EAcAc in the pores of matrix, which corresponds to an endothermic peak in DSC curves. The decomposition of PDMS composites starts from 350 °C to 500 °C and is related to the exothermic peaks in DSC curves (20-22). It can be seen that the PDMS-$BaTiO_3$ (1-2) sample decomposes at the highest temperature and in two distinct steps displayed by another derivative peak from 500 °C to 700 °C. This can be explained by the structural model, where PDMS-$BaTiO_3$ (1-2) has the most cross-linked structure that requires the highest decomposition temperature and it may also need a second step to fully decomposed. On further heating, an exothermic peak appears around 680 °C can be ascribed to the formation of SiC or the cross-linking of polymer chains (23). For PDMS-$BaTiO_3$ (1-2). this also corresponds to the second decomposition temperature. At lower temperature, the cross-linked chains don't fully decompose until heated to this higher temperature. From the results of the TGA curves, it is shown that the higher the ratio of $BaTiO_3$, the lower the total weight loss. This is because, for a unit mass, composites with a higher ratio of $BaTiO_3$ contain lower amount of PDMS which is the main factor of decomposition weight loss. The exothermic peak at 810 °C is the anatase TiO_2 in the

matrix changing to a rutile structure. The exothermic peak around 870 °C is the tetragonal crystallization of $BaTiO_3$.

3.4.2 Effect of curing temperature

As proposed in the hypothesis and seen from the SEM images, the network of hybrids structure may consist of pores of nanometer dimensions containing isopropanol solvent, which is hard to remove until heated. One temperature of 60 °C below and the other temperature of 100 °C above the boiling point of isopropanol were chose as the annealing temperatures. After the PDMS-$BaTiO_3$ hybrid nanocomposites were initially synthesized, they were dried in the ambient air, and heated up in an oven at 60 °C or 100 °C. Samples with the same composition, but annealed at different temperatures were characterized to examine the effect of temperature on the refractive index, dielectric constant and thermal properties of the resulting hybrid films.

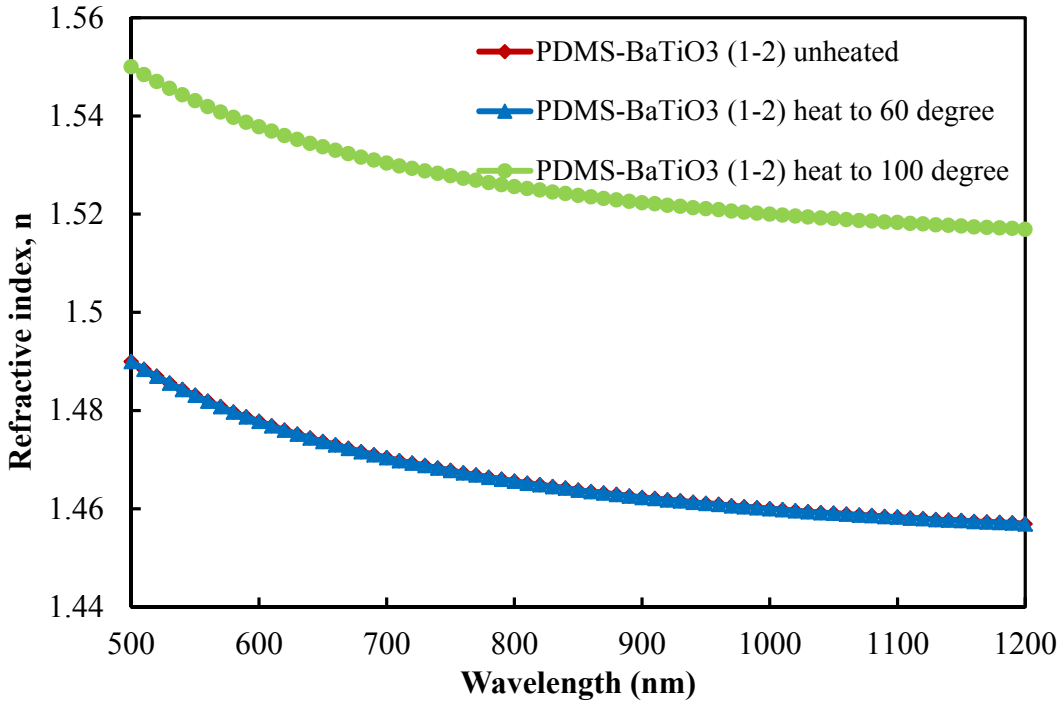

Figure 3.12 Refractive index of PDMS-$BaTiO_3$ (1-2) annealed at different temperatures

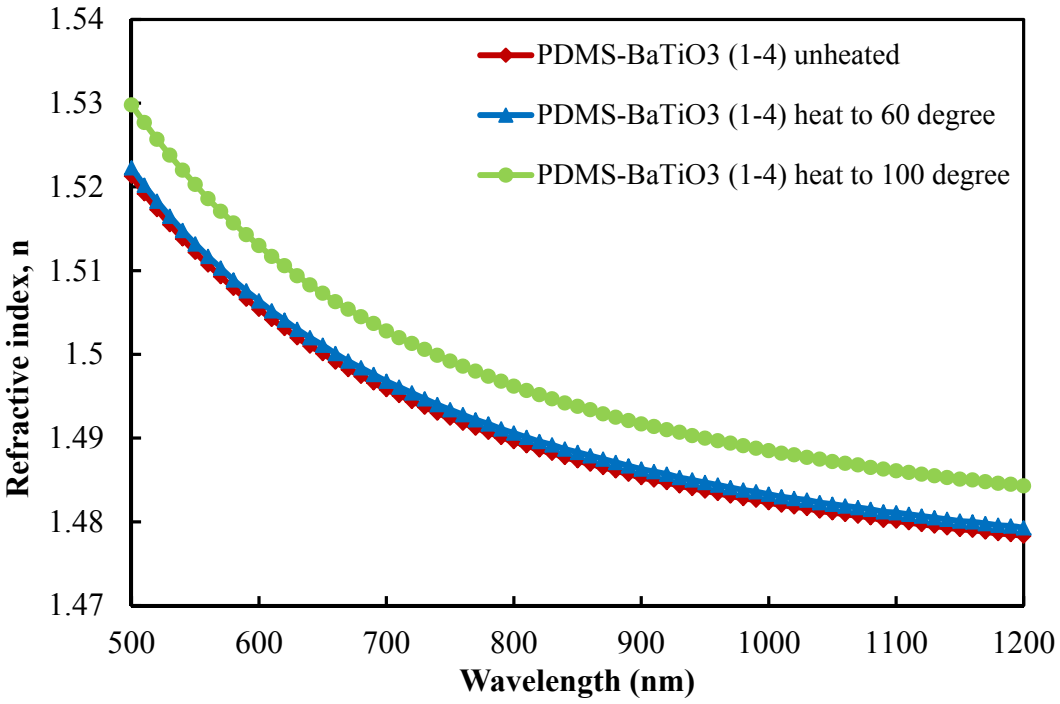

Figure 3.13 Refractive index of PDMS-$BaTiO_3$ (1-4) annealed at different temperatures

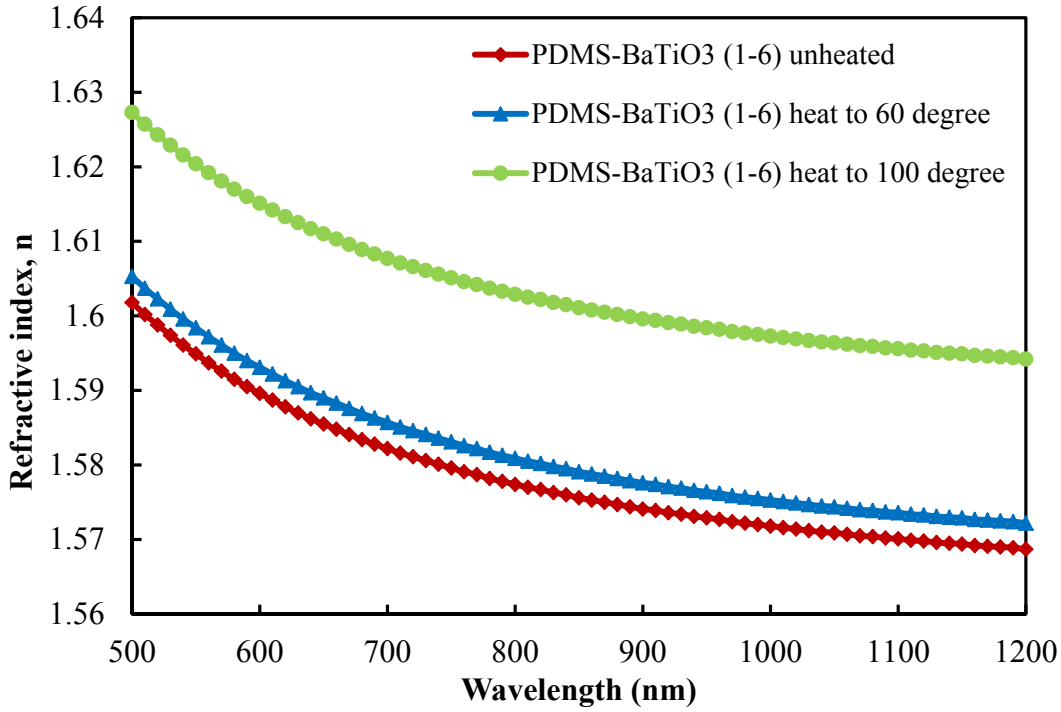

Figure 3.14 Refractive index of PDMS-$BaTiO_3$ (1-6) annealed at different temperatures

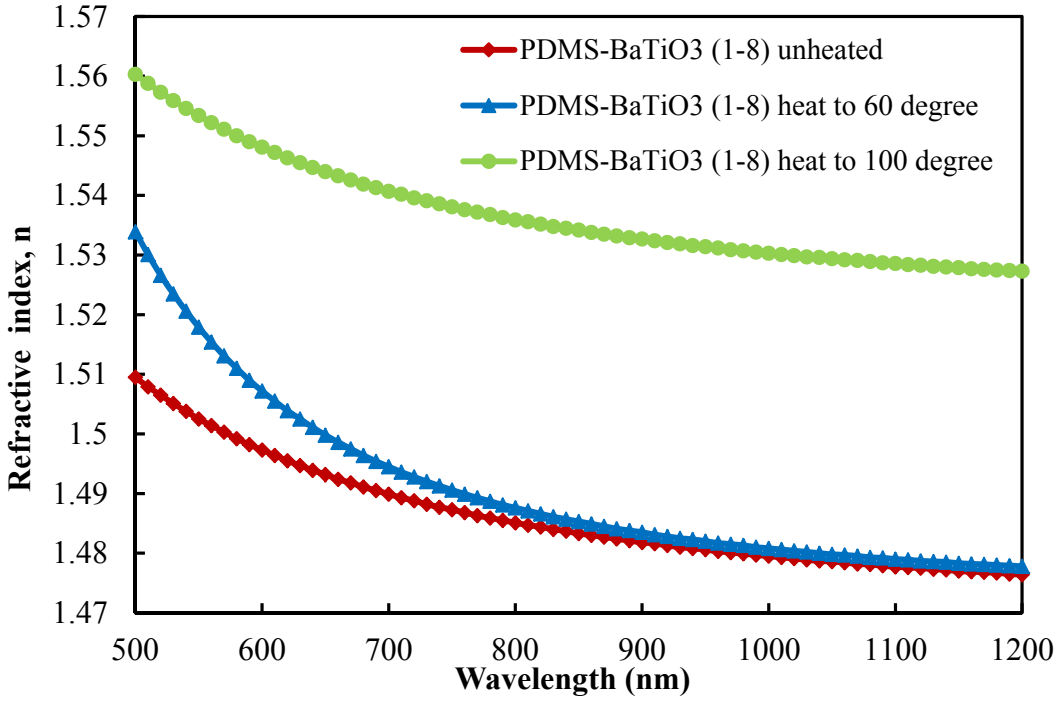

Figure 3.15 Refractive index of PDMS-$BaTiO_3$ (1-8) annealed at different temperatures

PDMS-$BaTiO_3$ composite samples were spin-coated on silicon wafers and tested on ellipsometer for refractive index. The coated wafers were air dried and then heated in an oven for 6 hours at 60 °C and 100 °C respectively. As shown in the Figures 3.12 through 3.15, the air dried and the 60 °C annealed PDMS-$BaTiO_3$ samples have almost the same refractive index over the measured wavelength range of 500-1200 nm. It appears that the lower annealing temperature of 60 °C does not change the structure of PDMS-$BaTiO_3$ composites or the amorphous $BaTiO_3$ state in the system. However, when annealed at 100 °C, the refractive indices are significantly increased. This is because annealing at 100 °C, although the state of $BaTiO_3$ is not altered, some of the residual solvent and the chemical modifier EAcAc in the network pores are evaporated out and the refractive index increases as a result.

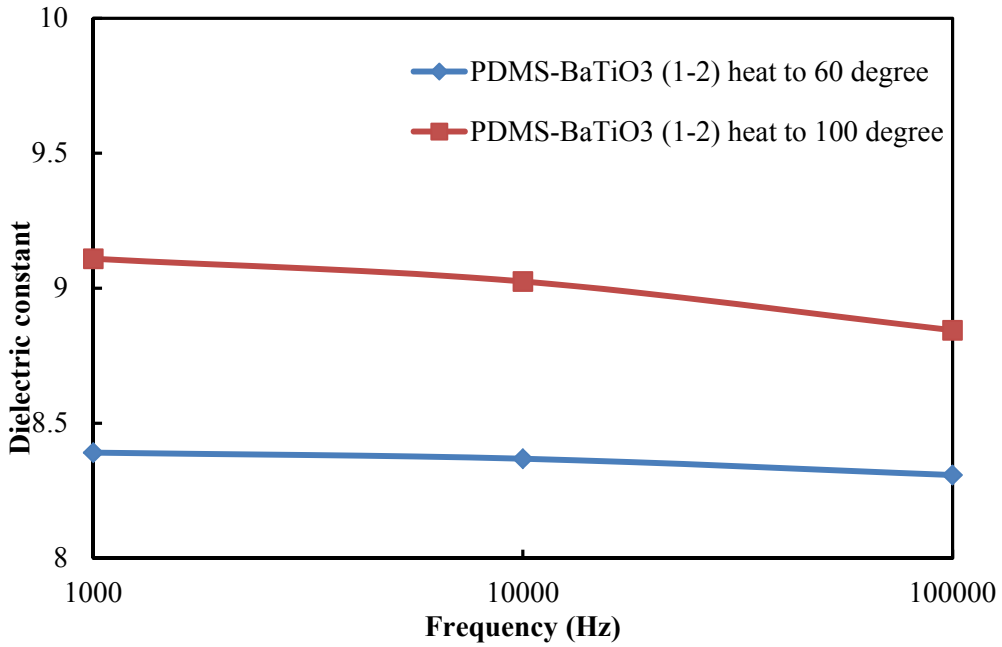

Figure 3.16 Dielectric constant of PDMS-$BaTiO_3$ (1-2) annealed at different temperatures

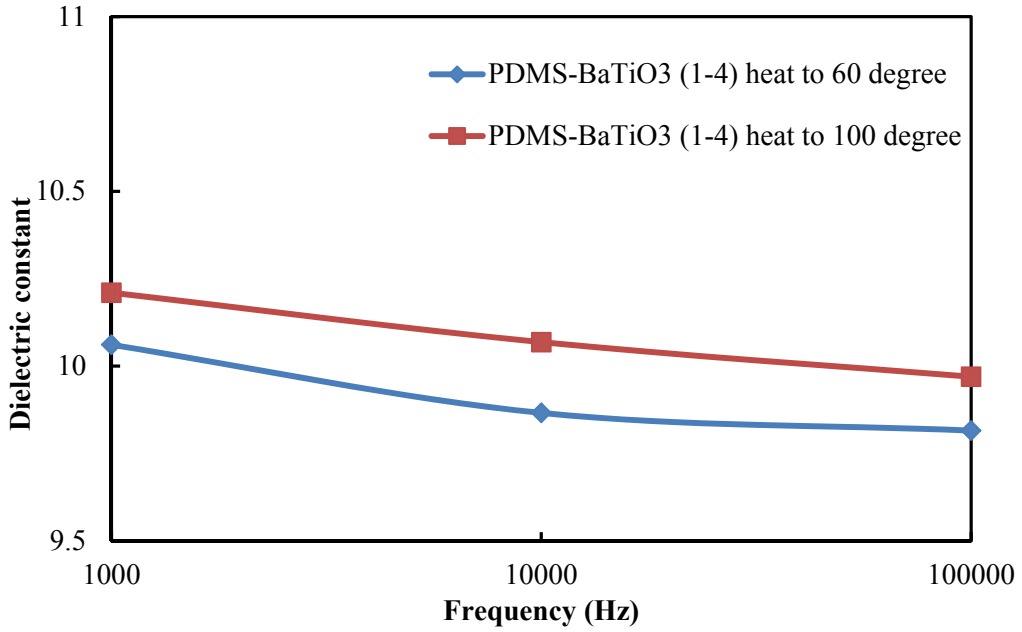

Figure 3.17 Dielectric constant of PDMS-$BaTiO_3$ (1-4) annealed at different temperatures

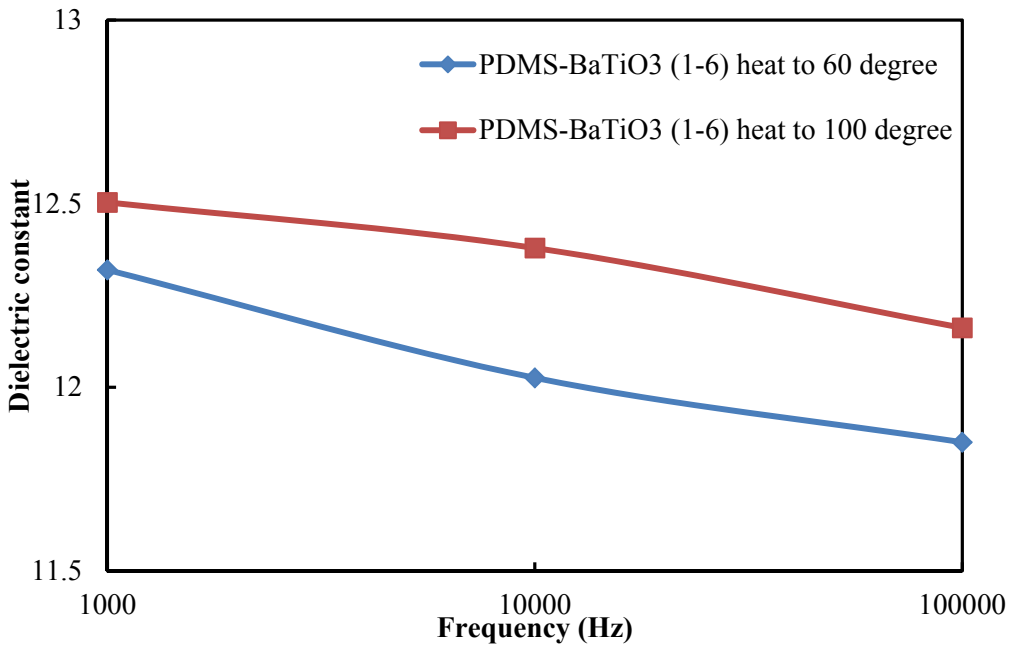

Figure 3.18 Dielectric constant of PDMS-$BaTiO_3$ (1-6) annealed at different temperatures

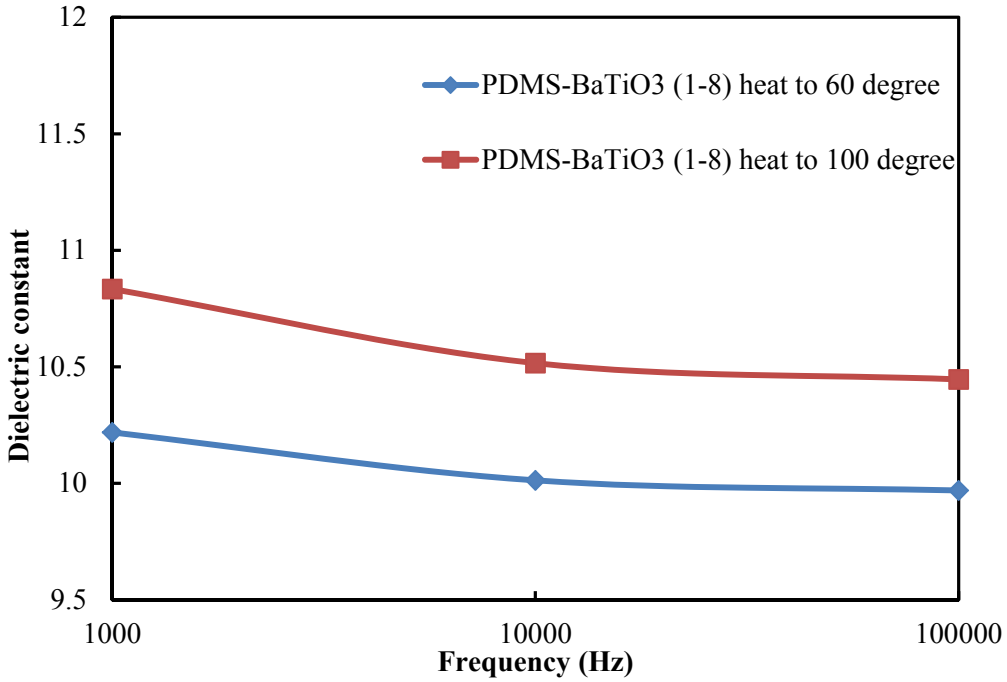

Figure 3.19 Dielectric constant of PDMS-$BaTiO_3$ (1-8) annealed at different temperatures

The dielectric constants of the PDMS-$BaTiO_3$ composites annealed at different temperatures are depicted in Figures 3.16 through 3.19. It can be seen that there is a slight decrease for dielectric constant with increasing frequency in the range of 10^3-10^5 Hz. When the annealing temperature is raised from 60 °C to 100 °C, the dielectric constants are significantly increased to higher values, most likely due once again to the evaporation of the solvent and the chemical modifier EAcAc from the pores of the composites during annealing.

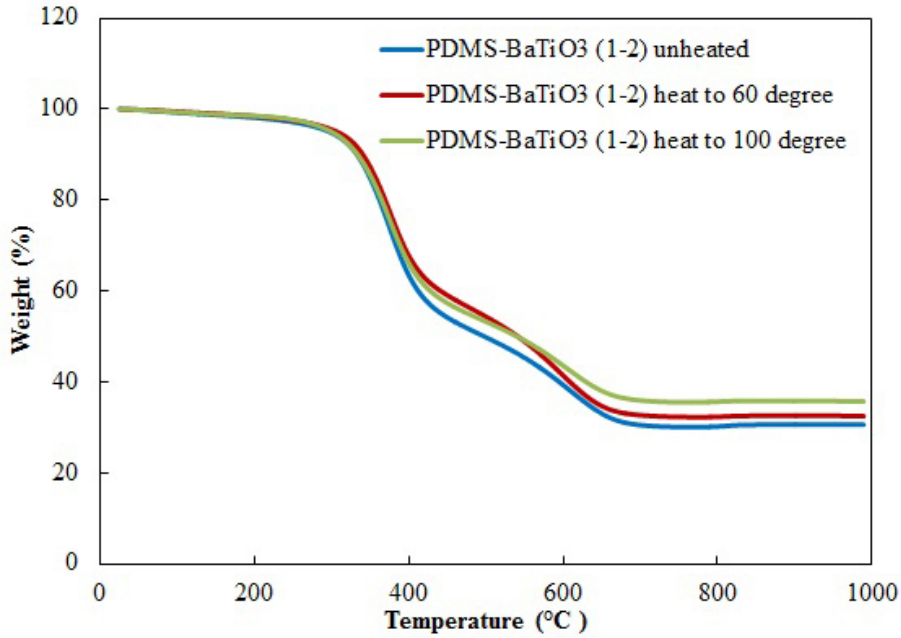

Figure 3.20 TGA curve of PDMS-$BaTiO_3$ (1-2) annealed at different temperatures

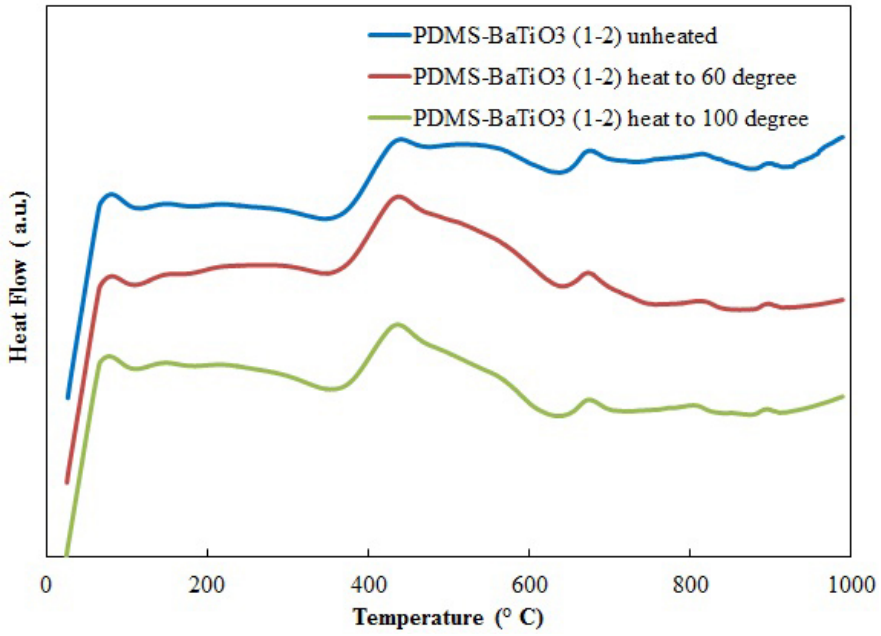

Figure 3.21 DSC curve of PDMS-$BaTiO_3$ (1-2) annealed at different temperatures

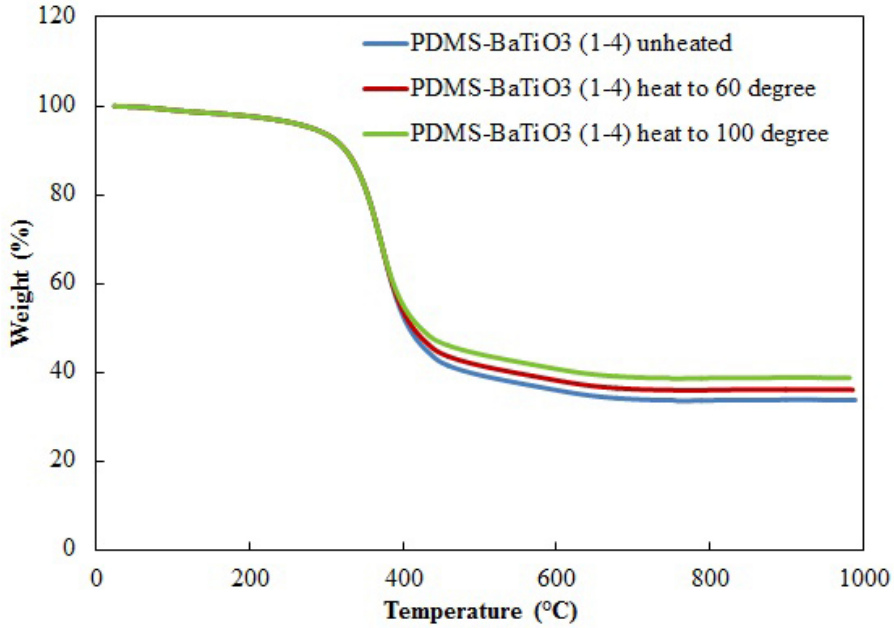

Figure 3.22 TGA curve of PDMS-$BaTiO_3$ (1-4) annealed at different temperatures

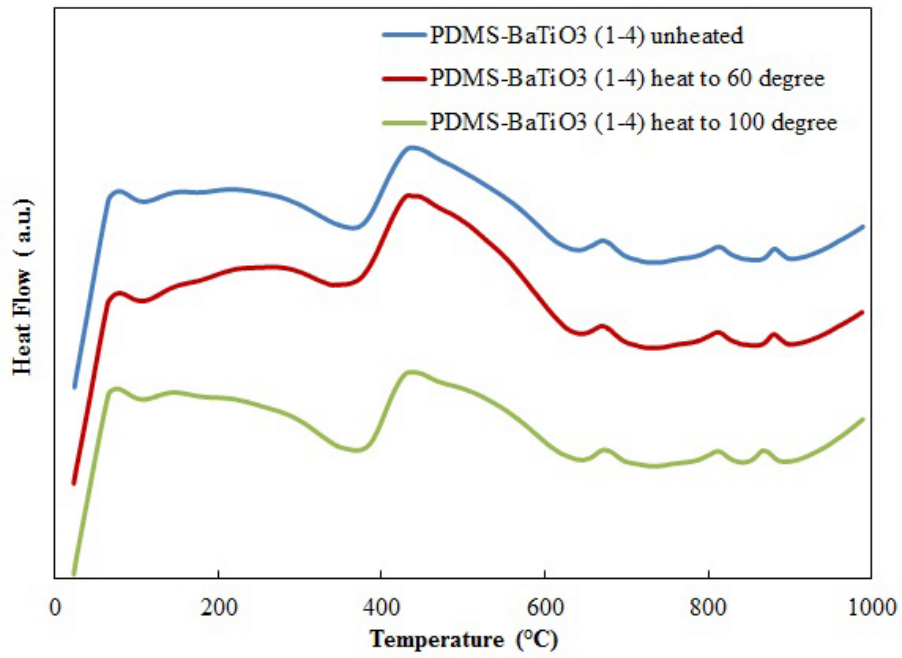

Figure 3.23 DSC curve of PDMS-$BaTiO_3$ (1-4) annealed at different temperatures

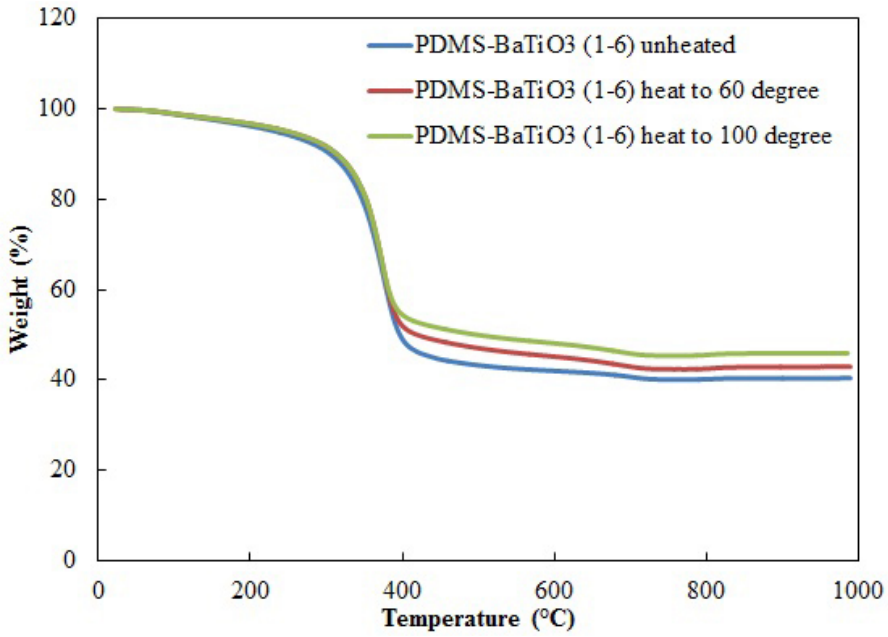

Figure 3.24 TGA curve of PDMS-BaTiO3 (1-6) annealed at different temperatures

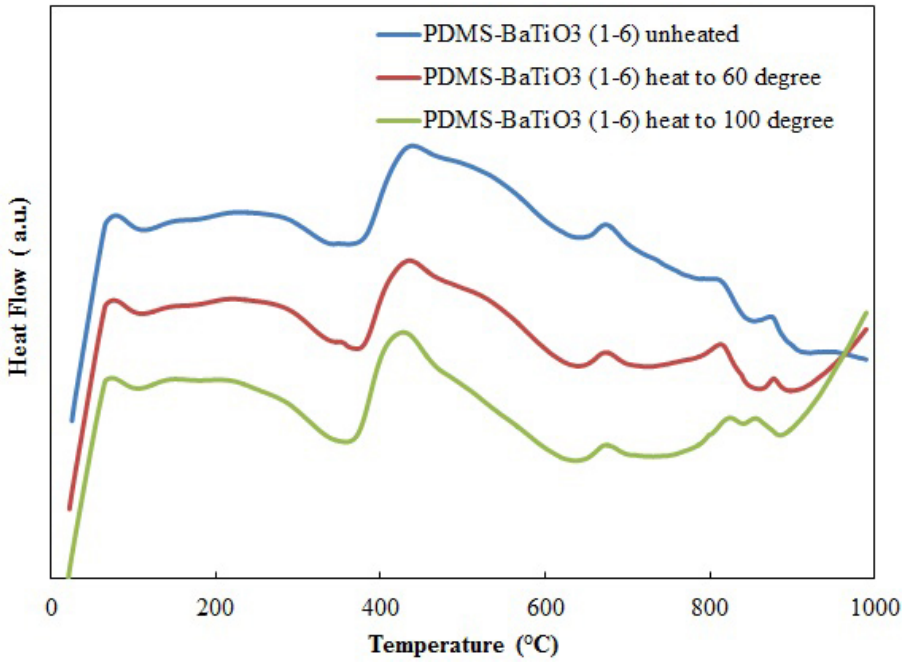

Figure 3.25 DSC curve of PDMS-BaTiO3 (1-6) annealed at different temperatures

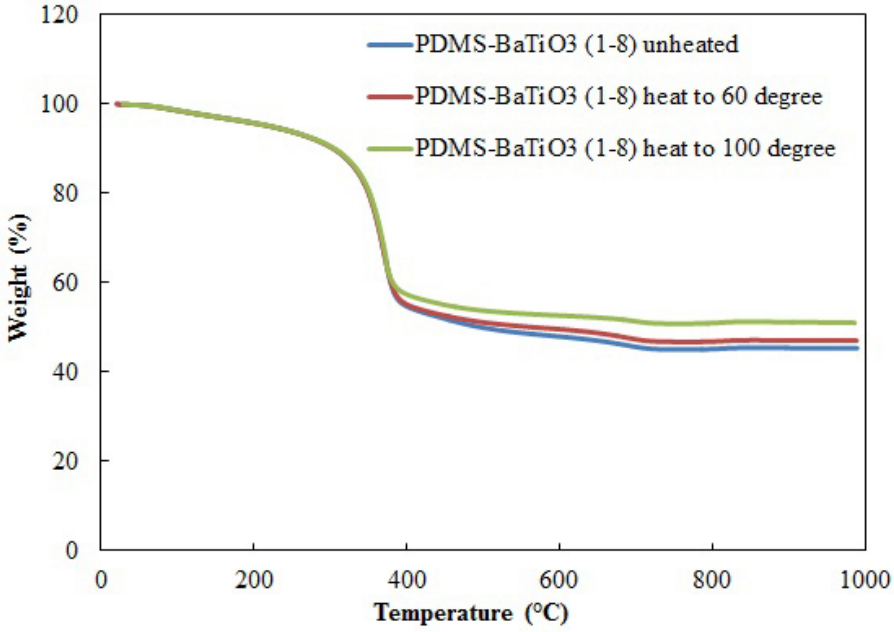

Figure 3.26 TGA curve of PDMS-$BaTiO_3$ (1-8) annealed at different temperatures

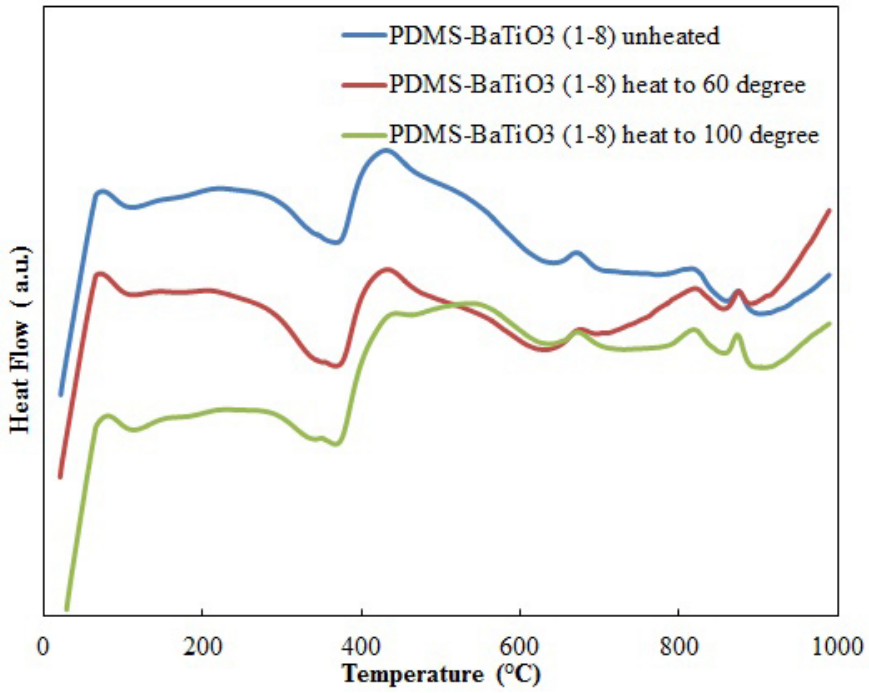

Figure 3.27 DSC curve of PDMS-BaTiO3 (1-8) annealed at different temperatures

As shown in the TGA-DSC curves above, the higher the annealing temperature, the lower the percentage the weight loss. This weight loss reduction is caused by the release of the trapped isopropanol and EAcAc in the pores, or residually bonded EAcAc. As discussed above, titanium is fully hydrolyzed during curing which means that most of the bonded EAcAc would release from the hybrids. However, since the EAcAc is difficult to remove, some still connected with titanium may not evaporate until annealed at higher temperatures.

3.5 Conclusion

The chemical and structural model proposed has been verified by the results of our characterization. Titanium isopropoxide was modified by EAcAc to form a compound

with a lower hydrolysis rate and then reacted with barium to generate amorphous Ba-Ti particles. When PDMS was introduced into the system, it cross-linked with the Ba-OH on the surfaces of the particles to produce hybrids nanocomposites. After curing and releasing EAcAc from the system, the final structure of the hybrids contain amorphous $BaTiO_3$ particles connected with PDMS and uniformly dispersed in the matrix, some amorphous TiO_2 particles may also be distributed in the network. The hybrids produced contain pores in nanometer range containing residual solvents. Nanocomposites with wide molar ratios of titanium and barium precursors to PDMS were successfully synthesized, from 2-1 to 8-1. The lower the ratio of titanium and barium precursors, the more cross-linked the structure created, with smaller and the fewer barium titanate particles present. The refractive index and dielectric constant increased with the amount of $BaTiO_3$ in the system. The highest refractive index and dielectric constant obtained was 1.6 and 12.2 respectively with sample PDMS-$BaTiO_3$ (1-6). However, when the ratio of $BaTiO_3$ to PDMS reached as high as 8 to 1, phase separation occurs and the refractive index and dielectric constant dropped to much lower values. Some residual EAcAc associated with the titanium precursor is released during annealing. When the composites were annealed at 60 °C, no significant effect on the hybrid properties was observed. However, upon increasing the annealing temperature to 100 °C, the refractive index and dielectric constant were improved due to removal of residual EAcAC and solvents.

3.6 References

1. Windlass, H., et al. Colloidal processing of polymer ceramic nanocomposite integral capacitors. Ieee Transactions on Electronics Packaging Manufacturing. 2003; 26(2): 100-105.
2. Ramesh, S., et al. Dielectric nanocomposites for integral thin film capacitors: Materials design, fabrication, and integration issues. Ieee Transactions on Advanced Packaging. 2003; 26(1): 17-24.
3. Kobayashi, Y., et al. Fabrication and dielectric properties of the BaTiO3-polymer nano-composite thin films. Journal of the European Ceramic Society. 2008; 28(1): 117-122.
4. Rao, Y., et al. Novel polymer-ceramic nanocomposite based on high dielectric constant epoxy formula for embedded capacitor application. Journal of Applied Polymer Science. 2002; 83(5): 1084-1090.
5. Bhattacharya, S.K., R.R. Tummala. Integral passives for next generation of electronic packaging: application of epoxy/ceramic nanocomposites as integral capacitors. Microelectronics Journal. 2001; 32(1): 11-19.
6. Kozuka, H., A. Higuchi. Stabilization of poly(vinylpyrrolidone)-containing alkoxide solutions for thick sol-gel barium titanate films. Journal of the American Ceramic Society. 2003; 86(1): 33-38.
7. Tsay, J.D., T.T. Fang. Effects of temperature and atmosphere on the formation mechanism of barium titanate using the citrate process. Journal of the American Ceramic Society. 1996; 79(6): 1693-1696.
8. Choudhury, A. Dielectric and piezoelectric properties of polyetherimide/BaTiO3 nanocomposites. Materials Chemistry and Physics. 2010; 121(1-2): 280-285.
9. Y. Kobayashi, T.T., T. Tabata, T. Miwa, M. Konno. Fabrication and dielectric properties of the BaTiO3-polymer nanocomposite thin films. Journal of the European Ceramic Society. 2008; 28: 117-122.
10. Chandradass, J., D.S. Bae. Preparation and properties of barium titanate nanopowder/epoxy composites. Materials and Manufacturing Processes. 2008; 23(2): 117-123.

11. Wen, J., J.E. Mark. Precipitation of Silica-Titania Mixed-Oxide Fillers into Poly(Dimethylsiloxane) Networks. Rubber Chemistry and Technology. 1994; 67(5): 806-819.
12. Yabuta, T., et al. Synthesis of blood compatible PDMS-based organic-inorganic hybrid coatings. Journal of Sol-Gel Science and Technology. 2004; 31(1-3): 273-276.
13. Tangwiwat, S., S.J. Milne. Barium titanate sols prepared by a diol-based sol-gel route. Journal of Non-Crystalline Solids. 2005; 351(12-13): 976-980.
14. Shindou, T., et al. Effect of composition on surface properties of polydimethylsiloxane-based inorganic/organic hybrid films. Journal of Sol-Gel Science and Technology. 2004; 30(3): 229-237.
15. Nakade, M., M. Ogawa. Synthesis and characterization of zinc oxide fine particles coated with titania/PDMS hybrid. Journal of Materials Science. 2007; 42(12): 4254-4259.
16. Maria J. Mosquera, D.M.d.l.S., Lucila Valdez-Castro, Luis Esquivias. New route for producing crack-free xerogels: obtaining uniform pore size. Journal of Non-Crystalline Solids. 2008; 354: 645-650.
17. Sung Chul Bae, H.L., Zhiqun Lin, Steve Granick. Chemical Imaging in a Surface Forces Apparatus: Confocal Raman Spectroscopy of confined Poly(dimethylsiloxane). Langmuir. 2005; 21: 5685-5688.
18. Zhu, X.H., et al. Morphology and atomic-scale surface structure of barium titanate nanocrystals formed at hydrothermal conditions. Journal of Crystal Growth. 2009; 311(8): 2437-2442.
19. Bliss, C.L., J.N. McMullin, C.J. Backhouse. Rapid fabrication of a microfluidic device with integrated optical waveguides for DNA fragment analysis. Lab on a Chip. 2007; 7(10): 1280-1287.
20. MASATO NAKADE, KOSUKE ICHIHASHI, MAKOTO OGAWA. Microporous materials derived from the thermal decomposition of the titania/PDMS hybrid particles. Journal of Porous Materials. 2005; 12: 79-85.

21. T. Howard, T. C. Kendrick. Thermal analysis of polydimethylsiloxane. I. Thermal degradation in controlled atmospheres. Journal of Polymer Sicence: Part A-2. 1969; 7: 537-549.
22. S. R. Gomes, F. M. A. Margaca, D. Faria Silva, L. M. Ferreira, I. M. Miranda Salvado, A. N. Falcao. Novel way to control PDMS cross-linking by gamma-irradiation. Nuclear Instruments and Methods in Physics Research B. 2008; 266: 1105-1108.
23. Shukla, S.K., et al. Some thermal studies of polysilanes and polycarbosilanes. Thermochimica Acta. 2004; 424(1-2): 209-217.

4. In situ Synthesis of High Refractive Index PDMS/Metal Oxide Nanocomposites

Qiaoyu Lu and Michael E. Mullins
Department of Chemical Engineering, Michigan Technological University, 1400 Townsend Drive, Houghton, MI 49931, U.S.A.

4.1 Abstract

Organic-inorganic hybrids have been prepared with tailorable and enhanced properties which are unachievable using polymers or ceramics alone. By combining the flexibility of polymers with the electronic and optical properties of ceramic materials, these hybrids offer great potential for many optical, electrical and mechanical applications. Silicone polymers because of their desirable surface properties, excellent physical properties, heat stability, and high resistance to chemical and UV attack, have been widely used. Hybrid siloxane-metal oxide gels have been prepared via sol-gel techniques, by using hydroxyl-terminated polydimethylsiloxanes (PDMS) crosslinked by metallic alkoxides, M(OR)n. In this technique, the use of organic solvents permits organic and inorganic components to be combined at a molecular level with the desired composition. By varying the type and percentage of metal alkoxides during synthesis, transparent and homogeneous organic-inorganic hybrid materials with unique properties were obtained. Also a secondary metal oxide species was introduced to synthesize binary metal oxide-PDMS hybrids. Systematic experiments were carried out to study the effect of the reaction conditions and metal alkoxides-PDMS ratios on the properties of the final hybrids. These

---

The material contained in this chapter was previously published in MRS proceedings.

composition and the properties of the transparent inorganic-organic hybrids were investigated and characterized by ellipsometer and Fourier Transform Infrared (FTIR) spectroscopy. Experimental results showed that the refractive index of the hybrid materials exhibits a proportional relationship with the metal oxide content, the higher the metal oxide content the higher the refractive index. The refractive index was increased from 1.4 of PDMS to 1.7 of metal oxide-PDMS hybrid with highest prepared metal oxide loading. From the FTIR spectra, the structures of the hybrids for various metal oxide-PDMS compositions were examined.

4.2 Introduction

The organic-inorganic hybrids have received special attention in recent years because of their versatile composition, structure, and properties. By combining properties of organic and inorganic components, these hybrids have numerous applications in optical, mechanical, chemical, electrical and biological fields. There are many methods can be used to obtain organic-inorganic composite materials, among which the sol-gel technique has been widely used (1-5). In this technique, metal alkoxides or metal chlorides as precursors undergo hydrolysis and polycondensation reactions to form a metal oxide network at low temperatures and incorporate the organic component into inorganic oxide network at molecular level. This approach has several advantages as compared to other techniques, such as low costs, low temperature of heat treatment, unique ability to achieve molecular level uniformity in the synthesis of organic-inorganic composites, and strong adhesion of the coating to the substrates(6,7).

The high elasticity, excellent relaxation properties, hydrophobicity and transparent of polydimethylsiloxane (PDMS) have made it widely studied as an organic precursor in the polymer sol-gel reaction (8-19). Two types of PDMS, hydroxyl terminated and methyl terminated, are suitable candidates for the synthesis of hybrids which can co-condensate with metal alkoxides to form a covalently bonded network. By introducing metal oxide components into PDMS-based hybrids, optical properties such as refractive index may be increased to a much higher level by the incorporated metallic ions. Aside from tetraethoxysilane, which was primarily used as the inorganic component to incorporate with PDMS in the past, other metal alkoxides of Ti, Zr, Al, Ta, etc. are now incorporated into the hybrids to improve the mechanical, thermal and optical properties.

Because of its high chemical and thermal stability, photocatalytic activity and refractive index, titania is widely used to make titania-containing hybrid nanocomposites. In our work, by controlling the basic reaction mechanism, transparent PDMS-TiO_2 hybrids were synthesized using titanium isopropoxide as the metal alkoxide precursor. The molar ratio of $Ti(OR)_4$/PDMS ranges from 5:1 to 20:1. In addition to titanium dioxide, we also prepared PDMS-binary metal oxide hybrids. Barium titanate is an important ceramic material due to its high refractive index and especially high dielectric constant. However, due to high reactivity, the preparation of PDMS-$BaTiO_3$ has not been reported yet. In this paper, barium titanate binary metal oxide was synthesized *in situ* to prepare PDMS-$BaTiO_3$ using the sol-gel technique. Ethyl acetoacetate as a chelating agent was used to inhibit titanium alkoxide reaction with water in the system. The structure, optical and electronic properties of the synthesized PDMS-based nanocomposites were studied.

4.3 Experiment

Titanium isopropoxide (TTIP) Ti $(OCH(CH_3)_2)_4$ (97%) and barium acetate (99%) purchased from Sigma Aldrich were used as precursors of inorganic components. Hydroxy terminated poly(dimethylsiloxane) (PDMS) with an average molecular weight of 3500 was provided by the Dow Corning Corporation. Isopropanol and ethanol (anhydrous, PHARMCO-AAPER) were used as solvents. Ethyl acetoacetate (EAcAc) (Sigma Aldrich) was used as a chemical modifier of the metal alkoxide to decrease the hydrolysis rate. Water was distilled and deionized. All the chemicals were used without further purification.

4.3.1 Synthesis of PDMS-TiO_2

First, 0.6ml of titanium isopropoxide (TTIP) was mixed with 1ml isopropanol (IPA). The appropriated amount of PDMS was diluted with isopropanol in another bottle and sonicated for 5 min. Then the TTIP-IPA solution was dripped into PDMS-IPA bottle which was stirred and heated in an oil bath at 70°C. After stirring for 30 min, the sample was removed from the heat and spin coated on silicon wafer to test refractive index. The rest of the sample was poured out to an aluminum dish to make a film. The wafer and the film were annealed in an oven at 50°C for 1d, 70°C for 1d and 100°C for 1d. The compositions of the PDMS-TiO_2 composites are summarized in Table 4.1.

Table 4.1

Composition of PDMS-TiO_2 nanocomposites.

Sample	Molar ratio of TTIP:PDMS	Molar ratio of Ti:Si (theoretical value)	TTIP wt% (theoretical value)
TTIP-PDMS (5-1)	5:1	5:47	29%
TTIP-PDMS (10-1)	10:1	10:47	45%
TTIP-PDMS (15-1)	15:1	15:47	55%
TTIP-PDMS (20-1)	20:1	20:47	62%

4.3.2 Synthesis of PDMS-$BaTiO_3$

Titanium isopropoxide and barium acetate were used as precursors. Ethyl acetoacetate was used as a chemical modifier. The synthesis of PDMS-$BaTiO_3$ was carried out as follows. Titanium isopropoxide (TTIP) mixed with isopropanol was poured into PDMS/isopropanol solution which is stirred and heated in an oil bath at 70°C, the sol was continuously stirred for 30 min. The mixed solution of titanium isopropoxide, isopropanol and ethyl acetoacetate was added into the PDMS solution while stirring at room temperature. Then an equimolar amount of barium acetate dissolved in the mixture of deionized water, ethanol and isopranol was added into this system. The molar ratio of TTIP, EAcAc, barium acetate and deionized water was 1: 4: 1: 200. The sample was poured to an aluminum dish and annealed in an oven at 50°C for 1d, 70°C for 1d and 100°C for 1d.

4.3.3 Characterization

Infrared spectra of the PDMS-based inorganic/organic hybrid films were measured by using a FT-IR spectrometer (BRUKER IFS66). For refractive index measurement, the

PDMS-based sols were first spin-coated on silicon wafer and tested on an ellipsometer (VASE, J.A. Woollam Co., Inc.).

4.4 Discussion

All the PDMS-TiO_2 hybrid films with different compositions were transparent, indicating that no visible precipitate was formed. If aggregates are formed from excess titanium alkoxide, they must be much smaller than the light wavelength. As a typical example, a photograph of the synthesized transparent and flexible PDMS-TiO_2 hybrid film (TTIP-PDMS (15-1)) is shown in Figure 4.1. The structure of the PDMS-TiO_2 hybrid films were examined by FT-IR spectrometer. Figure 4.2 shows the FT-IR spectra of unreacted PDMS and TTIP-PDMS (5-1) after reaction. The broad peak around 3200-3400 cm^{-1} was assigned to the terminal hydroxyl (-OH) groups of PDMS. After the sol-gel reaction, the absorption peak corresponding to the hydroxyl groups disappears (as shown in Figure 4.2 (b)), indicating that most of the –OH groups were reacted with titanium isopropoxide. Figure 4.3 shows the FT-IR spectra of PDMS-TiO_2 films with different compositions. The absorption peaks at around 1400, 1260 and 800 cm^{-1}were assigned to CH_3 groups derived of PDMS (20), while the peak at around 1000-1100 cm^{-1} can be assigned to Si-O-Si of PDMS. In a previous study (21), an absorption band at 960 cm^{-1} was ascribed to Ti-O-Si. This absorption band was not clearly seen in the hybrid film of TTIP-PDMS (5-1), which may be because the relative amounts of Ti-O-Si bonds were small. For the hybrid films of TTIP-PDMS (10-1), TTIP-PDMS (15-1) and TTIP-PDMS (20-1), the intensity of the absorption band at 960 cm^{-1} were almost the same, which indicates that the excess

titanium alkoxide formed nano sized titania in these hybrid films. Figure 4.4 shows the refractive index of composite films for TTIP-PDMS (5-1), TTIP-PDMS (10-1), TTIP-PDMS (15-1) and TTIP-PDMS (20-1) measured at a wavelength in the range from 500-1000nm. As shown in the figure, the refractive index increased with higher titanium alkoxide concentration. For TTIP-PDMS (5-1), TTIP-PDMS (10-1), TTIP-PDMS (15-1) hybrid films, refractive index decreased with the increase of wavelength, but not obvious. However, when the initial titanium alkoxide up to a content of 62% (TTIP-PDMS (20-1)), the wavelength had a huge effect on the refractive index, the longer the wavelength the smaller the refractive index. This is considered to be due to the higher amount of titania formed in the composite which causes the refractive index of the composite to be more like that of titania. In this sample, the refractive index decreases more obviously with the increase of wavelength.

The structure of the PDMS-$BaTiO_3$ hybrid film was measured by FT-IR spectrometer and is shown in Figure 4.5. In the figure, the band assigned to Ti-O-Si at 960 cm^{-1} is shifted to a lower wavenumber, around 920-910 cm^{-1}. Such change should be caused by the incorporation of barium bonded to titanium to form barium titanate in the system.

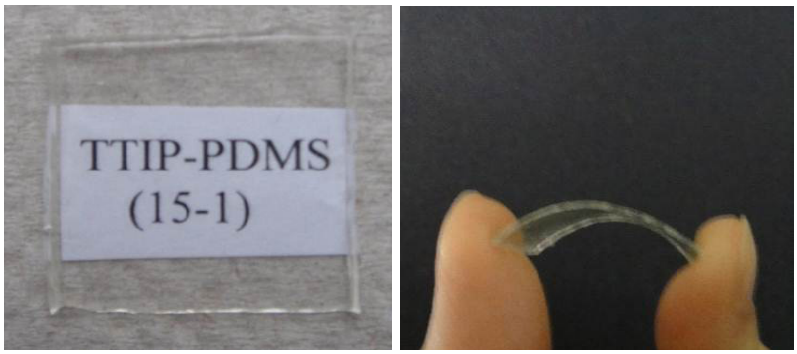

Figure 4.1 Photographs of the synthesized film (TTIP-PDMS (15-1))

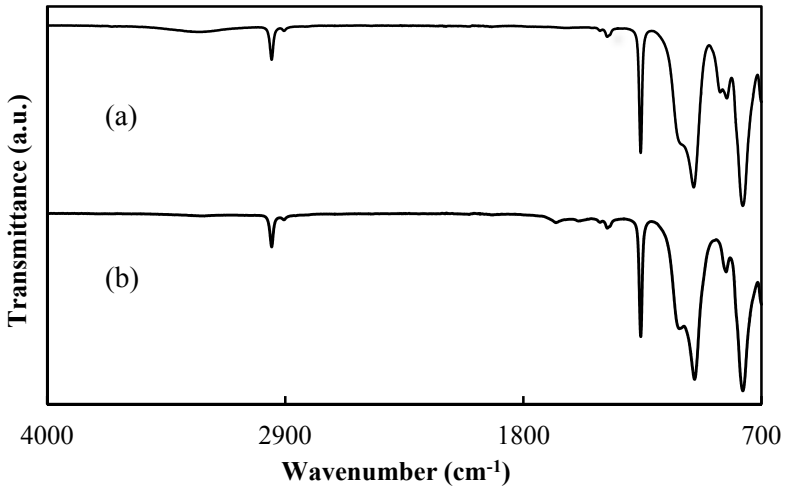

Figure 4.2 FT-IR spectra of (a) PDMS and (b) TTIP-PDMS (5-1)

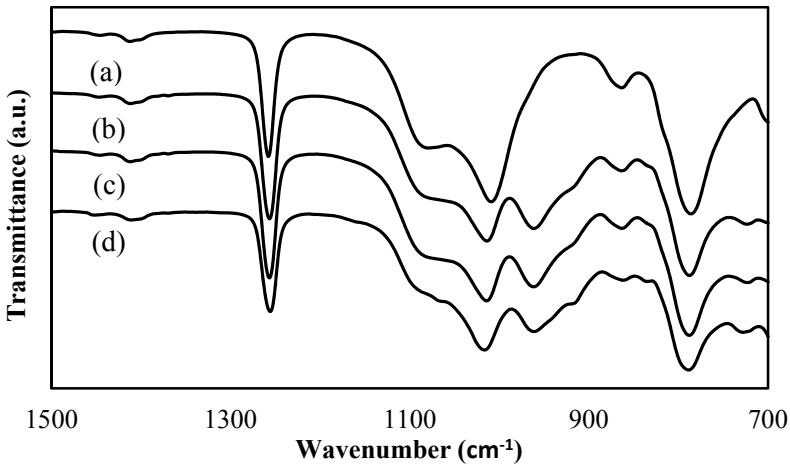

Figure 4.3 FT-IR spectra of PDMS-TiO_2 hybrid films (a) TTIP-PDMS (5-1), (b) TTIP-PDMS (10-1), (c) TTIP-PDMS (15-1), (d) TTIP-PDMS (20-1)

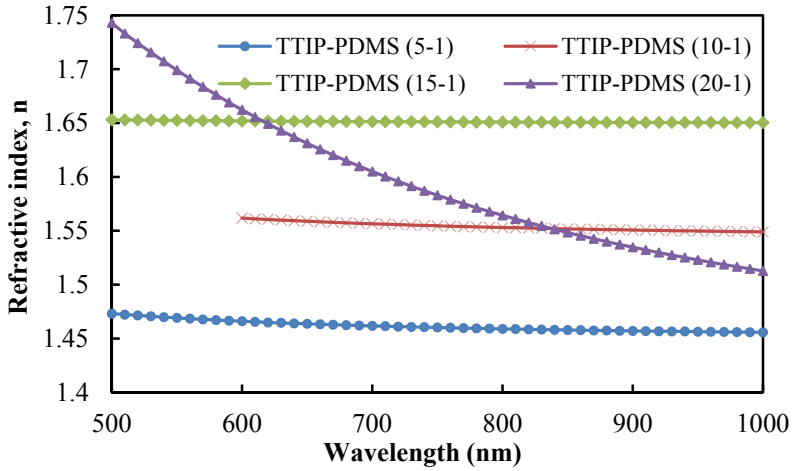

Figure 4.4 Refractive index of PDMS-TiO_2 hybrid films at various compositions

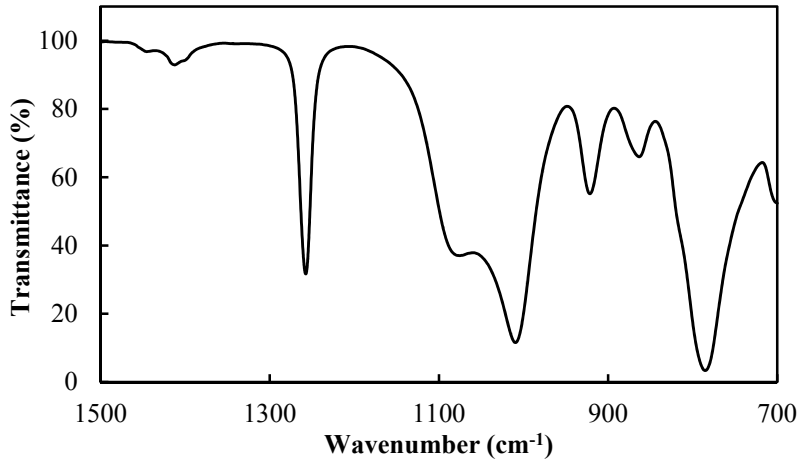

Figure 4.5 FT-IR spectra of PDMS-$BaTiO_3$ hybrid film

4.5 Conclusions

Transparent and flexible PDMS-TiO_2 hybrid films were synthesized with various compositions. The refractive index of the films increased with the increase of the inorganic (titanium) component. When the amount of titanium component was high up to 62%, the structure of the film changed so the refractive index decreased a lot with the

increase of the wavelength. PDMS-$BaTiO_3$ hybrid films were also successfully synthesized.

4.6 References

1. H. Schmidt. Inorganic–organic composites by sol-gel techniques. Journal of Sol-Gel Science and Technology. 1994; 1: 217–231.
2. O. Lev, Z. Wu, S. Bharathi, V. Glezer, A. Modestov, J. Gun, L. Rabinovich, S. Sampath. Sol-gel materials in electrochemistry. Chemistry of Materials. 1997; 9: 2354–2375.
3. C. Sanchez, B. Julia´n, P. Belleville, M. Popall. Applications of hybrid organic-inorganic nanocomposites. Journal of Materials Chemistry. 2005; 15: 3559–3592.
4. Shindou, T., et al. Surface properties of polydimethylsiloxane-based inorganic/organic hybrid films deposited on polyimide sheets by the sol-gel method. Journal of Sol-Gel Science and Technology. 2003; 27(1): 15-21.
5. Husing, N., et al. Novel siloxane-silica nanocomposite aerogels and xerogels. Journal of Sol-Gel Science and Technology. 2003; 26(1-3): 73-76.
6. B.D. Fabes, D.R. Uhlmann. Strengthening of glass by sol-gel coatings. Journal of American Ceramics Society. 1990; 73: 978–988.
7. B. Simionescu, M. Aflori, M. Olaru. Protective coatings based on silsesquioxane nanocomposites films for building limestones. Construction and Building Materials. 2009; 23: 3426–3430.
8. Wang, S.B., J.E. Mark. In situ Precipitation of Reinforcing Titania Fillers. Polymer Bulletin. 1987; 17(3): 271-277.
9. C. S. Parkhurst, W. F. Doyle, L. A. Silverman, S. Singh, M. P. Andersen, D. McClurg, G. E. Wnek, D. R. Uhlmann. Siloxane modified SiO_2-TiO_2 Glasses via Sol-Gel. Materials Research Society Symposium Proceedings. 1986; 73: 769.
10. E. Taylor-Smith, K. M. Choi. Synthesis & Characterization of Optically-Active Lanthanide-Doped Hybrid Inorganic-Organic Systems. Materials Research Society Symposium Proceedings. 1999; 576: 433.

11. J. D. Mackenzie. Sol-Gel Optics I. edited by D. R. Ulrich. Bellingham, WA: SPIE; 1990. 1328p.
12. S. Dire´, F. Babonneau, C. Sanchez, J. Livage. Sol-gel Synthesis of Siloxane-oxide Hybrid coatings [$Si(CH_3)_2O$, MO_x: M= Si, Ti, Zr, Al] with luminescent properties. Journal of Materials Chemistry. 1992; 2: 239.
13. C. Guermeur, J. Lambard, J. F.Gerard, C. Sanchez. Hybrid polydimethylsiloxane-zirconium oxo nanocomposites. Part 1 Characterization of the matrix and the siloxane-zirconium oxo interface. Journal of Materials Chemistry. 1999; 9: 769.
14. B. Alonso, J. Maquet, B. Viana, C. Sanchez. Hybrid organic-inorganic polydimethylsiloxane–vanadium–oxo materials crosslinked at the molecular level. New Journal of Chemistry. 1998; 22: 935.
15. F. Babonneau, L. Bois, Livage. Structural Characterization of Gels Prepared from Co-Hydrolysis of Tetraethoxysilane and Dimethyldiethoxysilane. Journal of Materials Research Society Symposium Proceedings. 1992; 271: 237.
16. F. Babonneau, L. Bois, J. Livage, S. Dire´. Structural Investigation of Sol-Gel-Derived Hybrid Siloxane-Oxide Materials Using Si MAS-NMR Spectroscopy. Materials Research Society Symposium Proceedings. 1992; 286: 289.
17. F. Babonneau, J. Maquet. Nuclear magnetic resonance techniques for the structural characterization of siloxane–oxide hybrid materials. Polyhedron. 2000; 19: 315.
18. C. L. Shutte, J. R. Fox, R. D. Boyer, D. R. Ulhmann. Ultrastructure Processing of Advanced Materials. edited by D. R. Ulhmann and D. R.Ulrich. New York: J. Wiley & Sons; 1992.
19. F. Babonneau. ^{29}Si, ^{17}O Liquid NMR and ^{29}Si CP-MAS NMR Characterization of Siloxane-Oxide Materials, [$(CH_3)_2SiO/TiO_2$, $(CH_3)_2SiO/ZrO_2$]. Materials Research Society Symposium Proceedings. 1994; 346: 949.
20. S. Katayama, Y. Kubo, N. Yamada. Characterization and Mechanical Properties of Flexible Dimethylsiloxane-Based Inorganic/Organic Hybrid Sheets. Journal of American Ceramic Society. 2002; 85: 1157.

21. TAKUYA SHINDOU. Effect of Composition on Surface Properties of Polydimethylsiloxane-based Inorganic/Organic Hybrid Films. Journal of Sol-gel Science and Technology. 2004; 30: 229-237.

5. Conclusions and Future Work

5.1 Conclusions

An *in situ* sol-gel technique was applied to fabricate organic-inorganic hybrid nanocomposites using reactive metal precursors such as titanium isopropoxide and barium acetate within a PolyDiMethylSiloxane (PDMS) matrix. Transparent and homogeneous PDMS-TiO_2 and PDMS-$BaTiO_3$ hybrid nanocomposite films were prepared over a wide range of compositions. Hybrids of PDMS-TiO_2 were fabricated with a low molecular weight silanol terminated PDMS and titanium isopropoxide; whereas PDMS-$BaTiO_3$ were prepared using silanol terminated PDMS, titanium isopropoxide, barium acetate, with the introduction of EAcAc as the chemical modifier to slow the hydrolysis rate of the titanium precursor. Several different ratios of the metal precursors, hybrids of PDMS-TiO_2 and PDMS-$BaTiO_3$ were synthesized to evaluate the effect of composition on the hybrid's chemical structure, physical, electronic, and optical properties. The chemical structure of the hybrids was characterized by a combination of FTIR and FT-Raman. FESEM was employed to examine the morphology of cross-sections of the hybrid sample films. The optical and electronic properties of the nanocomposites were evaluated by ellipsometry and electrical capacitance respectively. A simultaneous DSC/TGA instrument was utilized to determine the hybrid's thermal properties. The PDMS-TiO_2 and PDMS-$BaTiO_3$ hybrid films prepared at ambient conditions were also annealed at 60 °C and 100 °C to explore the influence on the optical, electronic, and thermal properties of the final products.

From the results of the experiments, a chemical and structural model was proposed for the synthesis of PDMS-TiO_2 hybrids. It was demonstrated that PDMS was first cross-linked by the titanium precursor via the silanol end groups to form a PDMS-TiO_2 hybrid. Excess or unbounded titanium isopropoxide reacts during curing to produce titanium dioxide within the final hybrid structure network which contains pores in the sub-micron range. The titanium dioxide generated is located at the PDMS cross linking sites, and is dispersed uniformly within the matrix in an amorphous state. As the molar ratio of titanium isopropoxide to PDMS increases from 5:1 to 20:1, (i.e. a higher dosage of titanium precursor), the more condensed the structure created. Subsequently larger and more numerous amorphous titanium dioxide particles were produced. The refractive index and dielectric constants of the hybrids increased with an increased ratio of TiO_2 in the system up to a point. The highest refractive index and dielectric constant obtained were 1.74 and 15.5 respectively with the PDMS-TiO_2 molar ratio of 1:15. However, when the ratio of TiO_2 to PDMS reached as high as 20:1, phase separation occurs and the refractive index and dielectric constant decreased to lower values. Annealing the films at60°C did not affect the properties of the hybrids significantly. However, upon increasing the annealing temperature to 100 °C, the refractive index, dielectric constant and thermal stability of the composites were greatly improved.

The reaction hypothesis and structural model for PDMS-$BaTiO_3$ nanocomposites were similarly validated by the results of our characterization. It was concluded that the final structure of the hybrids consisted of amorphous $BaTiO_3$ particles formed at the cross-linking sites with PDMS, and uniformly dispersed within the matrix, some amorphous

TiO_2 particles may also exist in the network. The produced hybrids contain some residual solvent held within pores of submicron dimensions, which may be removed upon heating. The lower the ratio of titanium and barium precursors, the more cross-linked the structure created, but fewer and smaller barium titanate particles were obtained. The refractive index and dielectric constant increased with the amount of $BaTiO_3$ in the system; with the highest values being 1.6 and 12.3 respectively for the PDMS-$BaTiO_3$ ratio of 1:6. However, when the ratio of $BaTiO_3$ to PDMS was increased to 8:1, phase separation occurred and the refractive index and dielectric constant decreased to lower values. When annealed at 60 °C, no significant effect on the properties of the composites was observed. Upon increasing the annealing temperature to 100 °C, the refractive index, and dielectric constant were significantly improved.

Several of the most important discoveries from this work are listed below:

1. Silanol terminated PDMS was crosslinked by titanium precursors to form PDMS-TiO_2 hybrids, and crosslinked by barium and titanium precursors to generate PDMS-$BaTiO_3$ hybrids. The extra metal precursors create amorphous TiO_2 and $BaTiO_3$ particles dispersed within the polymer matrix.
2. The hybrids of PDMS-TiO_2 and PDMS-$BaTiO_3$ demonstrated much higher refractive indices and dielectric constants compared to pure PDMS by the introduction of TiO_2 and $BaTiO_3$ in the system. The larger the ratio of TiO_2 and $BaTiO_3$ in the composites, the higher the refractive index and dielectric constant attained. However, for samples PDMS-TiO_2 (1-20) and PDMS-$BaTiO_3$ (1-8), phase separation occurred and the refractive index and dielectric constant decreased to lower values.

3. The hybrid composites have porous structures with pore sizes in nanometer range. Annealing these composites at 60 °C showed no significant effects, whereas upon annealing at 100 °C, the refractive index and dielectric constant of the hybrids were improved by the releasing of solvent trapped in pores.

5.2 Future Work

The technique and structural model provided in this work have presented a general understanding for the fabrication of PDMS-TiO_2 and PDMS-$BaTiO_3$ hybrids. However, there are some more details and related issues have left to be resolved to better recognizing the chemistry and obtain products with improved properties.

It is recommended that silanol terminated PDMS with different molecular weight should be introduced in the synthesis to investigate its effect on the properties of the final hybrids. In this experiment, only one molecular weight of PDMS was cross-linked with metal oxide to fabricate nanocomposites, in the following work various molecular weights could be utilized and characterize their influences. Also other hydroxyl terminated polymers may react with metal precursors based on the same process to synthesize hybrids for different applications. Polymers with hydroxyl side bonds are also worth trying to increase the cross-linking percentage, using which method the inorganic loading can be increased without scarifying flexibility of hybrids.

Although the structural models of the *in situ* sol-gel reaction for PDMS-TiO_2 and PDMS-$BaTiO_3$ have been proposed, the chemistry of the *in situ* reactions still need to be explored further. Especially, the hybrids of PDMS-$BaTiO_3$ need to be better understood where water was in the solution and the relative rates of hydrolysis for titanium and barium need to be controlled. This may be realized by using an *in situ* real-time reaction monitoring. After better evaluating the reaction chemistry, hybrid nanocomposites with precise properties can be produced.

Mechanical measurements should be done on the final hybrids to provide mechanical properties of the product and give further insight into the differences in the network structures of various compositions. It can be measured by a compression testing machines. Also a rheometer is worth trying for the rheological properties of the hybirds, based on which results the relationship between network structure and hybrid composition may be determined. Also for the application of electro rheological fluid, rheology is one of the main factors needs to be known.

The ratios of Ti to Si and Ba to Si given in this work are theoretical values, the real amount of TiO_2 in PDMS-TiO_2 and $BaTiO_3$ in PDMS-$BaTiO_3$ are required to know in the future. An atomic absorption spectrometry can be applied to measure the ratio of Ti to Si and Ba to Si. Furthermore, it will be better if the amount of metal oxide that crosslinked and free dispersed are both known in the future.

The reaction between the mixed metal precursors should be better controlled. More

studies are desired to be capable of fabricating a perfect stoichiometry metal oxide without any impurities. In this experiment, chemical modifier EAcAc was employed to slow down the hydrolysis rate of titanium isopropoxide. However, it is hard to remove and may affect the final property of the hybrids. An improved method or modifier should be developed instead.

6. References

1. B K G Theng. Interactions of clay minerals with organic polymers. Some practical applications. Clays and Clay Minerals. 1970; 18: 357.
2. Pedro Henrique Cury Camargo, Kestur Gundappa Satyanarayana*, Fernando Wypych. Nanocomposites: Synthesis, Structure, Properties and New Application Opportunities. Materials Research. 2009; 12(1):1-39.
3. Lange FF. Effect of microstructure on strength of Si_3N_4-SiC composite system. Journal of the American Ceramic Society. 1973; 56(9):445-450.
4. Becher PF. Microstructural design of toughened ceramics. Journal of the American Ceramic Society. 1991; 74(2):255-269.
5. Harmer M, Chan HM, Miller GA. Unique opportunities for microstructural engineering with duplex and laminar ceramic composites. Journal of the American Ceramic Society. 1992; 75(2):1715-1728.
6. Niihara K. New design concept of strctural ceramics-ceramic nanocomposite. Journal of the Ceramic Society of Japan *(*Nippon Seramikkusu Kyokai Gakujutsu Ronbunshi). 1991; 99(6):974-982.
7. Nakahira A, Niihara K. Strctural ceramics-ceramic nanocomposites by sintering method: roles of nano-size particles. Journal of the Ceramic Society of Japan. 1992; 100(4):448-453.
8. Ferroni LP, Pezzotti G, Isshiki T, Kleebe HJ. Determination of amorphous interfacial phases in Al_2O_3/SiC nanocomposites by computer-aided high-resolution electron microscopy. Acta Materialia. 2001; 49(11):2109-2113.
9. She J, Inoue T, Suzuki M, Sodeoka S, Ueno K. Mechanical properties and fracture behavior of fibrous Al_2O_3/SiC ceramics. Journal of European Ceramic Society. 2000; 20(12):1877-1881.
10. Tjong SC, Wang GS. High-cycle fatigue properties of Al-based composites reinforced with in situ TiB_2 and Al_2O_3 particulates. Materials Science and Engineering: A. 2004; 386(1-2):48-53.

11. Fischer H. Polymer nanocomposites: from fundamental research to specific applications. Materials Science and Engineering: C. 2003; 23(6-8):763-772.
12. Jordan J, Jacob KI, Tannenbaum R, Sharaf MA, Jasiuk I. Experimental trends in polymer nanocomposites: a review. Materials Science and Engineering: A. 2005; 393(1-2):1-11.
13. Ray SS, Bousmina M. Biodegradable polymers and their layered silicate nanocomposites: in greening the 21st century materials world. Progress in Matererials Science. 2005; 50(8):962-1079.
14. Akita H, Hattori T. Studies on molecular composite. I. Processing of molecular composites using a precursor polymer for poly (P-Phenylene benzobisthiazole). Journal of Polymer Science: Part B: Polymer Physics. 1999; 37(3):189-197.
15. Akita H, Kobayashi H. Studies on molecular composite. III. Nano composites consisting of poly (P-phenylene benzobisthiazole) and thermoplastic polyamide. Journal of European Ceramic Society. 1999; 37(3):209-218.
16. Akita H, Kobayashi H, Hattori T, Kagawa K. Studies on molecular composite. II. Processing of molecular composites using copolymers consisting of a precursor of poly (P-phenylene benzobisthiazole) and aromatic polyamide. Journal of European Ceramic Society. 1999; 37(3):199-207.
17. Chang JH, An YU. Nanocomposites of polyurethane with various organoclays: thermomechanical properties, morphology, and gas permeability. Journal of European Ceramic Society. 2002; 40(7):670-677.
18. Zavyalov SA, Pivkina AN, Schoonman J. Formation and characterization of metal-polymer nanostructured composites. Solid State Ionics. 2002; 147(3-4):415-419.
19. Kamigaito O. What can be improved by nanometer composites? Journal of Japan Society of Powder Metalurgy. 1991; 38: 315-321.
20. Wang B., Wilkes G. L. New Ti-PTMO and Tr-PTMO Ceramer Hybrid Materials Prepared by the Sol-Gel Method: Synthesis and Characterization. Journal of Polymer Science Part A: Polymer Chemistry. 1991; 29: 905-909.
21. Wang B., Wilkes G. L., Hedrick J. C., Liptak S. C. McGrath J. E. New high refractive index organic/inorganic hybrid materials from sol-gel processing. Macromolecules. 1991; 24: 3449-3450.

22. Wang B., Wilkes G. L., Smith C. D., McGrath J. E. High Refractive Index Hybrid Ceramer Materials Prepared from Titanium Tetraisopropoxide and Poly(arylene ether phosphine oxide) Through Sol-Gel Processing. Polymer Communications. 199; 32: 400-402.
23. Chen W. C., Lee S. J., Lee L. H., Lin J. L. Synthesis and Characterization of Trialkoxysilane-Capped Poly(methyl methacrylate)-Titania Hybrid Optical Thin Films. Jouranl of Materials Chemistry 1999; 9(12): 2999-3003.
24. Lee L. H., Chen W. C. High refractive-index thin films prepared from trialkoxysilane-capped poly(methyl methacrylate)-titania materials. Chemistry of Materials. 2001; 13(3): 1137-1142.
25. L. Zimmermann, M. Weibel, W. Caseri, U. W. Suter. High refractive index films of polymer nanocomposites. Journal of Materials Research. 1993; 8: 1742.
26. F. Papadimitrakopoulos, P. Wisniecki, D. E. Bhagwagar. Mechanically attrited silicon for high refractive-index nanocomposites. Chemistry of Materials. 1997; 9(12): 2928.
27. D. L. Thomsen, T. Phely-Bobin, F. Papadimitrakopoulos. Zinc-Bisquinoline Coordination Assemblies of High Refractive Index and Film Uniformity. Journal of the American Chemical Society. 1998; 120: 6177.
28. M. Weibel, W. Caseri, U. W. Suter, H. Kiess, E. Wehrli. Polymer nanocomposites with 'ultrahigh' refractive index. Polymers for Advanced Technologies. 1991; 2: 75.
29. T. Kyprianidou-Leodidou, W. Caseri, U. W. Suter. Size variations of PbS particles in high-refractive-index nanocomposites. Journal of Physical Chemistry. 1994; 98: 8992.
30. B. Wang, G. L. Wilkes, J. C. Hedrick, S. C. Liptak, J. E. Mcgrath. New High Refractive Index Organic/Inorganic Hybrid Materials from Sol-Gel Processing. Macromolecules. 1991; 24: 3449.
31. B. Wang, H. Huang, G. L. Wilkes. Polymeric Materials: Science and Engeering. 1990; 63: 892.
32. B. Wang, G. L. Wilkes, C. D. Smith, J. E. McGrath. High Refractive Index Hybrid Ceramer Materials Prepared from Titanium Tetraisopropoxide and Poly(arylene

ether phosphine oxide) Through Sol-Gel Processing. Polymer Communication. 1991; 32: 400.

33. M. Yoshida, P. N. Prasad. Sol-gel-processed SiO2/TiO2/poly(vinylpyrrolidone) composite materials for optical waveguides. Chemistry of Materials. 1996; 8: 235.
34. W. F. Su, H. K. Yuan, Polym. Prepr. (Am. Chem. Soc., Div. Polym. Chem.) 2000; 41: 574.
35. L. H. Lee, W. C. Chen. High refractive-index thin films prepared from trialkoxysilane-capped poly(methylmethacrylate)-titania materials. Chemistry of Materials. 2001; 13: 1137.
36. C. C. Chang, W. C. Chen. High-refractive-index thin films prepared from amino alkoxysilane-capped pyromellitic dianhydride-titania hybrid materials. Journal of Polymer Science Part A: Polymer Chemistry. 2001; 39: 3419.
37. B. M. Novak. Hybrid Nanocomposite Materials—between inorganic glasses and organic polymers. Advanced Materials. 1993; 5(6): 422.
38. P. Judeinstein, C. Sanchez. Hybrid Organic-Inorganic Materials : A Land of Multidisciplinarity. Journal of Materials Chemistry. 1996; 6: 511.
39. C. Sanchez, F. Ribot, B. Lebeau. Molecular design of hybrid organic-inorganic nanocomposites synthesized via sol-gel chemistry. Journal of Materials Chemistry. 1999; 9: 35.
40. C. K. Chan, S. L. Peng, I. M. Chu, S. C. Ni. Effects of heat treatment on the properties of poly(methyl methacrylate)/silica hybrid materials prepared by sol-gel process. Polymer. 2001; 42: 4189.
41. Q. Hu, E. Marand. In situ formation of nanosized TiO2 domains within poly(amide–imide) by a sol–gel process. Polymer. 1999; 40(17): 4833.
42. C. Sanchez, B. Alonso, F. Chapusot, F. Ribot, P. Audebert. Molecular design of hybrid organic-inorganic materials with electronic properties. Journal of Sol-Gel Science and Technology. 1994; 2(1-3): 161.
43. M. Yoshida, P. N. Prasad. Sol-gel-processed SiO2/TiO2/poly(vinylpyrrolidone) composite materials for optical waveguides. Chemistry of Materials. 1996; 8: 235.
44. Z. Ahmad, J. E. Mark. Polyimide-ceramic hybrid composites by the sol-gel route. Chemistry of Materials. 2001; 13: 3320.

45. Y. Wei, J. M. Yeh, D. Jin, X. Jia, J. Wang. Composites of electronically conductive polyaniline with polycrylate-silica hybrid sol-gel materials. Chemistry of Materials. 1995; 7(5): 969.
46. Y. Wei, D. Jin, D. J. Brennan, D. N. Rivera, Q. Zhuang, N. J. DiNardo, K. Qiu, Atomic Force Microscopy Study of Organic-Inorganic Hybrid Materials. Chem. Mater. 1998; 10(3): 769.
47. W. E. van Zyl, M. Garcìa, B. A. G. Schrauwen, B. J. Kooi, J. T. M. de Hosson, H. Verweij. Hybrid polyamide/silica nanocomposites: Synthesis and mechanical testing. Macromolecular Materials and Engineering. 2002; 287(2): 106.
48. J. Jang, H. Park. In situ sol-gel process of polystyrene/silica hybrid materials: Effect of silane-coupling agents. Journal of Applied Polymer Science. 2002; 85(10): 2074.
49. M.I. Sarwar, Z. Ahmad. Interphase bonding in organic–inorganic hybrid materials using aminophenyltrimethoxysilane. European Polymer Jouranl. 2000; 36: 89-94.
50. R.A. Zoppi, C.R. de Castro, I.V.P. Yoshida, S.P. Nunes. Hybrids of SiO2 and poly(amide 6-b-ethylene oxide). Polymer. 1997; 38: 5705.
51. W. C. Chen, S. J. Lee, L. H. Lee, J. L. Lin. Synthesis and characterization of trialkoxysilane-capped poly(methyl methacrylate)-titania hybrid optical thin films. Journal of Materials Chemistry. 1999; 9: 2999.
52. B. M. Novak. Hybrid nanocomposite materials-between inorganic glasses and organic polymers. Advanced Materials. 1993; 5: 422.
53. H. R. Allcock. Inorganic—Organic Polymers. Advanced Materials. 1994; 6: 106.
54. P. Judeinstein, C. Sanchez. Hybrid Organic-Inorganic Materials: A Land of Multidisciplinarity. Journal of Materials Chemistry. 1996; 6: 511.
55. D. Pomogailo. Hybrid polymer-inorganic nanocomposites. Russian Chemical Reviews. 2000; 69(1): 53.
56. G. Kickelbick. Concepts for the incorporation of inorganic building blocks into organic polymers on a nanaoscale. Progress in Polymer Science. 2003; 28: 83.
57. F. Mammeri, E. Le Bourhis, L. Rozes, C. Sanchez. Mechanical properties of hybrid organic-inorganic materials. Journal of Materials Chemistry. 2005; 15: 3787.
58. C. Sanchez, G. J. de, A. A. Soler-Illia, F. Ribot, T. Lalot, C. R. Mayer, V. Cabuil. Designed hybrid organic-inorganic nanocomposites from functional nanobuilding

blocks. Chemistry of Materials. 2001; 13: 3061.

59. C. Sanchez, F. Ribot, B. Lebeau. Molecular design of hybrid organic-inorganic nanocomposites synthesized via sol-gel chemistry. Journal of Materials Chemistry. 1999; 9(1): 35.
60. G. Schottner. Hybrid Sol-Gel-Derived Polymers: Applications of Multifunctional Materials. Chemistry of Materials. 2001; 13: 3422.
61. P. Innocenzi, B. Lebeau. Organic-inorganic hybrid materials for non-linear optics. Journal of Materials Chemistry. 2005; 15: 3821.
62. C. Sanchez, B. Lebeau, F. Chaput, J.-P. Boilot. Optical Properties of Functional Hybrid Organic-Inorganic Nanocomposites. Advanced Materials. 2003; 15(23): 1969.
63. L. Nicole, C. Boissi_ere, D. Grosso, A. Quach, C. Sanchez. Mesostructured hybrid organic-inorganicthin films. Journal of Materials Chemistry. 2005; 15: 3598.
64. C. Sanchez, B. Julian, P. Belleville, M. Popall. Applications of hybrid organic-inorganic nanocomposites. Journal of Materials Chemistry. 2005; 15: 3559.
65. A.-L. Penard, T. Gacoin, J.-P. Boilot. Functionalized sol-gel coatings for optical applications. Accounts of Chemical Research. 2007; 40(9): 895.
66. W. Que, Z. Sun, Y. Zhou, Y. L. Lam, Y. C. Chan, C. H. Kam. Optical and mechanical properties of TiO2/SiO2/organically modified silane composite films prepared by sol–gel processing. Thin Solid Films, 2000; 359(2): 177.
67. B. Yang, Y. Liu, C. Lu, Chin. Pat. ZL2005 1 0016828.7, 2005.
68. M. Yoshida, P. N. Prasad. Sol-gel-processed SiO2/TiO2/poly(vinylpyrrolidone) composite materials for optical waveguides. Chemistry of Materials. 1996; 8: 235.
69. B. Wang, H. Huang and G. L. Wilkes. Polymeric Materials: Science and Engeering. 1990; 63: 892.
70. B. Wang, G. L. Wilkes, J. C. Hedrick, S. C. Liptak, J. E. McGrath. New high refractive index organic/inorganic hybrid materials from sol-gel processing. Macromolecules. 1991; 24: 3449.
71. B. Wang, G. L. Wilkes, C. D. Smith, J. E. McGrath. High Refractive Index Hybrid Ceramer Materials Prepared from Titanium Tetraisopropoxide and Poly(arylene

ether phosphine oxide) Through Sol‐Gel Processing. Polymer Communications. 1991; 32(13): 400.

72. L. H. Lee, W. C. Chen. High-Refractive-Index Thin Films Prepared from Trialkoxysilane-Capped Poly(methyl methacrylate)- Titania Materials. Chemistry of Materials. 2001; 13: 1137.
73. C. C. Chang and W. C. Chen. High-refractive-index thin films prepared from amino alkoxysilane-capped pyromellitic dianhydride-titania hybrid materials. Journal of Polymer Science Part A: Polymer Chemistry. 2001; 39(19): 3419.
74. H. W. Su, W. C. Chen. High Refractive Index Polyimide-Nanocrystalline Titania Hybrid Optical Materials. Journal of Materials Chemistry. 2008; 18: 1139.
75. W. C. Chen, W. C. Liu, P. T. Wu, P. F. Chen. Synthesis and characterization of oligomeric phenylsilsesquioxane-titania hybrid optical thin films. Materials Chemistry and Physics. 2004; 83(1): 71.
76. C. Lu, Z. Cui, C. Guan, J. Guan, B. Yang and J. Shen. Research on preparation, structure and properties of TiO2/polythiourethane hybrid optical films with high refractive index. Macromolecular Materials and Engeering. 2003; 288: 717.
77. M. Moffitt, A. Eisenberg. Size Control of Nanoparticles in Semiconductor-Polymer Composites. 1. Control via Multiplet Aggregation Numbers in Styrene-Based Random Ionomers. Chemistry of Materials. 1995; 7(6): 1178.
78. M. Moffitt, L. McMahon, V. Pessel, A. Eisenberg. Size Control of Nanoparticles in Semiconductor-Polymer Composites. 2. Control via Sizes of Spherical Ionic Microdomains in Styrene-Based Diblock Ionomers. Chemistry of Materials. 1995; 7(6): 1185.
79. R. S. Kane, R. E. Cohen and R. Silbey. Synthesis of PbS Nanoclusters within Block Copolymer Nanoreactors. Chemistry of Materials. 1996; 8(8): 1919.
80. R. S. Kane, R. E. Cohen, R. Silbey. Synthesis of doped ZnS nanoclusters within block copolymer nanoreactors. Chemistry of Materials. 1999; 11: 90.
81. J. Huang, Y. Yang, B. Yang, S. Liu, J. Shen. Synthesis of the CdS nanoparticles in polymer networks. Polymer Bulletin. 1996; 36(3): 337.
82. G. Carrot, S. M. Scholz, C. J. G. Plummer, J. G. Hilborn. Synthesis and

Characterization of Nanoscopic Entities Based on Poly(caprolactone)-Grafted Cadmium Sulfide Nanoparticles. Chemistry of Materials. 1999; 11(12): 3571

83. T. Kypriandou-Leodidou, H. J. Althaus, Y. Wyser, D. Vetter, M. Buchler, W. Caseri, U. W. Suter. High refractive index materials of iron sulfides and poly(ethylene oxide). Journal of Materials Research. 1997; 12: 2198.
84. L. Zimmermann, M. Weibel, W. Caseri, U. W. Suter. High refractive index films of polymer nanocomposites. Journal of Materials Research. 1993; 8: 1742.
85. T. Kypriandou-Leodidou, W. Caseri, U. W. Suter. Size variation of PbS particles in high-refractive-index nanocomposites. Journal of Physical Chemistry. 1994; 98(36): 8992.
86. M. Gao, Y. Yang, B. Yang, F. Bian, J. Shen. Synthesis of PbS Nanoparticles in Polymer Matrices. Journal of the Chemical Society, Chemical Communications. 1994, 2779.
87. M. Gao, Y. Yang, B. Yang, J. Shen. Effect of the surface chemical modification on the optical properties of polymer-stabilized PbS nanoparticles. Journal of the Chemical Society, Faraday Transactions. 1995; 91: 4121.
88. Y. Yang, J. Huang, S. Liu, J. Shen. Preparation, characterization and electroluminescence of ZnS nanocrystals in a polymer matrix. Journal of Materials Chemistry. 1997; 7(1): 131.
89. J. Wang, W. Chen, A. Liu, G. Lu, G. Zhang, J. Zhang, B. Yang. Controlled Fabrication of Cross-Linked Nanoparticles/Polymer Composite Thin Films through the Combined Use of Surface-Initiated Atom Transfer Radical Polymerization and Gas/Solid Reaction. Journal of the American Chemical Society. 2002; 124(45): 13358-13359.
90. C. Lu, C. Guan, Y. Liu, Y. Cheng, B. Yang. PbS/polymer nanocomposites optical materials with high refractive index. Chemistry of Materials. 2005; 17: 2448-2454.
91. S. Lee, H. J. Shin, S. M. Yoon, D. K. Yi, J. Y. Choi, U. Paik. Refractive index engineering of transparent ZrO_2-polydimethylsiloxane nanocomposites. Journal of Materials Chemistry. 2008; 18: 1751-1755.
92. N. Nakayamaa and T. Hayashi. Preparation and characterization of TiO_2 and polymer nanocomposite films with high refractive index. Journal of Applied Polymer

Science. 2007; 105(6): 3662-3672.

93. M. Avella, M. E. Errico, E. Martuscelli. Novel PMMA/CaCO3 nanocomposites abrasion resistant prepared by an in situ polymerization process. Nano Letters. 2001; 1(4): 213-217.
94. H. Zhang, Z. Cui, Y. Wang, K. Zhang, X. Ji, C. Lu, B. Yang, M. Gao. From water-soluble CdTe nanocrystals to fluorescent nanocrystal-polymer transparent composites using polymerizable surfactants. Advanced Materials. 2003; 15: 777-780.
95. C. H. Hung, W. T. Whang. Effect of surface stabilization of nanoparticles on luminescent characteristics in ZnO/poly(hydroxyethyl methacrylate) nanohybrid films. Journal of Materials Chemistry. 2005; 15(2): 267-274.
96. S. M. Khaled, R. Sui, P. A. Charpentier, A. S. Rizkalla. Synthesis of TiO_2-PMMA Nanocomposite: Using Methacrylic Acid as a Coupling Agent. Langmuir. 2007; 23: 3988-3995.
97. M. M. Demir, P. Castignolles, U. Akbey, G. Wegner. In-situ bulk polymerization of dilute Particle/MMA dispersions. Macromolecules, 2007; 40(12): 4190-4198.
98. H. Althues, R. Palkovits, A. Rumplecker, P. Simon, W. Sigle, M. Bredol, U. Kynast, S. Kaskel. Synthesis and Characterization of Transparent Luminescent ZnS:Mn/PMMA Nanocomposites. Chemistry of Materials. 2006; 18(4): 1068-1072.
99. M. Inkyo, Y. Tokunaga, T. Tahara, T. Iwaki, F. Iskandar, C. J. Hogan, K. Okuyama. Beads Mill-Assisted Synthesis of Poly Methyl Methacrylate (PMMA)-TiO2 Nanoparticle Composites. Industrial Engineering Chemistry Research. 2008; 47: 2597-2604.
100. M. M. Demir, K. Koynov, U. Akbey, C. Bubeck, I. Park, I. Lieberwirth, G. Wegner. Optical Properties of Composites of PMMA and Surface-Modified Zincite Nanoparticles. Macromolecules. 2007; 40: 1089-1100.
101. Uhlmann D. R., Teowee G. Sol-gel science and technology: Current state and future prospects. Journal of Sol-Gel Science and Technology. 1998; 13: 153-162.
102. Mackenzie J. D., Bescher E. P. Structures, properties and potential applications of ormosils. Journal of Sol-Gel Science and Technology. 1998; 13(1-3): 371-377.
103. H. A. Macleod. Thin Film Optical Filters. 2nd ed. UK: Adam Hilger Ltd, Bristol; 1986.

104. A. Thelen. Design of Optical Interference Coatings. New York: McGraw-Hill; 1989.
105. L. Martinu, D. Poltras. Plasma deposition of optical films and coatings: A review. Journal of Vaccumm Science & Technology A. 2000; 18: 2619-2645.
106. H. G. Shanbhogue, C. L. Nagendra, M. N. Annapurna, S. A. Kumar, G. K. M. Thutupalli. Multilayer antireflection coatings for the visible and near-infrared regions. Applied Optics. 1997; 36: 6339-6351.
107. E. Spiller, I. Haller, R. Feder, J. E. E. Baglin and W. N. Hammer. Graded-index AR surfaces produced by ion implantation on plastic materials. Applied Optics. 1980; 19(17): 3022-3026.
108. B. S. Dunn, J. D. Mackenzie, E. J. A. Pope, H. K. Schmidt, M. Yamane. Sol–Gel Optics. 4th ed. San Diego, CA: SPIE; 1997. 452 p.
109. E. Brinley, S. Seal, R. Folks, E. Braunstein, L. Kramer, S. Seal. High efficiency SiO_2–TiO_2 hybrid sol-gel antireflective coating for infrared applications. Journal of Vacuum Science and Technology A. 2006; 24: 1141.
110. K. C. Krogman, T. Druffel, M. K. Sunkara. Anti-reflective optical coatings incorporating nanoparticles. Nanotechnology. 2005; 16(7): S338-343.
111. C. Vassallo. Optical Waveguide Concepts. New York: Elsevier; 1991.
112. C. Xu, L. Eldada, C. Wu, R. A. Norwood, L. W. Shacklette, J. T. Yardley, Y. Wei. Photoimageable, low shrinkage organic-inorganic hybrid materials for practical multimode channel waveguides. Chemistry of Materials. 1996; 8: 2701-2703.
113. Y. K. Kwon, J. K. Han, J. M. Lee, Y. S. Ko, J. H. Oh, H. S. Lee, E. H. Lee. Organic–inorganic hybrid materials for flexible optical waveguide applications. Journal of Materials Chemistry. 2008; 18(5): 579-585.
114. Y. Enami, G. Meredith, N. Peyghambarian, M. Kawazu and A. K.-Y. Jen. Hybrid Electro-optic Polymer/Selective Buried Sol-gel Waveguides for the Integration of Phase-Modulator at 1.55 mm. Applied Physics Letters. 2003; 82(4): 490.
115. M. Yoshida, M. Lal, N. D. Kumar, P. N. Prasad. TiO_2 nano-particle-dispersed polyimide composite optical waveguide materials through reverse micelles. Journal of Materials Science. 1997; 32: 4047.
116. S. Motakef, T. Suratwala, R. L. Roncone, J. M. Boulton, G. Teowee, G. F. Neilson, D. R. Uhlmann. Processing and optical properties of inorganic-organic hybrids

(polycerams). I. MPEOU-based waveguides. Journal of Non-Crystalline Solids. 1994; 178: 31-36.

117. S. Jeong, J. Moon. Fabrication of inorganic–organic hybrid films for optical waveguide. Journal of Non-Crystalline Solids. 2005; 351: 3530-3535.

118. D. C. Oliveira, A. G. Macedo, N. J. O. Silva, C. Molina, R. A. S. Ferreira, P. S. Andr_e, K. Dahmouche, V. D. Z. Bermudez, Y. Messaddeq, S. J. L. Ribeiro, L. D. Carlos. Photopatternable di-ureasil-zirconium oxocluster organic-inorganic hybrids as cost effective integrated optical substrates. Chemistry of Materials. 2008; 20(11): 3696-3705.

119. R. Buestrich, F. Kahlenberg, M. Popall, P. Dannberg, R. Muller- Fiedler, O. S. Rosch. Ormocers for optical interconnection technology. Journal of Sol–Gel Science and Technology. 2001; 20(2): 181-186.

120. X. Luo, C. Zha, B. L. Davies. Preparation and optical properties of titania-doped hybrid polymer via anhydrous sol–gel process. Journal of Non-Crystalline Solids. 2005; 351(1): 29-34.

121. Y. Shi, C. Zhang, H. Zhang, J. H. Bechtel, L. R. Dalton, B. H. Robinson ,W. H. Steier. Halfwave Voltage Polymeric Electro-optic Modulators Achieved by Controlling Chromophore Shape. Science. 2000; 288: 119-122.

122. J. A. Delaire, K. Nakatani. Linear and Nonlinear Optical Properties of Photochromic Molecules and Materials. Chemical Reviews. 2000; 100: 1817-1846.

123. A. Martucci, P. Innocenzi, J. Fick, J. D. Mackenzie. Zirconia-ormosil films doped with PbS quantum dots. Journal of Non-Crystalline Solids. 1999; 244: 55-62.

124. F. Gan. Optical nonlinearity of hybrid and nano compostie materials prepared by the Sol-Gel method. Journal of Sol–Gel Science and Technology. 1998; 13: 559-563.

125. F. Qin, J. L.Shi, C. Y.Wei, J. L.Gu. Large incorporation amount and enhanced nonlinear optical properties of sulfide nanoparticles within mesoporous thin films. Journal of Materials Chemistry. 2008; 18(6): 634-636.

126. H. Yuwono, J. Xue, J. Wang, H. I. Elim, W. Ji, Y. Li, T. J. White. Transparent nanohybrids of nanocrystalline TiO_2 in PMMA with unique nonlinear optical behavior. Journal of Materials Chemistry. 2003; 13: 1475-1479.

127. H. Yuwono, B. Liu, J. Xue, J. Wang, H. I. Elim, W. Ji, Y. Li, T. J. White. Controlling the crystallinity and nonlinear optical properties of transparent TiO_2 PMMA nanohybrids. Journal of Materials Chemistry. 2004; 14: 2978-2987.
128. C. Sciancalepore, T. Cassano, M. L. Curri, D. Mecerreyes, A. Valentini, A. Agostiano, R. Tommasi, M. Striccoli. TiO_2 nanorods / PMMA co-polymer based nanocomposites: highly homogeneous linear and nonlinear optical material. Nanotechnology. 2008; 19: 205705-205713.
129. M. Haw. Holographic data storage: The light fantastic. Nature. 2003; 422: 556.
130. T. J. Trout, J. J. Schmieg, W. J. Gambogi, A. M. Weber. Optical photopolymers: design and applications. Advanced Materials. 1998; 10: 1219-1224.
131. F. del Monte, O. Martı´nez, J. A. Rodrigo, M. L. Calvo, P. Cheben. A Volume Holographic Sol-Gel Material with Large Enhancement of Dynamic Range by Incorporation of High Refractive Index Species. Advanced Materials. 2006; 18: 2014-2017.
132. R. A. Vaia, C. L. Dennis, L. V. Natarajan, V. P. Tondiglia, D. W. Tomlin, T. J. Bunning. One-step, micrometer-scale organization of nano- and mesoparticles using holographic photopolymerization: A generic technique. Advanced Materials. 2001; 13: 1570-1574.
133. N. Suzuki, Y. Tomita and T. Kojima. Holographic recording in TiO2 nanoparticle-dispersed methacrylate photopolymer films. Applied Physics Letters. 2002; 81: 4121-4123.
134. C. S_anchez, M. J. Escuti, C. van Heesch, C. W. M. Bastiaansen, D. J. Broer, J. Loos, R. Nussbaumer. TiO2 nanoparticle-photopolymer composites for volume holographic recording. Advanced Functional Materials. 2005; 15: 1623-1629.
135. N. Suzuki, Y. Tomita. Highly transparent ZrO2 nanoparticle-dispersed acrylate photopolymers for volume holographic recording. Optics Express. 2006; 14: 12712.
136. O. V. Sakhno, L. M. Goldenberg, J. Stumpe and T. N. Smirnova. Surface Modified ZrO_2 and TiO_2 Nanoparticles Embedded in Organic Photopolymers for Highly Effective and UV-Stable Volume Holograms. Nanotechnology. 2007; 18(10): 105704.

137. G. Garnweitner, L. M. Goldenberg, O. V. Sakhno, M. Antonietti, M. Niederberger, J. Stumpe. Large-Scale Synthesis of Organophilic Zirconia Nanoparticles and Their Application in Organic–Inorganic Nanocomposites for Efficient Volume Holography. Small 2007; 3: 1626.
138. G. Schottner, K. Rose, U. Posset. Scratch and abrasion resistant coatins on plastic lenses-state of the art, current developments and perspectives. Journal of Sol–Gel Science and Technology. 2003; 27: 71-79.
139. D. K. Hwang, J. H. Moon, Y. G. Shul, K. T. Jung, D. H. Kim, D. W. Lee. Scratch resistant and transparent UV-protective coating on polycarbonate. Journal of Sol–Gel Science and Technology. 2003; 26: 783-787.
140. Bhattacharya, S. K., Tummala, R. R. Next generation integral passives: materials, processer, and integration of resistors and capacitors on PWB substrates. Journal of Materials Science: Materials in Electronics. 2000; 11: 253-268.
141. Bhattacharya, S. K., Tummala, R. R. Integral passives for next generation of electronic packaging: application of epoxy/ceramic nanocomposites as integral capacitors. Microelectronics Journal. 2001; 32: 11-19.
142. Rao, Y., Ogitani, S., Kohl, P., Wong, C. P. Novel polymer–ceramic nanocomposite based on high dielectric constant epoxy formula for embedded capacitor application. Journal of Applied Polymer Science. 2002; 83(5): 1084-1090.
143. Robertson, J. High dielectric constant oxides. The European Physical Journal-Applied Physics. 2004; 28: 265–291.
144. Dang, Z. M., Zhou, T., Yao, S. H., Yuan, J. K., Zha, J. W., Song, H. T., Li, J. Y., Chen, Q., Yang, W. T., Bai, J. B. Advanced Calcium Copper Titanate/Polyimide Functional Hybrid Films with High Dielectric Permittivity. Journal of Advanced Materials. 2009; 21(20): 2077–2082.
145. Rao, Y., Ogitani, S., Kohl, P., Wong, C. P. Novel polymer–ceramic nanocomposite based on high dielectric constant epoxy formula for embedded capacitor application. Journal of Applied Polymer Science. 2002; 83(5): 1084–1090.
146. Kim, C., Wang, Z. M., Choi, H. J., Ha, Y. G., Facchetti, A., Marks, T. J. Printable cross-linked polymer blend dielectrics. Design strategies, synthesis, microstructures, and electrical properties, with organic field-effect transistors as testbeds. Journal of

the American Chemical Society. 2008; 130: 6867–6878.

147. Ortiz, R. P., Facchetti, A., Marks, T. High-k Dielectrics for Low-Voltage Organic Field-Effect Transistors. Journal of Chemical Reviews. 2010; 110: 205–239.

148. Dimitrakopoulos, C. D., Purushothaman, S., Kymissis, J., Callegari, A., Shaw, J. M. Low-voltage organic transistors on plastic comprising high-dielectric constant gate insulators. Science. 1999; 283: 822–824.

149. Homes, C. C., Vogt, T., Shapiro, S. M., Wakimoto, S., Ramirez, A. P. Optical response of high-dielectric-constant perovskite-related oxide. Science 2001; 293: 673–676.

150. Carlson, C. M., Rivkin, T. V., Parilla, P. A., Perkins, J. D., Ginley, D. S., Kozyrev, A. B., Oshadchy, V. N., Pavlov, A. S. Large dielectric constant ($\varepsilon/\varepsilon 0>6000$) $Ba_{0.4}Sr_{0.6}TiO_3$ thin films for high-performance microwave phase shifters. Applied Physics Letters. 2000; 76(14): 1920–1922.

151. Scott, J. F. High dielectric constant thin films for dynamic random access memories. Annual Review of Materials Science. 1998; 28: 79–100.

152. Kotecki, D. E. A review of high dielectric materials for DRAM capacitors. Integrated Ferroelectrics. 1997; 16(1/4): 1–19.

153. Pelrine, R., Kornbluh, R., Kofod, G. High-Strain Actuator Materials Based on Dielectric Elastomers. Advanced Materials. 2000; 12: 1223–1225.

154. Jiang, S. L., Yu, Y., Zeng, Y. K. Novel Ag–$BaTiO_3$/PVDF three-component nanocomposites with high energy density and the influence of nano-Ag on the dielectric properties. Current Applied Physics. 2009; 9(5): 956–959.

155. Raval, H. N., Tiwari, S. P., Navan, R. R., Mhaisalkar, S. G., Rao, V. R. Solution-Processed Bootstrapped Organic Inverters Based on P3HT With a High-k Gate Dielectric Material. IEEE Electron Device Letters. 2009; 30(5): 484–486.

156. Khan, M. Z. R., Hasko, D. G., Saifullah, M. S. M., Welland, M. E. Trapped charge dynamics in a sol-gel based TiO_2 high-k gate dielectric silicon metal-oxide-semiconductor field effect transistor. Journal of Physics: Condensed Matter. 2009; 21: 215902.

157. Mark, J.E. Some novel polymeric nanocomposites. Accounts of Chemical Research. 2006; 39: 881–888.

158. Mark, J.E. Ceramic-modified elastomers. Current Opinion in Solid State & Materials Science. 1999; 4: 565–570.
159. Brinker, C., Scherer, G. Sol–Gel Science: the Physics and Chemistry of Sol–Gel Processing. Boston: Academic Press; 1990.
160. De Luca, M.A., Jacobi, M.M., Orlandini, L.F. Synthesis and characterization of elastomeric composites prepared from epoxidised styrene butadiene rubber, 3-aminopropyltriethoxysilane and tetraethoxysilane. Journal of Sol-Gel Science and Technology. 2009; 49: 150–158.
161. De Luca, M.A., Machado, T.E., Notti, R.B., et al. Synthesis and characterization of epoxidized styrene-butadiene rubber/silicon dioxide hybrid materials. Journal of Applied Polymer Science. 2004; 92: 798–803.
162. Kohjiya, S., Kato, A., Ikeda, Y. Visualization of nanostructure of soft matter by 3D-TEM: nanoparticles in a natural rubber matrix. Progress in Polymer Science. 2008; 33: 979–997.
163. Kohjiya, S., Katoh, A., Shimanuki, J., et al. Three-dimensional nano-structure of in situ silica in natural rubber as revealed by 3D-TEM/electron tomography. Polymer. 2005. 46: 4440–4446.
164. Breiner, J.M., Mark, J.E., Beaucage, G. Dependence of silica particle sizes on network chain lengths, silica contents, and catalyst concentrations in in situ-reinforced polysiloxane elastomers. Journal of Polymer Science: Polymer Physics. 1999; 37: 1421–1427.
165. Dewimille, L., Bresson, B., Bokobza, L. Synthesis, structure and morphology of poly(dimethylsiloxane) networks filled with in situ generated silica particles. Polymer. 2005; 46: 4135–4143.
166. Bokobza, L. New developments in rubber reinforcement. Kgk-Kaut Gummi Kunst. 2009; 62: 23–27.
167. Bokobza, L. Elastomeric composites. I. Silicone composites. Journal of Applied Polymer Science. 2004; 93: 2095–2104.
168. Murugesan, S., Mark, J.E., Beaucage, G. Structure-property relationships for poly(dimethylsiloxane) networks in situ filled using titanium 2-ethylhexoxide and zirconium n-butoxide. ACS Symposium Series. 2003; 838: 163–169.

169. Murugesan, S., Sur, G.S., Mark, J.E., et al. In situ catalyst generation and controlled hydrolysis in the sol–gel precipitation of zirconia and titania particles in poly(dimethylsiloxane). Journal of Inorganic and Organometallic Polymers. 2004; 14: 239–252.
170. Julian, B., et al. Synthesis and characterization of transparent PDMS-metal-oxo based organic anorganic nanocomposites. Chemistry of Materials. 2003; 15(15): 3026-3034.
171. Pomogailo, A.D. Polymer sol-gel synthesis of hybrid nanocomposites. Colloid Journal. 2005; 67(6): 658-677.
172. Niederberger, M. Nonaqueous sol-gel routes to metal oxide nanoparticles. Accounts of Chemical Research. 2007; 40(9): 793-800.
173. Nandi, M., et al. Molecular-Level Ceramic Polymer Composites. 2.1 Synthesis of Polymer-Trapped Silica and Titania Nanoclusters. Chemistry of Materials. 1991; 3(1): 201-206.
174. Mourey, T.H., et al. Hydrolysis and Condensation Coupling of (Trimethoxysilyl)Phenyl-Terminated Polystyrene Macromonomers. Macromolecules. 1992; 25(1): 45-52.
175. Chujo, Y., et al. Block Copolymer of 2-Methyl-2-Oxazoline with Silica-Gel - an Organic-Inorganic Hybrid Polymer. Makromolekulare Chemie-Macromolecular Symposia. 1991; 42(3): 303-312.
176. Noell, J.L.W., et al. The Preparation and Characterization of New Polyether Ketone-Tetraethylorthosilicate Hybrid Glasses by the Sol-Gel Method. Journal of Applied Polymer Science. 1990; 40(7-8): 1177-1194.
177. Glaser, R.H., G.L. Wilkes. Polymer Modified Mixed Metal Alkoxide-Metal Acetyl Acetonate Sol-Gel Materials. Polymer Bulletin. 1989; 22(5-6): 527-532.
178. Coltrain, B.K., et al. Role of Trialkoxysilane Functionalization in the Preparation of Organic-Inorganic Composites. Chemistry of Materials. 1993; 5(10): 1445-1455.
179. Macwan, D.P., P.N. Dave, S. Chaturvedi. A review on nano-TiO2 sol-gel type syntheses and its applications. Journal of Materials Science. 2011; 46(11): 3669-3686.

180. Hu, Q., E. Marand. In situ formation of nanosized TiO2 domains within poly(amide-imide) by a sol-gel process. Polymer. 1999; 40(17): 4833-4843.
181. Chen, W.C., et al. Synthesis and characterization of poly(methyl silsesquioxane) titania optical thin films. Journal of Materials Chemistry. 2002; 12(12): 3644-3648.
182. Lee, L.H., W.C. Chen. High refractive-index thin films prepared from trialkoxysilane-capped poly(methyl methacrylate)-titania materials. Chemistry of Materials. 2001; 13(3): 1137-1142.
183. Nussbaumer, R.J., et al. Polymer-TiO2 nanocomposites: A route towards visually transparent broadband UV filters and high refractive index materials. Macromolecular Materials and Engineering. 2003; 288(1): 44-49.
184. Zhang, J., et al. New observations on the optical properties of PPV/TiO2 nanocomposites. Polymer. 2001; 42(8): 3697-3702.
185. Yabuta, T., et al. Synthesis of blood compatible PDMS-based organic-inorganic hybrid coatings. Journal of Sol-Gel Science and Technology. 2004; 31(1-3): 273-276.
186. Shindou, T., et al. Effect of composition on surface properties of polydimethylsiloxane-based inorganic/organic hybrid films. Journal of Sol-Gel Science and Technology. 2004; 30(3): 229-237.
187. Pena-Alonso, R., et al., Surface chemical and physical properties of TEOS-TBOT-PDMS hybrid materials. Journal of Sol-Gel Science and Technology. 2006; 38(2): 133-145.
188. Nakade, M., M. Ogawa. Synthesis and characterization of zinc oxide fine particles coated with titania/PDMS hybrid. Journal of Materials Science. 2007; 42(12): 4254-4259.
189. Bae, S.C., et al. Chemical imaging in a surface forces apparatus: Confocal Raman spectroscopy of confined poly(dimethylsiloxane). Langmuir. 2005; 21(13): 5685-5688.
190. Aprile, C., et al. Long-lived (minutes) photoinduced charge separation in a structured periodic mesoporous titania containing 2,4,6-triphenylpyrylium as guest. Dalton Transactions. 2008; 40: 5465-5470.

191. Jang, J., et al. Self-reference quantitative phase microscopy for microfluidic devices. Optics Letters. 2010; 35(4): 514-516.
192. Shukla, S.K., et al. Some thermal studies of polysilanes and polycarbosilanes. Thermochimica Acta. 2004; 424(1-2): 209-217.
193. Windlass, H., et al. Colloidal processing of polymer ceramic nanocomposite integral capacitors. Ieee Transactions on Electronics Packaging Manufacturing. 2003; 26(2): 100-105.
194. Ramesh, S., et al. Dielectric nanocomposites for integral thin film capacitors: Materials design, fabrication, and integration issues. Ieee Transactions on Advanced Packaging. 2003; 26(1): 17-24.
195. Kobayashi, Y., et al. Fabrication and dielectric properties of the BaTiO3-polymer nano-composite thin films. Journal of the European Ceramic Society. 2008; 28(1): 117-122.
196. Rao, Y., et al. Novel polymer-ceramic nanocomposite based on high dielectric constant epoxy formula for embedded capacitor application. Journal of Applied Polymer Science. 2002; 83(5): 1084-1090.
197. Bhattacharya, S.K., R.R. Tummala. Integral passives for next generation of electronic packaging: application of epoxy/ceramic nanocomposites as integral capacitors. Microelectronics Journal. 2001; 32(1): 11-19.
198. Kozuka, H., A. Higuchi. Stabilization of poly(vinylpyrrolidone)-containing alkoxide solutions for thick sol-gel barium titanate films. Journal of the American Ceramic Society. 2003; 86(1): 33-38.
199. Tsay, J.D., T.T. Fang. Effects of temperature and atmosphere on the formation mechanism of barium titanate using the citrate process. Journal of the American Ceramic Society. 1996; 79(6): 1693-1696.
200. Choudhury, A. Dielectric and piezoelectric properties of polyetherimide/BaTiO3 nanocomposites. Materials Chemistry and Physics. 2010; 121(1-2): 280-285.
201. Y. Kobayashi, T.T., T. Tabata, T. Miwa, M. Konno. Fabrication and dielectric properties of the BaTiO3-polymer nanocomposite thin films. Journal of the European Ceramic Society. 2008; 28: 117-122.

202. Chandradass, J., D.S. Bae. Preparation and properties of barium titanate nanopowder/epoxy composites. Materials and Manufacturing Processes. 2008; 23(2): 117-123.
203. Wen, J., J.E. Mark. Precipitation of Silica-Titania Mixed-Oxide Fillers into Poly(Dimethylsiloxane) Networks. Rubber Chemistry and Technology. 1994; 67(5): 806-819.
204. Yabuta, T., et al. Synthesis of blood compatible PDMS-based organic-inorganic hybrid coatings. Journal of Sol-Gel Science and Technology. 2004; 31(1-3): 273-276.
205. Tangwiwat, S., S.J. Milne. Barium titanate sols prepared by a diol-based sol-gel route. Journal of Non-Crystalline Solids. 2005; 351(12-13): 976-980.
206. Shindou, T., et al. Effect of composition on surface properties of polydimethylsiloxane-based inorganic/organic hybrid films. Journal of Sol-Gel Science and Technology. 2004; 30(3): 229-237.
207. Nakade, M., M. Ogawa. Synthesis and characterization of zinc oxide fine particles coated with titania/PDMS hybrid. Journal of Materials Science. 2007; 42(12): 4254-4259.
208. Maria J. Mosquera, D.M.d.l.S., Lucila Valdez-Castro, Luis Esquivias. New route for producing crack-free xerogels: obtaining uniform pore size. Journal of Non-Crystalline Solids. 2008; 354: 645-650.
209. Sung Chul Bae, H.L., Zhiqun Lin, Steve Granick. Chemical Imaging in a Surface Forces Apparatus: Confocal Raman Spectroscopy of confined Poly(dimethylsiloxane). Langmuir. 2005; 21: 5685-5688.
210. Zhu, X.H., et al. Morphology and atomic-scale surface structure of barium titanate nanocrystals formed at hydrothermal conditions. Journal of Crystal Growth. 2009; 311(8): 2437-2442.
211. Bliss, C.L., J.N. McMullin, C.J. Backhouse. Rapid fabrication of a microfluidic device with integrated optical waveguides for DNA fragment analysis. Lab on a Chip. 2007; 7(10): 1280-1287.
212. Shukla, S.K., et al. Some thermal studies of polysilanes and polycarbosilanes. Thermochimica Acta. 2004; 424(1-2): 209-217.

213. H. Schmidt. Inorganic–organic composites by sol-gel techniques. Journal of Sol-Gel Science and Technology. 1994; 1: 217–231.
214. O. Lev, Z. Wu, S. Bharathi, V. Glezer, A. Modestov, J. Gun, L. Rabinovich, S. Sampath. Sol-gel materials in electrochemistry. Chemistry of Materials. 1997; 9: 2354–2375.
215. C. Sanchez, B. Julia´n, P. Belleville, M. Popall. Applications of hybrid organic-inorganic nanocomposites. Journal of Materials Chemistry. 2005; 15: 3559–3592.
216. Shindou, T., et al. Surface properties of polydimethylsiloxane-based inorganic/organic hybrid films deposited on polyimide sheets by the sol-gel method. Journal of Sol-Gel Science and Technology. 2003; 27(1): 15-21.
217. Husing, N., et al. Novel siloxane-silica nanocomposite aerogels and xerogels. Journal of Sol-Gel Science and Technology. 2003; 26(1-3): 73-76.
218. B.D. Fabes, D.R. Uhlmann. Strengthening of glass by sol-gel coatings. Journal of American Ceramics Society. 1990; 73: 978–988.
219. B. Simionescu, M. Aflori, M. Olaru. Protective coatings based on silsesquioxane nanocomposites films for building limestones. Construction and Building Materials. 2009; 23: 3426–3430.
220. Wang, S.B., J.E. Mark. In situ Precipitation of Reinforcing Titania Fillers. Polymer Bulletin. 1987; 17(3): 271-277.
221. C. S. Parkhurst, W. F. Doyle, L. A. Silverman, S. Singh, M. P. Andersen, D. McClurg, G. E. Wnek, D. R. Uhlmann. Siloxane modified SiO_2-TiO_2 Glasses via Sol-Gel. Materials Research Society Symposium Proceedings. 1986; 73: 769.
222. E. Taylor-Smith, K. M. Choi. Synthesis & Characterization of Optically-Active Lanthanide-Doped Hybrid Inorganic-Organic Systems. Materials Research Society Symposium Proceedings. 1999; 576: 433.
223. J. D. Mackenzie. Sol-Gel Optics I. edited by D. R. Ulrich. Bellingham, WA: SPIE; 1990. 1328p.
224. S. Dire´, F. Babonneau, C. Sanchez, J. Livage. Sol-gel Synthesis of Siloxane-oxide Hybrid coatings [$Si(CH_3)_2O$, MO_x: M= Si, Ti, Zr, Al] with luminescent properties. Journal of Materials Chemistry. 1992; 2: 239.

225. C. Guermeur, J. Lambard, J. F.Gerard, C. Sanchez. Hybrid polydimethylsiloxane-zirconium oxo nanocomposites. Part 1 Characterization of the matrix and the siloxane-zirconium oxo interface. Journal of Materials Chemistry. 1999; 9: 769.

226. B. Alonso, J. Maquet, B. Viana, C. Sanchez. Hybrid organic-inorganic polydimethylsiloxane–vanadium–oxo materials crosslinked at the molecular level. New Journal of Chemistry. 1998; 22: 935.

227. F. Babonneau, L. Bois, Livage. Structural Characterization of Gels Prepared from Co-Hydrolysis of Tetraethoxysilane and Dimethyldiethoxysilane. Journal of Materials Research Society Symposium Proceedings. 1992; 271: 237.

228. F. Babonneau, L. Bois, J. Livage, S. Dire´. Structural Investigation of Sol-Gel-Derived Hybrid Siloxane-Oxide Materials Using Si MAS-NMR Spectroscopy. Materials Research Society Symposium Proceedings. 1992; 286: 289.

229. F. Babonneau, J. Maquet. Nuclear magnetic resonance techniques for the structural characterization of siloxane–oxide hybrid materials. Polyhedron. 2000; 19: 315.

230. C. L. Shutte, J. R. Fox, R. D. Boyer, D. R. Ulhmann. Ultrastructure Processing of Advanced Materials. edited by D. R. Ulhmann and D. R.Ulrich. New York: J. Wiley & Sons; 1992.

231. F. Babonneau. ^{29}Si, ^{17}O Liquid NMR and ^{29}Si CP-MAS NMR Characterization of Siloxane-Oxide Materials, [$(CH_3)_2SiO/TiO_2$, $(CH_3)_2SiO/ZrO_2$]. Materials Research Society Symposium Proceedings. 1994; 346: 949.

232. S. Katayama, Y. Kubo, N. Yamada. Characterization and Mechanical Properties of Flexible Dimethylsiloxane-Based Inorganic/Organic Hybrid Sheets. Journal of American Ceramic Society. 2002; 85: 1157.

233. TAKUYA SHINDOU. Effect of Composition on Surface Properties of Polydimethylsiloxane-based Inorganic/Organic Hybrid Films. Journal of Sol-gel Science and Technology. 2004; 30: 229-237.

Appendix A. Preparation of Polymeric Nanoparticles From Ternary Polymer/Solvent/Nonsolvent Systems

A.1 Introduction

Polymeric nanoparicles are polymer based particles having size between 1 to 1000 nm (1). They have been extensively studied in the last decades for biomedical applications, mainly in drug delivery (2). Numerous methods can be used to prepare polymeric nanoparticles, including microphase inversion (3), nanoprecipitation (4), solvent evaporation (5), emulsification (6), and salting out (7), among which nanoprecipitation is known as the commonly applied technique due to its simple and convenient. Nanoprecipitation is based on a ternary polymer/solvent/nonsolvent system, where the solvent and the nonsolvent are miscible. In such a system, since the polymer is not able to dissolve in the nonsolvent, diffusion of the organic polymer solution into the nonsolvent will lead to the precipitation of the polymer into small colloidal particles. This process consists of several steps, such as particle nucleation, molecular growing, and aggregation. By using this method, the properties and the sizes of the resulting particles depend on numerous factors, such as the polymer behavior in the organic phase, the nature and ratio of the external phase, the initial polymer concentration, and the ratio between solvent and nonsolvent etc. This relationship is complicated and difficult to be modeled. In this experiment, we set up an apparatus based on light scattering modified by a computer which can be notified as soon as the particle forms. By applying this apparatus, it makes the fabrication of particles in nano-sized feasible and easier.

A.2 Experiments

A.2.1 Apparatus Schematic

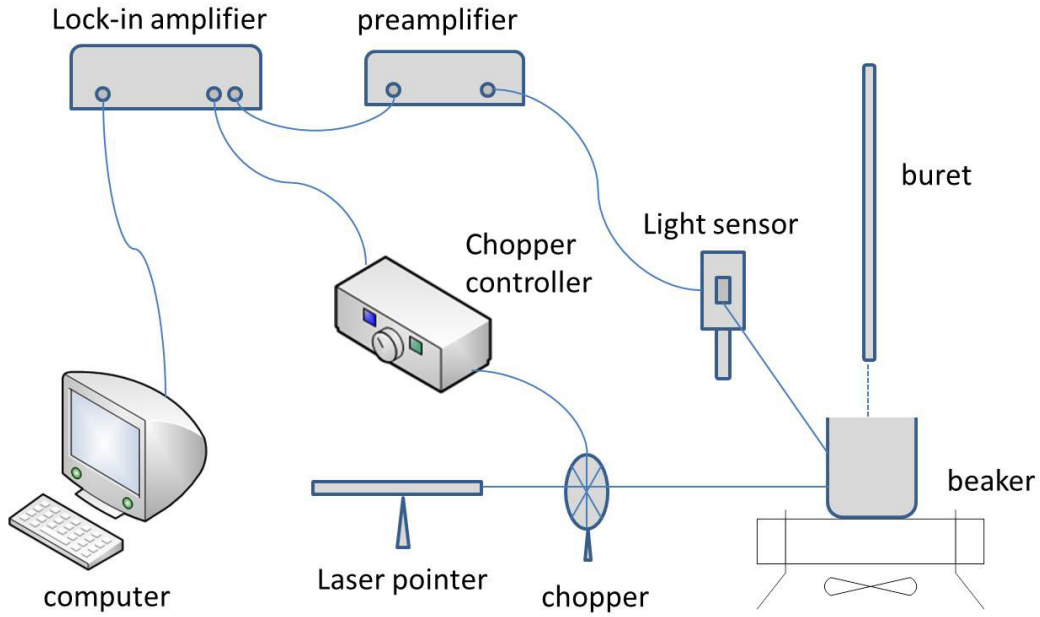

Figure A.1 Apparatus schematic of light scattering

As shown in Figure A.1, an intermittent laser light with frequency settled by a chopper is sent to the beaker. The chopper is controlled by a controller connecting to the lock-in amplifier. The nonsolvent is dripped from buret into the beaker containing a polymer solution. When the polymer particle forms, the laser light passing through is scattered and detected by the light sensor. The generated signal from the sensor is pre-amplified and finally sent to the lock-in amplifier, which can recognize the right signal from noise by comparing it with the source laser frequency. The whole process is monitored by a computer.

A.2.2 Materials

Polylactic acid (PLLA) (Grade 6202D) produced by NatureWorks LLC and Polyvinyl alcohol (PVA) (98-99%) purchased from Sigma-Aldrich were used as polymers. 1,2-dichloroethane (≥99%) from Sigma-Aldrich and methanol (FisherChemical) were the solvent and nonsolvent of PLLA respectively. Deionized water was the solvent of PVA and acetone (FisherChemical) was employed as nonsolvent. All the chemicals were used without further purification.

A.2.3 Polymer/solvent/nonsolvent systems

Two different systems were tested using this light scattering apparatus:

1) Polylactic acid (PLLA)/ 1, 2-dichloroethane/methanol

2) Polyvinyl alcohol (PVA)/water/acetone

Both of these two systems were prepared using polymer concentrations of 1.5 w/v%. Two kinds of titration methods, forward titration (FT) and back titration (BT), were employed to proceed with the experiment. For forward titration, 1.5 w/v% of polymer solution was charged into a beaker, the nonsolvent was added dropwise until the signal changed on the computer. For backward titration, the nonsolvent was charged into a beaker, the polymer solution was added dropwise from a burette into this beaker until it cause a signal change notified by computer.

A.3 Results and Discussions

The obtained polymeric particle suspensions were characterized by a Malvern Zetasizer Nano ZS for particle size. The results are shown below.

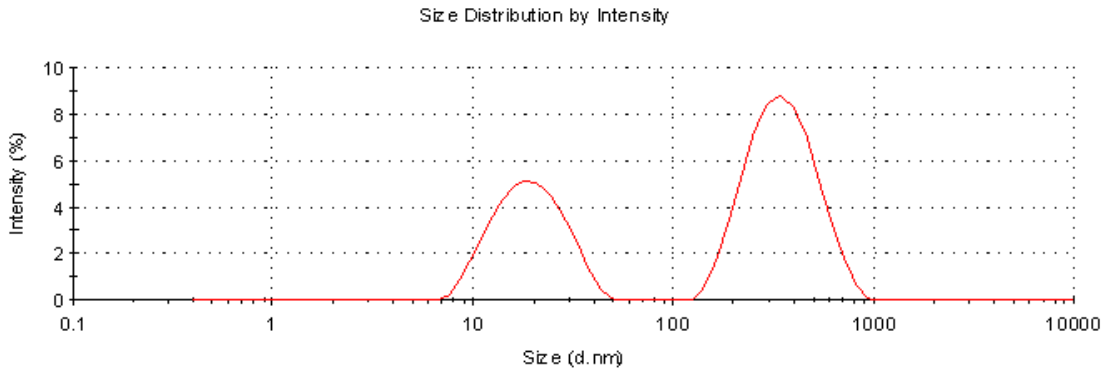

Figure A.2 PLLA particle size distribution prepared by BT

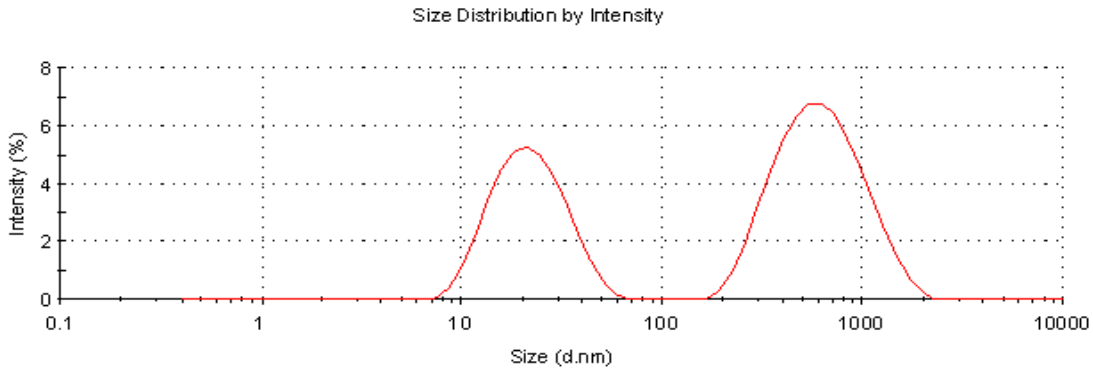

Figure A.3 PLLA particle size distribution prepared by FT

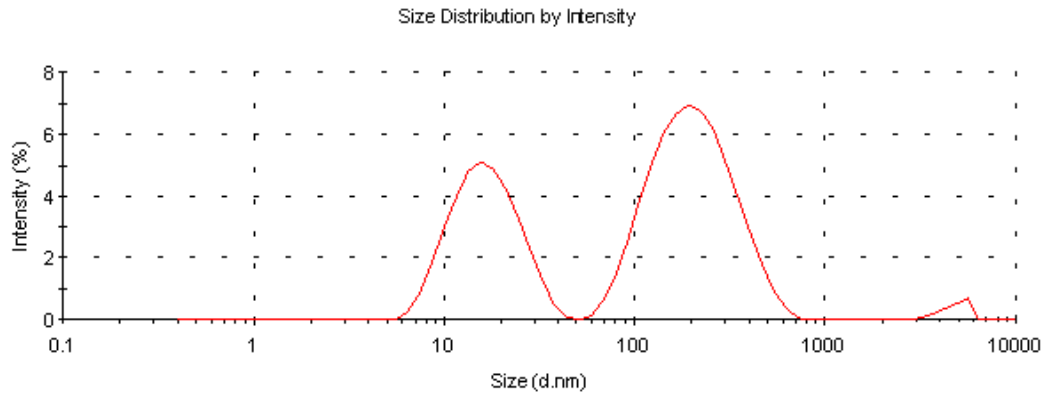

Figure A.4 PVA particle size distribution prepared by BT

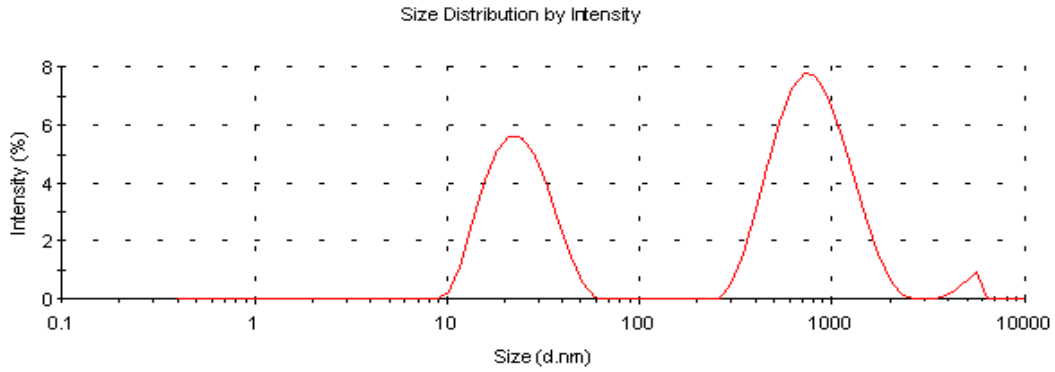

Figure A.5 PVA particle size distribution prepared by FT

According to the results, for both of these two systems, nano-sized polymeric particles were obtained by using this set-up apparatus. Based on the particle size distribution curves, it can be found that the BT method can achieve smaller particles than the FT method. The BT method was used for preparation of very fine nanoparticles in the following experiments.

A.4 References

1. Couvreur, P., C. Dubernet, F. Puisieux. Controlled Drug-Delivery with Nanoparticles - Current Possibilities and Future-Trends. European Journal of Pharmaceutics and Biopharmaceutics. 1995; 41(1): 2-13.
2. Igor Y. Perevyazko, A.V., Christian Pietsch, Stephanie Schubert, Georgy M. Pavlov, Ulrich S. Schubert. Nanoprecipitation of Poly(methyl methacrylate)-Based Nanoparticles: Effect of the Molar Mass and Polymer Behavior. Polymer Chemistry. 2012; 50: 2906-2913.
3. Zhang, G.Z., et al. Formation of novel polymeric nanoparticles. Accounts of Chemical Research. 2001; 34(3): 249-256.
4. Ezpeleta, I., et al. Gliadin nanoparticles for the controlled release of all-trans-retinoic acid. International Journal of Pharmaceutics. 1996; 131(2): 191-200.
5. Scholes, P.D., et al. The Preparation of Sub-200 Nm Poly(Lactide-Co-Glycolide) Microspheres for Site-Specific Drug Delivery. Journal of Controlled Release. 1993; 25(1-2): 145-153.
6. Niwa, T., et al. Preparations of Biodegradable Nanospheres of Water-Soluble and Insoluble Drugs with D,L-Lactide Glycolide Copolymer by a Novel Spontaneous Emulsification Solvent Diffusion Method, and the Drug Release Behavior. Journal of Controlled Release. 1993; 25(1-2): 89-98.
7. Allemann, E., R. Gurny, E. Doelker. Preparation of Aqueous Polymeric Nanodispersions by a Reversible Salting-out Process - Influence of Process Parameters on Particle-Size. International Journal of Pharmaceutics. 1992; 87(1-3): 247-253.

Appendix B. Fabrication of (Gelatin-g-PMMA)-TiO_2 Hybrid Nanocomposites by Sol-Gel Route

B.1 Introduction

Polymer-inorganic hybrids are attracting great attentions because of their ability to combine advantages of polymers and inorganic materials. These hybrids have promising potential applications in electro-optics (1,2), biology (3,4), and material sciences (5) etc.

A large number of polymers, synthetic and natural, have been applied to prepare polymer-inorganic hybrids. Among synthetic polymers, poly (glycolic acid) (6), poly (lactic acid) (7), and poly (methyl methacrylate) (8) are frequently used. Natural polymers include chitosan (9), cellulose (10), and gelatin (11). Gelatin is widely employed due to its self-assembling, nontoxic, biodegradable, and inexpensive. However, the films made of gelatin are tough and brittle, and easily to be swelled in water. In our experiments, methyl methacrylate (MMA) was grafted onto gelatin chains to obtain gelatin-g-PMMA which owns improved biocompatibility and long-term stability.

Titanium dioxide (TiO_2) is one of the most extensively studied metal oxides. It possesses outstanding properties, including chemical resistance, good mechanical strength, and well insulation. In our experiments, (gelatin-g-PMMA)-TiO_2 hybrids were fabricated by sol-gel reaction to obtain nanocomposites with enhanced thermal stability, optical transparency, and mechanical properties.

B.2 Experiments

B.2.1 Apparatus Schematic

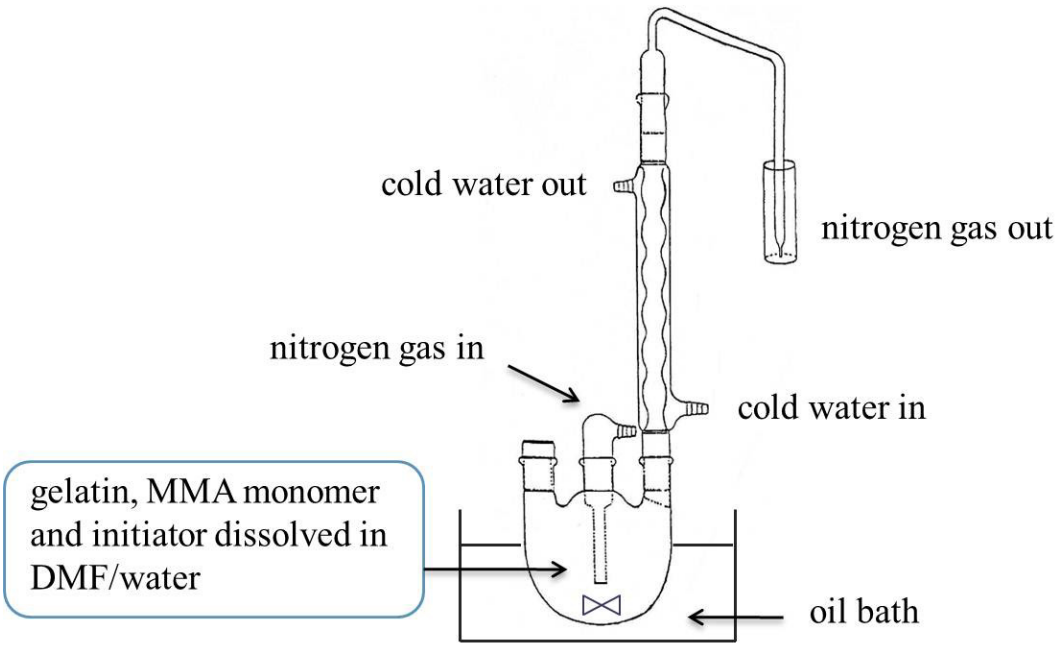

Figure B.1 Schematic of Gelatin-g-PMMA polymerization

The apparatus used for the polymerization of Gelatin-g-PMMA is shown above. Cold water was flowing through the reactor to condensate evaporated reactants back to the flask. During the experiment, the flask was heated in an oil bath at 70 °C and purged with nitrogen gas.

B.2.2 Materials

Gelatin (225 bloom), and methyl methacrylate (MMA) purchased from Sigma Aldrich were used to produce Gelatin-g-PMMA polymers. 2, 2-azobis-(2-methylpropionamide dihydrochloride) (V50) from Sigma Aldrich was employed as the initiator. Titanium isopropoxide (97%) provided by Sigma Aldrich was applied as the titanium precursor. Dimethylformamide (DMF) (Sigma Aldrich), isopropanol (anhydrous, PHARMCO-AAPER), and distilled and deionized water were utilized as solvents. Hydrochloric acid (38%) was used to change the pH of the solution.

B.2.3 Preparation of (Gelatin-g-PMMA)-TiO_2 Hybrids

To synthesize grafted polymer of Gelatin-g-PMMA, 3.2 g of gelatin in 80 ml D.I. water and 0.8 g of MMA in 20 ml DMF were charged into a 250 ml three-neck flask purged with nitrogen. 67.8 mg of V50 as the initiator in 20 ml DMF was dripped into this combination. Then the reaction was heated under reflux for 12 h. Finally a white suspension of grafted polymers was obtained. Certain amount of titanium isopropoxide (10 wt %) dissolved in isopropanol/DMF was added into this polymer suspension, and this combination was dripped into sufficient deionized water stirred at room temperature. Hydrochloric acid was introduced to adjust the pH of this suspension to be around 1.

B.3 Results and Discussions

After stirring at room temperature for 6 h, this suspension was filtered using filter papers with a diameter of 25 nm, and then characterized by FE-SEM (Hitachi S-4700) for the morphology of the particles.

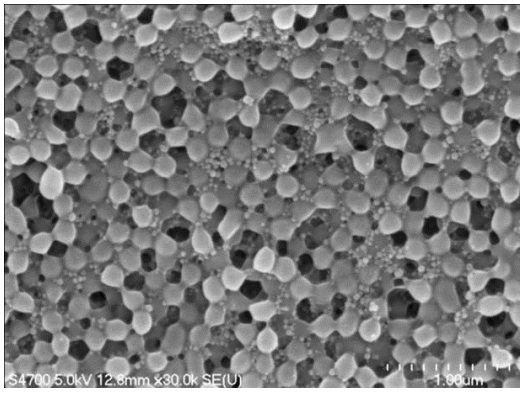

Figure B.2: (Gelatin-g-PMMA)-TiO_2 (pH=7)

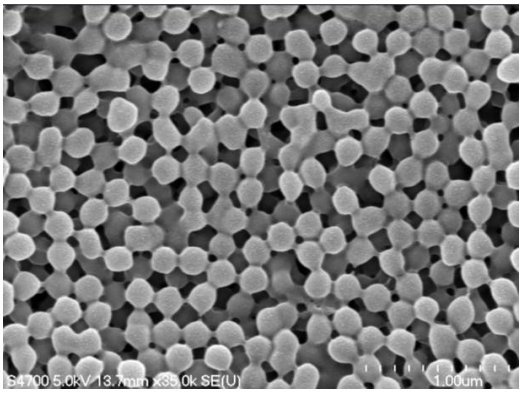

Figure B.3: (Gelatin-g-PMMA)-TiO_2 (pH=1)

It is known that gelatin is hydrophilic and PMMA is hydrophobic. The hypothesis is when dripping this polymer suspension into water, gelatin-g-PMMA would form core-shell particles containing TiO_2 particles inside as the core. From the results shown in the figures above, although gelatin-g-PMMA polymer particles were fabricated in nano dimension with uniform size, TiO_2 particles aggregated outside instead of being enclosed by polymer shell. By decreasing the pH of the solution, fewer TiO_2 particles were detected and they were in much smaller size absorbed on the particle surfaces. That may be because titanium isopropoxide is stable in hydrous solution with pH=1, so most of the titanium was filtered out with the solution.

B.4 References

1. Dey, A., et al. Characterization and dielectric properties of polyaniline-TiO2 nanocomposites. Nanotechnology. 2004; 15(9): 1277-1283.
2. Tsai, T.Y., et al. Electro-optical properties of a twisted nematic-montmorillonite-clay nanocomposite. Nanotechnology. 2005; 16(8): 1053-1057.
3. D., L. Polymeric Organic/Inorganic Hybrids for Electro-Responsive Applications. Michigan Technological University, M.S. Thesis, 2000.
4. Paunesku, T., et al. Biology of TiO2-oligonucleotide nanocomposites. Nature Materials. 2003; 2(5): 343-346.
5. Pope, M.T., A. Muller. Polyoxometalate Chemistry - an Old Field with New Dimensions in Several Disciplines. Angewandte Chemie-International Edition in English. 1991; 30(1): 34-48.
6. Kawanishi, M., et al. New type of biodegradable porous scaffolds for tissue-engineered articular cartilage. Materials Science & Engineering C-Biomimetic and Supramolecular Systems. 2004. 24(3): 431-435.
7. Whang, K., et al. A Novel Method to Fabricate Bioabsorbable Scaffolds. Polymer. 1995; 36(4): 837-842.
8. Singh, V., Tiwari, A., Tripathi, D. N., Sanghi, R. Microwave synthesized of Chitosan-graft-poly(methylmethacrylate): An Efficient Zn^{2+} ion binder. Carbohydrate Polymer. 2006; 65(1): 35-41.
9. Amsden B.G., S.U., Knight D.K., Shapka S.N., Methacrylated glycol chitosan as a photo- polymerizable biomaterial. Biomacromolecules. 2007; 8: 3758-3766.
10. Khan, F. Photoinduced graft-copolymer synthesis and characterization of methacrylic acid onto natural biodegradable lignocellulose fiber. Biomacromolecules. 2004; 5(3): 1078-1088.
11. Griffiths, P.C., et al. Interaction between a partially fluorinated alkyl sulfate and gelatin in aqueous solution. Langmuir. 2004; 20(4): 1161-1167.

Appendix C. Extra Data

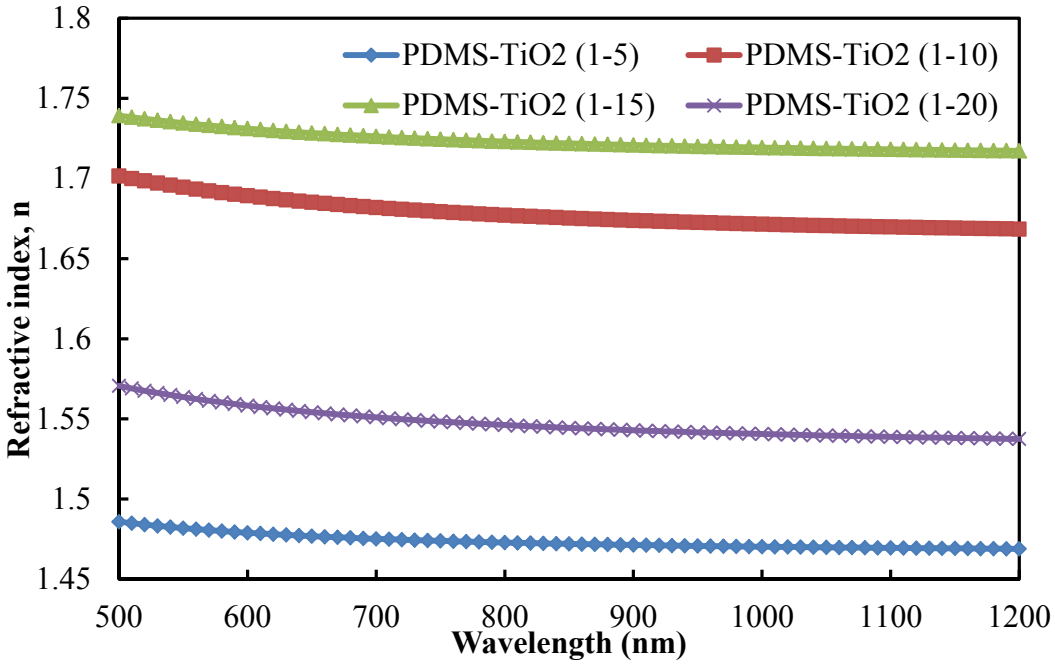

Figure C.1 Refractive index of PDMS-TiO_2 hybrid nanocomposites

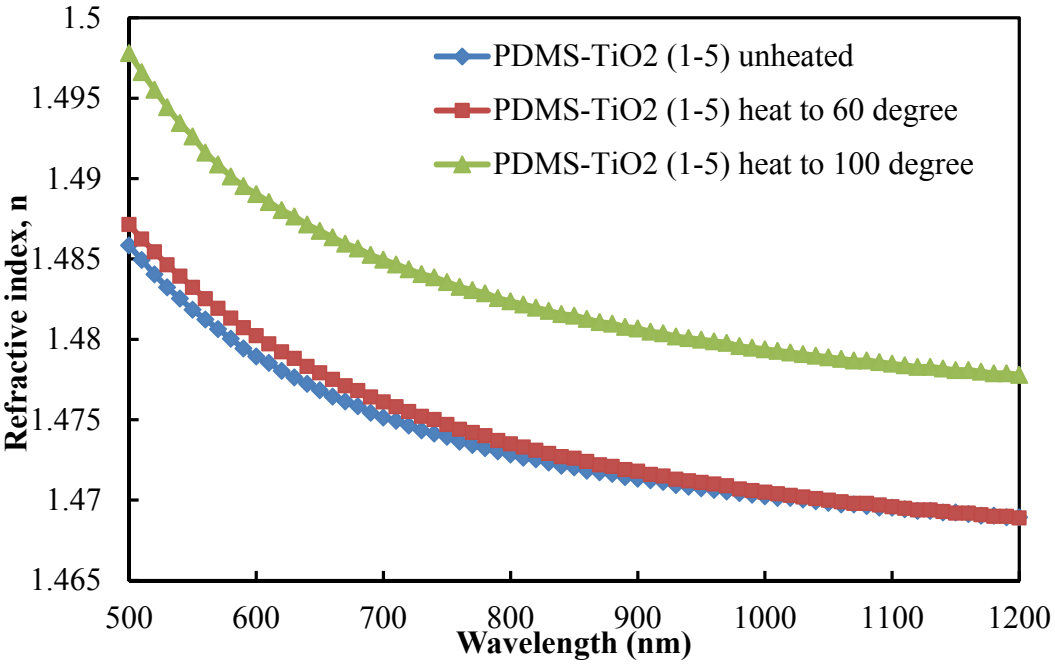

Figure C.2 Refractive index of PDMS-TiO_2 (1-5) annealed at different temperatures

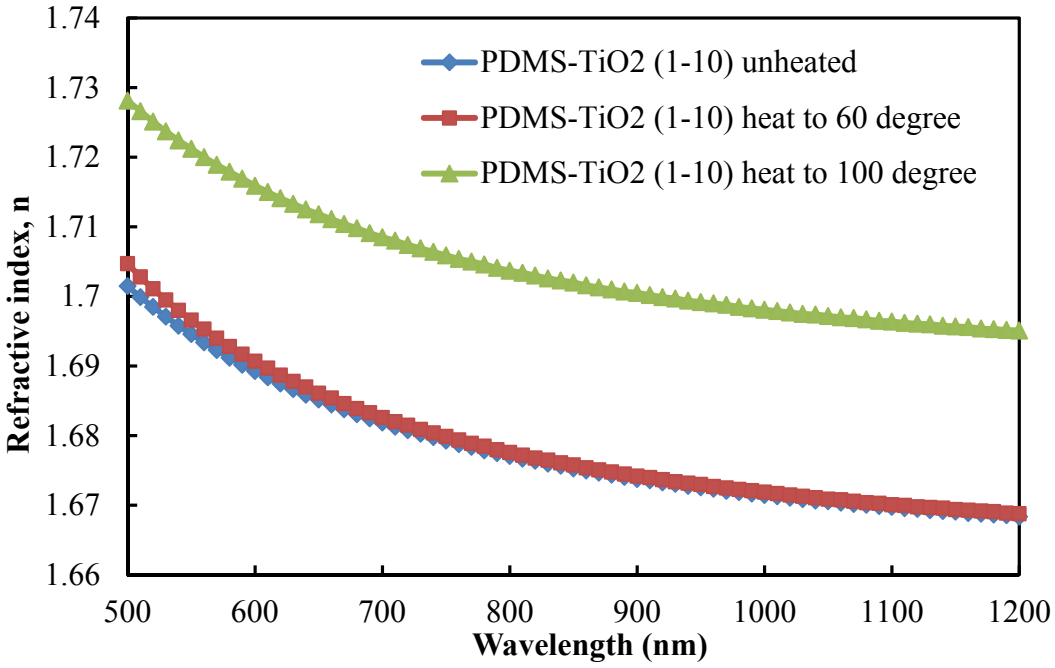

Figure C.3 Refractive index of PDMS-TiO_2 (1-10) annealed at different temperatures

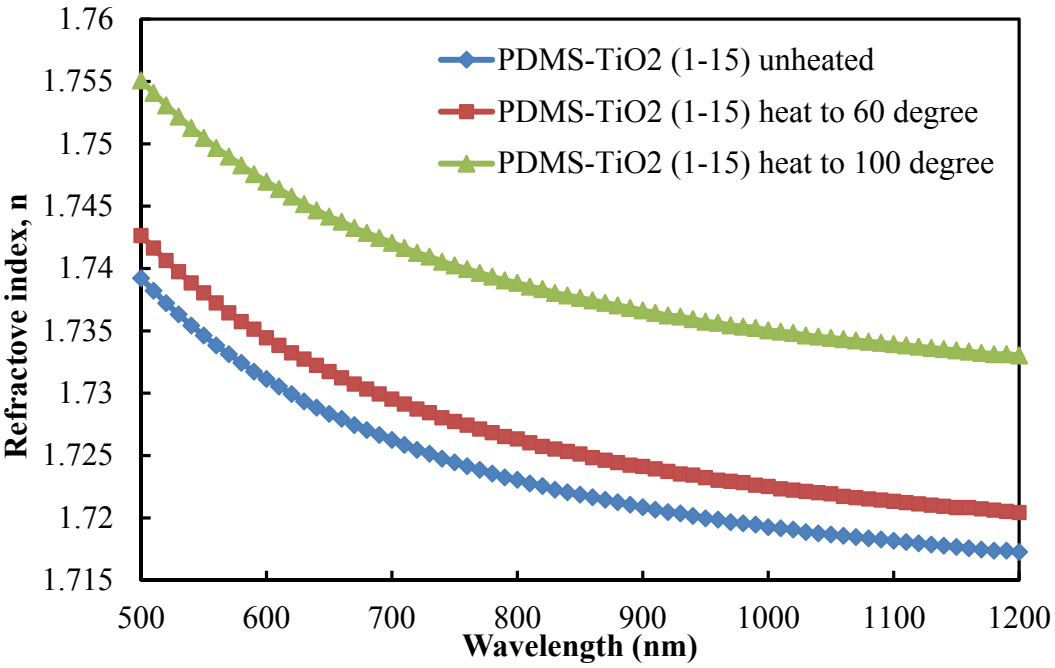

Figure C.4 Refractive index of PDMS-TiO_2 (1-15) annealed at different temperatures

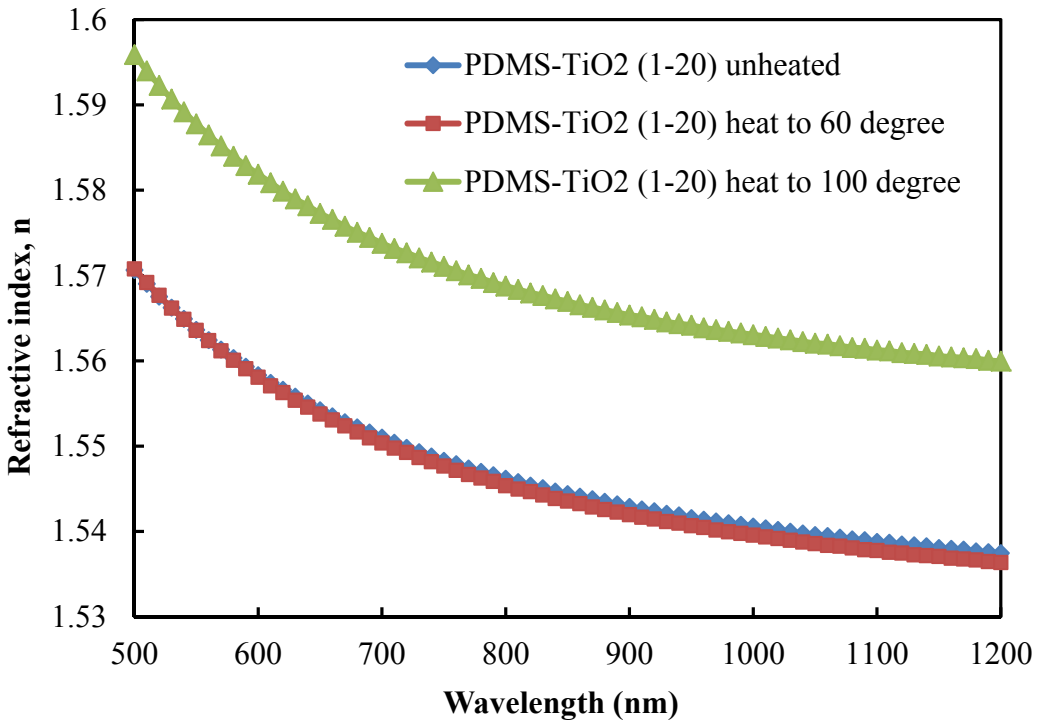

Figure C.5 Refractive index of PDMS-TiO_2 (1-20) annealed at different temperatures

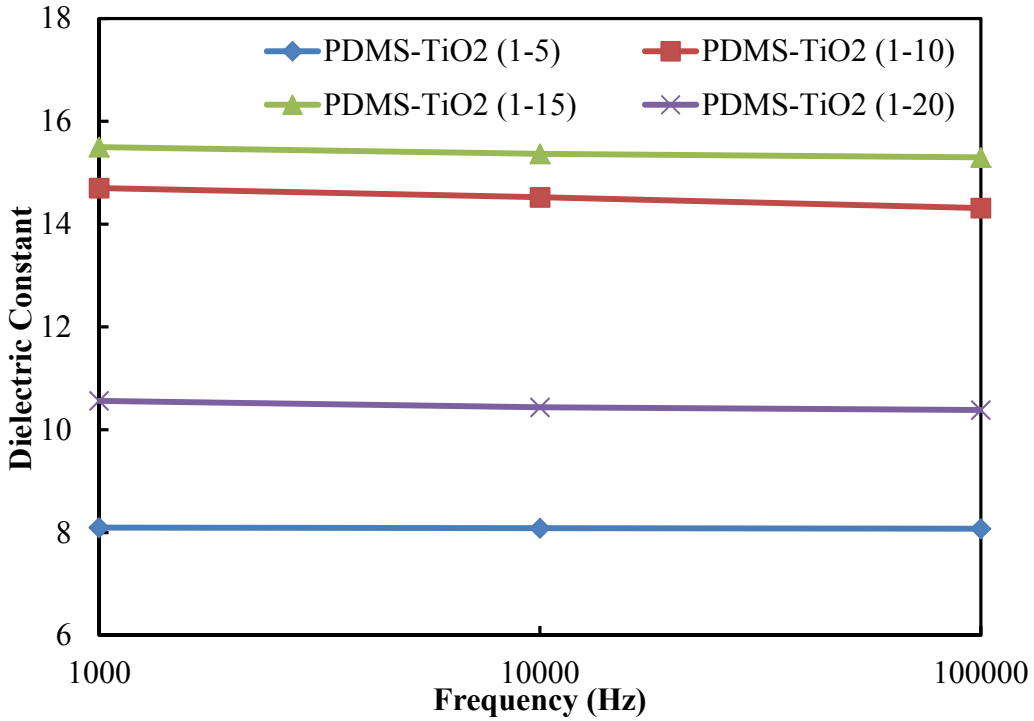

Figure C.6 Dielectric constant of PDMS-TiO_2 hybrid nanocomposites

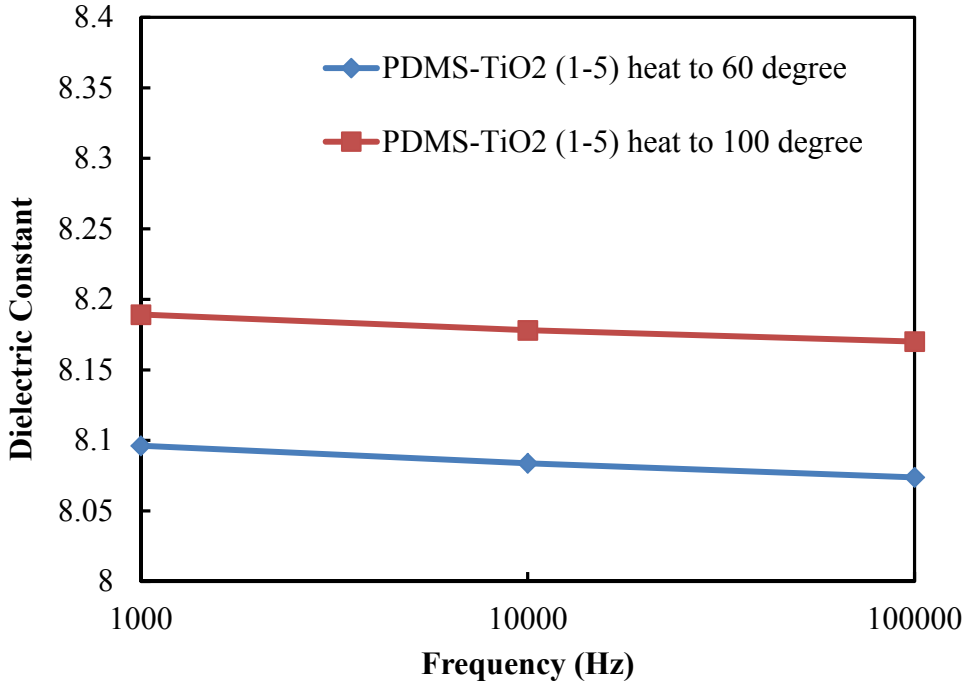

Figure C.7 Dielectric constant of PDMS-TiO_2 (1-5) annealed at different temperatures

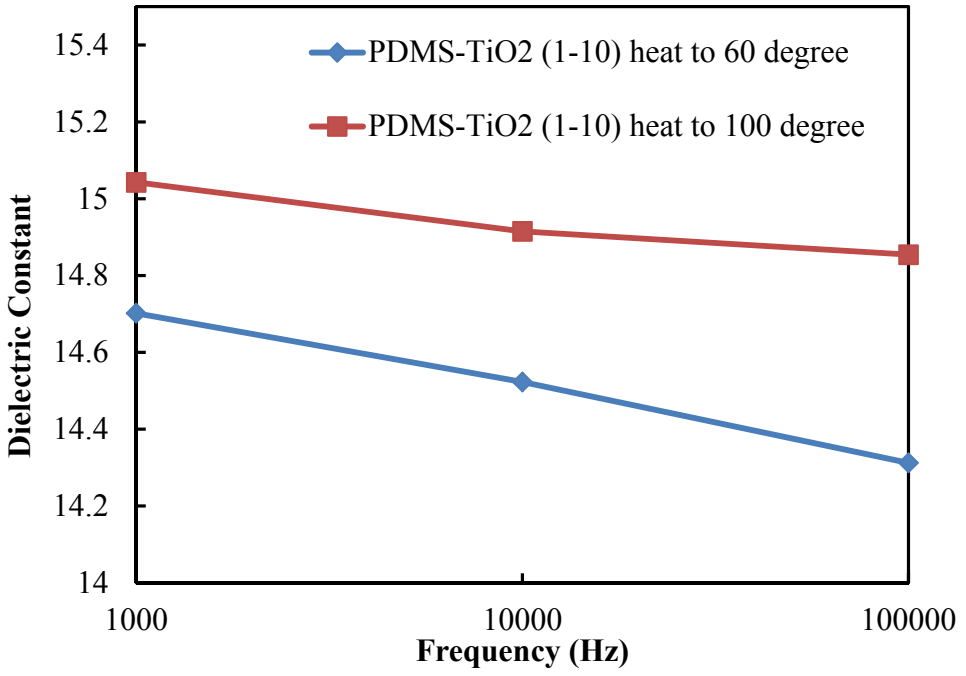

Figure C.8 Dielectric constant of PDMS-TiO_2 (1-10) annealed at different temperatures

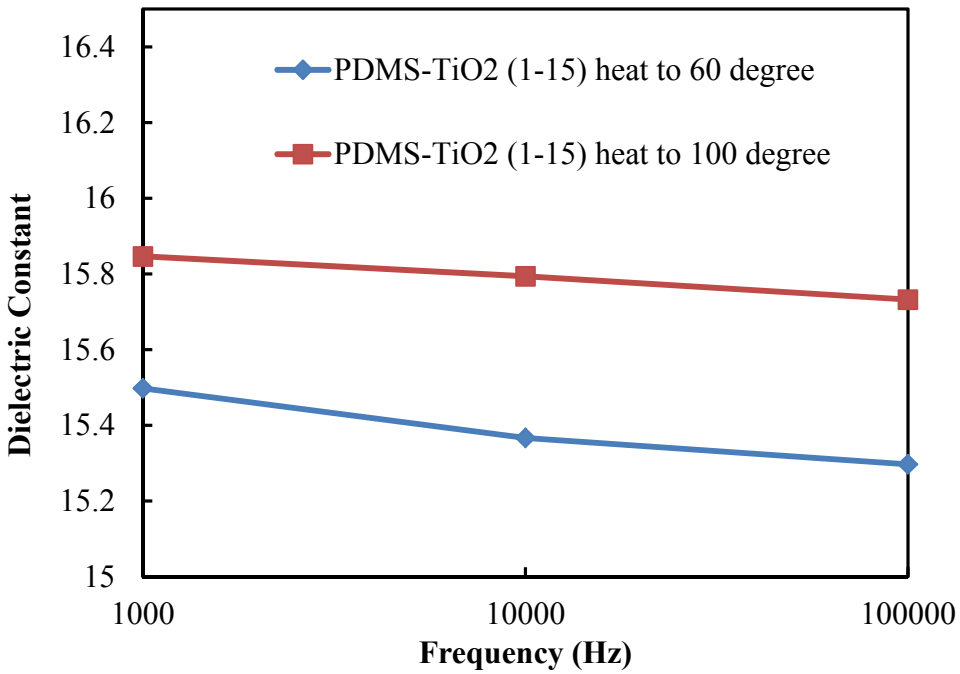

Figure C.9 Dielectric constant of PDMS-TiO_2 (1-15) annealed at different temperatures

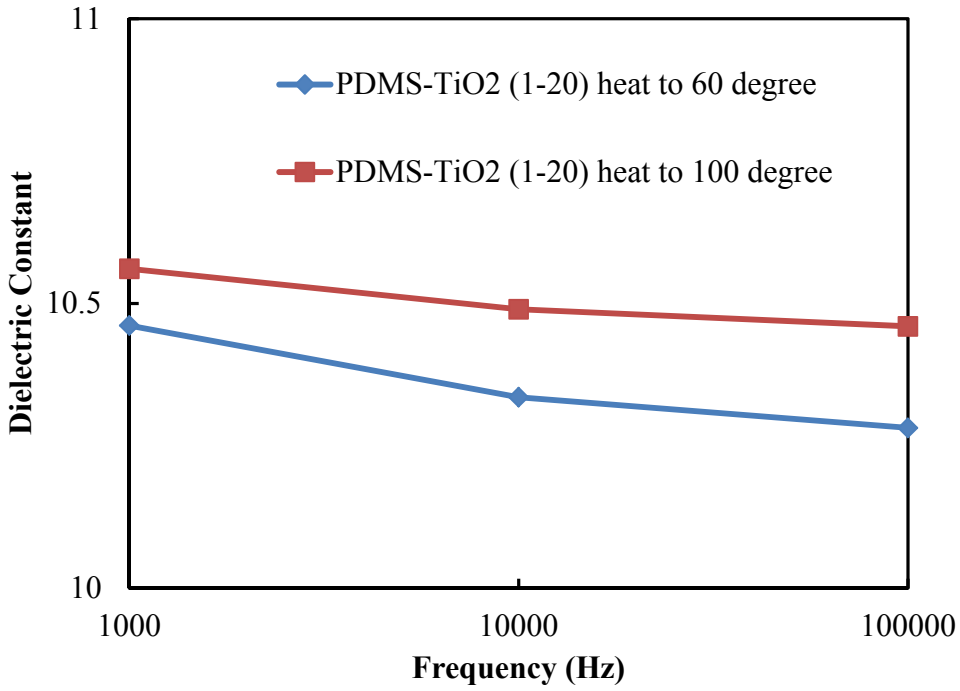

Figure C.10 Dielectric constant of PDMS-TiO_2 (1-20) annealed at different temperatures

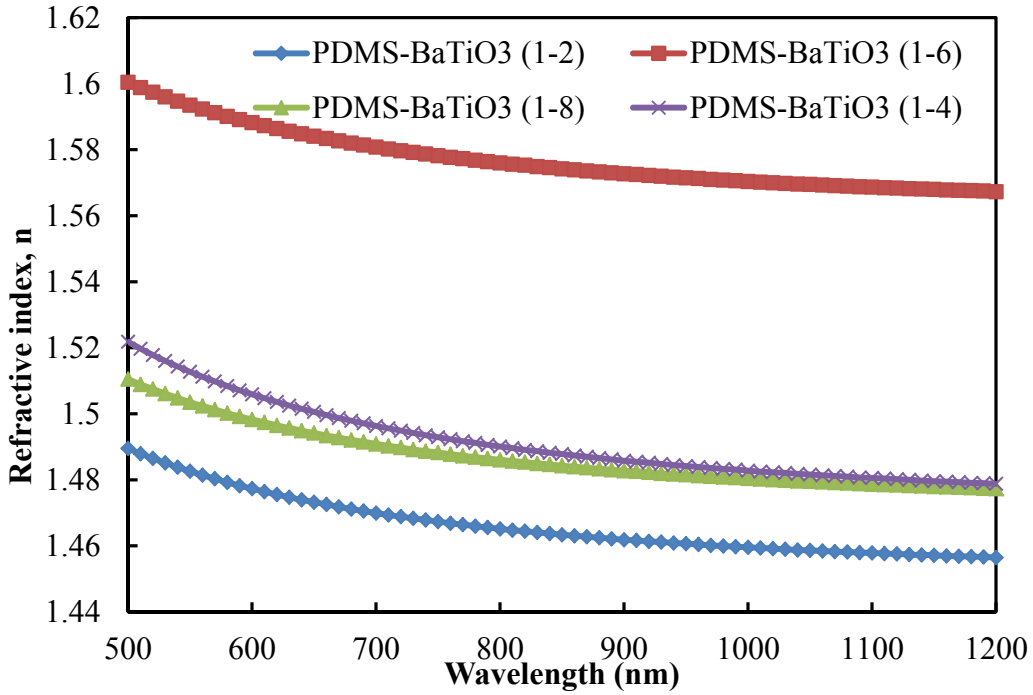

Figure C.11 Refractive index of PDMS-$BaTiO_3$ hybrid nanocomposites

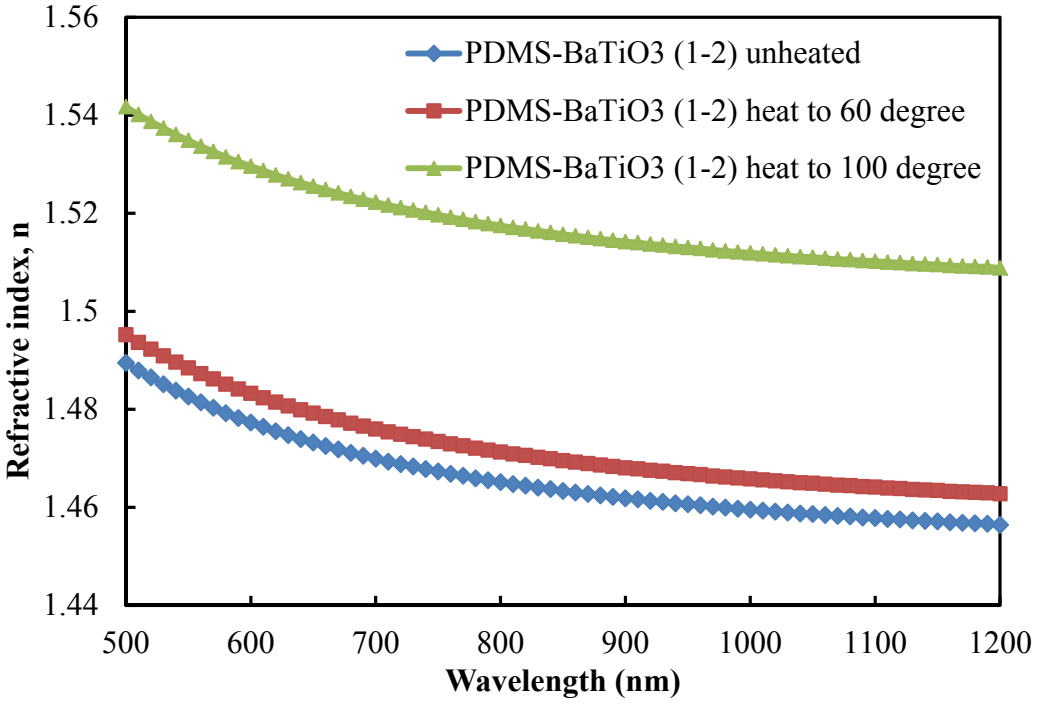

Figure C.12 Refractive index of PDMS-$BaTiO_3$ (1-2) annealed at different temperatures

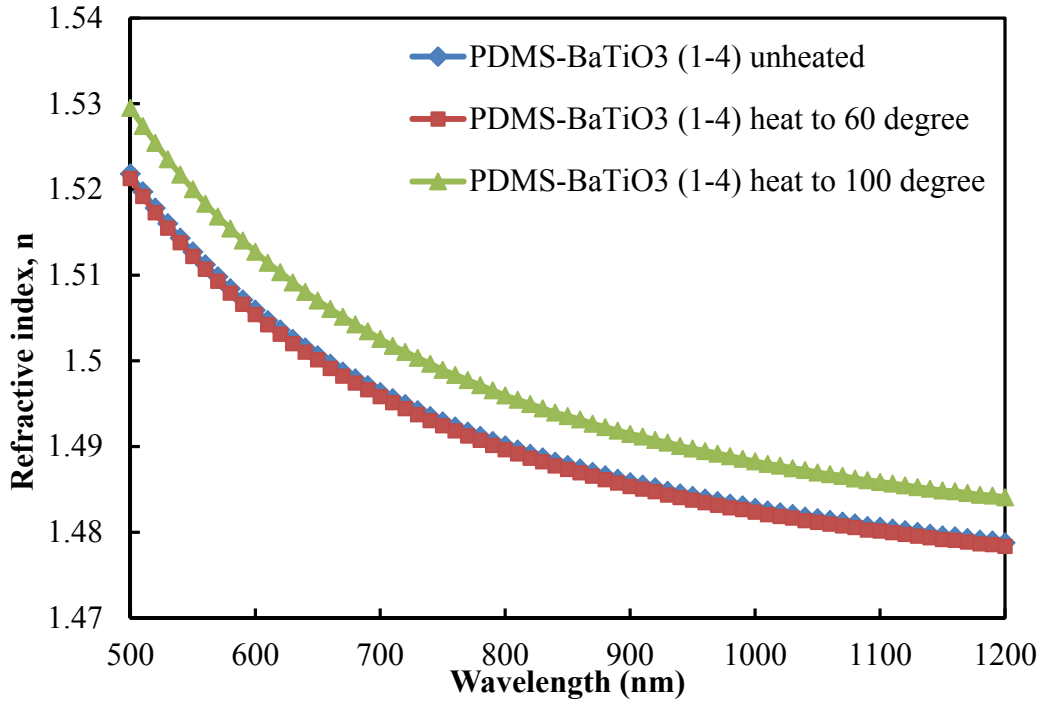

Figure C.13 Refractive index of PDMS-$BaTiO_3$ (1-4) annealed at different temperatures

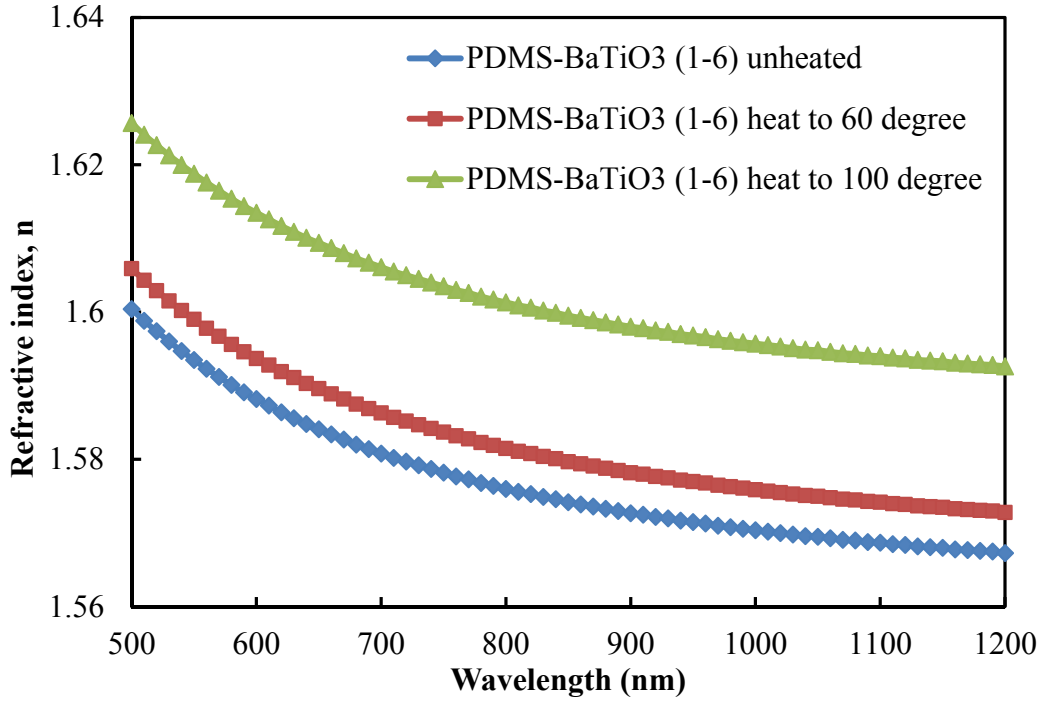

Figure C.14 Refractive index of PDMS-$BaTiO_3$ (1-6) annealed at different temperatures

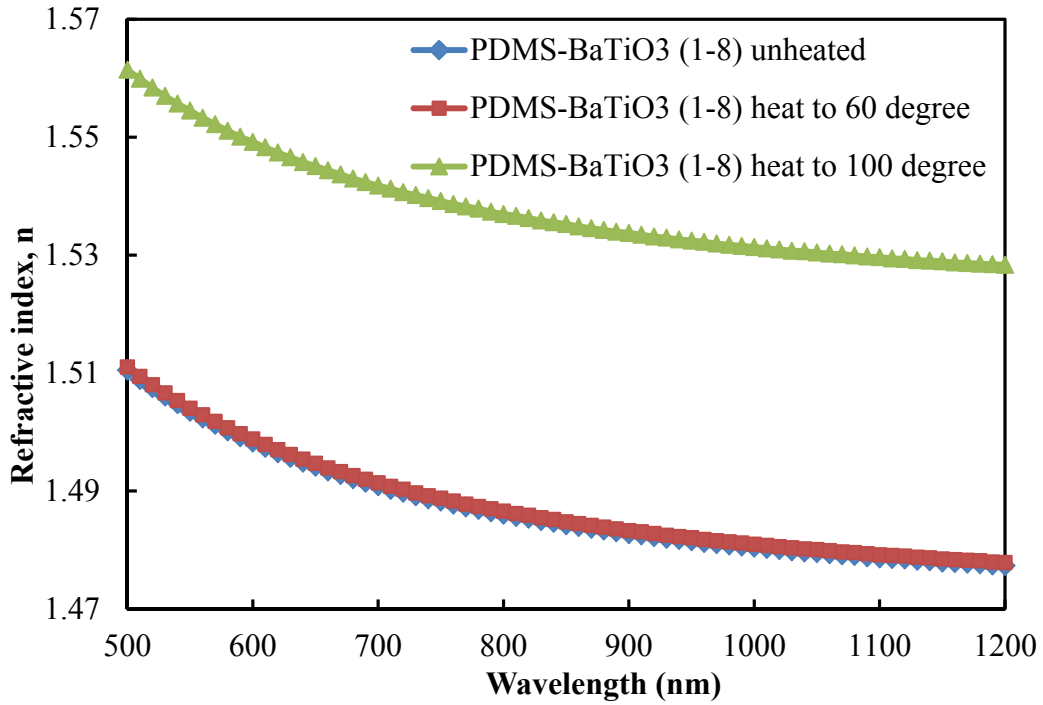

Figure C.15 Refractive index of PDMS-$BaTiO_3$ (1-8) annealed at different temperatures

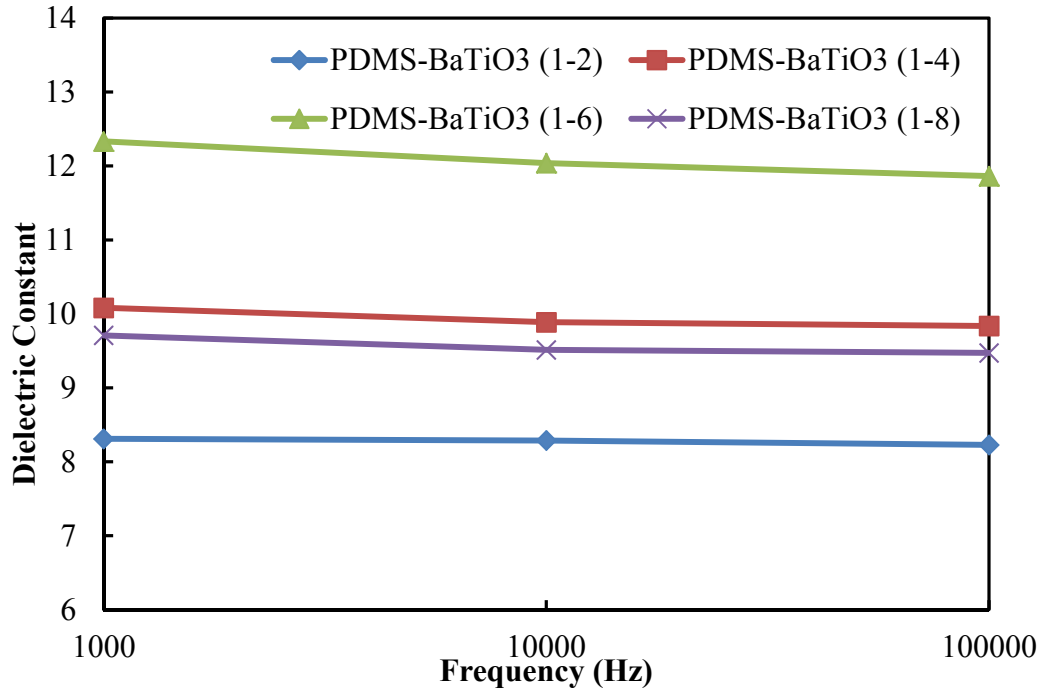

Figure C.16 Dielectric constant of PDMS-$BaTiO_3$ hybrid nanocomposites

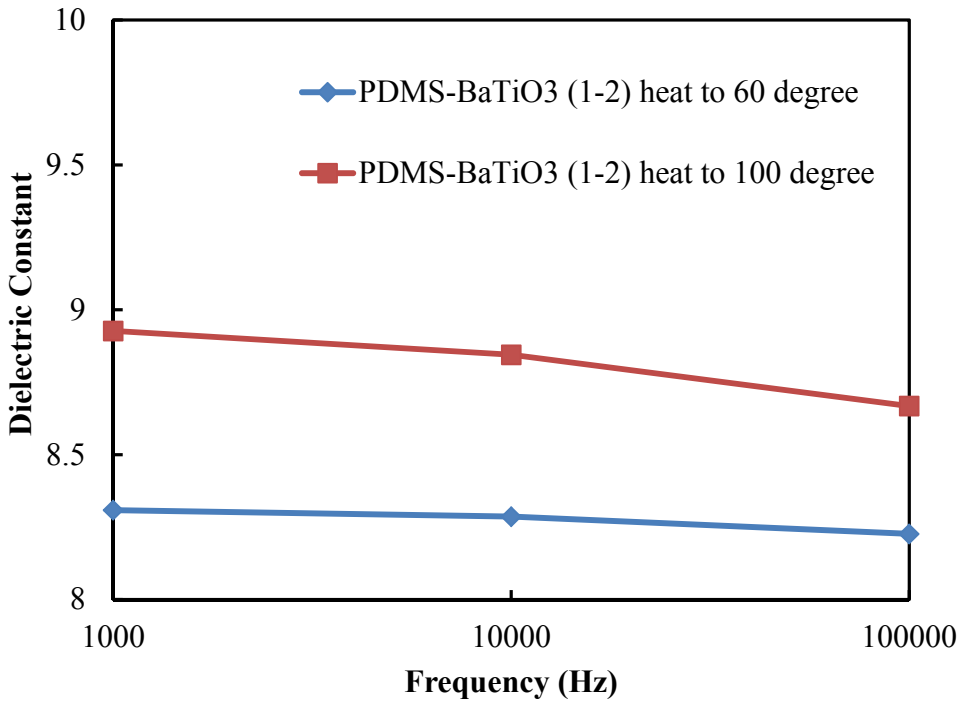

Figure C.17 Dielectric constant of PDMS-$BaTiO_3$ (1-2) annealed at different temperatures

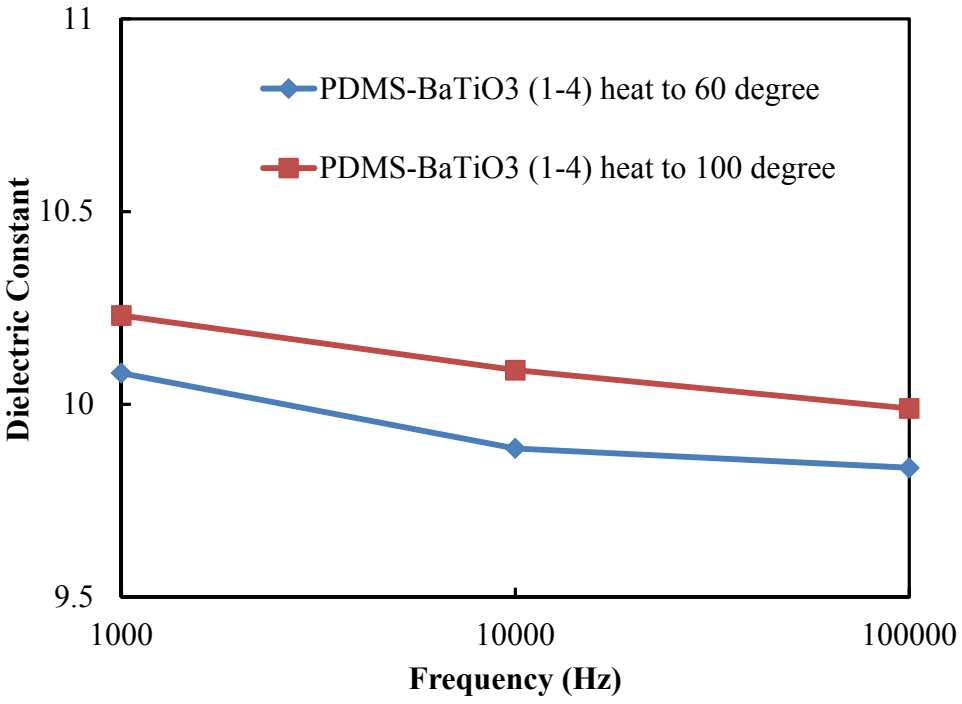

Figure C.18 Dielectric constant of PDMS-$BaTiO_3$ (1-4) annealed at different temperatures

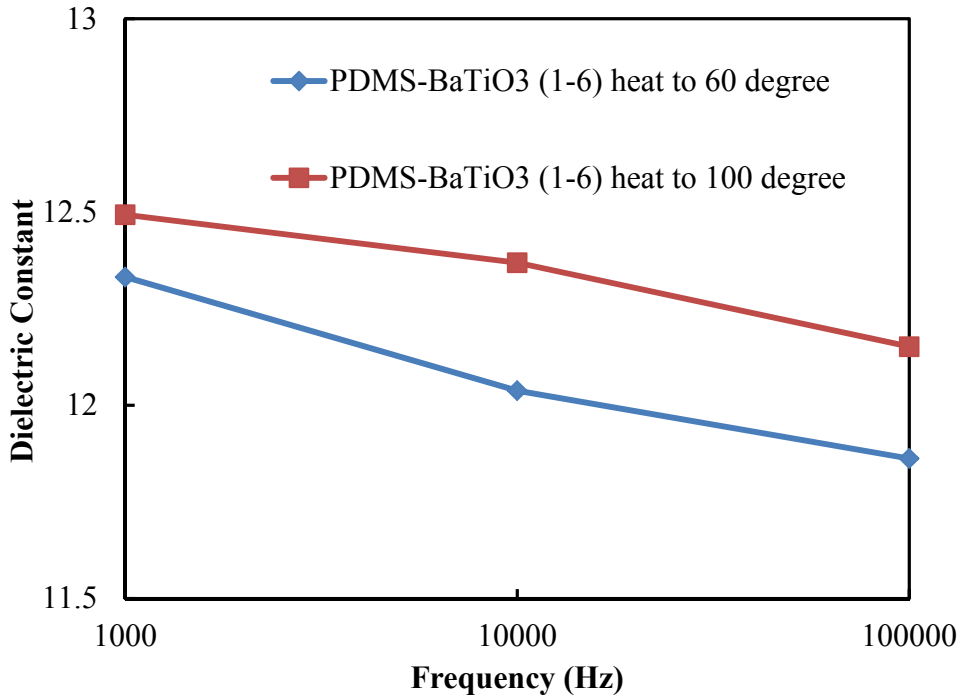

Figure C.19 Dielectric constant of PDMS-$BaTiO_3$ (1-6) annealed at different temperatures

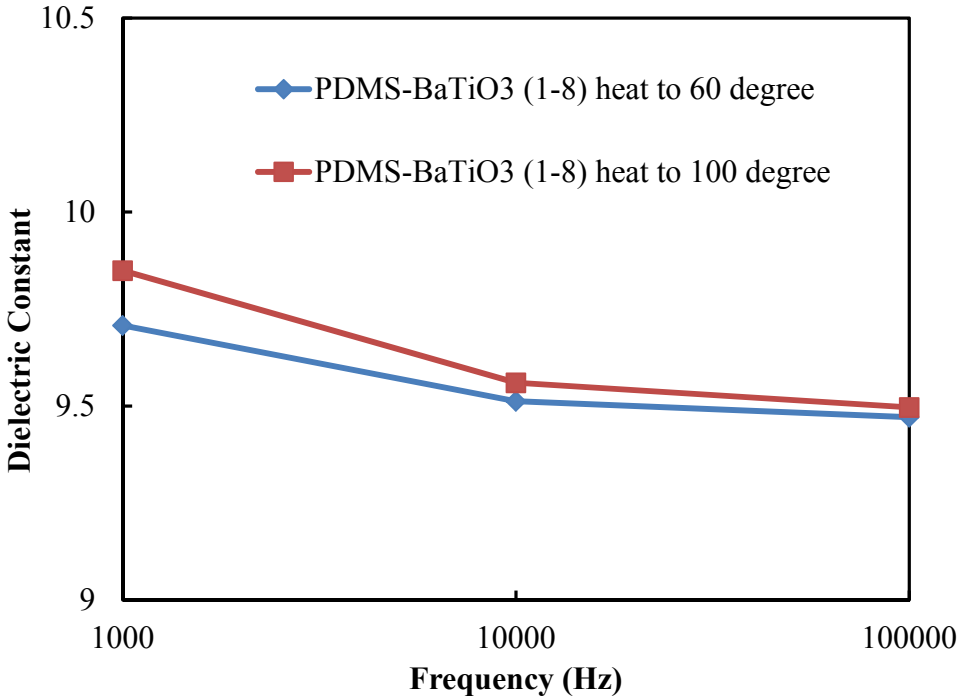

Figure C.20 Dielectric constant of PDMS-$BaTiO_3$ (1-8) annealed at different temperatures

Appendix D. Copyright

Cambridge University Press

Reprint Permission

August 6, 2012

Qiaoyu Lu

1908 Woodmar Drive Apt.B

Houghton, MI 49931

906-370-7836

qlu@mtu.edu

Reference

In situ Synthesis of High Refractive Index PDMS/Metal Oxide Nanocomposites

Qiaoyu Lu and Michael E. Mullins

MRS Proceedings, Volume 1400, Symposium S (2012), s06-02 (6 pages)

Reprint Description

Title: Synthesis of PDMS-Metal Oxide Hybrid Nanocomposites Using An In Situ Sol-Gel Route, by Qiaoyu Lu

Institution: Michigan Technological University

Format: Dissertation

Rights/Acknowledgement

Permission is granted for nonexclusive rights to reprint your journal article in your dissertation as described above. This permission requires full acknowledgement:

In situ Synthesis of High Refractive Index PDMS/Metal Oxide Nanocomposites, by Qiaoyu Lu and Michael E. Mullins
MRS Proceedings, Volume 1400, Symposium S (2012), s06-02

This permission is subject to the following:

a.) the material to be reprinted must be original to you as the Cambridge University Press journal author and must not involve material obtained from a third party; any material copyrighted by or credited in the journal article to another source may require further clearance by you from the original source, and Cambridge University Press is not liable for the use of third party material

b.) you must inform your co-author in advance of your reprinting the article and ensure that your co-author has no objections

c.) you must forward or refer to Cambridge University Press all republication requests that you may receive involving the material published by Cambridge University Press

Sincerely,

_____

Marc P. Anderson

Rights and Permissions Manager

Cambridge University Press

32 Avenue of the Americas

New York, N.Y. 10013-2473

tel.: 212-924-3900; 212-337-5048 (direct)

email: manderson@cambridge.org

_____

Cambridge Academic and Professional Books

Cambridge Books Online

Cambridge Journals Online

Cambridge English Language Learning

_____